**Lay-up Optimisation of Fibre Metal Laminates**

*Development of a Design Methodology for Wing Structures*

**Ilhan Şen**

A design optimisation methodology for fibre metal laminates has been developed with intention to design wing structures that satisfy fatigue and damage tolerant criteria. The methodology enables the exploration of the design space of fibre metal laminates by finding lay-up solutions for flat plates and also reveals the contribution of individial criteria to the obtained solutions. Furthermore, the method is capable of designing a lower wing skin consisting of fibre metal laminates and an upper wing skin consisting of aluminium while assuring compatibility between the wing cross-sections. The procedure is improved by decreasing the computation time of the optimisation by considering approximations for the evaluation methods while assuring the accuracy. The influence of optimisation settings, approximations and different design criteria are extensively investigated and the results to support and demonstrate the working of the design methodology are presented.

TU Delft

9 789461 864925

Ilhan Şen

**Lay-up Optimisation of Fibre Metal Laminates**

*Development of a Design Methodology for Wing Structures*

# Lay-up Optimisation of Fibre Metal Laminates

## *Development of a Design Methodology for Wing Structures*

**Ilhan Şen**

## Invitation

to the defence of
my PhD thesis.

**Lay-up Optimisation of Fibre Metal Laminates**

*Development of a Design Methodology for Wing Structures*

on Thursday
22th October 2015 at 15:00 hours

in the Senaatszaal of
the Delft University
of Technology at
Mekelweg 5 in Delft.

Prior to the defence,
at 14:30, I will present a
short outline of
the research work
in my thesis.

After the ceremony,
there will be a
reception in the
Vliegtuighal of the
Faculty of
Aerospace Engineering at
Kluyverweg 1 in Delft.

Ilhan Şen

# Lay-up Optimisation of Fibre Metal Laminates

Development of a Design Methodology for Wing Structures

**Ilhan Şen**

# Lay-up Optimisation of Fibre Metal Laminates

Development of a Design Methodology for Wing Structures

**Proefschrift**

ter verkrijging van de graad van doctor

aan de Technische Universiteit Delft,

op gezag van de Rector Magnificus prof. ir. K. C. A. M. Luyben,

voorzitter van het College voor Promoties,

in het openbaar te verdedigen op donderdag 22 oktober 2015 om 15:00 uur

door

**Ilhan Şen**

Master of Science in Aerospace Engineering

geboren te 's-Gravenhage, Nederland.

Dit proefschrift is goedgekeurd door de promotor:

Prof. dr. ir. R. Benedictus

Copromotor: Dr. ir. R. C. Alderliesten

Samenstelling promotiecommissie:

| | |
|---|---|
| Rector Magnificus | voorzitter |
| Prof. dr. ir. R. Benedictus | Technische Universiteit Delft, promotor |
| Dr. ir. R. C. Alderliesten | Technische Universiteit Delft, copromotor |
| | |
| Onafhankelijke leden: | |
| Prof. dr. ir. R. Marissen | Technische Universiteit Delft |
| Prof. ir. F. S. K. Bijlaard | Technische Universiteit Delft |
| Prof. dr. ir. A. de Boer | Universiteit Twente |
| Prof. P. M. Weaver | University of Bristol |
| Dr. J.-C. Ehrström | Constellium |

This work was funded by the Constellium Technology Center (C-TEC) in Voreppe, France.

*Keywords:* Fibre Metal Laminates, Lay-up Optimisation, Fatigue & Damage Tolerance, Wing Design

*Published by:* Uitgeverij BOXPress || Proefschriftmaken.nl



ISBN 978-94-6186-492-5

An electronic version of this dissertation is available at
http://repository.tudelft.nl/.

*There's a fine line between genius and insanity.*
*I have erased this line.*

Oscar Levant

# Preface

This thesis is the output of a special period in my life which I experienced as being fun, full of happiness, relaxing, but also once in a while stressful. It was a period of hard work where I learned a lot. I hope this thesis will have a valuable contribution to science and it will pioneer the research topics related to the design and optimisation of fibre metal laminates.

I would like to express my appreciation and admiration to René Alderliesten. I have learned a lot from him and consider myself very fortunate to have him as a supervisor. He was very supportive and he is really dedicated to his work and research. I would like to express the same appreciation and admiration to Rinze Benedictus for giving me the opportunity for performing my research in his research group. Furthermore, I would like to thank all other colleagues from the Structural Integrity & Composites group. I had a great time the last four years. Thanks a lot!

I would also like to thank Constellium for funding my research. I hope the design tool that I have prepared for them will be of great value, and may boost their research on hybrid aluminium solutions for aerospace applications. Hereby, I would like to give special thanks to Frédéric Bron and Guillaume Delgrange for being valuable to me with their supportive advises.

Finally, to conclude, I would like to thank my family and beloved ones for supporting me during this knowledge and wisdom acquisition period.

Anyhow, I would like to wish you a lot of reading pleasure…

*Ilhan Şen*
*Delft, October 2015*

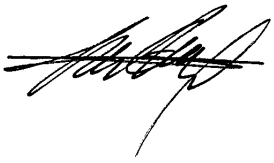

# Contents

# List of Figures

# List of Tables

# Acronyms

**A/C** Aircraft

**AF** Approximate Function

**ARALL** Aramid Reinforced Aluminium Laminate

**CARALL** Carbon Fibre Reinforced Aluminium Laminate

**CCT** Centre Cracked Tensile

**CFRP** Carbon Fibre-Reinforced Polymer

**CLT** Classical Laminate Theory

**CTE** Coefficient of Thermal Expansion

**CTOA** Crack Tip Opening Angle

**CTOD** Crack Tip Opening Displacement

**FCI** Fatigue Crack Initiation

**FCP** Fatigue Crack Propagation

**F&DT** Fatigue and Damage Tolerance

**FML** Fibre Metal Laminates

**GA** Genetic Algorithms

**GLARE** Glass Laminate Aluminium Reinforced Epoxy

**MVF** Metal Volume Fraction

**PM** Prediction Method

**RS** Residual Strength

**SCF** Stress Concentration Factor

**S-N** Cyclic stress - Cycles to failure

**SS** Static Strength

**TiGr** Titanium Graphite

**TW** Tsai-Wu

# Nomenclature

| Symbol | Units | Description |
|---|---|---|
| $a$ | mm | Half crack length |
| $a_c$ | mm | Half critical crack length |
| $a_e$ | - | Engine weight correction factor |
| $a_i$ | mm | Half initial crack length |
| $A$ | - | Stiffness matrix of laminate |
| $A$ | $mm^2$ | Area |
| $b$ | mm | Half delamination length |
| $b_l$ | m | Stringer spacing lower panel |
| $b_{rib}$ | mm | Rib spacing |
| $b_{str}$ | mm | Stringer spacing |
| $b_u$ | m | Stringer spacing upper panel |
| $b_w$ | m | Wing box width |
| $c$ | mm | Wing chord length |
| $C_{cg}$ | - | Paris crack growth coefficient |
| $C_d$ | - | Paris delamination coefficient |
| $C_{1,2,3,4}$ | - | Constants for S-N curve |
| $E$ | MPa | Young's (elastic) modulus |
| $f$ | Hz | Frequency |
| $f$ | - | Load factor |
| $G$ | MPa | Shear modulus |
| $h$ | - | Grade (vector/variable) |
| $h$ | mm | Height |
| $I_{xx}$ | $mm^4$ | Moment of inertia around the x-axis |
| $I_{xz}$ | $mm^4$ | Products of inertia around the xz-axis |
| $I_{zz}$ | $mm^4$ | Moment of inertia around the z-axis |
| $K_{br}$ | - | Bridging stress intensity factor |
| $k_c$ | | Buckling coefficient |
| $K_{ff}$ | - | Far-field stress intensity factor |
| $K_{ic}$ | - | Fracture toughness property |
| $K_{st}$ | - | Straps stress intensity factor |
| $K_{stiffened}$ | - | Stress intensity factor of stiffened panel |
| $K_t$ | - | Stress concentration factor |

| | | |
|---|---|---|
| $K_{tip}$ | - | Stress intensity factor in metal layer |
| $K_{unstiffened}$ | - | Stress intensity factor of unstiffened panel |
| $l$ | mm | Length |
| $L$ | mm | Specimen length |
| $L$ | N | Lift |
| $L_{seg}$ | mm | Segment length |
| $\overline{L}$ | | Design vector (phenotype) |
| $m$ | - | Thickness of metal layer (vector/variable) |
| $M$ | Nm | Bending moment |
| MVF | - | Metal volume faction |
| $MS$ | - | Margin of safety |
| $n$ | - | Load factor |
| $n$ | - | Number of metal layer (vector/variable) |
| $n$ | - | Number of layers |
| $n_{cg}$ | - | Paris crack growth exponent |
| $n_d$ | - | Paris delamination exponent |
| $N$ | cycles | Number of cycles |
| $N$ | N | External loading vector |
| $p_{\max}$ | - | Maximum fraction of thickness step |
| $p_{\text{lam}}$ | - | Actual laminate fraction of thickness step |
| $p_w$ | m | Start position of wing box |
| $P$ | - | Undefined property of the fibre layers |
| $P$ | N | Initial applied load |
| $P$ | N/mm | Running load |
| $Q$ | - | Stiffness matrix of a layer |
| $R$ | - | Stress ratio |
| $R^2$ | - | Coefficient of determination |
| $RF$ | - | Reserve factor |
| $S$ | MPa | Stress |
| $S_a$ | MPa | Stress amplitude |
| $T$ | ° | Cure temperature |
| $t$ | m | Wing thickness |
| $t$ | mm | Thickness |
| $t_b$ | mm | Required thickness for Euler buckling |
| $t_{ft}$ | mm | Required thickness for fracture toughness |
| $t_{lc}$ | mm | Required thickness for local buckling |
| $\Delta t$ | mm | Thickness step |
| $V$ | N | Shear force |
| $w_e$ | mm | Element width |
| $W$ | mm | Specimen width |

| | | |
|---|---|---|
| $W$ | kg | Aircraft weight |
| $W$ | kg | Weight of a cross-section segment |
| $W_{\text{lam}}$ | kg/m² | Weight per unit of an element |
| $W_{\text{cross}}$ | kg/m | Weight per unit of span length for a cross-section |
| $W_e$ | kg | Engine weight |
| $W_f$ | kg | Fuel weight |
| $W_w$ | kg | Wing weight |
| $x$ | - | Design solution |
| $x$ | m | Position on the wing chord / local x-coordinates |
| $\overline{x}$ | - | Design vector (genotype) |
| $x_0$ | - | Initial input solution |
| $x_h$ | - | Variable representing the grade |
| $x_m$ | - | Variable representing the thickness of metal layers |
| $x_n$ | - | Variable representing the number of metal layers |
| $X$ | m | X-coordinate |
| $y$ | m | Half thickness on wing air foil / local y-coordinates |
| $Y$ | m | Y-coordinate / location on the wing |
| $Z$ | m | Z-coordinate |
| | | |
| $\alpha$ | 1/° | Coefficient of thermal expansion |
| $\beta$ | - | Geometry correction factor |
| $\gamma$ | - | Shear strain |
| $\Gamma$ | ° | Wing dihedral |
| $\epsilon$ | - | Strain |
| $\eta$ | - | Stiffening ratio |
| $\eta_b$ | - | Wing box width as fraction of chord |
| $\eta_p$ | - | Start position of wing box as fraction of chord |
| $\Lambda$ | ° | Wing sweep angle |
| $\nu$ | - | Poisson's ratio |
| $\rho$ | kg/m³ | Density |
| $\sigma$ | MPa | Stress |
| $\sigma_b$ | MPa | Bearing stress |
| $\sigma_b$ | MPa | Buckling stress |
| $\sigma_{cr}$ | MPa | Local buckling stress |
| $\sigma_y$ | MPa | Bending stress |
| $\tau$ | MPa | Shear stress |

| **Subscript** | **Description** |
|---|---|
| al | Aluminium |
| bottom | Bottom cover |

| | |
|---|---|
| c | Compression load |
| cap | Wing cap |
| cr | Critical |
| e | Engine |
| e | Equivalent |
| f | Fibre layer |
| f | Fuel |
| fci | Fatigue crack initiation |
| fcp | Fatigue crack propagation |
| fml | Fibre metal laminate |
| front | Front spar |
| i | Element number |
| $k_1$ | Kink number 1 |
| $k_2$ | Kink number 2 |
| lam | Laminate |
| m | Metal layer |
| m | Mean |
| metal | Metal |
| mid | Midpoint between top and bottom panel |
| nom | Nominal |
| net | Net section |
| nl | Neutral line |
| peak | Peak value |
| ply | Fibre ply |
| r | Root |
| rear | Rear spar |
| req | Requirement |
| rs | Residual strength |
| s | Shear load |
| spar | Wing spar |
| sk | Skin |
| st | Stringer |
| S-N | Stress-Cycles |
| t | Tension load |
| t | Tip |
| top | Top cover |
| x | x-direction |
| xy | xy-direction |
| xz | xz-direction |
| y | y-direction |

| | |
|---|---|
| y / yld | Yielding |
| yz | yz-direction |
| u / ult | Ultimate |
| | |
| 0 | Initial |
| 1 | 1-direction, longitudinal direction |
| 12 | 12 - direction |
| 2 | 2-direction, lateral direction |
| 21 | 21 - direction |

# 1

# Introduction

## 1.1. Motivation

There has always been the goal of improving the performance of a structure by means of innovative solutions and optimising the material for their specific application. Ideally, for aircraft, this improved performance is to be achieved while decreasing the structural weight. Aluminium was for centuries the main material for the stressed skin construction in aircraft structures. Nowadays, however, the step is made to other solutions to further improve the performance of aircraft structures. Materials such as carbon and glass fibre composites and bonded hybrid metal-composite solutions, like Fibre Metal Laminates (FML), were developed for this purpose. The successful exploitation of GLARE FML in the Airbus A380 fuselage and carbon fibre reinforced plastic (CFRP) in the Boeing 787 and Airbus A350 fuselage showed the great potential of applying these materials in aircraft structures.

The lower wing skin is one of the primary structures of an aircraft. Its design is governed by several criteria that assure a safe transportation. Currently, a limiting factor for this part is the fatigue and damage tolerance (F&DT). Unfortunately, despite the progress of developing low density alloys such as aluminium-copper-lithium, it is hard to further improve the F&DT performance, because only small improvements are achieved with large investments in the design. Therefore, wing solutions based on new materials are required to further improve the F&DT performance to obtain a more efficient structure. Improving the fatigue and damage tolerance of the lower wing skin by means of FML or CFRP would result in a significant weight and maintenance cost reduction compared to aluminium due to the improved fatigue and damage tolerance properties of these materials.

From the weight perspective without looking at cost or manufacturing, there are basically

two lower wing skin solutions possible. The first option is to use CFRP for the lower wing, but this requires the upper wing to be CFRP to prevent high differences in structural stiffness and thermal expansion between the upper and lower wing. Unfortunately, this way the weight saving obtained by the improved F&DT lower wing is expected to be nullified by the worse buckling behaviour of CFPR compared to aluminium which will lead to a heavier upper wing. The second option is to design a lower wing consisting of FML. In this case, the upper wing will remain aluminium due to the similar structural stiffness and thermal expansion. This means the lower wing will have an improved F&DT performance, while the upper wing keeps its good buckling performance. Theoretically, the latter wing solution would give significant weight saving compared to a complete aluminium wing structure, as proven earlier with the design of a lower wing skin with ARALL for the Fokker F-27 [1].

Plenty of studies were performed to characterize and understand the behaviour of FML, especially the F&DT properties, because that is the area where the performance gain is expected. In the literature, many studies have been presented to describe the properties, like fatigue crack initiation [2–4], fatigue crack propagation [5–9], blunt-notch strength [10], bearing strength [11], residual strength [12, 13] and impact damage [14]. As a result, prediction methods were developed to predict the corresponding behaviour for FML. The focus was predominantly to characterise and understand FML, because many aspects of FML are still unknown. This focus explains why the literature lacked design methods for FML structures, because first more understanding about the material is needed before proceeding to the design for application. Furthermore, the earlier developed prediction methods had an empirical character based solely on observations rather than theory and were only used to predict the properties of small number of lay-ups (single material models). Later, the focus shifted to create generic prediction methods based on theory and physical mechanism that can predict the properties of a large number of lay-ups.

FML has an increased design freedom compared to aluminium, because the lay-ups can be specifically designed to the requirements by simply changing the number, thickness or orientation of the fibre and metal layers. The properties of FML depend on the lay-up, and therefore, the prediction methods for the properties listed above are useful to determine the corresponding property to check whether the selected lay-ups satisfy the design requirements related to this property. In the past, FML were only designed and certified based largely on single material models, and therefore, all other potential solutions were not considered in the design process. In this so-called solution-based analysis, the prediction methods were used to determine the properties, while the lay-up solutions were manually evaluated and selected based on their performance. This strong focus on single material models restricted the actual search for a more advanced and better solution in the design space. The recently developed prediction methods tend to get a more generic character, and therefore, these prediction methods can be used for the development of a generic design method for FML.

In the literature, steps were set towards a design method for FML. For example, Cooper [15] proposed a design approach for FML in which a FML sizing module based on the ultimate tensile strength failure criteria is integrated together with a manufacturability module into a wing design framework. This approach has the potential to be extended to incorporate the F&DT criteria and forms the basis of FML optimisation. Currently, the optimisation is limited to the required minimum number of metal layers in FML for a user-specified grade and material thickness, instead of giving the possibility to explore a large design space for other potential solutions. The need is for a design procedure in which all possible lay-ups are obtained based on the design requirements and ranked according to their performance and weight. This way a fast overview of potential solutions are obtained which could be used to correlate the design requirement to the lay-ups parameters and to identify different lay-ups that might have better performance or weight ratio.

## **1.2.** Research scope

The goal of this study is to develop a design optimisation methodology for FML that satisfies F&DT criteria. The methodology should enable exploration of the design space of FML by finding lay-up solutions for flat plates. The optimisation methodology should also reveal the contribution of individual criteria to the obtained solutions. Furthermore, it is aimed to design a lower wing skin consisting of FML where the F&DT and additional design criteria are met. To achieve these goals, both engineering and scientific objectives must be met, which are stated below.

### **1.2.1.** Engineering objective

The engineering objective of this study is to develop a design tool that is capable of dimensioning an aircraft wing structure build using FML with F&DT design criteria. This objective is met using the following sub-objectives:

- *Develop a parametric model for an aircraft wing to determine the running loads for various load cases.*
- *Extend the model to evaluate and optimise aluminium configurations on the basis of specific design criteria.*
- *Develop an optimisation routine for FML based on F&DT criteria and its prediction methods.*
- *Develop approximate functions for the prediction methods to simplify the evaluation of lay-ups.*
- *Improve the optimisation routine by replacing the prediction methods with its approximates.*

- *Combine the aluminium and FML optimisation to perform a cross-section optimisation.*
- *Extend the model by adding the cross-section optimisation to the aircraft wing model to obtain the required lay-ups and thickness with minimised weight for the wing.*

### **1.2.2.** Scientific objective

To describe the scientific objective, the prediction method for a property $Y$ is assumed to be represented by the following function:

$$Y = a_1 X_1 + a_2 X_2 + \dots + a_n X_n \tag{1.1}$$

In which $X_1, \dots, X_n$ represent parameters to define the FML lay-up and $a_1, \dots, a_n$ are the coefficients of the function depending on other aspects, such as material type and model settings.

The property $Y$ is related to different lay-up parameters of FML and the prediction methods developed for FML strictly predict the property for a given lay-up, and therefore, it works only in one direction.

To obtain the lay-up for a given value of $Y$, the function should be reversed and would be formulated as:

$$\begin{bmatrix} X_1 \\ X_2 \\ \vdots \\ X_n \end{bmatrix} = f(Y) \tag{1.2}$$

Basically, the lay-up parameters would become a function of the property. However, the situation for a prediction method is complexer and for two reasons it is not possible to revert mathematically the analysis process and to obtain lay-ups as output for given design criteria as input. Firstly, the methods are not invertible due to the structure (e.g. the iterative process wherein the growth is calculated incrementally) of the prediction methods.

Secondly, FML are characterized by a number of parameters which is usually smaller than the number of design variables, thus different sets of design variables can produce similar results [16]. In other words, various lay-ups have similar material behaviour. As a result, a reversed mathematical function cannot result in a unique answer. The challenge is to understand how these methods could be reversed and then find the reversed approach so that the lay-ups are obtained as design solutions for given design requirements. The scientific contribution is delivered in finding and describing a method to reverse the prediction method to obtain the lay-ups for a given property.

Due to the not uniqueness of the solution for a given property, a range of lay-ups are obtained that fulfil the property requirement. Hereby, a design space for the property $Y$ is created. Combining with other criteria, such as $W$ and $Z$, more design spaces are created for each individual property. From scientific perspective, it is key to understand how the different design spaces relate to each. If there is overlap between the spaces, this area will contain the solutions that satisfy multiple design criteria. For this reason, an approach is required to identify the overlapping regions and to select the optimal design solution using an objective, such as minimum weight.

## 1.3. Methodology

The methodology for both the engineering and scientific objectives is presented below.

### 1.3.1. Methodology to engineering objective

The engineering objectives of the project are achieved by step-wise implementing the tool and extending it to a complete design method for an aircraft wing structures where the lower wing skin is consisting of FML. Therefore, the research was divided into different phases:

*Development of optimisation routine for aluminium at wing level*
: The study started with the development of a wing box design tool for aluminium. The design and failure criteria for aluminium and different load cases for aircraft were investigated and together with the geometry and load calculations implemented in the tool. The aim was to use this tool as structure for the FML variant of the design tool.

*Research on prediction methods for FML and their implementation as design criteria*
: The research was extended from aluminium to FML and the important material properties and prediction methods were investigated. The various F&DT criteria were evaluated and the available methods were implemented so that the properties of a given lay-up could be predicted. Additionally, research was performed on manufacturing aspects and design considerations to understand the important aspects of designing FML for aircraft structures.

*Development of optimisation routine for FML at element level*
: The lay-up optimisation procedure is developed in which the different F&DT design criteria are used to find the optimal lay-ups for flat-plate panels. Research was performed on optimisation algorithms and the implementation of the prediction methods into the procedure was done. The design criteria were step-wise implemented in the optimisation routine and issues with respect to accuracies of the solutions were investigated.

*Development of approximations for the prediction methods*

Due to the structure of the prediction methods, the optimisation procedure became time consuming. Therefore, research was performed on finding relationships between the lay-ups and their properties to create an approximate function which could replace the prediction methods in the optimisation procedure with goal to speed up the design procedure.

*Development of optimisation routine for FML at wing level*

Finally, the tool is extended by combining the lay-up optimisation procedure for element and the aluminium wing design tool while switching to cross-section optimisation, so that additional constraints were implemented to assure compatibility between wing segments. The optimal solution for a FML lower wing skin and aluminium upper wing skin were obtained and different wing solutions were investigated and compared with respect to their weight.

### **1.3.2.** Methodology to scientific objective

The scientific objective of the project is achieved by identifying the possibilities to reverse the methodology. The standard approach to reverse a model is basically reversing and rewriting the equations, such that desired input parameter is given as output. In complex models with unique solutions, the desired input parameter could similarly be obtained using a solver function.

The prediction methods for FML in their current state cannot be incorporated into an design optimisation tool. The methods only predict properties for a given lay-up and loading. Multiple lay-ups have (approximately) the same properties, meaning that the solution is not unique. As a consequence, forming the reversed relation is not possible. Hence, an alternative approach is needed to create a reversible relationship between lay-up parameters and properties. The new relationship should represent the original method and maintain the underlying physics, while fulfilling the design tool requirements. The desired relationship can be derived in essentially four ways:

1. *Iterative (brute force)*

Repeating the original methodology and filling a database. The required lay-up is obtained using a 'look-up' function in this database. This option is eliminated, because a function is preferred rather than a database.

2. *Black box using machine learning algorithms (i.e. neural networks)*

Trying to find a correlation between the input and output variables. This also requires a database in which the output is listed for varying input parameters. This database is used

to create a black box or neural network, without knowledge on the physics and interactions of variables.

3. *Approximate function*

An alternative technique to the black box approach is to search manually for trends between the variables and try to understand the relation. This relationship is then addressed as a function which represents the original model.

4. *Problem limitation*

In this approach, the methodology is broken into parts and the non-reversible parts are isolated for which then approximate functions are obtained. The remainder of the method is reversed using the standard approach (mathematical reversing). The functions for the isolated parts, which will have a unique solution, could be obtained by making assumptions and fixing variables. This approach maintains the physics explicit in the analytical equations, but the resulting design space is limited to given material selection and other defined parameters.

With the use of these four methods, the prediction methods could be reversed. However, multiple solutions will have the same output, and therefore, it is necessary to select the solutions based on an objective, such as weight, cost or manufacturability. For this reason, an optimisation algorithm is needed to identify the solutions that satisfies the requirement and compares the solutions for the weight objective. This approach would also include solutions with better performance and lower weight instead of solutions that exactly fulfil the requirement.

## **1.4.** Thesis overview

This thesis describes the development of the design optimisation procedure for FML in the following chapters:

**Chapter 2 — Fibre metal laminates** gives an overview of the prominent properties and prediction methods of FML. The prediction methods are investigated and properties are selected to be applied as F&DT design criteria for FML. Furthermore, additional design considerations that play a role when applying FML to a structure are discussed.

**Chapter 3 — State-of-the-art in design optimisation** lists the current optimisation procedures for structural design of composites and FML.

**Chapter 4 — Design methodology** discusses the design optimisation method for the aircraft wing by presenting the procedure, the load cases, the optimisation algorithm, the evaluation criteria and the procedure of the model.

**Chapter 5 — Constraint approximation** presents the study to replace the prediction methods by an approximation function to improve the computation time of the optimisation procedure.

**Chapter 6 — Lay-up optimisation** presents the method for the lay-up optimisation at element level. The optimal lay-ups are obtained for different F&DT design criteria and a brief discussion is given about various aspects that influence the design solutions.

**Chapter 7 — Application to aircraft wings** presents the extension of the lay-up optimisation procedure to wing level by performing a cross-section optimisation. A design case is presented in which different cross-section solutions are optimised and compared with each other based on the minimised weight objective. At last, the wing optimisation method is discussed by identifying its limitations.

**Chapter 8 — Conclusions and recommendations** restates the objectives of this thesis and discusses the results of the research. The important conclusions from the entire work will be briefly noted in a concise summary and recommendations for further study are also discussed.

## References


[1] J. W. Gunnink and P. A. van der Schee, *Design of the arall f-27 lower wing fatigue panel,* Composite Structures **4**, 162 (1987).

[2] J. Homan, *Fatigue initiation in fibre metal laminates,* International Journal of Fatigue **28**, 366 (2006).

[3] P.-Y. Chang, P.-C. Yeh, and J.-M. Yang, *Fatigue crack initiation in hybrid boron/glass/aluminum fiber metal laminates,* Material Science and Engineering A **496**, 273 (2008).

[4] S. Spronk, I. Şen, and R. Alderliesten, *Predicting fatigue crack initiation in fibre metal laminates based on metal fatigue test data,* International Journal of Fatigue **70**, 428 (2015).

[5] R. Marissen, *Fatigue crack growth in ARALL*, Ph.D. thesis, Delft University of Technology (1988).

[6] Y. Guo and X. Wu, *A phenomenological model for predicting crack growth in fibre-reinforced metal laminates under constant-amplitude loading,* Composite Science and Technology **59**, 1825 (1999).

[7] R. Alderliesten, *Analytical prediction model for fatigue crack propagation and delamination growth in glare,* International Journal of Fatigue **29**, 628 (2007).

[8] S. Khan, *Fatigue Crack & Delamination Growth in Fibre Metal Laminates under Variable Amplitude Loading*, Ph.D. thesis, Delft University of Technology (2013).

[9] G. Wilson, *Fatigue Crack Growth Prediction for generalized fiber metal laminates and hybrid materials*, Ph.D. thesis, Delft University of Technology, Delft (2013).

[10] O. Bosker, *Blunt notch strength,* in *Fiber Metal Laminates an Introduction*, edited by A. Vlot and J. Gunnink (Kluwer Academic Publishers, 2001).

[11] R. Rooijen, van, *Bearing strength characteristics of standard and steel reinforced glare*, Ph.D. thesis, Delft University of Technology (2006).

[12] T. Vries, de, *Residual strength,* in *Fiber Metal Laminates an Introduction*, edited by A. Vlot and J. Gunnink (Kluwer Academic Publishers, 2001).

[13] R. Rodi, *Residual strength in Fibre Metal Laminates*, Ph.D. thesis, Delft University of Technology, Delft (2012).

[14] F. Moriniére, *Low-Velocity Impact on Fibre-Metal Laminates*, Ph.D. thesis, Delft University of Technology (2014).

[15] C. Cooper, *Development of a Methodology to Support Design of Complex Aircraft Wings*, Ph.D. thesis, Delft University of Technology, Delft (2011).

[16] R. LeRiche and R. Hafka, *Improved genetic algorithms for minimum thickness composite laminate design,* Composites Engineering **5**, 143 (1995).

# 2

# Fibre metal laminates

*The aim of optimising FML lay-ups for fatigue and damage tolerance properties with final application in wing structures was stated in the previous chapter. To familiarise with the material, in this chapter, the concept of FML is introduced together with the different variants. Furthermore, a part of the knowledge about FML is discussed by describing the important static, fatigue and damage tolerance properties. Wherein, the important prediction methods for the prediction of the F&DT properties are identified and summarised. Finally, an overview is given about the design considerations for FML regarding the application in an airframe structure. A part of these methods are selected to be included in the design optimisation procedure.*

## 2.1. Concept

FML represent a hybrid material concept that combines thin sheets of metal with in-between fibre/epoxy layers to improve the fatigue and damage tolerance behaviour over that of monolithic metal. The alternating thin metal sheets and prepreg layers (fibres embedded in adhesive) are bonded together to one laminate [1]. A typical layout of FML is given in Fig. 2.1. The fibre orientation and the stacking sequence can be selected depending on the application. Examples of the FML concept are ARALL, GLARE, CARALL and TiGr. The common used metals are aluminium, magnesium, steel or titanium and the fibres are aramid, glass, carbon, PE or M5. The combination of the metal and fibres provide benefits over conventional monolithic materials for a wide range of applications, mainly in the aerospace industry.

The characteristics of FML are obtained by combining the advantages and disadvantages of the individual constituents. The properties of FML strongly depend on different components

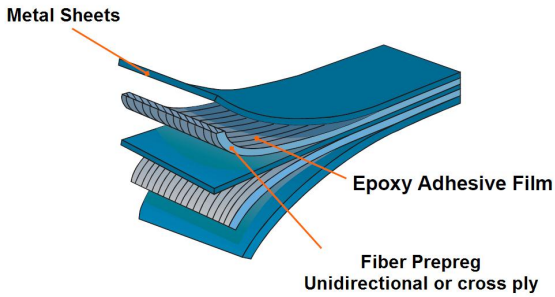


Figure 2.1: Typical lay-out of FML [1].

(type or resin, type of fibre, type of metal) and their proportions (volume fraction and thickness). The number and type of potential fibres used in FML is based on strength, density, ultimate strain, bonding and corrosion properties [2]. The choice of sheet material is mainly based on available thickness and properties of the bare material. The adhesive should have good shear and toughness properties but also provide good bonding between the metal and fibres, and it should be moisture resistant [2].

### 2.1.1. Grades

A simple coding system was developed to identify and distinguish the different configurations of FML. GLARE and ARALL are standardised in this way. The so-called different grades are used in the design, production and certification process [3]. The thickness of the aluminium, the orientation and the number of fibre plies in-between the aluminium sheets determine the grade. GLARE has 6 grades and ARALL has 4 grades, which are listed with their main beneficial characteristics in Table 2.1. The laminates have a symmetrical lay-up to avoid secondary bending effects due to unsymmetrical internal stresses. An example of this coding system is:

GLARE 2B-5/4-0.5

Defined as:

- GLARE 2B: The grade with fibre orientations according to the GLARE 2B definition as listed in Table 2.1.
- 5/4: The number of layers: 5 metal layers and 4 fibre layers
- 0.5: The metal layer thickness: 0.5 mm.

This coding system will be used to identify the design options in the optimisation procedure, but without any restrictions on the sheet thickness or layer number. More detail on the lay-up definition will be given in section 4.4.2.

| FML grade | Metal layers Aluminium alloy | Thickness[a] (mm) | Fibre layers Orientation[b,c] (°) | Thickness[a] (mm) | Characteristics |
|---|---|---|---|---|---|
| *GLARE* | | | | | |
| GLARE 1 | 7475-T761 | 0.3 – 0.4 | 0/0 | 0.25 | Fatigue, strength, yield stress |
| GLARE 2A | 2024-T3 | 0.2 – 0.5 | 0/0 | 0.25 | Fatigue, strength |
| GLARE 2B | 2024-T3 | 0.2 – 0.5 | 90/90 | 0.25 | Fatigue, strength |
| GLARE 3 | 2024-T3 | 0.2 – 0.5 | 0/90 | 0.25 | Fatigue, strength, impact |
| GLARE 4A | 2024-T3 | 0.2 – 0.5 | 0/90/0 | 0.375 | Fatigue, strength in 0° |
| GLARE 4B | 2024-T3 | 0.2 – 0.5 | 90/0/90 | 0.375 | Fatigue, strength in 90° |
| GLARE 5 | 2024-T3 | 0.2 – 0.5 | 0/90/90/0 | 0.5 | Impact |
| GLARE 6A | 2024-T3 | 0.2 – 0.5 | +45/ – 45 | 0.25 | Shear, off-axis properties |
| GLARE 6B | 2024-T3 | 0.2 – 0.5 | −45/ + 45 | 0.25 | Shear, off-axis properties |
| GLARE HS | 7475-T761 | 0.3 – 0.4 | *d* | *d* | |
| *ARALL* | | | | | |
| ARALL 1 | 7075-T6 | 0.3 | 0/0 | 0.22 | Fatigue, strength |
| ARALL 2 | 2024-T3 | 0.3 | 0/0 | 0.22 | Fatigue, damage tolerant |
| ARALL 3 | 7475-T761 | 0.3 | 0/0 | 0.22 | Fatigue, toughness |
| ARALL 4 | 2024-T8 | 0.3 | 0/0 | 0.22 | Fatigue, elevated temperature properties |

Table 2.1: Commercially available standardised GLARE and ARALL grades [4, 5].

[a] The thickness corresponds to thickness of single fibre layer or aluminium sheet

[b] All aluminium rolling directions in standard laminates are in the same orientation; the rolling direction is defined as 0°, the transverse rolling direction is defined as 90°

[c] The number of orientations in this column is equal to the number of fibre plies (prepregs) in each fibre layer

[d] High strength (HS) GLARE has any of the fibre layups as in GLARE 2 to GLARE 5.

### **2.1.2.** Material definition

In this study, the design options for FML comprise design solutions analogous to GLARE grades. For this reason, the material properties of GLARE constituents are used to define the laminates. The mechanical and physical properties of GLARE constituents are given in Table 2.2. GLARE (except GLARE 1 and HS) is based on aluminium 2024-T3 and unidirectional S2-glass fibres embedded with FM94 adhesive. This prepreg has a nominal fibre volume fraction (FVF) of 59% and a nominal post-cure thickness of 0.133 mm [5]. The laminate is cured in an autoclave with maximum pressure between 6 to 11 bar and a curing temperature of 120° [6].

The design method aims to be generic, and therefore, other metal and fibre properties are possible to be defined as constituent material for the lay-ups with the requirement that prediction methods are able to evaluate to design criteria. This topic will be discussed later in detail.

### **2.1.3.** Thermal stress

Variations in temperature cause thermal stresses in a laminate when layers have a different coefficient of thermal expansion (CTE) in the same global direction. A thermal stress field exists when the laminate is held at a temperature different from the curing temperature.

| Material properties | | Aluminium 2024-T3 | S2-glass/FM94 epoxy |
|---|---|---|---|
| Tensile modulus (MPa) | $E_1$ | 72,400 | 48,900 |
| | $E_2$ | 72,400 | 5,500 |
| Shear modulus (MPa) | $G_{12}$ | 26,900 | 5,550 |
| Poisson's ratio (-) | $\nu_{12}$ | 0.33 | 0.33 |
| | $\nu_{21}$ | 0,33 | 0,0371 |
| Coefficient of | $\alpha_1$ | $22 \cdot 10^{-6}$ | $6.1 \cdot 10^{-6}$ |
| thermal expansion (1/°) | $\alpha_2$ | $22 \cdot 10^{-6}$ | $26.2 \cdot 10^{-6}$ |
| Cure temperature (°) | $T$ | - | 125 |
| Thickness fibre ply (mm) | $t_{ply}$ | - | 0.133 |
| Density (kg/m$^3$) | $\rho$ | 2780 | 1980 |

Table 2.2: Mechanical and physical properties of GLARE constituents [7].

It could thus also be named curing stress or residual stress. The metal layers have residual tensile stresses and the fibre layers have residual compression stresses [8]. For several GLARE laminates, the residual stresses at different loading angles are listed in Table 2.3. The thermal stresses have a contribution to the internal stresses in a laminate, and therefore, influence positively the fatigue properties of FML by causing a higher fatigue life. This contribution is calculated using the classical laminate theory (CLT), which will be discussed in section 2.3.5.

| Lay-up | Residual stress (MPa) | | |
|---|---|---|---|
| | 0° | 22.5° | 45° |
| GLARE 2A-3/2-0.3 | 27.9 | 19.2 | 9.1 |
| GLARE 3-3/2-0.5 | 17.6 | 18.0 | 17.1 |
| GLARE 4B-3/2-0.3 | 24.5 | 35.3 | 53.6 |

Table 2.3: Residual stresses in aluminium layers of several GLARE types at different loading angles, which are determined with the method described in [9].

## 2.2. FML configurations

The nature of FML gives great freedom in selecting the constituents of the laminate. The desired lay-up can be tailored for a specific application by varying the fibre direction, the number of layer and the thickness of layer. However, this will only change the grade, see for example Table 2.1. A completely new FML is created by changing the aluminium sheet with titanium or the glass fibres with carbon fibres. There are basically two types of FML defined:

1. Standard FML
2. Custom FML

The standard FML is assumed to have thin sheets, consists of the same alloy in all metal layers, has the same thickness in metal layers and is stacked by alternating the fibre and

metal layers with the outer layers to be metal to achieve a symmetric lay-up. On the other hand, a custom FML could have layers with different material or thickness for the metal or fibre layers. It could have an additional adhesive layer or a thick metal layer, or the lay-up could be stacked arbitrary resulting in an asymmetrical lay-up. The definition of standard and custom FML will be used to state the complexity of lay-ups.



### **2.2.1.** Metal and fibre types

Theoretically, any alloy can be used in combination with fibres to create a laminate. Currently, the 2000 and 7000 aluminium series are used as metal layer, because of their good crack propagation resistance or high strength. The metal layers can be easily changed depending on the specific applications or requirements. For example, the aluminium 6000 series are known for their good weldability and compression properties, though it is rarely used in the aerospace industry. The aluminium 5000 series are alloyed with magnesium and have a lower density, but also decreased static properties compared to the 6000 series. Research on FML with 5000 aluminium series has shown that the weight benefit is nullified due to the loss in static properties [10]. Research is also performed on FML with aluminium-lithium (Al-Li), and this FML solution has the potential to achieve weight savings and improved fatigue properties, but for a higher material cost price [11].

Replacing glass fibres with carbon fibres is beneficial due to the higher stiffness of carbon fibres. An example of FML with aluminium and carbon fibre is CARALL. This solution offers a very low crack growth rate and good impact properties and it has the benefit of reducing the stiffness differences in the aircraft structures when it is used in combination with monolithic aluminium [2]. However, a disadvantage is galvanic corrosion, which consequently can be avoided by the pretreatment of aluminium or by isolating the carbon fibres. Replacing aluminium with titanium creates the so-called TiGr solution. This combination with carbon fibres does not lead to galvanic corrosion. An advantage of FML with titanium is their high strength, low density, fatigue and impact properties, but the material cost is very high [12].

### **2.2.2.** Thick configurations

With the intention to develop a design optimisation method for FML and its application for aircraft wing, thicker FML solutions are required. A simple way is to increase the layer number or the layer thickness to reach the desired wing thickness while keeping to the concept of GLARE. The industry made efforts to develop alternative solutions to increase the stiffness and manufacturability of thick lay-ups. Their intention was also to manufacture laminates faster and to reach the required wing thickness easily.

Initially, Gunning [12] introduced a concept to gain a thicker laminate by using a thick alu-

minium plate tapered in the wing tip direction and reinforced with FML at both sides. This concept is shown in Fig. 2.2.

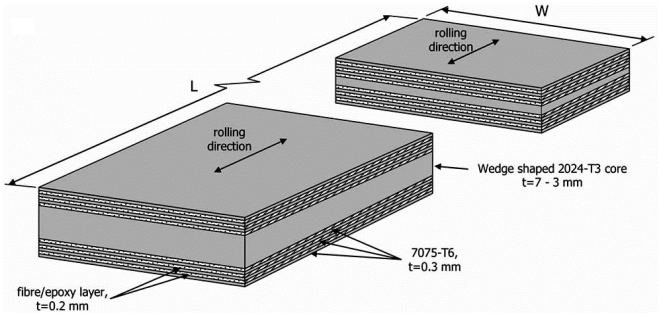


Figure 2.2: Concept of thick aluminium plate reinforced with FML [12].

Later, Gunnink and Roebroeks [12, 13] developed a new concept where the FML is reinforced by aluminium on both sides. However, the fatigue cracks initiating in the outer aluminium sheets propagated directly into the first sheets of the FML. This problem was solved by placing fibres in the adhesive between the FML and the outer aluminium sheets. The first concepts used the stiffer Zylon fibres for this purpose, as shown in Fig. 2.3. The problem in the latter design was that large delaminations were formed as soon as the outer sheets started to show fatigue cracking. For this reason, a special low fibre volume adhesive called BondPreg has been developed to prevent the high delamination rates.

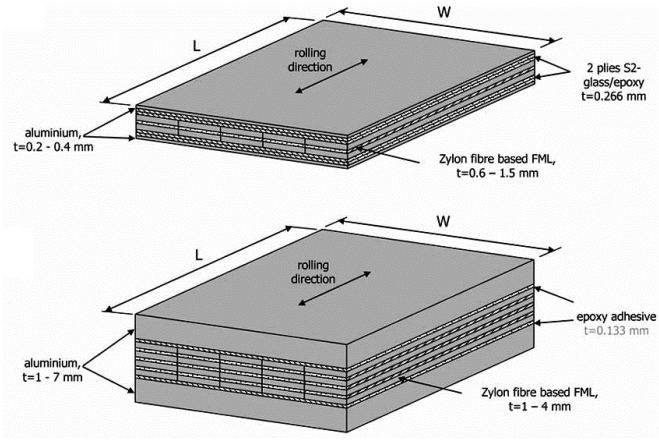


Figure 2.3: Concept of FML reinforced with aluminium on both sides [12].

CentrAl is created by the application of BondPreg between the FML and the thicker aluminium sheets, see Fig. 2.4 for this concept. The CentrAl concept is specifically developed for (curved) wing panels. The outer aluminium sheets can be manufactured and formed before

bonding them onto the FML. The FML core, preferably GLARE 1 or 2 can be machined to thinner straps to fit the curvature of the mold. The FML straps can be butt-joined together in an easier concept than the splices used for GLARE, but self-evidently the performance of the joint might differ. The lower wing panel tapering is relatively easy by positioning the ply drop-off on the outside of the laminate (at the inside of the wing-box) or inter-laminar [13].



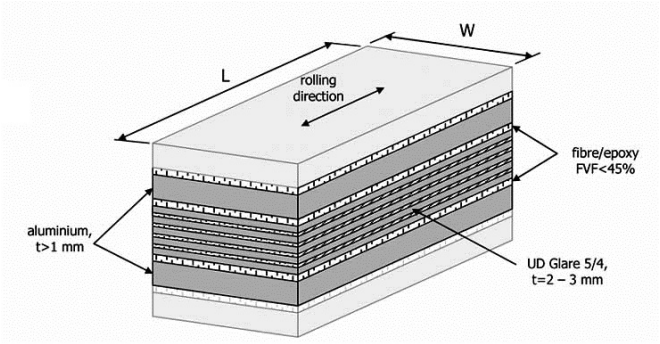


Figure 2.4: CentrAl configuration [12].

Due to the increased thickness of the outer sheets the fatigue crack growth in CentrAl is not as good as GLARE. By decreasing the outer sheet thicknesses of CentrAl the fatigue life could be further increased [13]. Further improvements were achieved by using post-stretching on the FML straps. Other benefits of CentrAl are improved machineability and the thick outer sheets give better support for counter sunk bolts. Furthermore, the application of newer alloy types are easily implemented and can help to improve the overall stiffness of the laminate.

This kind of custom FML, which consider multi-alloy and different metal layer thicknesses, are definable in the design optimisation procedure. Therefore, all kind of different lay-up solutions could be assessed as long as there are prediction methods available to evaluate the laminate properties. More information follows later on this topic.

## 2.3. Static properties

The static properties of a laminate play a dominant role in the design process. A full understanding of the static properties is needed to design a structure for maximum strength and strain. The static strength consists of yielding and ultimate strength for compression, tension and shear, and the blunt notch and bearing strength in case of a notch. This section describes briefly the static properties and aims to compare it with the properties of aluminium. Finally, two methods are described that are used to predict the static properties of FML based on the static properties of the constituent materials, and a failure criterion is given that is commonly used to check the static strength.

### 2.3.1. Static strength and strain

The tensile and compressive properties of FML, such as the elastic modulus, yield strength, ultimate strength and ultimate strain are directly related to those of the single constituents.

The elastic modulus of FML depends on the direction of the fibres. In the fibre direction, the stiffness is mainly related to the fibre stiffness, while the matrix has less influence. Transverse to the fibre direction, both the fibre and matrix stiffness are at comparable importance. In off-axis direction, the shear modulus of the fibre layer is the most important parameter. In conclusion, the metal and fibre stiffness are the most important parameters influencing the stiffness and the matrix is only of minor importance on the stiffness [14].

The yield strength of FML is directly related to the metal yield strength, because that is the only constituent that shows yielding. The yield strength can be increased by either using a different metal alloy or using fibres with a higher stiffness. Furthermore, the residual tensile stress in the metal layer reduces the FML yield strength effectively. Therefore, reducing the curing temperature which consequently reduces the residual stress, might increase the yield strength [14]. The ultimate strength of FML is defined by the strength of the metal and fibre layer. The full strength level of both components is never used due to large differences in failure strain. Therefore, it is necessary to increase the strength of the component with the lowest failure strain [14].

The shear modulus depends on the shear modules of its constituents. Replacing (one of) the constituents for one with a higher shear modulus, the laminate shear modulus could be increased. However, due to the isotropic behaviour of the metal, replacing the metal is the most efficient choice. With respect to the fibres, adding fibres in $\pm 45^{\circ}$ direction also results in improvements [14, 15].

### 2.3.2. Blunt notch strength

The blunt notch strength is defined as the strength of a structure containing a hole and it is valid for open holes as well as for filled holes. Since typically many holes exist in aircraft structures for joining purposes and other cut-outs, the blunt notch behaviour of a material is an important design parameter [15]. Especially, for orthotropic materials, such as FML and CFRP, the blunt notch strength often appears to be very critical due to the limited ductility. In Fig. 2.5, GLARE, ARALL 1 and ARALL 2 are compared with aluminium 2024-T and 7075-T6. Both aluminium alloys are rather sensitive for blunt notches, because large deformations are possible at the root of the notch allowing increased loading until net section yielding occurs [16]. ARALL and GLARE show a severe decrease of the tensile stress for increasing stress concentration factor $(K_t)$, which is mainly related to the fact that the fibres cannot deform plastically. In other words, for FML, a higher notch sensitivity can be observed as a result

of delamination of fibres. [14]. However, the orientation of the fibres does not have large influences on the blunt notch strength [16].

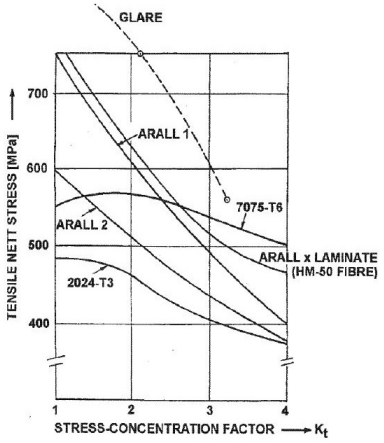


Figure 2.5: Blunt notch behaviour in FML [16].

There is a correlation between the blunt notch strength and the ultimate strength of FML, and therefore, stronger FML have a higher blunt notch strength [14]. For example in Fig. 2.5, ARALL 1 has a higher blunt notch strength than ARALL 2, because of the different aluminium alloy. The difference in the slightly different behaviour is caused by strain hardening, which affects the notch sensitivity. In case of plain aluminium sheets, a material with a low amount of strain hardening results in a lower notch sensitivity [14].

### **2.3.3.** Bearing strength

The bearing strength is a measure for the ability to withstand bearing loads applied within a hole and is thus an important parameter for joint design. Similar to the blunt notch properties, the fibres are very ineffective to cope with bearing due to their relatively low shear properties. For this reason, the bearing strength of FML is generally lower than of monolithic aluminium [14]. The bearing strength of FML is predicted by assuming a simplified bi-linear behaviour analogous to the elastic-plastic metal behaviour, because the bearing response of a fibre is not linear and shows a progressive strength decrease. It is assumed that the strength of the fibre decreases when the metal starts yielding. Figure 2.6 shows an illustration of this bi-linear behaviour.

The bearing properties of FML can be increased with the use of higher strength metals. Additionally, the fibre layer can be improved by considering higher stiffness or off-axis fibres. For practical reasons, thin stainless steel sheets with high bearing strength can be used as local reinforcement. It is also possible to use aluminium as reinforcement layer, but this will

involve higher layer thicknesses.

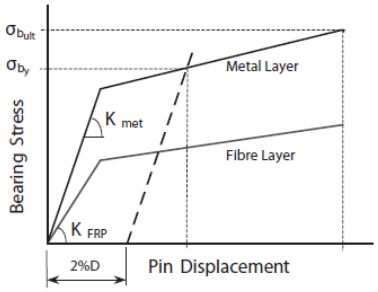


Figure 2.6: Bi-linear behaviour of the bearing strength [14].

### 2.3.4. Summary of static properties

The static properties of several GLARE grades are compared with monolithic aluminium in Fig. 2.7. The ultimate strength and gross blunt notch strength are higher due to higher ultimate strength of the fibre layers compared to aluminium 2024-T3. However, the yield strength and elastic (Young's) modulus are lower due to the lower modulus of the fibres. The shear modulus and bearing strength are lower due to the ineffectiveness of the fibres under those loading conditions. The large difference between yield and ultimate strength illustrates the extensive strain hardening that the material exhibits [15].

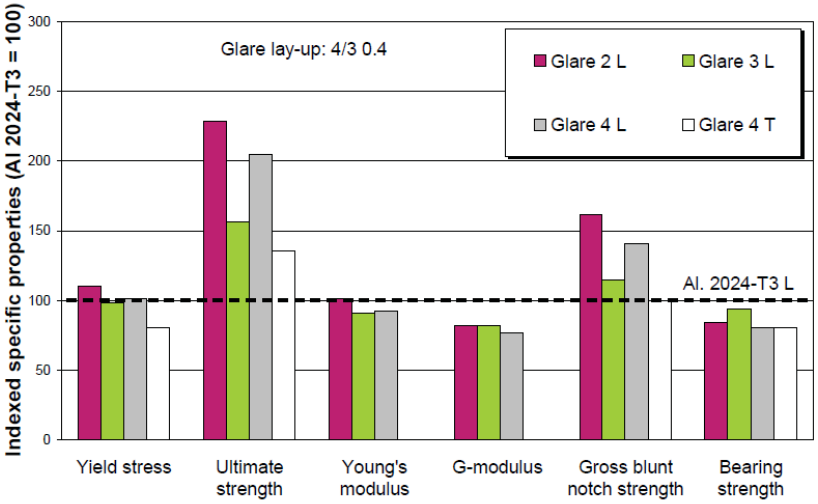


Figure 2.7: Static properties of GLARE compared to aluminium 2024-T3 [15].

### **2.3.5.** Predicting static properties

Two methods are used to determine the static material properties of a laminate: the metal volume fraction (MVF) method and classical laminate theory (CLT) method. The MVF method is able to give quick and reliable property prediction for the laminate based on the properties of the constituents materials and their volume fraction in the laminate. Whereas, the CLT method is a more advanced method that combines the properties of each layer to calculate the layer stresses and the static properties of the laminate.



#### Metal volume fraction

The most common method for predicting strength values (tension, compression, shear, bearing, and blunt notch) is to use the MVF. This approach is also called 'the rule of mixtures' method, which is commonly used for composite analysis [17]. The MVF is defined as the ratio of the sum of the thicknesses of the individual metal layers and the total thickness of the laminate.

$$\text{MVF} = \frac{\sum t_m}{t_{\text{lam}}} \tag{2.1}$$

where, $t_m$ is the metal sheet thickness and $t_{\text{lam}}$ is the total laminate thickness. An MVF of $1$ means monolithic aluminium for which the material properties are known. When the MVF is $0$ the laminate is based purely on the properties of the prepreg (theoretical). This approach assumes a linear relationship between material properties at MVF = $1$, the so-called 'metal layer contribution', and the average of tested laminate data. This line is extrapolated to MVF = $0$, this data point is called 'fibre layer contribution', see Fig. 2.8. This approach results in a formula which can be used to obtain a single laminate property based on the contribution of the metal and prepreg [17].

$$P_{\text{fml}} = \text{MVF} \cdot P_m + (1 - \text{MVF}) \cdot P_f \tag{2.2}$$

where the variables $P$ are the property of interest of the FML, metal or prepreg, and MVF is the ratio of the laminate thickness that is metal, see Eq. (2.1). The MVF method has the ability to predict tensile modulus, yield, and ultimate strengths; compressive modulus and yield strength; shear modulus and yield strength; bearing yield and ultimate strengths; and blunt notch ultimate strength (for a single hole geometry). However, experimental data with constituent material properties is needed to do so. Experimental FML data is also required, because the fibre properties are sometimes unavailable.

The problem is that the method is an empirical relationship that does not rely upon mechanics for prediction of any of the strength parameters. It therefore requires a large number of experiments to determine the correct constituent material properties. Currently, the method is only valid in-between $0.45$ and $0.85$, because outside these ranges the data is not validated.

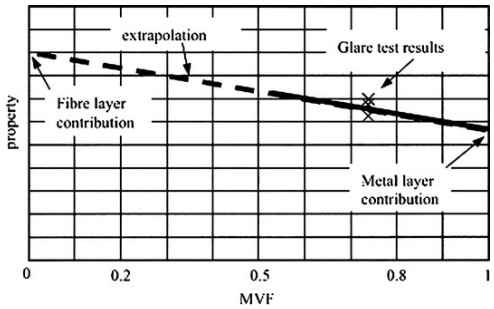


Figure 2.8: Concept of metal volume fraction [17].

Extensive testing took place on GLARE 3 and GLARE 4 during the development phase of GLARE as A380 fuselage material and the currently used GLARE laminates are within this range. Below and above these limits a factor might have to be applied to counteract the difference in prediction result. On average, a excellent correlation between the predicted values with the MVF method and test results were obtained with a maximum a few percent off. It is assumed that by dividing the typical values by factor 1.1, minimum values are obtained and conservatism is introduced [5, 17]. Therefore, the metal volume fraction approach using a rule of mixtures is a reliable method to predict mechanical properties and to calculate each of the stiffness and strength properties of FML [18].

### Classical laminate theory

Classical laminate theory (CLT) is a method of analysing fibre-reinforced materials by systematically developing stiffness relationships for individual lamina and combining these single lamina into a composite plate to determine the stiffness of laminate. The CLT method is a commonly used approach in the literature to determine the layer stresses and strains in composite laminates under given loading conditions [19, 20].

This method is also widely used for FML like in other studies regarding the property prediction of FML, e.g. fatigue crack initiation [7, 9], fatigue crack propagation [21, 22], residual strength [23] and impact damage [24]. The reason to include CLT is that this method allows for a straightforward inclusion of layers with several orientations into the calculation. With the CLT method, the internal stress states due to external loading and the residual stress in FML are calculated and also the tensile and compressive stress-strain curves are predicted.

The CLT is applicable to FML, because the orthotropic laminate definition is applicable to isotropic metal layers and linear elastic behaviour is assumed. Furthermore, different coefficient of thermal expansion (CTE) are considered for the calculation of residual stress and plasticity is ignored, because this is not applicable to the prediction models used in this study. The remaining assumptions for CLT include the following:

- All plies are considered thin relative to their width and length, which usually implies $t < 0.1W$. This assumption is made so the plies can be assumed to be in a state of plane stress, which means $\sigma_z = \tau_{yz} = \tau_{xz} = 0$ and thus free straining in the z – direction.
- Every layer is assumed to be orthotropic, which means it contains three planes of symmetry and it is linearly elastic.
- The z-axes of all plies are aligned
- All plies are perfectly bonded to each other, which enforces strain compatibility throughout the laminate
- The Kirchhoff hypothesis is assumed to hold, which means that all deformations of the laminate are a function of the mid-plane in-plane deformation, a rotation and a translation in z-direction. This implies that the z-coordinate does not change under deformation and that deformations thus need to remain small, and that a cross-section that was flat before deformation is still flat after deformation
- Out-of-plane loads on the laminate are considered negligible.

As long as these assumptions for CLT apply to thin FML, the theory can be used even when the elastic constants of layers are different.

The general stress-strain for a FML layer is related by a stiffness matrix $[Q]$. Depending on the type of layer, such as metal or prepreg, the stiffness matrix is related to the elastic modulus and Poisson's ratio of the specific material.

$$\begin{Bmatrix} \sigma_x \\ \sigma_y \\ \tau_{xy} \end{Bmatrix} = [Q] \begin{Bmatrix} \epsilon_x \\ \epsilon_y \\ \gamma_{xy} \end{Bmatrix} \tag{2.3}$$

Defining the stiffness matrix for each layer creates the possibility to find the stiffness matrix for the laminate $[\mathbf{A}]$, this gives the relation between the mid-plane strains $(\boldsymbol{\epsilon})$ and the external loading $(N)$. Neglecting the bending loads and mid-plane curvature the following relation is obtained for symmetric laminates:

$$(N) = [\mathbf{A}]\,(\boldsymbol{\epsilon}) \tag{2.4}$$

with for the stiffness matrix,

$$A_{ij} = \sum_{k=1}^{n_f} (\bar{Q}_{ij,f})_k (t_f)_k + \sum_{l=1}^{n_m} (\bar{Q}_{ij,m})_l (t_m)_l \tag{2.5}$$

The stiffness matrix of the laminate gives the specific properties, such as the moduli of elasticity, of a laminate. Once the external loading is known the strain and the related layer

stress is obtained. Again, using the same theory the residual stress in a layer is derived to:

$$\{\sigma\}^r = [Q]\{\alpha_{\text{lam}} - \alpha\}\Delta T \tag{2.6}$$



Combining the stress due to external loading and residual stress gives the total layer stress.

$$\{\sigma\} = [Q]\left([\mathbf{A}]^{-1}(N) + \{\alpha_{\text{lam}} - \alpha\}\Delta T\right) \tag{2.7}$$

The CLT method forms the basis of FML analysis and it is used in many prediction models to determine the general properties and internal stress of a laminate.

### Failure criteria for static strength

For static strength, many criteria exist to predict failure [20], such as the maximum stress, maximum strain, Tsai-Hill and Tsai-Wu failure theories. For reasons of simplification, the Tsai-Wu failure criterion is presented here. The criterion is not entirely based on physical phenomena, nevertheless it is a useful and widely used method to define failure of composite [20]. This criterion is used to find out whether failure occurs within the laminate. The criterion is described with the following equation:

$$\begin{gathered}\frac{\sigma_1^2}{S_{u,t1}S_{u,c1}} + \frac{\sigma_2^2}{S_{u,t2}S_{u,c2}} - \sqrt{\frac{1}{S_{u,t1}S_{u,c1}}\frac{1}{S_{u,t2}S_{u,c2}}} + \\ \left(\frac{1}{S_{u,t1}} - \frac{1}{S_{u,c1}}\right)\sigma_1 + \left(\frac{1}{S_{u,t2}} - \frac{1}{S_{u,c2}}\right)\sigma_2 + \frac{\tau_{12}^2}{S_{u,s}^2} \geq 1\end{gathered} \tag{2.8}$$

where $S_{u,ti}$ is the ultimate tensile strength in direction $i$, $S_{u,ci}$ the ultimate compressive strength in direction $i$, and $S_{u,s}$ the ultimate in-plane shear strength. The values $\sigma_1$ and $\sigma_2$ are the local stresses in the 1- and 2-direction of a ply. As soon as Eq. (2.8) surpasses a value of 1 for one or more layers, the laminate is said to have failed. The local stresses are calculated using CLT.

## **2.4.** Fatigue and damage tolerance properties

The airworthiness requirements for aircraft demand regular inspection of the aircraft and prescribes the allowed amount of damage to the aircraft structure. Thereupon, cracking initiated by fatigue loading or accidental damage may not propagate to catastrophic failure prior to detection [15]. Two types of damages are distinguished for FML [15]: Damage where only the metal layers are broken (fibres are still intact) and damage where both the metal and fibres are broken. The first type is typically fatigue damage and the latter is more a result of impact damage. The fatigue damage is described by the crack initiation and crack propagation property, whereas the residual strength property is a measure for the impact damage. Therefore, in this section, the fatigue crack initiation (FCI), fatigue crack propagation (FCP) and residual strength (RS) properties of FML is briefly discussed.

### **2.4.1.** Fatigue crack initiation

The fatigue life can be split in two phases [25]: 1) the number of loading cycles required to initiate a crack and 2) the number of cycles it takes that crack to propagate to failure. For aluminium, the crack initiation period starts with crack nucleation at the metal surface and is followed by crack growth of micro-structurally small cracks. Officially, the crack initiation period ends when the crack starts growing perpendicularly away from the material surface, which is thought to be visually detectable [25]. However, for FML, there is no clear transition from one phase to other. Alderliesten stated that a crack length less than 1 mm is preferred to exclude any effect of fibre bridging on the initiation life. While, a crack length higher than 1 mm is preferred to have small error with respect to the S-N data in the literature. Therefore, a crack length of 1 mm is selected as an appropriate limit of the initiation phase [26].

Crack initiation in FML is governed by the aluminium and the fibre layers. However, the fibres exhibit no sensitivity to cyclic loading by means of fibre bridging, but the fibre stiffness and CTE still affect the initiation behaviour. Initiation is a surface phenomenon and mainly based on the stress in the particular metal layer. Since the curing cycle introduces residual stresses in the single layers, the metal layers face a tensile stress when the laminate is unloaded. Therefore, the mean stress level of the metal layers is higher as compared with monolithic aluminium without residual stresses. Furthermore, the stiffness of the aluminium layers is higher than the prepreg layers, which also relatively increases the stress level. As an effect, the higher tensile stress results in larger stress amplitudes and thus a reduced initiation life compared to monolithic aluminium [3].

### **2.4.2.** Prediction of FCI

In the literature, methods to predict the fatigue crack initiation in FML is rather limited. Homan [7] took the first step towards a prediction method with his proposition to compare the number of cycles to crack initiation for GLARE to that of monolithic aluminium by looking at the stress levels in the metal layers rather than the net section stress of the FML. The subsequent use of this stress to get to a prediction of cycles to crack initiation, however, is left untreated. Homan and Schra [27] mention that the presence of residual stress in notched FML makes the stress concentration factor (SCF) depend on applied load, but no information is given on which SCF should be used to characterise the peak stress cycle in comparison to S-N data. No details are given, moreover, about the selection of one of the many stress ratios that can be computed for FML, for similar purpose. Chang et al. [28, 29] connect Homan's reasoning to two different models to create a S-N curve for a notched monolithic specimen to allow for a prediction of cycles to crack initiation of FML. Their explanations, however, do not go further than a rough description of the method by Homan and the connected model,

again leaving many implementation details to the reader.

Finally, Spronk et al. [9] created understanding of the complete methodology to predict the cycles to crack initiation in a notched FML. This methodology implies using Homan's method to find the stress amplitudes in the metal layers at the point of interest, and subsequently comparing these amplitudes to S-N data for monolithic aluminium from the literature to get to a prediction of the cycles to crack initiation. Since this method [9] is the only complete methodology existing for fatigue crack initiation, it is decided to include it in the optimisation procedure.

The method carries out the steps below to find the number of cycles to reach a crack initiation length of 1 mm:

1. Calculate the far-field stress in the metal layer using the CLT.
2. Find the stress cycle at the notch. This implies determining the stress concentration factor (SCF), stress ratio and the nominal stress at the notch.
3. Predict the cycles to crack initiation using S-N data obtained from database. If the SCF or mean stress / stress ratio of the S-N curve do not match the stress cycle then adapt the load cycle to match the mean stress using the Goodman line and adapt the load cycle to match the SCF using a load factor or interpolation method.

A schematic overview of this procedure is given in Fig. 2.9.

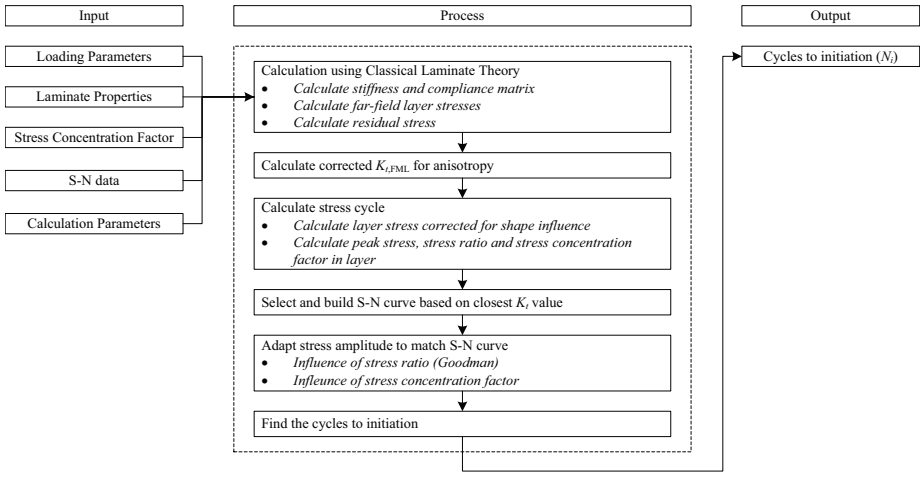


Figure 2.9: Overview of the fatigue crack initiation method.

### 2.4.3. Fatigue crack propagation

During the crack propagation phase, fatigue is not dependent on the surface conditions of the constituent layer, but on the crack growth resistance of the bulk constituent layer material. After fatigue initiation, a significant reduction of the crack growth rate can be measured, caused by the crack bridging mechanism of the fibres. While a fatigue crack grows in the metal layer, the fibres remain intact and take over part of the load that was normally carried by the metal. As a result, the stress intensity at the crack tip in the metal is reduced, resulting in a reduced crack propagation rate. Figure 2.10 illustrates the crack bridging mechanism as faced by the laminate.

For a surface crack (e.g. a scratch), the bridging stress is much higher, because not only fibres, but also the intact metal layers will restrain the crack opening and take over the load. The crack growth will thus be lower. However, a side effect is that secondary bending is introduced due to the eccentricity. Depending on the number of metal layers and the thickness, this effect is significant or can be neglected.

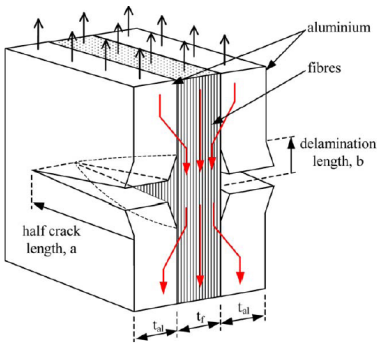


Figure 2.10: Crack bridging mechanism in FML [3].

Crack propagation in GLARE is clearly slower than monolithic aluminium, which is visible in Fig. 2.11 that shows the crack growth curves for aluminium 2024-T3 versus those of GLARE 3 and 4B. The exact difference in crack growth in different FML lay-ups depends on several parameters, such as the thickness of metal layers, the number of interfaces and the direction of fibres.

A side effect of the crack bridging mechanism is delamination. The load transfer from the cracked metal layer to the bridging fibres introduces shear stresses at the interface. Delamination growth is a function of the shear stress and occurs simultaneously with crack propagation. In Fig. 2.12, a cracked metal layer is shown with the corresponding delamination shape around the crack. Furthermore, a sketch of the mechanisms for a crack propagating from a saw cut is given. Notice that the saw-cut goes through all layers, both fibres and metal.

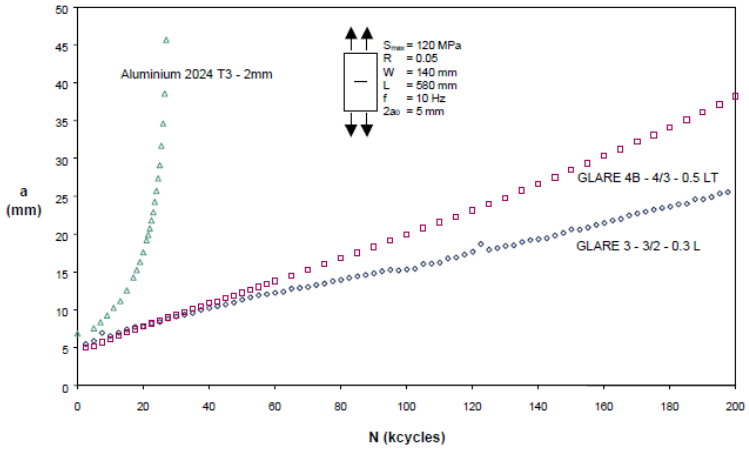


Figure 2.11: Crack growth curves for two GLARE grades compared with aluminium [3].

The fatigue crack only propagates in the metal layers, while the fibres stay intact. Therefore, next to crack bridging also delamination is observed in the wake of the propagated crack.

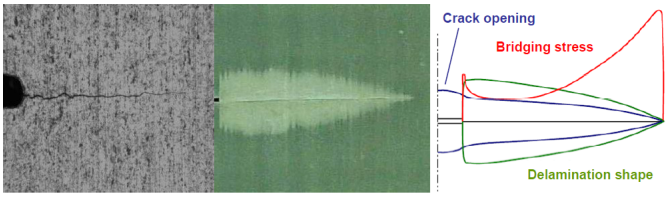


Figure 2.12: Crack in metal layer, delamination area and schematic view of crack [3, 21].

### 2.4.4. Prediction of FCP

A number of analytical approaches have been developed for FML to predict fatigue crack propagation. Most share two common assumptions: superposition of stress intensity factors and crack growth according to the stress intensity factors at the metal crack tips. Initially, Marissen [30] developed an analytical model for crack and delamination growth for ARALL. Guo and Wu [31] and Alderliesten [32, 33] used the same framework, improved the inappropriate assumptions and created a more generalized model, but the models were limited to simple configurations, like GLARE. Recently, Wilson [22] developed a generalized analytical model for FML of arbitrary lay-up, including different metal alloys, different thickness layers, and different combinations of reinforcing composite layers. This model is also capable of predicting the cracks growing separately in each layer. All these models only consider constant

amplitude loading, and therefore, Khan [34] developed an add-on to these methodologies that describes the fatigue mechanisms under variable amplitude loading.

After reviewing these methodologies it is decided to adopt Alderliesten's method [33] to be included in the evaluation procedure. Despite the more advanced model of Wilson [22] for arbitrary lay-up, the model of Alderliesten [33] is chosen, because the optimisation procedure described in this study is limited to lay-ups build-up of GLARE. This means single metal alloy, fixed thickness of all metal layers and a ply orientation of $0^\circ$ or $90^\circ$ are considered. For these configurations, the Alderliesten model is capable of delivering accurate predictions. Variable amplitude loading is not considered, assuming that the ranking will not alter by variable loading. The developed procedure is intended to be universal, meaning the prediction method can be replaced with any other model capable of making accurate predictions for the lay-ups in the design range.



The analytical model of Alderliesten [33] predicts the propagation of 'through cracks' (same length in all metal layers) in FML when constant amplitude loading is applied. This method describes the crack propagation of the fatigue cracks in the aluminium layers and the corresponding delamination growth at the aluminium-fibre interfaces perpendicular to the crack.

The method iteratively carries out the steps below to find the number of cycles to reach a certain crack length:

1. Calculate the crack opening due to maximum and minimum far-field stress.
2. Calculate the deformation of the prepreg layer under maximum and minimum far-field stress.
3. Calculate the bridging stress intensity by applying displacement compatibility at the crack surface at maximum and minimum far-field stress. This displacement is comprised of the results of the two previous steps, the extension of the fibre layer due to a combination of far-field fibre stress and bridging stress, and due to the reduction of crack opening due to the fibre bridging effect. This displacement compatibility requires a discrete solution, because an integration of the non-uniform bridging stress cannot be carried out.
4. Calculate the effective stress intensity ratio from the far-field stress intensity and the bridging stress intensity, again at maximum and minimum far-field stress.
5. Compute the maximum and minimum delamination strain energy release rates.
6. Calculate the crack- and delamination growth rates from the effective stress intensity ratio and the strain energy release rate ratio, respectively.
7. Apply the calculated crack- and delamination increments to the current coordinates and interpolate to find the updated delamination shape.

A schematic overview of this procedure is given in Fig. 2.13.

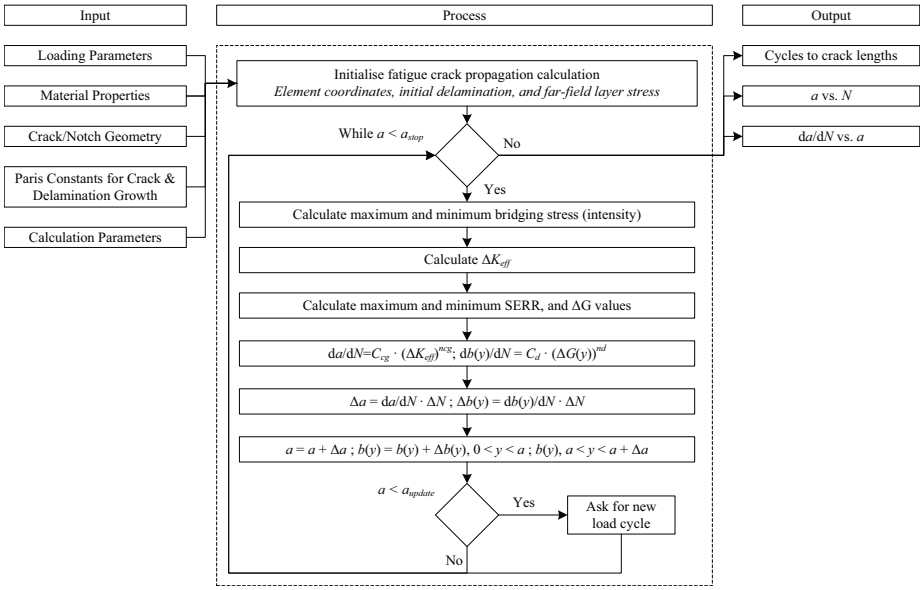


Figure 2.13: Overview of the fatigue crack propagation model.

### 2.4.5. Residual strength

The residual strength of a structure is defined as the remaining static strength of a material in case of any structural damage. For FML, two types of damage have to be differentiated; impact damage and fatigue damage. For impact damage, it is assumed that both metal and fibres layers are damaged, while for fatigue damage, the damage is restricted to the metal layers only. The type of damage has an effect on the residual strength behaviour of the laminate. For fatigue damage, the residual strength is higher than for impact damage. In case of accidental damage, the fracture behaviour in FML is similar to that of monolithic metals: initially stable crack growth takes place, followed by rapid unstable crack extension until failure occurs.

For clarity, the cracking behaviour during a residual strength test on GLARE 2A Centre Cracked Tension-specimen (CCT) is visualised in Fig. 2.14. Initially, the crack propagates by means of a cyclic fatigue loading, where the fibre stay intact and bridge the crack in the metal layers. This crack extension is visible in Fig. 2.14a. Hereafter, when static loading is applied, the fatigue crack will open as visible in Fig. 2.14b, and at approximately 90% of the residual strength the first fibres will fail in the tip of the crack (Fig. 2.14c). The fibres will take as much load as they can until they break, then the entire load is redistributed to the aluminium layers which will consequently fail, which is observed in Fig. 2.14d.

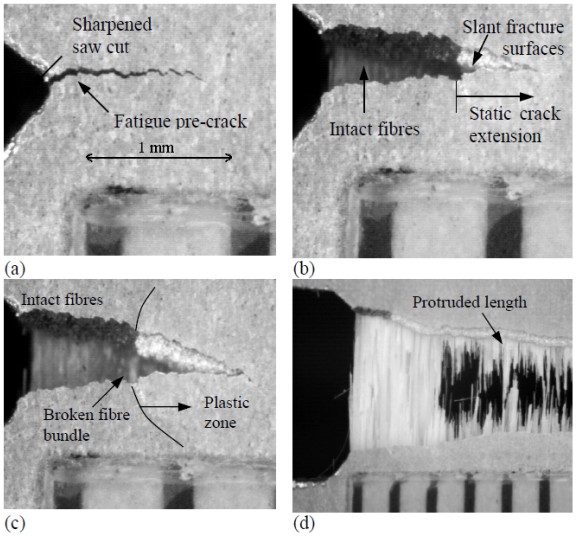


Figure 2.14: Crack growth sequence for a GLARE 2A CCT-specimen [35].

### **2.4.6.** Prediction of RS

Prediction methods describing the failure mechanism occurring during the residual strength failure sequence in FML have been developed. Afaghi-Khatibi et al. [36] evaluated the residual strength by means of an effective crack growth model. Jin and Batra [37] proposed a prediction model based on Dugdale strip yielding zone in the aluminium layers and a strip damage zone in the fibre composite layers at the crack tip. Vermeeren [38] and De Vries [15] used the R-curve method to predict the residual strength for FML and De Vries [39] proposed the use of the crack tip opening angle (CTOA) method as an alternative to the R-curve. Rodi [23] proceeded on the CTOA method and developed a prediction model for residual strength which analytically described the failure mechanisms within FML subjected to monotonically increasing load.

The latter model is selected for the evaluation of lay-ups because of its extensive validation with wide range of test data and its availability. The model of Rodi [23] handles the through-the-thickness crack damage and fatigue crack scenarios. In the model, FML are treated as build-up materials, where metal and fibres carry part of the load and interact with each other. The metal crack growth is modelled under quasi-static load using CTOA, while the static delamination process is treated using the strain energy release rate approach. The interaction between the constituents, including plastic deformation of the metallic layers, fibre bridging and fibre failure are implemented. Only the through-the-thickness crack scenario is adopted in the evaluation procedure.

The model iteratively carries out the steps below to find the residual strength of a laminate:

1. Calculate the far-field stress acting in each metal and fibre layers using CLT [20].
2. Calculate the crack opening in the metal and fibre layers by taken into account fibre failure, plastic zone ahead of the crack tip and permanent plastic deformation in the wake of the crack. Fibres contribute either with an opening effect, in case of fibre failure, or a closing effect, in case of fibre bridging. Fibre failure is reached in those locations where the calculated fibre strain exceeds the ultimate strain of the fibre.
3. Calculate CTOA, which consists of the contribution due to the far-field stress in the metal layers and fibre layers.
4. Compare the calculated CTOA with value by the input curve for the current crack extension defined whether a new crack extension occurs. If the criterion is not met, the load is increased by a fixed amount and the length of the yielded bar-element $CTOD_c$ is set equal to zero. If the criterion is met, the current CTOD is stored and the crack length is extended with a fixed length.
5. Repeat the process till the current load level drops below 2% of the maximum load level, which is the residual strength of the laminate

A schematic overview of this procedure is given in Fig. 2.15.

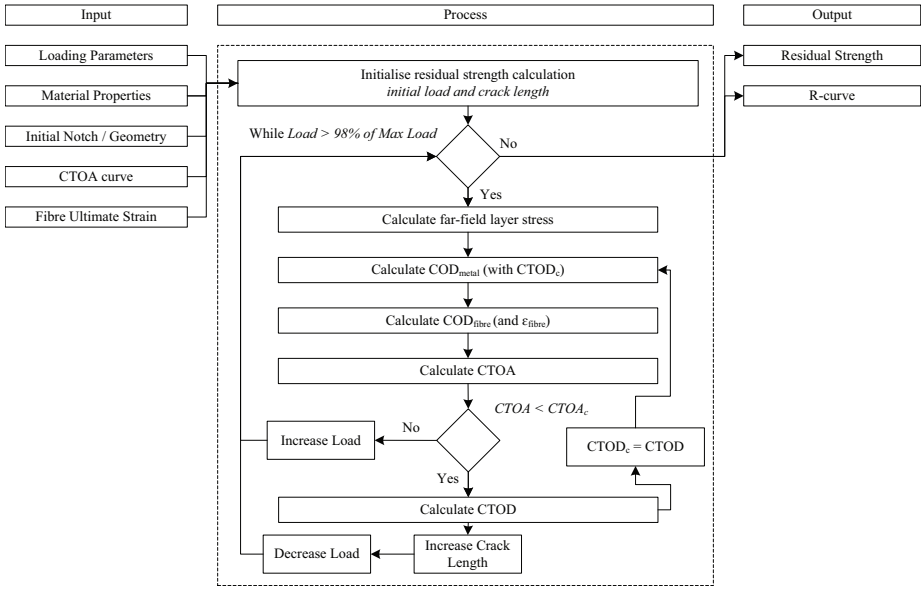


Figure 2.15: Overview of the residual strength model.

## 2.5. Selection of prediction methods

The reasoning behind the selection and remarks on the accuracy of the prediction methods are discussed in this section.



### 2.5.1. Reasoning behind selection

Before starting the design process of a structure with a selected material, it is necessary to know the behaviour and properties of this material. For this reason, an overview of the important static, fatigue and damage tolerance properties were given in the previous section. For metals, the most properties are known and easily predictable. Unfortunately, for FML, these fatigue and damage tolerance properties are difficult to obtain, because the material is not homogeneous and various lay-ups exist. From the literature, certain methodologies were presented to predict these properties of FML. These prediction models are important for the design of a FML structure. Knowing the material properties, design criteria can be set and the material can be assessed whether it passes or fails the criteria.

With the objective of designing a fatigue and damage tolerant wing structure, the fatigue crack initiation, fatigue crack propagation and the residual strength properties were selected to be included in the procedure. All other criteria were not considered. The selection was based on the availability of model, the possibility of implementation in the optimisation procedure, the accuracy of the model and the predictability of lay-ups.

The properties are assessed with specially developed prediction methodologies. The developed design optimisation method aims to be generic as possible, and for this reason, each design criteria can be easily replaced by a different one to evaluate the lay-ups.

### 2.5.2. Remarks on accuracy of prediction methods

The described prediction methods for crack initiation, crack propagation and residual strength are mainly validated for typical GLARE laminates. However, the optimisation methodology is not limited to GLARE, and for this reason, the validation of prediction methods for all other laminates in the design range is necessary to obtain fair optimisation results. In this study, the focus lies on the development of a design optimisation methodology for FML. Therefore, it is assumed that the evaluation of the lay-ups are based on accurate prediction results. Basically, it is expected that the methods give accurate results for lay-ups that have the same constituent material and lay-ups as GLARE and are not validated for these models. In case the design range is extended to custom FML, extra research might be required to confirm that the methods are applicable to these FML types. An additional accuracy issue regarding to the fatigue crack initiation method is discussed in appendix C.

Another issue is related to defining the design requirement values for the fatigue life. In real life, fatigue experiments show a fatigue life distribution (see Fig. 2.16), meaning for each experiment a different fatigue life is obtained. Usually for design purposes, the fatigue life is determined with a certain confidence limit to assure that gross of the laminates have at least this fatigue life. While, for the prediction only a single value is obtained. It is important to know how this predicted value is correlated to the life distribution of the specific lay-up. The challenge is to select a proper value for the design requirements to assure that obtained design solutions do indeed satisfy this fatigue life. This issue is left open for the designer.

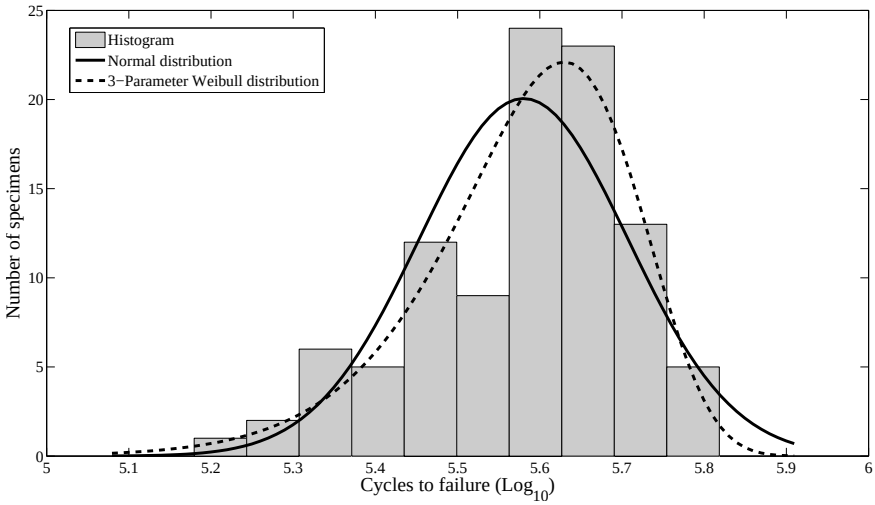


Figure 2.16: Example of a fatigue life distribution.

## **2.6.** Other design considerations

Next to the properties of the material, the manufacturing and design aspects play also an important role in the design process. FML share the benefits of being close to metals in terms of manufacturing and assembling the material and structure. Despite this, there are still differences in manufacturing processes, and therefore, new design challenges are introduced. Some of these design aspects are described in this section to make sure that during the optimisation procedure it could be taken into account to ease the manufacturability of the design solutions. These design aspects are, for example, the thickness steps, stringers design and joining methods.

### 2.6.1. Joining

Joining aircraft parts are commonly done by fasteners (rivets or bolds) and this technique could be used for FML. However, for example the blunt notch strength and ultimate strength vary per FML lay-up, which means the lay-up or laminate thickness should be tuned to make riveting possible. There is also the option to use bonding, which is more favourable compared to riveting in case of FML. The application and inspection of adhesive bonding is similar to aluminium. Leaving the fact that certification of bonded joints without fasteners are still not performed aside. Both joining methods are worth to investigate to acquire the most compromising joining method for the defined lay-up. Any joining aspect is not considered in this study.

#### Riveting

In case of riveted joints, the static failure modes of FML are determined in the same way as for aluminium, using the static allowables of the FML panel. Pin loading and rivet pull through require some special attention. Pin loading failure can occur due to bearing or delamination buckling. For bearing this happens when the yield strength is insufficient or the ultimate strength is exceeded. GLARE has worse bearing properties than monolithic aluminium due to the ineffectiveness of the fibres. Rivet pull through also differs for FML, because the prepreg layers contribute less to the strength in rivet direction, but contribute more to the bending behaviour.

#### Bonding

Bonded joints are favourable compared to riveting in case of FML, because the stress concentration is minimized due to the adhesive joints that spread the load path over the entire overlap area. There is also no fretting between the sheets, because the adhesive layer prevents metal to metal contact. Furthermore, the blunt notch behaviour is often a critical design parameter, and therefore, it is more beneficial to use bonding as joining method, because no holes are required and all the fibres stay intact and thus crack bridging is not locally reduced.

### 2.6.2. Stringers

#### Stringer stiffness

Alderliesten [12] stated that at some locations in a stiffened fuselage skin panel, monolithic aluminium stringers might result in insufficient performance. The relatively high elastic modulus of the aluminium stringers would attract more load from the skin panels, which creates fatigue problems in the stringers. For this reason, stringers with an elastic modulus

similar to the FML skin panel or increased fatigue resistance were required to be applied in the stiffened fuselage skins. Consequently, FML stringers were developed to meet these requirements [40]

2

### Stiffening effect on crack propagation

In the fatigue propagation calculation method only the skin panels are considered by assuming a geometry constant equal to 1 ($\beta = 1$). However, in real life the stringers have a contribution on the crack propagation behaviour. Depending on the location of the stringers, the stress intensity factor is changing along the skin panels. There are two ways to attach the stringers on the skin: rivets or adhesives, as discussed above. Consequently, two methods are available to predict the geometry constant and the relating stress intensity factor.

The first method, the method of Poe [41], calculates the stress intensity factor for riveted stringers of uniform size and spacing. An extension of this method is also made on stiffened panels with bolted stringers and with integral stringers. The stress intensity factor for panels with integral stringers are calculated by assuming that the stringers are attached to the sheet with very closely spaced rivets. As the rivet spacing approaches zero, this situation approaches the case of integral stringers [41].

The second method is developed by Rodi and Rans [42, 43], this method calculates the stress intensity factor for stiffened panels attached with adhesives or prepreg. The method considers three options for the stiffening contribution:

- Intact stiffeners ahead of the crack tip. These stiffeners provide additional stiffness and load redistribution ahead of the crack tip, reducing the crack growth in the skin panel.
- Broken stiffeners behind the crack tip. These stiffeners transmit load into the skin panel along the crack flanks, exacerbating crack growth in the skin panel.
- Bridging stiffeners over the crack. These stiffeners bridge load over the crack, reducing crack growth in the skin panel in a manner analogous to that of a bonded patch repair.

The stress intensity factor in the metal layer is, according to this method, a function of three stress system:

$$K_{tip} = K_{ff} + K_{br} + K_{st} \tag{2.9}$$

where, $K_{ff}$ is the far-field stress and has a positive contribution on the stiffening, $K_{br}$ is the bridging stress and has a negative contribution, and $K_{st}$ is the straps stress with negative or positive contribution.

The geometry constant is given as the ratio between the stress intensity factor of the stiffened and unstiffened panel.

$$\beta = \frac{K_{stiffened}}{K_{unstiffened}} \tag{2.10}$$

This method could be joined with the fatigue crack propagation method described in section 2.4.4 to include the stiffening contribution while calculating the crack growth of a FML panel.



### **2.6.3.** Thickness step

FML allow a more tailored sheet thickness distribution in comparison with monolithic metals. In theory, extra layers can be added where the stress levels are high, or layers can be removed in case of lower stress levels. This is introducing additional production steps and thickness steps in the structure. There are four reasons for thickness steps in aircraft structures: gradual thickness reduction due to bending moment (in wing span direction), local reinforcements (doublers around a man-hole), connection of a stiffener (stringer or rib) and end of overlap area in joints (lap-joint).

Every thickness step involves stress concentrations, which have to be minimized as much as possible. Furthermore, thickness steps often introduce secondary bending, because the outer surface has to be kept smooth for aerodynamic reasons and thus only internal thickness steps are possible that are not symmetric. Secondary bending and stress concentrations due to thickness steps can be minimized by applying a smooth gradient, instead of an abrupt ending of multiple layers. Two ways how this can be done are shown in Fig. 2.17. An internal ply drop-off is easier to manufacture, but interlaminar drop-offs show better properties, especially since delamination is unlikely to occur. However, interlaminar drop-offs are restricted to thin aluminium layers, because formability constraints prohibit self-forming of thicker layers.

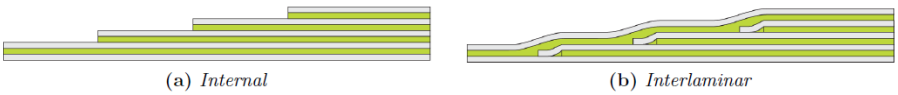

(a) *Internal* (b) *Interlaminar*

Figure 2.17: Internal ply drop-off (a) and interlaminar ply drop-off (b) [44]

A rules-of-thumb exist with respect to thickness steps and ply drop-offs [44]. The first rule is related to the stress concentration at the end of a layer, which is visualized in 2.18a. The ratio $\frac{b}{a} < 0.33$, which means that a doubler may have a maximum thickness of $33\%$ of the laminate underneath [44]. If the presented ratio is not satisfied, either delamination or crack initiation in the metal layer will occur. In case of crack initiation, the crack will propagate until the fibres in length direction are reached, where deflection of the crack in fibre direction will take place via delamination. This results in a decreased effective thickness. To prevent this, a gradual thickness reduction should be applied. For that situation also a rule-of-thumb exist, being that the distance between two thickness steps $(c)$ (see Fig. 2.18) should be minimum $25$ mm [44].

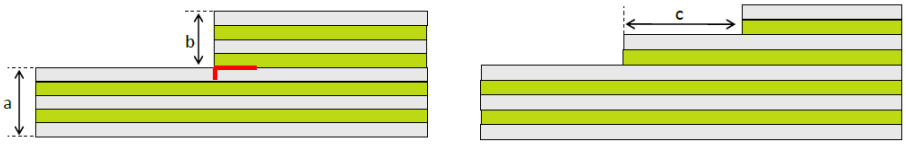


(a) *Thickness step and possible failure modes* (b) *Gradual thickness reduction*

Figure 2.18: Rules-of-thumb for ply drop-offs. [44]

### **2.6.4.** Compatibility requirement

When optimising a large wing panel, it is required that the optimised wing panel can be produced. A solution with many different lay-ups optimised per (small) wing segment is impossible to manufacture. For this reason, limitations on the design solutions are needed to assure compatibility between the lay-ups. Only lay-ups with similar compositions (same grade and same metal layer thickness) can be produced by simply adding or removing additional layers depending on the load acting on each segment. With this requirement only one type of lay-up is considered along the wing length, meaning the number of design choices will be limited. The importance is to find an optimal design for the complete wing instead of the optimal for a segment where for the wing the manufacturing plays a larger role. The optimal states that the solution fulfils the F&DT criteria while being compatible by means of manufacturing. Selecting same grade and same metal layer thickness will solve many problems related to manufacturing. However, to overcome the limited design choices, different solution can be manually compared by the design methodology to consider them for the design of the wing.

## **2.7.** Conclusions

The topics discussed in this chapter are fundamental to understand the properties and failure mechanisms in FML, because in the design process of FML these properties are the link to the design requirements. Therefore, a full understanding and good prediction of the FML properties are required to assure an accurate evaluation and to obtain a satisfying design solution. In this study, the F&DT criteria are selected as focal point to design a wing structure. For this reason, three criteria are selected to be included in the optimisation method to assure that the obtained design solution satisfy F&DT philosophy. The fatigue crack initiation, fatigue crack propagation and residual strength properties are selected to evaluate the laminates in the upcoming chapters. The CLT method forms the basis of these prediction methods to calculate the internal stresses for each laminate, and therefore, it is extensively used in the procedure. A summary of the methodologies considered for property prediction of FML is given in Table 2.4.

| Property | Methodology | Feature | Restrictions |
|---|---|---|---|
| Static properties | Classical Laminate Theory [20]<br>Tsai-Wu [20] | Custom FML[a]<br>Custom FML[a] | Not based on physical phenomena |
| Crack initiation | Homan [7] (extended by Spronk / Şen [9]) | Standard FML [b] | |
| Crack propagation and delamination growth | Alderliesten [45]<br>Wilson [22] | Standard FML [b]<br>Custom FML[a] | |
| Residual strength | Rodi [23] | Standard FML[b], Static and fatigue cracks | Fatigue crack part not working optimal |
| Stiffening contribution | Poe [41]<br>Rans / Rodi [42, 43] | Mechanical: Rivets or bolts<br>Bonding: Adhesive or prepreg | Empirical model<br>Constant delamination length and prepreg part not implemented yet |

Table 2.4: Summary of the available prediction methods for FML

[a] Includes standard FML, thick sheets, multi-alloy, variable thickness, adhesive layer and asymmetric laminate

[b] Thin sheets, single alloy, fixed layer thickness and symmetric lay-up

## References


[1] A. Vlot, R. Alderliesten, P. Hooijmeijer, J. Kanter, de, J. Sinke, and M. Ypma, *Fibre metal laminates: a state of the art,* International Journal of Materials & Product Technology **17**, 79 (2002).

[2] T. Boer, de, *Next generation fibre metal laminates,* in *Fiber Metal Laminates an Introduction*, edited by A. Vlot and J. Gunnink (Kluwer Academic Publishers, 2001).

[3] R. Alderliesten and J. Homan, *Fatigue and damage tolerance issues of glare in aircraft structures,* International Journal of Fatigue **28**, 1116 (2006).

[4] G. Chai and P. Manikandan, *Low velocity impact response of fibre-metal laminates - a review,* Composite Structures **107**, 363 (2014).

[5] G. Roebroeks, *The metal volume fraction approach* (Structural Laminates Industries, Delft, 2000).

[6] J. Sinke, *Manufacturing principles for fiber metal laminates,* (2009).

[7] J. Homan, *Fatigue initiation in fibre metal laminates,* International Journal of Fatigue **28**, 366 (2006).

[8] S. Khan, R. Alderliesten, and R. Benedictus, *Post-stretching induced stress redistribution in fibre metal laminates for increased fatigue crack growth resistance,* Composites Science and Technology **69**, 396 (2009).

[9] S. Spronk, I. Şen, and R. Alderliesten, *Predicting fatigue crack initiation in fibre metal*

*laminates based on metal fatigue test data,* International Journal of Fatigue **70**, 428 (2015).

[10] R. Alderliesten, C. Rans, and R. Benedictus, *The applicability of magnesium based fibre metal laminates in aerospace structures,* Composite Science and Technology **68**, 2983 (2008).

[11] G. Freischmidt, R. Coutts, and M. Janardhana, *Aluminium/lithium alloy-carbon fibre/epoxy laminated hybrid composite material - part i preliminary results,* Journal of Material Science Letters **13**, 1027 (1994).

[12] R. Alderliesten, *On the development of hybrid material concepts for aircraft structures,* Recent Patents on Engineering **3**, 25 (2009).

[13] G. Roebroeks, P. Hooijmeijer, E. Kroon, and M. Heinimann, *The development of central,* First International Conference on Damage Tolerance of Aircraft Structures (2007).

[14] R. Rooijen, van, *Bearing strength characteristics of standard and steel reinforced glare*, Ph.D. thesis, Delft University of Technology (2006).

[15] T. Vries, de, *Blunt and sharp notch behavior of glare laminates*, Ph.D. thesis, Delft University of Technology (2001).

[16] G. Roebroeks, *Towards Glare: The development of a fatigue insensitive and damage tolerant aircraft material*, Ph.D. thesis, Delft University of Technology (1991).

[17] M. IJpma, *Material design allowables and qualification,* in *Fiber Metal Laminates an Introduction*, edited by A. Vlot and J. Gunnink (Kluwer Academic Publishers, 2001).

[18] H. Wu, L. Wu, W. Slagter, and J. Verolme, *Use of rule of mixtures and metal volume fraction for mechanical property predictions of fibre-reinforced aluminium laminates,* Journal of Material Science **29**, 4583 (1994).

[19] W. Peng, J. Chen, J. Wei, and W. Tu, *Optimal strength design for fiber-metal laminates and fiber-reinforced plastic laminates,* Journal of Composite Materials **45**, 237 (2011).

[20] C. Kassapoglou, *Design and Analysis of Composite Structures: With Applications to Aerospace Structures* (John Wiley & Sons Inc., 2010).

[21] R. Alderliesten, *Fatigue Crack Propagation and Delamination Growth in Glare*, Ph.D. thesis, Delft University of Technology, Delft (2005).

[22] G. Wilson, *Fatigue Crack Growth Prediction for generalized fiber metal laminates and hybrid materials*, Ph.D. thesis, Delft University of Technology, Delft (2013).

[23] R. Rodi, *Residual strength in Fibre Metal Laminates*, Ph.D. thesis, Delft University of Technology, Delft (2012).

[24] F. Moriniére, *Low-Velocity Impact on Fibre-Metal Laminates*, Ph.D. thesis, Delft University of Technology (2014).

[25] J. Schijve, *Fatigue of Structures and Materials* (Springer, 2009) iSBN-13: 978-1-4020-6807-2.

[26] R. Alderliesten, *Fatigue & damage tolerance of hybrid materials & structures - some myths, facts & fairytales,* in *ICAF 2009, Bridging the Gap between Theory and Operational Practice*, edited by M. Bos (Springer Netherlands, 2009) pp. 1245–1260.

[27] J. J. Homan and L. Schra, *Application of aluminium alloy 2024-T3 fatigue life data to Glare laminates, GTP methods projects 2.4.3.2-B, 2.4.3.3-B and 2.3.3.4-B*, NLR Report NLR-CR-2002-185 (National Aerospace Laboratory of the Netherlands, 2002).

[28] P.-Y. Chang, J.-M. Yang, H. Seo, and H. T. Hahn, *Off-axis fatigue cracking behaviour in notched fibre metal laminates,* Fatigue & Fracture of Engineering Materials & Structures **30**, 1158 (2007).

[29] P.-Y. Chang, P.-C. Yeh, and J.-M. Yang, *Fatigue crack initiation in hybrid boron/glass/aluminum fiber metal laminates,* Material Science and Engineering A **496**, 273 (2008).

[30] R. Marissen, *Fatigue crack growth in ARALL*, Ph.D. thesis, Delft University of Technology (1988).

[31] Y. Guo and X. Wu, *A phenomenological model for predicting crack growth in fibre-reinforced metal laminates under constant-amplitude loading,* Composite Science and Technology **59**, 1825 (1999).

[32] R. Alderliesten, *Fatigue,* in *Fiber Metal Laminates an Introduction*, edited by A. Vlot and J. Gunnink (Kluwer Academic Publishers, 2001).

[33] R. Alderliesten, *Analytical prediction model for fatigue crack propagation and delamination growth in glare,* International Journal of Fatigue **29**, 628 (2007).

[34] S. Khan, *Fatigue Crack & Delamination Growth in Fibre Metal Laminates under Variable Amplitude Loading*, Ph.D. thesis, Delft University of Technology (2013).

[35] T. Vries, de, *Residual strength,* in *Fiber Metal Laminates an Introduction*, edited by A. Vlot and J. Gunnink (Kluwer Academic Publishers, 2001).

[36] A. Afaghi-Khatibi, L. Ye, and Y.-W. Mai, *Evaluations of effective crack growth and residual strength of fibre-reinforced metal laminates with a sharp notch,* Composites Science and Technology **56**, 1079 (1996).

[37] Z. Jin and R. Batra, *Residual strength of centrally cracked metal/fiber composite laminates,* Material Science and Engineering A **216**, 117 (1996).

[38] C. Vermeeren, *The residual strength of fibre metal laminates: Glare 2 and glare 3,* International Sampe Technical Conference Series , 471 (1998).

[39] T. Vries, de and A. Vlot, *The influence of the constituent properties on the residual strength of glare,* Applied Composite Materials **8**, 263 (2001).

[40] T. D. Jong, E. Kroon, and J. Sinke, *Formability,* in *Fibre Metal Laminates an Introduction*, edited by A. Vlot and J. Gunnink (Springer Netherlands, Delft, 2001) pp. 337–354.

[41] C. Poe, Jr., *Fatigue crack propagation in stiffened panels,* American Society for Testing and Materials **Damage Tolerance in Aircraft Structures**, 79 (1971).

[42] R. Rodi, *The effect of external stiffening elements on the fatigue crack growth in Fibre Metal Laminate*, Master's thesis, Universita Degli Studi Di Pisa, Pisa (2006).

[43] C. Rans, R. Rodi, and R. Alderliesten, *Analytical prediction of mode i stress intensity factors for cracked panels containing bonded stiffeners,* Engineering Fracture Mechanics **97**, 12 (2013).

[44] A. Keizer, *Evaluation of an FML lower wing panel design*, Master's thesis, Delft University of Technology, Delft (2011), available via `http://repository.tudelft.nl/`.

[45] R. Alderliesten, *Analytical prediction model for fatigue crack propagation and delamination growth in glare,* International Journal of Fatigue **29**, 628 (2007).

# 3

# State-of-the-art in design optimisation

*In the previous chapter, the concept of FML is introduced and its important properties alongside the available prediction methodologies are discussed. In this chapter, the process of designing an aircraft structure is introduced and the requirements for the optimisation procedure are determined. An evaluation is made for the optimisation algorithms based on these requirements and the best optimisation algorithm is selected to be implemented in the design optimisation methodology.*

## **3.1.** Introduction

The design process of an aircraft wing is an integral part of the design process of an entire aircraft. In the literature, a lot of work has been performed to both parametrically and statistically model aircraft wings. For example, Torenbeek [1] approaches the aircraft design process in a statistical way. With this method, parameters for new wing designs can be estimated using historic data of previous aircraft. Others studies, like [2–4] followed similar methods to perform conceptual aircraft design. The procedure of designing an aircraft structure is roughly performed as followed [5]:

1. Determine the design requirements.
2. Make an initial estimate of the weight based on previous aircraft data.
3. Determine the necessary critical performance parameters, such as wing loading.
4. Make an initial configuration lay-out: shape and size of the structure.

5. Obtain a better weight estimate.
6. Perform a performance analysis: does the design meet or exceed requirements? If not return to step 3.
7. At the end of the preceding iterative process, perform an optimisation procedure: is it the best design?



Şen [6] presented a design method for a parametric fuselage design based on statistical weight estimations of Torenbeek that follows a similar procedure. Other models have also been developed to automate this design process, but these methods consider only stiffened-skin design with aluminium. For aluminium, commonly the skin thickness is optimised based on the allowable stress set by the design requirements. As there is one variable and the allowable stress is defined per material, the optimisation becomes straight forward by finding the maximum thickness that equals the skin stress to the allowable stress. When new material solutions are considered, the design procedure is affected and becomes complex depending on the new material. In case of FML or composites, more variables are used to build up the laminate and the design allowables are not defined per material, but are changing per lay-up. This means an additional level of complexity is added to step 6 and 7, giving no clue in what direction the initial configuration should be changed if the step is returned to 3. In this case, it is for the designer difficult to achieve convergence. However, in this study, the above-mentioned procedure is still pursued for the implementation of the wing design procedure for FML, but with difference that the design procedure is approached by finding ways to over win the complexity introduced by FML.

The properties of FML are determined with the prediction methods as discussed in the previous chapter. There is a possibility to reverse the prediction process and convert it to a design process. This way the design allowables defined for the specific property are given as input to obtain the lay-ups as output. However, the multiple variables make it impossible to obtain a single optimal solution, simply there are more than one solutions that would satisfy the requirements. To overcome these problems, a search procedure (optimisation algorithm) is needed that can follow the iterative process by making deliberate choices for possible design solutions and assuring that the calculated design allowables for these solutions are indeed met by the laminate itself. While doing this the optimal or near-optimal solution are obtained. The optimal solution is defined as the lightest solution that satisfy all design requirements. This optimisation procedure is then implemented in a framework that considers a parametric definition for the wing geometry and statistical weight estimations for the load calculation. This way the lay-up optimisation of FML is linked to a wing structure to close the loop in the design process. More information on the wing definition and the load calculations are given in Appendix A.

For the purpose described above, the requirements for selecting a suitable optimisation algorithm for FML are defined. Hereafter, the optimisation algorithms are shortly discussed

and a choice is made for the implementation of the design optimisation procedure.

## 3.2. Requirements for lay-up optimisation

When optimising aluminium for a wing skin panel, the only variable is the thickness if the alloy is selected beforehand. However, in case of FML, more variables play a role, and for this reason, an optimisation method is required to find the best solution between all the variable combinations. Reviewing the literature, there is a lack of such a design optimisation method for FML. The closest to the current problem are only optimisation procedures for composite laminates. Composite laminates have a similar build up as FML with the difference that FML has additional metal layers. But the overall definition of the lay-up is similar, and therefore, the optimisation methods to design composites lay-ups could be applied to FML as well. For this reason, lay-up optimisation of composite is selected as starting point to define a suitable method for FML.



Design of composites commonly focusses on minimising the laminate thickness [7–14] or maximising the static strength or allowable buckling load of a laminate [15–18]. Design of the laminates has often been formulated as continuous optimisation problems, with ply thickness [7–9, 15] and ply orientation angles [9, 16] as design variables.

However, in practice, the design variables should be discrete variables, because composite laminates are fabricated using prepregs with a specific thickness. The fibre orientations are chosen from a finite set of angles during the design process, because of the difficulty of exactly orientating fibres along a given direction. If layer thicknesses and fibre orientation angles are taken as continuous variables in an optimisation process, the optimum values should be converted to the nearest discrete manufacturable values. In that case, the resulting design may not be optimal and the converted values might violate design constraints [14].

Therefore, it is better to include directly the manufacturing constraints by considering discrete values for the fibre angle or layer thickness. The use of discrete variables makes the optimisation of composite lay-ups a stacking sequence optimisation. Studies were performed for stacking sequence optimisation while for example the ply orientation, the laminate thickness, the ply thickness and/or the number of plies were fixed [10, 12, 13, 16].

The idea of stacking sequence optimisation could be implemented for FML, but the FML lay-ups have additional metal layers as stated before and this should be taken into account. This means a different lay-up definition is required. With the certification of GLARE [19], lay-ups were standardised and defined as a grade (see Section 2.1.1). This approach is also used to define lay-ups in the optimisation procedure. Instead of setting all variables free, the solutions are structured by defining the grades as variable, while the metal layers thickness and the stacking numbers are varied to create a large design space. In the grade,

the compositions of the fibre layers are defined as stacking order, amount and orientation of the fibre plies. This method has the benefit that the obtained optimal lay-ups are not completely random and thus easier to manufacture. For manufacturing reasons again, the ply thicknesses are fixed, the ply orientation angles are limited to a small set of angles, such as $0^\circ$, $90^\circ$ and $\pm 45^\circ$ and the metal sheet thicknesses are limited to producible sheet thicknesses. The orientation limitations are mainly incorporated in the grade definition and the sheet thicknesses by the step size of the variables.



Within the optimisation routine different objectives could be defined, such as minimum thickness, minimum weight, minimum cost or other objectives. Even multiple objectives are possible. The minimum thickness objective is not a minimum weight for FML like it is for composite. Because in FML two different materials are considered in the laminate, and the weight is also affected with the volume fraction of both materials.In conclusion, the optimisation of FML will be a discrete stacking sequence optimisation problem with minimum weight as objective. This problem can be formulated as an integer programming problem [20]. For this reason, an algorithm is required that can cope with discrete variables to implement the design optimisation procedure of FML.

## 3.3. Optimisation algorithms

Optimisation algorithms suitable for lay-up optimisations are investigated. A detailed review of available optimisation algorithms for composite structures is given by Ghiasi et al. [21]. Many different algorithms can be used to find optimal solution for a lay-up. The available algorithms are basically divided into two categories:

1. Gradient-based methods
2. Direct search methods

Gradient-based methods are generally faster than other algorithms and can find local minima in a small number of iterations. These methods, however, are limited to problems with continuous design variables, meaning discrete variables are not supported. Furthermore, the method requires the first or second derivatives of the objective function. The design solutions are dependent on the initial guess, because the method finds local optima often as solution. For small number of design variables and a smooth objective function, the gradient-based methods are favourable. These methods are commonly not used for composite lay-up design, because the derivatives functions are either unavailable or difficult to determine. Examples are Vanishing the function's first gradient, Steepest descent (SD), Conjugate gradient (CG) and Quasi-Newton (QN) methods [21].

In contrast, direct search methods are popular, because there is no need for a derivative and are more suitable for composite lay-up design. They are also popular because of their

capabilities of handling of both continuous and discrete variables. Furthermore, these methods always find the global optima of an objective function and work with a population of design solutions. However, they usually have a low rate of convergence depending on the objective and constraints functions. Genetic algorithms (GA) has been the most popular method together with simulated annealing (SA). Other examples are partitioning methods, enumeration search, simplex method, random and greedy search, scatter search (SS) [21].



### **3.3.1.** Genetic algorithms

FML design requires integer optimisations because the thicknesses are restricted to discrete variables and to predefined grades in which ply orientations are restricted to discrete angles and ply thicknesses are fixed. All gradient based algorithms are eliminated, because they only cope with continuous variables. From the direct search methods, GA has been the most popular method of tackling this problem and it is extensively used in the design of composite laminates from flat plates till structures, examples can be found in [10–13, 15, 16, 18, 22–24]. GA is a search technique based on a survival of the fittest concept and uses natural selection and genetics to create a design population in which it finds the optimal solution by performing random probability searches [10]. The advantage of GA is that they give the designer a family of near optimal designs with small variation in their performance index instead of single design, while the global optimisation methods always search for single global value [25]. For these reasons, in this study, GA is selected as optimisation algorithm for the lay-up optimisation of FML. The GA procedure and operators will be discussed in detail in Section 3.3.

### **3.3.2.** Implementation issue

The main limitation of GA in stacking sequence optimisations comes from the high number of evaluations that is required to assess all design solutions. This goes along with increased computational time, especially when using prediction methods or finite element analyses [26–28]. As expected, the same issue was encountered in this study as well. Therefore, an approximation for the objective function is considered for the laminate evaluation to improve the computation time. The approximate functions will be discussed in Chapter 5. Another major concern associated with GA is premature convergence, this happens if the initial population is not appropriately selected [21]. This issue will be extensively discussed in Chapter 7.

## 3.4. Conclusions

A design approach has been proposed based on statistical estimation of the loads and parametric definition of the wing. Within this approach, an optimisation routine is required to search for the optimal solution. Based on requirements set by FML design, GA is selected as optimisation algorithm to be implemented in the design methodology. FML lay-ups are decided to be defined as discrete variables to comply with manufacturing constraints, and GA handle discrete variables as proven by many (composite) lay-up optimisation studies. The optimisation becomes a stacking sequence optimisation due to discrete variables. Integer-based programming, where the integers refer to a specific design value, is selected. The design methodology will be discussed in Chapter 4. In the literature, it is stated that the application of GA will have implementation issues, such as high computation time due to high number of evaluations or premature convergence based on initial population. These issues will be respectively discussed in Chapter 5 and Chapter 7.



## References

[1] E. Torenbeek, *Synthesis of Subsonic Airplane Design* (Kluwer Academic Publishers Group, Delft, 1982).

[2] S. Brandt, R. Stiles, J. Bertin, and R. Whitford, *Introduction to Aeronautics, A Design Perspective*, 2nd ed. (AIAA Education Series, AIAA Inc., Reston, VA, 2004).

[3] D. Raymer and J. Przemieniecki, *Aircraft Design: A Conceptual Approach*, 4th ed. (AIAA Education Series, Reston, VA, 2006).

[4] J. Anderson, J.D., *Aircraft performance and Design* (McGraw-Hill, Boston, 1999).

[5] C. Cooper, R. Alderliesten, G. La Rocca, and R. Benedictus, *In search of a knowledge based preliminary design method of complex aircraft wings,* in *7th Annual Conference on Systems Engineering Research 2009 (CSER 2009)* (2009).

[6] I. Şen, *Aircraft Fuselage Design Study*, Master's thesis, Delft University of Technology, Delft (2010), available via `http://repository.tudelft.nl/`.

[7] L. Schmit and B. Farshi, *Optimum laminate design for strength and stiffness,* International Journal for Numerical Methods in Engineering **7**, 519 (1973).

[8] L. Schmit and B. Farshi, *Optimum design of laminated fibre composite plates,* International Journal for Numerical Methods in Engineering **11**, 623 (1977).

[9] H. Fukunage and G. Vanderplaats, *Strength optimization of laminates composites with respect to layer thickness and/or layer orientation angle,* Computer and Structures **40**, 1429 (1991).

[10] R. LeRiche and R. Hafka, *Improved genetic algorithms for minimum thickness composite laminate design,* Composites Engineering **5**, 143 (1995).

[11] R. LeRiche and J. Gaudin, *Design of dimensionally stable composites by evolutionary optimization,* Composite Structures **41**, 97 (1998).

[12] G. Soremekun, Z. Gürdal, R. Haftka, and L. Watson, *Composite laminate design optimization by genetic algorithm with generalized elitist selection,* Computers & Structures **79**, 131 (2001).

[13] O. Seresta, Z. Gürdal, D. Adams, and L. Watson, *Optimal design of composite wing structures with blended laminates,* Composites Part B: Engineering **38**, 469 (2007).

[14] M. Akbulut and F. Sonmez, *Optimum design of composite laminates for minimum thickness,* Computers and Structures **86**, 1974 (2008).

[15] K. Callahan and G. Weeks, *Optimum design of composite laminates,* Composites Engineering **2**, 149 (1992).

[16] J. Park, J. Hwang, C. Lee, and W. Hwang, *Stacking sequence design of composite laminates for maximum strength using genetic algorithms,* Composite Structures **52**, 217 (2001).

[17] G. Soremekun, Z. Gürdal, C. Kassapoglou, and D. Toni, *Stacking sequence blending of multiple composite laminates using genetic algorithms,* Composite Structures **56**, 53 (2002).

[18] R. LeRiche and R. Haftka, *Optimization of laminate stacking sequence for buckling load maximization by genetic algorithm,* AIAA journal **31**, 951 (1993).

[19] G. Roebroeks, *Glare features,* in *Fiber Metal Laminates an Introduction*, edited by A. Vlot and J. Gunnink (Kluwer Academic Publishers, 2001).

[20] G. Nemhauser and L. Wolsey, *Integer and combinatorial optimization* (Wiley, 1988).

[21] H. Ghiasi, D. Pasini, and L. Lessard, *Optimum stacking sequence design of composite materials part i: Constant stiffness design,* Composite Structures **90**, 1 (2009).

[22] Z. Gürdal, R. Haftka, and S. Nagendra, *Genetic algorithms for the design of laminated composite panel,* SAMPE journal **30**, 29 (1994).

[23] N. Kogiso, L. Watson, Z. Gürdal, and R. Haftka, *Genetic algorithms with local improvement for composite laminate design,* Structural Optimization **7**, 207 (1994).

[24] P. Sargent, D. Ige, and N. Ball, *Design of laminate composite lay-ups using genetic algorithm,* Engineering with Computers **11**, 59 (1995).

[25] A. Rama Mohan Rao and N. Arvind, *A scatter search algorithm for stacking sequence optimisation,* Composite Structures **70**, 383 (2005).

[26] F.-X. Irisarri, D. Bassir, N. Carrere, and J.-F. Maire, *Multiobjective stacking sequence optimization for laminated composite structures,* Composites Science and Technology **69**, 983 (2009).

[27] C. Lin and Y. Lee, *Stacking sequence optimization of laminated composite structures using genetic algorithm with local improvement,* Composite Structures **63**, 339 (2004).

[28] A. Muc and W. Gurba, *Genetic algorithms and finite element analysis in optimization of composite structures,* Composite Structures **54**, 275 (2001).

# 4

# Design methodology

*In Chapter 2, the prediction methods for the evaluation of the design criteria were introduced and in Chapter 3, a selection of suitable algorithms for optimising lay-ups were presented. As a follow-up, in this chapter, the design optimisation method to perform a FML lay-up optimisation for F&DT criteria is presented. The optimisation procedure is based on genetic algorithms considers lay-up optimisation for an element and for a wing cross-section. For this reason, different definitions for the design variables are proposed. Finally, the method is extended with the wing geometry and running load calculations to perform sizing for a wing structure with the lower wing consisting of FML and the upper wing consisting of aluminium.*

## **4.1.** Introduction

The method aims to size the wing by finding the optimum lay-up distribution over the lower wing skin. The method determines the minimum weight design that meets both the F&DT requirements, and the compatibility requirements for manufacturing. The method is used to:

- *Find an optimal solution by identifying possible solutions in the design space (ranking).*
- *Perform sensitivity analysis by changing the design requirements and identifying the influences on the optimal solution, the laminate thickness or weight.*
- *Perform weight comparison for wing solutions with different grades or metal layer thicknesses.*

The design optimisation method has a modular structure and has therefore the possibility to run independently. The model is divided into the following modules with corresponding functionalities:

Prediction module

- Predict the FCI, FCP and RS properties for given lay-ups.
- Determine the Tsai-Wu failure criteria for given lay-ups.

Regression module

- Create an approximate function for the FCI, FCP and RS prediction methods for given parameters.



Optimisation module

- Perform element lay-up optimisation for given load and requirements.
- Perform cross-section lay-up optimisation for given load and requirements.

Geometry- and load module

- Determine running loads for given wing dimensions, A/C weight and load cases.

Wing design module

- Perform wing optimisation based on cross-section optimisation and wing loads.

The interaction between the modules is described in detail in the next sections. All modulus combined form the wing design methodology.

## 4.2. Prediction module

The prediction module is used to determine the necessary properties of each design solution for the evaluation process. Predictions are either performed by the prediction methods or their approximate function created for a specific set of input parameters. In case of predictions with approximate functions, the function coefficients were determined beforehand with the regression module. For predictions with the prediction methods, the FCI, FCP and RS prediction methods described in Section 2.4 were included in this module for the F&DT evaluation. A schematic overview of this module is given in Fig. 4.1.

## 4.3. Regression module

The regression module is used to determine the approximate function for the prediction methods. The regression analysis and the procedure of obtaining the approximations for the prediction methods will be discussed in Chapter 5. In this module, the number of metal layers, thickness of metal layers are varied and a database is created with the corresponding

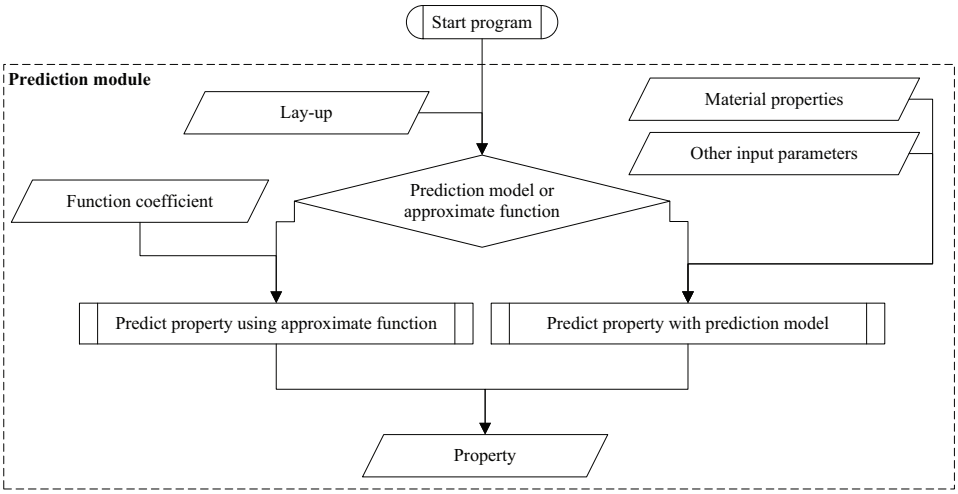


Figure 4.1: Structure of the prediction module.

property. This process is performed per grade and in case of FCI and FCP, the laminate stress is also varied. Using regression analysis, the function coefficients of the approximate function are obtained, which in turn could be used in the optimisation procedure to replace the prediction methods during the fitness evaluation. A schematic overview of the regression module is given in Fig. 4.2.

## **4.4.** Optimisation module

The optimisation module performs the lay-up optimisation for FML that should satisfy the design constraints. The module starts with the initialisation of the input parameters. The running loads and the settings of the optimisation algorithm are given as input for this module. The parameters for the prediction models or the coefficients of the approximate functions are given as input to the fitness evaluation part. The algorithm creates potential solutions which are evaluated based on the fitness and constraint functions, meaning the design properties are predicted for each lay-up and compared to the design requirements, whether they satisfy or not. Here after, the potential solutions are ranked and the optimal lay-up is given as output. The design objective and constraint are presented in Section 4.4.1. The design variables to construct the lay-ups are defined in Section 4.4.2 for both the element and cross-section optimisation. Then, in Section 4.4.3 and 4.4.4, the fitness evaluation and the evaluation criteria are discussed. Finally, the working of the optimisation algorithm is discussed in Section 4.4.5.

The optimisation procedure is schematically illustrated in Fig. 4.3.

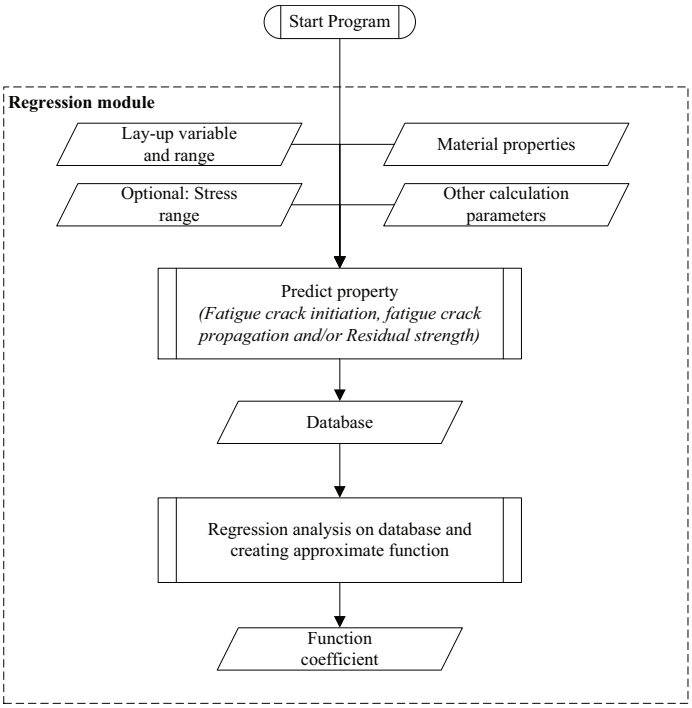


Figure 4.2: Structure of the regression module.

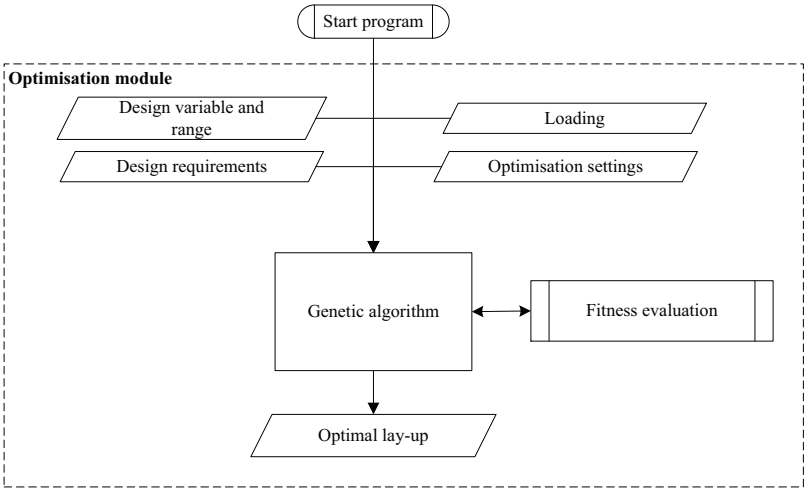


Figure 4.3: Structure of the optimisation module.

### **4.4.1.** Problem formulation

The optimisation problem aims to achieve a lay-up with minimized weight while satisfying the F&DT criteria and the additional compatibility criteria in case of cross-section optimisation. The optimisation problem can be formulated as:

$$\min W(\overline{x}) \tag{4.1}$$

subject to F&DT constraints:

$$N_{\text{fci}} \geq N_{\text{req}_{\text{fci}}} \tag{4.2}$$

$$N_{\text{fcp}} \geq N_{\text{req}_{\text{fcp}}} \tag{4.3}$$

$$S_{\text{rs}} \geq S_{\text{lam}} \tag{4.4}$$

and compatibility constraints (only for cross-section):

$$|t_i - t_{i-1}| \leq \Delta t_{\text{max}} \qquad i = 2 \dots j \tag{4.5}$$

or in terms of percentage with $t_i > t_{i-1}$:

$$\frac{t_i - t_{i-1}}{t_{i-1}} \leq p_{\text{max}} \qquad i = 2 \dots j \tag{4.6}$$

and with $t_i < t_{i-1}$:

$$\frac{t_{i-1} - t_i}{t_i} \leq p_{\text{max}} \qquad i = 2 \dots j \tag{4.7}$$

where $W$ is the laminate weight and $\overline{x}$ is design vector representing the lay-up of the laminate. The optimisation procedure is implemented using genetic algorithms (GA) as the optimisation algorithm. This algorithm requires a solution domain where the solutions are coded as a vector with integers. The definition of $\overline{x}$ is discussed in the next section, making a distinction between element or cross-section optimisation. Independent of the definition of $\overline{x}$, the algorithm requires a fitness function with constrained functions to evaluate the domain. The design solutions are evaluated and should satisfy the F&DT constraints.

The FCI criteria require that the FCI life $(N_{\text{fci}})$, that is the number cycles required to initiate a crack of 1 mm, is at least the required FCI life $(N_{\text{req}_{\text{fci}}})$. The FCP criteria requires that the lay-up will have at least a FCP life $(N_{\text{fcp}})$, that is needed to propagate the crack from detectable crack length until a critical crack length, equal or larger to the required FCP life $(N_{\text{req}_{\text{fcp}}})$. For the RS criteria, the laminate stress $(S_{\text{lam}})$ caused by the external load and the internal residual (thermal) stress, should not exceed the limit load $(S_{\text{rs}})$ of the laminate at a defined critical crack length.

In the cross-section constraints, $t_i$ and $t_{i-1}$ are the thickness of two neighbouring cross-section elements. The integer $i$ starts from the second element and proceeds to the last element $j$. The absolute thickness difference between the two elements should not exceed the maximum thickness step ($\Delta t_{\max}$). Another way to restrict the thickness step is in terms of maximum fraction ($p_{\max}$). This way the difference is better incorporated, because at higher thicknesses the allowed thickness step increases. An illustration of the thickness step between the elements is given in Fig. 4.4.



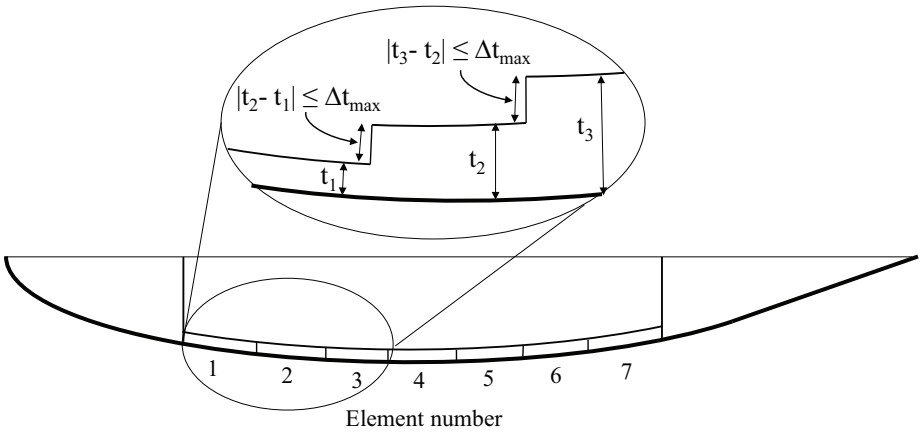


Figure 4.4: Illustration of the lower cross-section elements and the thickness step between the elements.

### **4.4.2.** Definition of variables

FML consist of thin metal layers bonded with layers of fibre composite [1]. Arbitrary lay-ups can be created by varying the properties of the metal and fibre layers such as, the thickness, the stacking sequence, the orientation or the amount of layers. The lay-ups of FML are defined in a systemic manner in which it is assumed that the laminates are balanced, symmetric and only one type of fibre and metal layer is used. The design optimisation method considers as stated before two different optimisation approaches: element and cross-section optimisation. Both require a different definition of the design variables, which will be discussed below.

#### Element optimisation

For element optimisation, the lay-up is defined by three parameters: the grade, the thickness of the metal layer and the number of metal layers (or the number of repetitions). The metal layers have the same thickness in all layers and the two outer layers consist of metal while the layers in-between are an alternation of the metal layers with the fibre layers. The fibre

layers consist of fibre plies with the amount and the orientation of these plies defined by the grade. The composition of the fibre layers are thereby fixed and only change when the grade is changed. In the grade, the composition of the fibre layers, like the stacking order, number of fibre plies and its orientations are specified.

In Fig. 4.5, a schematic overview of the laminate is given. There are basically four variables that are used to build up the laminate, namely the grade $(h)$, the number of metal layers $(n)$, the thickness of the metal layer $(m)$ and the thickness of single fibre ply $(f)$. The ply thickness for the fibre layer is assumed to be fixed, and therefore, not considered as a variable in the design procedure.


Figure 4.5: Lay-up definition of FML.

For the GA procedure, it is required to have a genetic representation of the laminate. GA works on the coding space (genotype) for genetic operations and in the solution space (phenotype) for evaluation and selection [2]. Therefore, the laminate representations should be decoded to the phenotypic solution space to evaluate the laminate using the crack initiation method then it should be encoded back to the genotypic coding space to apply the GA operators. This transformation is called mapping [3].

Each individual in the solution space is represented by a vector $L$ that describes the appearance of a laminate (phenotype).

$$\overline{L} = \begin{bmatrix} h & n & m \end{bmatrix} \tag{4.8}$$

This vector includes the three design variables mentioned above to build up the laminate. However, in the coding space the laminate is represented by vector $\overline{x}$ (chromosome) that describes the coded laminate (genotype) using integer coding.

$$\overline{x} = \begin{bmatrix} x_h & x_n & x_m \end{bmatrix} \tag{4.9}$$

The parameters $x_h$, $x_n$ and $x_m$ (genes) have fixed positions in the design vector (locus) and are integers referring to the position of the design value in the corresponding design vector $h$, $n$ and $m$ (alleles). An example design range are defined in the following vectors:

The grade:

$$h = \Big[< 0,0 > \quad < 90,90 > \quad < 0,90 > \quad < 0,90,0 > \quad < 90,0,90 > \quad < 0/90/90/0 >\Big] \tag{4.10}$$

in which each number represents the orientation of one ply, with the amount and stacking order described by the given numbers. For example, $< 0,0 >$ means two fibre plies with each laid in $0^{\circ}$ direction and $< 0/90/90/0 >$ means $4$ fibre plies which are stacked according to given order of orientations.

The number of metal layers:

$$n = \Big[2 \quad 3 \quad 4 \quad 5 \quad 6 \quad 7 \quad 8 \quad 9 \quad 10\Big] \tag{4.11}$$



The thickness of metal layers:

$$m = \Big[0.2 \quad 0.3 \quad 0.4 \quad 0.5 \quad 0.6 \quad 0.7 \quad 0.8 \quad 0.9 \quad 1.0\Big] \tag{4.12}$$

This design space consists of discrete variables and is customizable depending on the need of the user. In this example, the grades in vector $h$ are basically representing GLARE grades:

$$h = \Big[\text{GLARE 2A} \quad \text{GLARE 2B} \quad \text{GLARE 3} \quad \text{GLARE 4A} \quad \text{GLARE 4B} \quad \text{GLARE 5}\Big] \tag{4.13}$$

The number of metal layers are integers with a minimum of two layers. The thickness and its discretisation step should be defined by keeping in mind the minimum producible thickness, for aluminium 2024-T3 this is $0.2$ mm. The availability and producibility of different sheet thicknesses play also a role in defining the design space. In this case, it is decided to have a thickness step of $0.1$ mm. The thickness of a single fibre ply including the adhesive layer is assumed to be $0.133$ mm for S2-glass fibre with FM94 [4].

According to this design space, a coded laminate $x_1 = \Big[4 \quad 5 \quad 6\Big]$ represents the appearance $L = \Big[< 0,90,0 > \quad 6 \quad 0.7\Big]$ and is basically a GLARE 4A-6/5-0.7 laminate if aluminium 2024-T3 and S2-glass fibre with FM94 is selected as base materials.

### Cross-section optimisation

A cross-section optimisation is basically the simultaneous optimisation of different elements. By doing so, an optimal solution is obtained for the cross-section which includes compatibility or other design constraints between the elements rather than alone an optimisation based on F&DT properties. However, by considering three variables per element for a cross-section consisting for example of $10$ elements, the number of variables will increase to $30$. This means a very large design space is created, which will require high computation time to discover potential solution. With this large solutions it is difficult to find the global optimal

solution in the optimisation procedure. Additional to this, lots of constraints should be introduced to assure compatibility between elements, because different grades are difficult to manufacture together in one panel. To avoid this complexity, it is chosen to limit the design space by fixing the metal layer thickness and the grade. This means only the number of metal layers are set as variable and thus in case of $10$ elements, the number of variables remains $10$.

The cross-section is represented with vector $L$ in which $n_1 \dots n_j$ represent the number of metal layer in the cross-section element represented by the index value $1$ to $j$, where $j$ is the number of the last element.

$$\overline{L} = \begin{bmatrix} n_1 & n_2 & n_3 & n_4 & \dots & n_j \end{bmatrix} \tag{4.14}$$



The design solution vector $\overline{x}$ consist also of $j$ number of variables.

$$\overline{x} = \begin{bmatrix} x_1 & x_2 & x_3 & x_4 & \dots & x_j \end{bmatrix} \tag{4.15}$$

Each value in vector $\overline{x}$ represents indirectly the number of metal layers for each segment. $x_1$ to $x_j$ refer to a position in the design variable vector, which is for example:

$$n = \begin{bmatrix} 2 & 3 & 4 & 5 & 6 & 7 & 8 & 9 & \dots & 25 \end{bmatrix} \tag{4.16}$$

If GLARE 2A is selected as grade with a metal layer thickness of $0.4$ mm, the design vector $x_1 = \begin{bmatrix} 1 & 2 & 4 & 5 & 7 & 6 & 3 & 2 & 1 \end{bmatrix}$ refers to the cross-section solution with respectively $2$, $3$, $5$, $6$, $8$, $7$, $4$, $3$ and $2$ layers of GLARE 2A-0.4 in the cross-section, see Fig. 4.6 for an illustration.

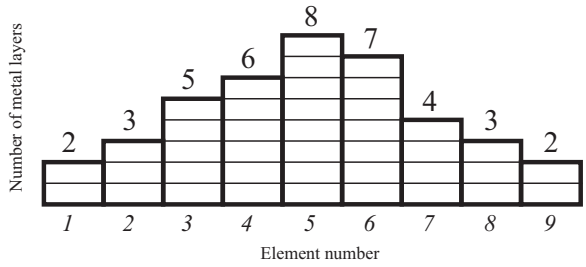


Figure 4.6: Illustration of the cross-section lay-up distribution.

### **4.4.3.** Fitness evaluation

The fitness evaluation of an individual requires the calculation of the laminate weight using the fitness function and the evaluation of the F&DT and other constraint functions. Every individual in the population is assigned a fitness value based on the overall performance,

which is measured by the total weight of the laminate and the value of the constraints [5]. The F&DT properties are checked with the design requirements and if violated, a penalty is applied to the fitness evaluation. If the constraint is satisfied then the fitness value is the total weight of the laminate, otherwise, the fitness value is the total weight of the laminate plus a penalty for the constraint violation. The laminates are ranked according to their fitness value, where the lowest weight laminate is ranked highest followed by the remaining. The laminate weight per unit width ($W_{\text{lam}}$) is calculated by:

$$W_{\text{lam}} = \rho_m \cdot n_m \cdot t_m + \rho_{\text{ply}} \cdot (n_m - 1) \cdot t_{\text{ply}} \cdot n_{\text{ply}} \tag{4.17}$$

where $\rho_m$ and $\rho_{\text{ply}}$ are the density of the metal and fibre layers respectively, $n_m$ is the number of metal layers, $t_m$ is the thickness of the metal layers, $n_{\text{ply}}$ is the number of plies in a fibre layer and $t_{\text{ply}}$ is the thickness of ply.



For the cross-section weight ($W_{\text{cross}}$), the weight of the elements are summed together giving the total cross-section weight and multiplying it with the element width ($w_e$).

$$W_{\text{cross}} = w_e \sum_{i=1}^{j} \rho_m \cdot n_m \cdot t_m + \rho_{\text{ply}} \cdot (n_m - 1) \cdot t_{\text{ply}} \cdot n_{\text{ply}} \tag{4.18}$$

$j$ is the total number of element in a cross-section and $i$ is the integer identifying the element in a cross-section.

The constraint margin $c$ is calculated by:

$$c = \begin{bmatrix} N_{\text{req}_{\text{fci}}} - N_{\text{fci}} \\ N_{\text{req}_{\text{fcp}}} - N_{\text{fcp}} \\ S_{\text{lam}} - S_{\text{rs}} \end{bmatrix} \tag{4.19}$$

GA attempts to achieve $c \geq \begin{bmatrix} 0 \\ 0 \\ 0 \end{bmatrix}$. If the value is positive, the laminate failed the F&DT constraint. For the cross-section the constraint margin is extended with the thickness constraints.

$$c = \left[ |t_i - t_{i-1}| - \Delta t_{\text{max}} \right] \tag{4.20}$$

or in terms of percentage with $t_i > t_{i-1}$:

$$c = \left[ \frac{t_i - t_{i-1}}{t_{i-1}} - p_{\text{max}} \right] \tag{4.21}$$

and with $t_i < t_{i-1}$:

$$c = \left[ \frac{t_{i-1} - t_i}{t_i} - p_{\text{max}} \right] \tag{4.22}$$

### **4.4.4.** Evaluation criteria

There are five major structural aspects that have to be considered during the design phase of an aircraft [6]:

- Static ultimate strength of undamaged structure
- Yield strength of undamaged structure
- Fatigue life of the airframe (crack initiation)
- Static residual strength of damaged structure
- Residual life of damaged structure (crack propagation)



Designing for these aspects will provide a structure which will meet the static strength and F&DT requirements of the aircraft. The three latter aspects are very important for the airworthiness and the economics of the present and future aircraft. The industry uses F&DT criteria to assure a safe operation of the aircraft in case of cracks or damages in the structure. For this purpose, a structural inspection program is developed for each aircraft and according to this program the aircraft is periodically inspected to assure all damages are detected and repaired before they become critical. The FAA requirements with respect to damage tolerance state that cracks present in the structure should not grow beyond a critical length that leads to catastrophic failure within inspection intervals.

For an aircraft, the inspection threshold and inspection interval are defined. The inspection threshold is the time of first inspection in flight and in general it is determined by the fatigue crack initiation with consideration of a relevant scatter factor. The inspection interval is the period between the repeated inspection in flights and it is determined from the crack growth period between the detectable crack length and the critical crack length under limit load. Therefore, in this study, the crack is assumed to nucleate and propagate up to 1 mm [7] for the fatigue initiation case. For the fatigue crack propagation analysis, the crack propagates from the detectable crack length until the critical crack length. The critical crack length is assumed to be the length of a bay according to the two-bay crack criterion. The two-bay-crack criterion states that a crack through a frame (and thus a crack in two bays) should not result in catastrophic failure [8]. An illustration of the two-bay-crack propagation is given in Fig. 4.7.

For the wing panels, a central crack with broken stringers is assumed, where the crack grows towards the neighbouring stringers in both opposite directions. The critical (half) crack length is selected to be equal to the stringer pitch ($2a_{\text{crit}} = 2b_{str}$) as the crack is assumed to occur at the skin panel below a broken stringer. The detectable crack length is defined as $2a_{\text{det}} = 2 \times 35$ mm and the critical crack length is thus defined as $2a_{\text{crit}} = 2 \times 150$ mm. Each element on the wing is analysed as a separate FML panel and the method assumes that only one crack occurs and that there are no multiple cracks influencing each other.

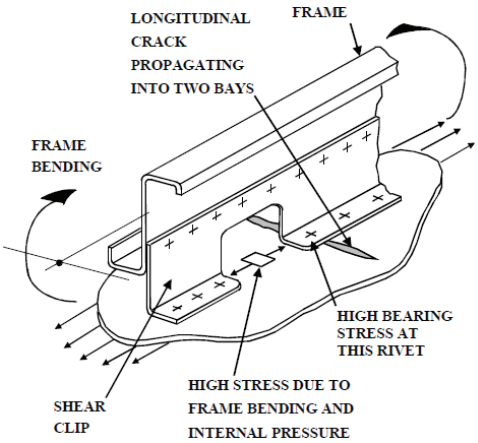


Figure 4.7: Two-bay longitudinal crack propagation [8].

In case, the crack detection is missed at the detectable length during inspection, the aircraft should be safe to fly until the next scheduled inspection, which should be before the critical crack length is reached. At critical crack length, the remaining strength of the structure drops below the limit load. In this case, the stresses in the wing panels should not exceed the limit load to prevent any structural failure. The ending of the crack propagation phase happens when the critical crack length is reached and this is the point where the residual strength is determined. Basically, the critical crack length is set to $2a_{\text{crit}} = 2 \times 150$ mm for the residual strength analysis. An illustration of the cracks in a panel for the three criteria is given in Fig. 4.8.

### 4.4.5. Optimisation algorithm

A genetic algorithm (GA) is used as a search technique to explore the design space and to obtain the optimal lay-up that satisfies the FCI, FCP and/or RS criteria. The algorithm uses operators, such as selection, mutation and crossover to generate design solutions within the design space that are evaluated. Based on their fitness values, these solutions are reproduced in the next generation with the goal of improving the fitness of the lay-up.

The search process starts with constructing a random initial population of individuals and evaluating the fitness of each member in this population. The population size determines the number of chromosomes (design solutions) that make up a generation. The fitness value of each individual determines the probability of being chosen as a future parent and of allowing them to pass their genes (design parameters) to the next generation.

A new generation of population is created by selecting parent design for mating. GA have

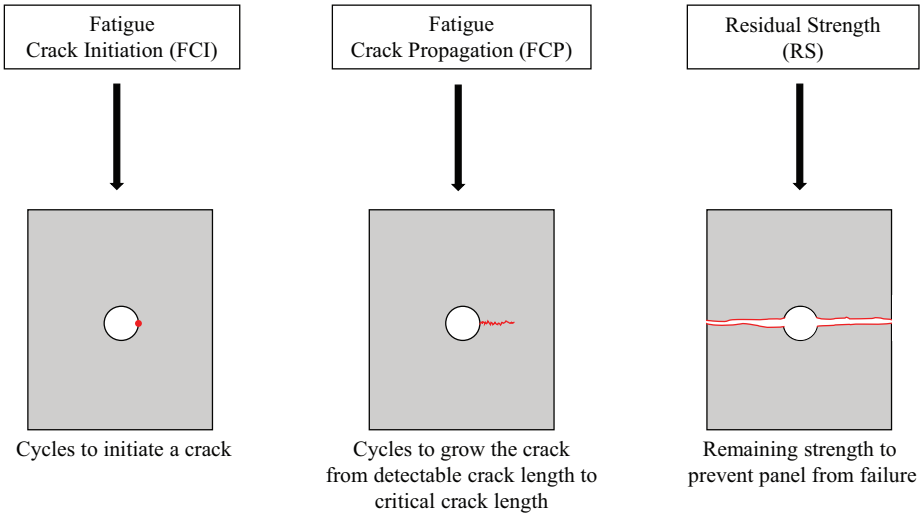


Figure 4.8: Crack representation for FCI, FCP and RS criteria.



various selection strategies, the old population is either replaced by a new one except for the best design which is always kept unchanged (elitist approach) [9], or a certain percentage of the old population is copied unchanged to the new population (generation gap/migration) [10]. These strategies are used to be sure that the best individual could be compared in the next generation and can produce off-springs. Especially in the case of full generation replacement, the choice for elitist approach can prevent not to lose the best individual when creating a new generation.

This newly created generation is subjected to cross-over and mutation operators to create a better and diverse population. Crossover is used to trade characteristics of two selected parent designs and to generate offspring by exchanging features of both strings at randomly selected crossover points [11]. The newly created off-springs are put into the next generation of the population. This idea of recombining parts of individual is to create better individuals. Mutation performs random changes in the string of a new individual with a low probability. Its purpose is to maintain diversity with the population and to protect the population against becoming uniform. An illustration of crossover and mutation is given in Fig. 4.9.

The fitness of each design solution is evaluated using the fitness and constraint functions. First, the coded laminates in the population are converted to suitable input parameters for the prediction methods (constraint function). After this, the corresponding property is predicted and compared with the design requirement. With the fitness function, the weight of each design solution is determined. If the laminate satisfy all the design criteria, then the weight is assigned as the fitness value of the solution. In case one or more criteria are not met, the fitness value is the weight plus a penalty factor, as explained before. The design solutions

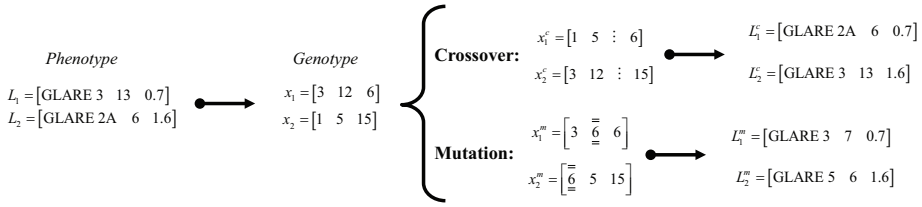


Figure 4.9: Genetic operations on the design vector for element optimisation.

are then ranked according to their fitness value. The lightest solutions are ranked high, while solutions not satisfying a design criteria are ranked low due to their high fitness value caused by the penalty factor. Lastly, the optimisation process is repeated until the solution converges to a single solution or the process stops when the maximum number of generations is reached. The last generation contains then the solution with the overall lowest weight that satisfies all design constraints. A schematic overview of the GA procedure is given in Fig. 4.10. This procedure is implemented in MATLAB with use of the built-in `ga`-function.

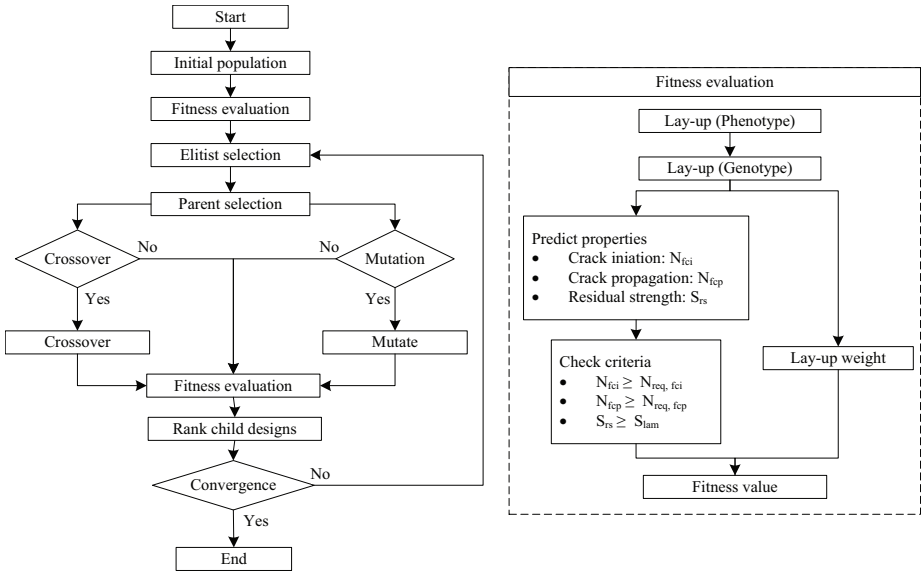


Figure 4.10: Optimisation procedure implemented with genetic algorithms.

### Optimisation settings

The settings for GA operators need to be properly set to ensure a good exploration of the design domain. Many times fixed setting do not work, and therefore, the settings need to be tuned if the design space or design criteria are changed. This means that the probability rates

of the operators and other parameters must be manually adapted till the settings assure a stable output for the design solution every time the optimisation is performed. In this study, the settings of De Jong [12] are used to perform the optimisation due to the best trade-off between accuracy and speed. These settings are listed in Table 4.1. In Section 6.2, a detailed analysis will be presented comparing different GA settings on their performance.

| Parameter | Value |
|---|---|
| Population size | 50 |
| Probability of crossover | 0.6 |
| Probability of mutation | 0.001 |
| Generation gap | 1 |
| Selection strategy | Elitist |

Table 4.1: Settings for genetic algorithm of De Jong [12].



## 4.5. Geometry- and load module

The calculations in the geometry- and load module are discussed in detail in Appendix A. With this module, the running loads on the wing structure are calculated. Initially, the wing shape is created based on dimensions of the reference aircraft and the wing is segmented lengthwise. The cross-section shape is similarly defined and segmented based on the stringer locations. Using an input skin thickness and elastic modulus, the moment of inertia of the each cross-section is calculated. The weight and lift distribution of the wing is then determined based on statistical aircraft data. Using these distributions, the force and bending moment lines are calculated for each segment in lengthwise direction. The force and bending moments are assumed to be constant for the segment length. Using the corresponding moment of inertia, the running loads on each cross-sectional elements are calculated. Then, the running load of each element is stored together with the coordinates of the corresponding element. The procedure of the running load calculation is given in Fig. 4.11.

## 4.6. Wing design module

The wing design module aims to create an optimised wing structure. This module combines the geometry- and load module with the optimisation module and optimises each wing cross-section for the applied load on the specific segment based on the selected load case. The procedure starts with the optimisation module which generates design solutions for the first cross-section using the genetic algorithm. For each individual solution, the thickness and elastic module is determined and forwarded to the geometry- and load module to obtain the running load for the corresponding solution. Afterwards, the design solutions are converted

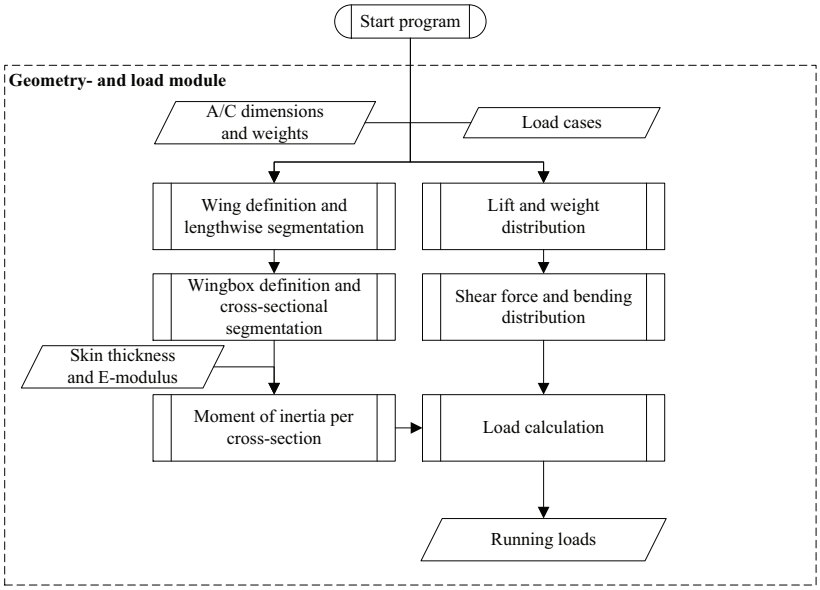


Figure 4.11: Structure of the geometry- and load module.



to input variables for the prediction module and the properties are then calculated. These values are then compared to the design requirements and the weight is determined. The optimisation process is repeated till the highest ranked solution is selected as optimal solution.

Hereafter, the method proceeds to the next cross-section and performs the same optimisation. Each cross-section is optimised independently from each other, because there are no constraints considered between the different cross-sections. Finally, the skin thickness, lay-up information and weight of each cross-section is obtained, so that a comparison study could be performed. In Fig. 4.12, a schematic overview of the wing design module is given.

### **4.6.1.** Load cases

Once the running loads are calculated, these are given as input for the optimisation module to design the laminate. Depending on the design criteria, the loads could be multiplied with a safety factor to be considered as ultimate load, fatigue load or buckling load. This is up to the designer.

De Jong et al. [13] presented a study for standardised load sequence on transport aircraft wing structures. The study concluded that all calculated load spectra for different aircraft are in a relatively small band, and hence, the establishment of a standardised spectrum is justified. From this load spectrum, it is deduced that the load encountered once every flight is 50% higher than the average 1G flight load. This is translated to a load factor of

1.5 experienced once a flight on the aircraft. Therefore, a safety factor of 1.5 should be considered on the load when designing the wing structure for fatigue.

The running loads are obtained for two load cases, namely *air* and *ground*. The standard air load case considers a steady flight, where the load factor is $n = 1$. There are two additional air load cases defined with $n = 2.5$ and $n = -1$. The critical load factor of $n = 2.5$ is selected for the structure design in this study and it is assumed that this 2.5G flight load case will include the effect of spectrum load, because the critical load factor is larger than the load factor spectrum load.

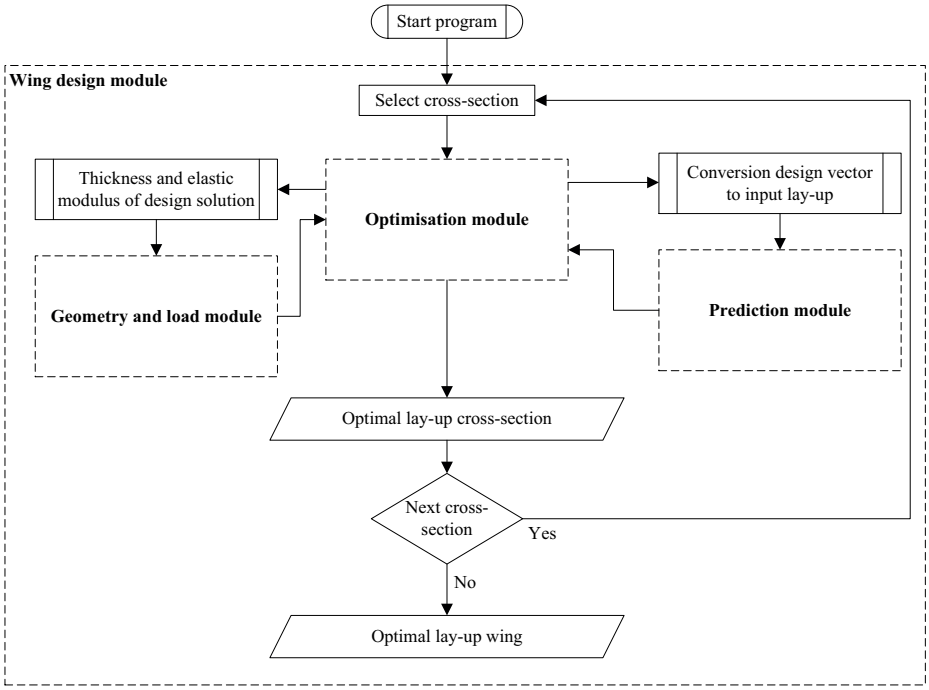


Figure 4.12: Structure of the wing design module.

For the lower wing skin design, the tensile loads are important for F&DT design and with a factor of 2.5 the largest tensile loads are obtained. For the upper skin, compression loads are required for the assessment of buckling criteria. Here again, the factor 2.5 gives the largest compressive loads at the upper wing skin. The load case of $n = 1$ and $n = -1$ are less critical, and for this reason, not considered in this study.

### 4.6.2. Contribution of upper panel

The design of the lower wing skin is linked to the overall design of the wing. Other parts such as the upper wing skin, stringers, webs and spar caps influence each other. For this reason, the design of these part has been considered as well. The moment of inertia calculation in the wing design procedure incorporates the different parts to obtain the correct running loads for the lower wing skin. On the other hand, the change of the lower wing skin thickness influences the running loads of the upper wing and visa versa due to the integrated design process.

The upper wing skin remains aluminium while the lower wing skin will be FML. The sizing of the upper wing skin is performed with the design methods for aluminium described in Appendix B. The optimisation procedure is adapted by considering additional design variables representing the skin thickness of each element on the upper part of the cross-section. Likewise, the algorithm generates solutions and determines the lightest solution satisfying the aluminium design criteria. In Section 7.3, the aluminium optimisation is discussed while performing a cross-section optimisation. Detailed evaluation of the aluminium upper wing panels is not given in this thesis.

## 4.7. Model output

The modular output of the method enables the designer to use each module separately for its specific purpose. Therefore, in this section, the output of the design method are listed.

Prediction module

- Cycles to initiation for given lay-up, stress and stress concentration factor.
- Cycles to propagation for given lay-up, stress and crack lengths.
- Residual strength for given lay-up and critical crack length.

Regression module

- Function coefficient of the approximate functions.

Geometry- and load module

- Coordinates of each element on the wing.
- Visual output of the wing and wingbox.
- Lift and weight distribution over the wing for given A/C data.
- Force and moment distribution over the wing for given load case.
- Stress and running load distribution over the wing for given skin thickness.

Optimisation module

- Ranking of design solutions based on weight.

Wing design module

- Distribution of layer number and skin thickness over the wing.
- Total weight of the wing solution
- Lay-up distribution per design criteria and identifying the limiting design criteria.

## 4.8. Local reinforcements

The lay-up optimisation routine has the potential to design local reinforcements for skin panels by considering the local reinforcement as an asymmetric lay-up. This is done by defining a fixed basis lay-up, which represents the existing skin panel and on top of this lay-up, another lay-up is attached with an adhesive or prepreg layer in between. The top lay-up is set as variable and the base lay-up is defined as a special type of grade. During the conversion of the design vector of the top lay-up to input for the prediction method, the laminate is generated based on both the basis and top lay-up. The main issue rising to consider local reinforcements is the capability of the prediction methods to determine the properties of the defined asymmetric laminate.



The FCI method discussed in Section 2.4.2 is a generic method that basically assumes that layers with the same internal stress will have similar FCI life provided that the notch and panel geometry are the same. In case of asymmetric lay-ups, it is expected that layers with the highest stress will be critical layer in which crack initiation will happen. Therefore, the FCI method of Spronk et al. [14] could be used by predicting the FCI life of the critical layer and checking if it satisfy the design life requirement. For FCP, the model of Alderliesten [15] summarised in Section 2.4.4 supports only typical FML with only fibres in 0° and 90°, having no support for asymmetric lay-ups. The FCP model of Wilson [16] allows an arbitrary lay-up definition. Using the prediction method developed by Wilson in the optimisation procedure, the asymmetric lay-up definition could be used to design local reinforcements. Unfortunately for RS, there are no analytical prediction methods available to consider asymmetric lay-ups. A separate assessment of the base and top lay-up is an option. But the influence of both lay-ups on each other is then ignored, making the evaluation not reliable.

Using these prediction methods will only assume that the local reinforcements are asymmetric lay-ups and will not evaluate the local reinforcement on delamination growth and stress concentrations. The design and optimisation of local reinforcements build with FML is not a content of this thesis.

## 4.9. Conclusions

The procedure of the design optimisation method for a wing consisting of FML has been presented. The method supports element optimisation in which the metal layer number, metal layer thickness and the grade are defined as variables to construct the lay-up. The method is used to find the optimal lay-up for a given load that meets the F&DT requirements.

The method is extended to a wing design method by linking the geometry and load calculations for the wing to the lay-up optimisation process. To simplify the design process and to assure compatibility between different elements, only the number of layers are selected as variable. While doing this an alternative optimisation procedure is developed that considers an optimised cross-section instead of an element. Additional thickness constraints are introduced to further improve the compatibility of elements with respect to manufacturing.



The results and discussion of the lay-up optimisation on element level will be discussed in Chapter 6. In Chapter 7, the result of the cross-section optimisation are presented and a final assessment of the complete wing is given by considering the optimisation of both the upper and lower wing skin, respectively designed for aluminium and FML.

## References

[1] G. Roebroeks, *Glare features,* in *Fibre Metal Laminates an Introduction*, edited by A. Vlot and J. Gunnink (Springer Netherlands, Delft, 2001) pp. 23–37.

[2] M. Gen and R. Cheng, *Genetic Algorithms and Engineering Design,* (John Wiley & Sons, 1997).

[3] D. Fogel, *Evolutionary Computation: Towards a New Philosophy of Machine Intelligence* (IEEE Press, New York, 1995).

[4] J. Homan, *Fatigue initiation in fibre metal laminates,* International Journal of Fatigue **28**, 366 (2006).

[5] O. Seresta, Z. Gürdal, D. Adams, and L. Watson, *Optimal design of composite wing structures with blended laminates,* Composites Part B: Engineering **38**, 469 (2007).

[6] I. Şen, *Aircraft Fuselage Design Study*, Master's thesis, Delft University of Technology, Delft (2010), available via `http://repository.tudelft.nl/`.

[7] R. Alderliesten, J. Schijve, and S. Zwaag, van der, *Application of the energy release rate approach for delamination growth in glare,* Engineering Fracture Mechanics **73**, 697 (2006).

[8] T. Swift, *Fail-safe design requirements and features, regulatory requirements,* (2003).

[9] D. Goldberg, *Genetic Algorithm in Search, Optimization and Machine Learning*, Vol. 412 (Addison-Wesley, Reading Menlo Park, 1989).

[10] C. Reeves, *Genetic algorithms,* in *Handbook of Metaheuristics*, edited by F. Glover and G. Kochenberger (Springer, Berlin, 2003).

[11] R. LeRiche and R. Hafka, *Improved genetic algorithms for minimum thickness composite laminate design,* Composites Engineering **5**, 143 (1995).

[12] K. D. Jong and W. Spears, *An analysis of the interacting roles of population size and crossover in genetic algorithms,* in *1st Workshop Parallel Problem Solving from Nature*, Vol. 496 (1991) pp. 38–47.

[13] J. Jonge, D. Schütz, H. Lowak, and J. Schijve, *Standardized Load Sequence for Flight Simulation Tests on Transport Aircraft Wing Structures*, NLR Report NLR TR 73029 U (National Aerospace Laboratory of the Netherlands, 1973).

[14] S. Spronk, I. Şen, and R. Alderliesten, *Predicting fatigue crack initiation in fibre metal laminates based on metal fatigue test data,* International Journal of Fatigue **70**, 428 (2015).

[15] R. Alderliesten and J. Homan, *Fatigue and damage tolerance issues of glare in aircraft structures,* International Journal of Fatigue **28**, 1116 (2006).

[16] G. Wilson, *Fatigue Crack Growth Prediction for generalized fiber metal laminates and hybrid materials*, Ph.D. thesis, Delft University of Technology, Delft (2013).

# 5

# Constraint approximation

*The previous chapters describe the prediction methods to be applied as evaluation criteria in the optimisation procedure. In this chapter, the process of approximating the FCI, FCP and RS prediction methods by means of regression analysis is described and their corresponding approximate function is given. The coefficients of this function is then found for GLARE 2, GLARE 4A and GLARE 4B laminates for a given design space and other design parameters. These functions with their coefficients replace the prediction methods in the optimisation procedure. This approach aims to speed up the optimisation process and solves specific issues with respect to the prediction method, which will be described in this chapter as well.*

## **5.1.** Introduction

The implementation of prediction methods as constraints in the optimisation procedure is very inefficient with respect to the computation time taken for optimisation. In this study, constraint approximations are considered to improve this computation time. With this approximation, the prediction methods are simplified to a single equation, where the coefficients of this equation represent the property of the lay-ups and the different input parameters of the methods. The process of obtaining the approximate function for the FCI, FCP and RS prediction methods is discussed in this chapter, and finally, the functions with their corresponding coefficients for GLARE are given. The approximate function is created by means of a regression analysis, which was performed on the models by analysing a database that contains fatigue or residual strength data for a range of lay-ups. A regression analysis is a statistical process for estimating the relationships among variables. This analysis helps, in this case, to understand how the fatigue life or residual strength of a laminate changes

when the lay-ups (and the applied stress) are varied, while the remaining variables (for example, the stress concentration factor, the stress ratio, the crack lengths, etcetera) are held constant. A database is created by running the prediction method for each design option (automated process). This database is later used to perform the regression analysis.

As told before, the main reason to replace the prediction models by approximations is that the evaluation of the design solutions using the FCP and RS prediction methods requires high computation time due to the many iterative calculations in the prediction methods. Additional reason for approximating the FCP prediction method is that the optimisation procedure combined with this prediction method encounters procedural errors when the laminate stress of the design solutions exceeds the yield strength in case high loads on thin laminates are applied [1]. The approximation function will resolve this problem, because the function will give a (not realistic) prediction and these design solutions are evaluated in the optimisation procedure. This way the optimisation procedure is not interrupted and these laminates are automatically excluded due to the high laminate stresses.



Next to this, the FCP prediction method is sometimes unable to predict the fatigue cycles of laminates with high metal sheet thickness ($t_m > 0.8$ mm) in combination of high stresses ($S_{\text{lam}} > 200$ MPa). When approximating, these data points are neglected and the function is obtained based on the available predictions. This way the approximation function will give a prediction for the design solutions based on interpolation between other predictions and assures that some lay-ups are not excluded in the optimisation procedure. The accuracy of the predictions of the missing points are assured, because the predictions are based on the trend laminates close to the laminate predicted. The reason that the prediction method is not giving a prediction has to do with the implementation of the prediction method rather than the validity of the method.

For the FCI prediction method, the constraint approximation is not necessary to speed up the optimisation procedure, because the optimisation procedure with the FCI prediction method is fast and the approximation did not significantly improve the computation time. The reason that the approximation of the FCI method is presented here is that this method initially was used to prove that the concept of approximation would work in terms of accuracy, because the time to construct the database was significantly lower compared to the FCP and RS prediction method.

The downside of using an approximation is that the database construction initially requires additional computation time, but once this database is obtained many optimisations can be performed at substantially less computation time. It is, therefore, important to define the design requirements properly prior to creating the approximate function to avoid the necessity to reconstruct databases. The approximate function has other benefits next to the improvement in computation time. For example, many prediction methods presented in the literature are not completely reproducible due to IP information that is not available.

Using approximate functions, properties can be predicted for FML without the need of implementing the prediction models itself. By all means within the validity and limitations of the prediction method which the function represents. Another benefit is that designers can replace the approximate function in the optimisation procedure with a function that relies on experimental data or curve fittings from experimental data, because the implementation of the optimisation procedure supports this in a similar way the approximate functions are implemented.

## **5.2.** Fatigue crack initiation

Wu et al. [2] stated that properties of FML lay-ups with the same MVF are not to be statistically different. This implies, for FCI criteria, that lay-ups with same MVF and same laminate stress will have the same internal stress, thus the same FCI life. However, this statement is only valid for lay-ups with the same grade. The MVF is related to the stress independent of the metal layer thickness $(t_m)$ or the metal layer number $(n_m)$. As long as the MVF is the same the $N_{\text{fci}}$ will be the same. If the grade is not the same, the laminate stress concentration factor $(K_{\text{FML}})$ will change together with the internal stress distribution due to the different fibre layer composition and this will result into a different relation between the MVF and the FCI life. For example, GLARE 2B will have the same MVF as GLARE 2A, but the fibres layers have a different influence on the internal stresses and thus resulting in different FCI predictions.



In Fig. 5.1, the fatigue life $(N_{\text{fci}})$ is plotted as function of the MVF for GLARE 2A laminates. In this figure, the statement of Wu et al. [2] is justified showing that no matter the number of layer or metal thickness is, the fatigue life is the same and showing a clear relationship between the MVF and the fatigue life.

There are two possibilities to create an approximate function for FCI. Either relating the MVF as parameter for the lay-up to the stress and fatigue life, or using the $n_m$ and $t_m$ as lay-up parameter. In previous work [3], the approximate function for FCI was created based on the MVF and the stress relation. Hereby, the created function had a high accuracy. However, for FCP and RS, the MVF is not directly correlated to FCP life $(N_{\text{fcp}})$ or residual strength $(S_{\text{rs}})$, because aspects like the number of interfaces also play a role in addition to the MVF of a lay-up. The approximate functions of FCP and RS, that will be discussed in the upcoming sections, are created using $n_m$ and $t_m$ as lay-up parameters. For consistency reasons, it is decided to take the same approach for FCI instead of the MVF as lay-up parameter.

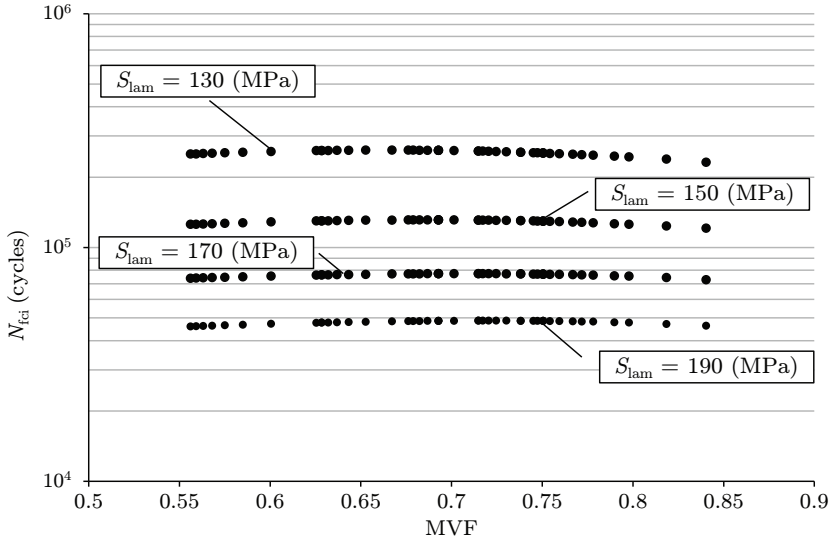


Figure 5.1: Fatigue crack initiation life ($N_{\text{fci}}$) as function of the metal volume fraction (MVF) for GLARE 2A with $K_t = 3.0$, $R = 0.05$ and prediction based on single S-N curve with $K_{t_{\text{S-N}}} = 2.0$ and $R_{\text{S-N}} = 0.0$ [4].

### **5.2.1.** Regression analysis

The regression analysis is started by selecting materials and setting constraints. It is chosen to use aluminium 2024-T3 and S2-glass fibre prepreg with FM94 adhesive as materials, because these materials are used in existing GLARE grades. The material properties are given in Table 2.2.

To present the approach a small range of lay-ups are chosen to obtain the approximate function. The metal thickness is hereby varied between $0.3$ and $0.9$ mm with steps of $0.1$ mm. The fibre ply thickness is selected as $0.133$ mm. The lay-up sequence is assumed to be constant and symmetric with $n_f = n_m - 1$ and $n_f = 2$ to $10$, according to the definition of GLARE 2A grades defined in Section 4.4.2. The prediction is based on a single S-N curve with $K_{t_{\text{S-N}}} = 2.0$ and $R_{\text{S-N}} = 0.0$ obtained from HSB 63111-01 [4]. The input parameters are summarised in Table 5.1.

The external laminate stress is applied in the longitudinal direction and all other applied stresses are assumed to be zero. The stress level is ideally varied between the fatigue limit stress and yield stress. Outside this region the FCI life will be infinite or the material will plastically deform. Beforehand it is not always known what this stress range will be and hence, predictions may result in the defined run-out value or no solution (NaN) is obtained.

| Constrained model variables | | |
|---|---|---|
| Stress concentration factor | $K_t$ | 3.0 |
| Stress ratio | $R$ | 0.05 |
| S-N curve stress concentration factor | $K_{t_{\text{S-N}}}$ | 2.0 |
| S-N data stress ratio | $R_{\text{S-N}}$ | 0.0 |
| Source S-N data: HSB Aluminium 2024-T3 [4] | | |
| **Free variables** | | |
| Laminate stress (MPa) | $S_{\text{lam}}$ | $130 - 200$ [step: 30] |
| Thickness of metal layer (mm) | $t_m$ | $0.3 - 0.9$ [step: 0.1] |
| Number of metal layers | $n_m$ | $2 - 10$ [step: 1] |
| **Constrained lay-up variables** | | |
| Number of fibre layers | $n_f$ | $n_m - 1$ |
| Thickness of fibre ply (mm) | $t_{\text{ply}}$ | 0.133 |
| Grade | | $(0,0)$ / GLARE 2A<br>$(0/90/0)$ / GLARE 4A<br>$(90/0/90)$ / GLARE 4B |

Table 5.1: Variables of the approximate function for fatigue crack initiation.

A loop is implemented around the prediction method with the aim creating a database that is used in further analysis. The applied laminate stress is varied between $130$ and $200$ MPa with steps of $10$ MPa and the range of lay-ups is also varied within the range of the number and thickness of metal layers. For each stress and lay-up combination, the FCI life $(N_{\text{fci}})$ was determined and stored in a database. The stored data is used to derive a relationship between the lay-up properties, applied stress and FCI life parameters. The NaN and fatigue limit (run-outs) solution influences the accuracy of the approximate functions, which is used to describe the centre section of a S-N curve. Therefore, the run-outs and NaN results are excluded and the function is created based on the trend of the centre part of the data set.

Fig. 5.2 shows the relationship between the FCI life $(N_{\text{fci}})$ and applied laminate stress $(S_{\text{lam}})$ for the different number of metal layers $(n_m)$ for $t_m = 0.6$ mm. The dataset follows a somewhat exponential trend, but there is no clear distinction between the lines to see the influence of $n_m$ on the FCI life. Similar graphs are obtained for other $t_m$. Taking the $\log_{10}$ of $N_{\text{fci}}$ and the $\ln$ of $S_{\text{lam}}$ and multiplying $\log_{10}(N_{\text{fci}})$ with $n_m$ will align the lines approximately parallel to each other. Each line is fitted with a linear function and the coefficients of these functions are linked to the corresponding $n_m$ value of the curves. This multiplication with $n_m$ assures that these coefficients will have a linear relationship with $n_m$, and therefore, it simplifies the process of obtaining the approximation with less coefficients as possible. If the multiplication was not performed, the coefficients would have to be fitted by a higher order function. Fig. 5.3 shows this relationship between the fatigue initiation life $n_m \cdot \log_{10}(N_{\text{fci}})$

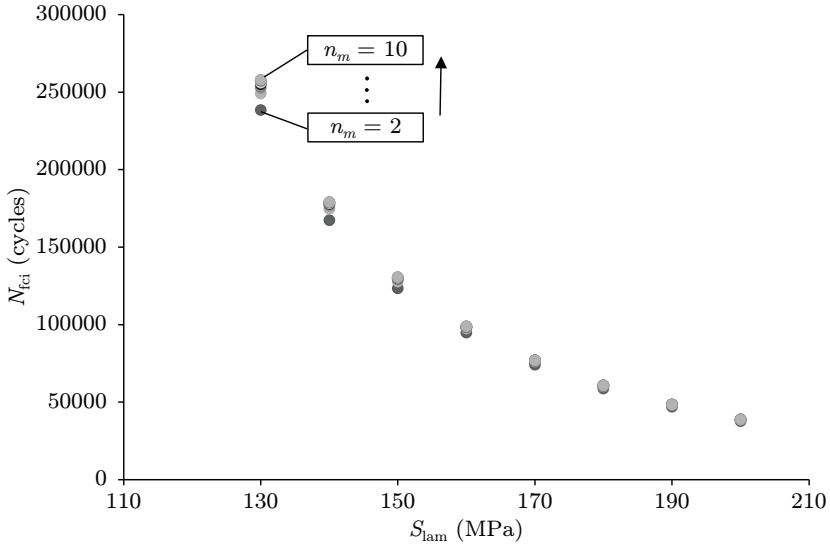


Figure 5.2: Data points of $N_{\text{fci}}$ plotted versus $S_{\text{lam}}$ for different $n_m$ at $t_m = 0.6$ mm.

and applied laminate stress ($S_{\text{lam}}$) for the $n_m$ range of $t_m = 0.6$ mm. There is thus a clear linear relationship, and these lines are described by the function in Eq. (5.1).

$$n_m \cdot \log_{10}(N_{\text{fci}}) = A_1 \cdot \ln(S_{\text{lam}}) + A_2 \tag{5.1}$$

In which coefficients $A_1$ and $A_2$ are a function of $n_m$ and are defined for each $t_m$. The process is repeated for other $t_m$ and the coefficients $A_1$ and $A_2$ are multiplied by the corresponding $t_m$, for the same reason as for $n_m$, which then results in a linear relationship. These relations between the $t_m \cdot A_1$ and $t_m \cdot A_2$-coefficients, and $n_m$ are shown in Fig. 5.4 and Fig. 5.5, respectively. These coefficients are described by a linear function, see Eq. (5.2) and Eq. (5.3). The linear curves are intersecting in one point on the y-axis ($n_m = 0$). For the presented case, the intersection point seems to be at the origin. However, for other design variables and grades, the intersection was at y-axis with larger distance from the origin. Therefore, the coefficient $a_1$ and $a_2$ are set to be constant instead of zero and are independent of $t_m$ due to this intersection at the y-axis.

$$t_m \cdot A_1 = B \cdot n_m + a_1 \tag{5.2}$$

$$t_m \cdot A_2 = C \cdot n_m + a_2 \tag{5.3}$$

To find the $a_1$ and $a_2$ coefficient, all function are separately fitted with a linear function and the average value of the second coefficients are determined. This averaged values are set to be equal to $a_1$ or $a_2$ and thus only the slope of the curves are considered as function

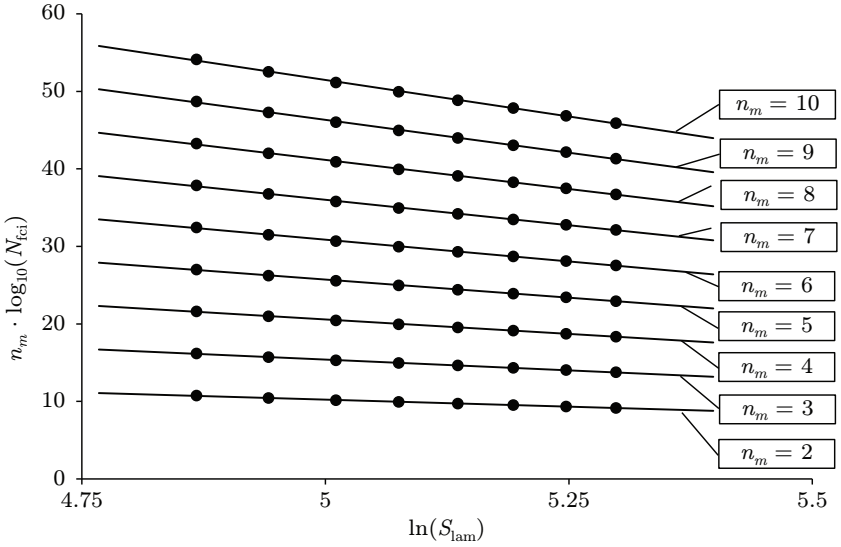


Figure 5.3: $n_m \cdot \log_{10}(N_{\text{fci}})$ as function of $\ln(S_{\text{lam}})$ for different $n_m$ at $t_m$ = 0.6 mm fitted with linear functions.

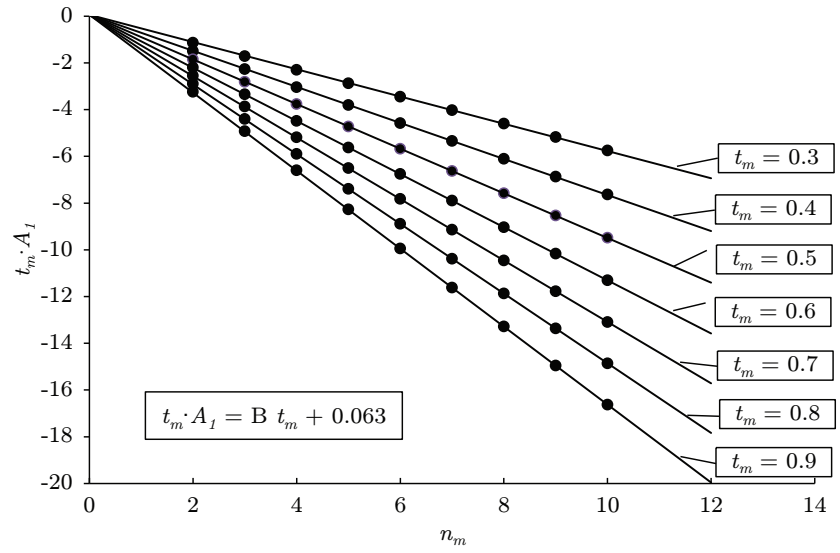


Figure 5.4: $A_1$-coefficient multiplied by the corresponding $t_m$ as function of $n_m$ for different $t_m$ fitted with linear functions with intersection at $(0, 0.063)$.

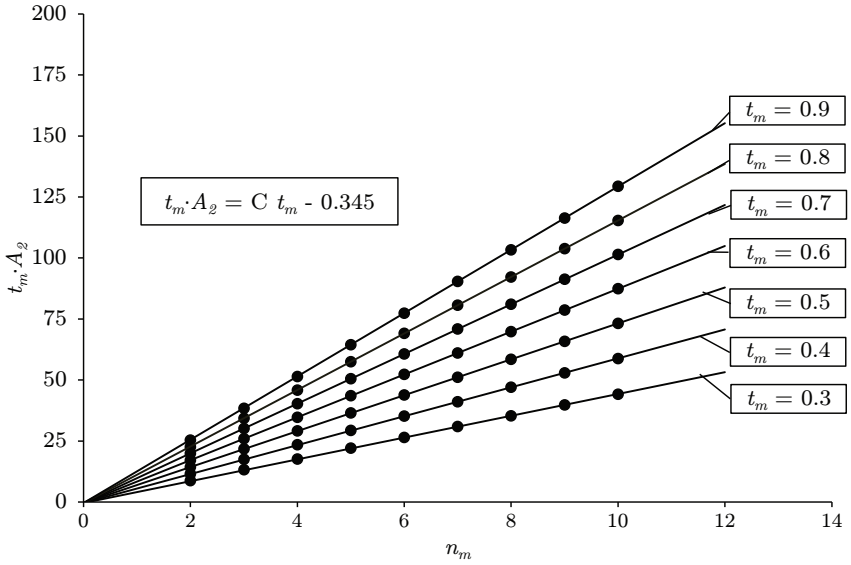


Figure 5.5: $A_2$-coefficient multiplied by the corresponding $t_m$ as function of $n_m$ for different $t_m$ fitted with linear functions with intersection at $(0, -0.345)$.

of $t_m$. Based on this averaged $a_1$ and $a_2$ value, the values of the $B$ and $C$ coefficients are redetermined. Both coefficients are then plotted against $t_m$ in Fig. 5.6 and 5.7, respectively. The linear relationships are described with:

$$B = b_1 t_m + b_2 \tag{5.4}$$

$$C = c_1 t_m + c_2 \tag{5.5}$$

In conclusion, a single relationship is created where $N_{\text{fci}}$ is written as a function of $S_{\text{lam}}$, $n_m$ and $t_m$.

$$\log_{10}(N_{\text{fci}}) = \frac{1}{n_m} \cdot \left[ \left( \frac{n_m}{t_m} (b_1 t_m + b_2) + a_1 \right) \ln (S_{\text{lam}}) + \left( \frac{n_m}{t_m} (c_1 t_m + c_2) + a_2 \right) \right] \tag{5.6}$$

The coefficients of the described case in Figs. 5.2 to 5.7 are summarised in Table 5.2.

| FCI function coefficients | | | | | |
|---|---|---|---|---|---|
| $a_1$ | 0.063 | $b_1$ | −1.804 | $c_1$ | 14.147 |
| $a_2$ | −0.345 | $b_2$ | −0.049 | $c_2$ | −0.258 |

Table 5.2: FCI function coefficients of GLARE 2A for the given case in Table 5.1 illustrated in Figs. 5.2 to 5.7.

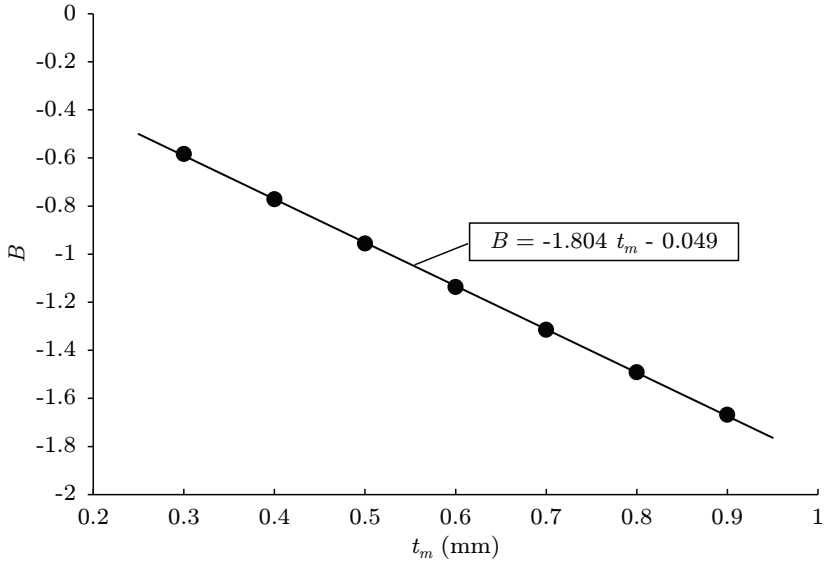


Figure 5.6: $B$-coefficient as function of $t_m$ fitted with a linear function.

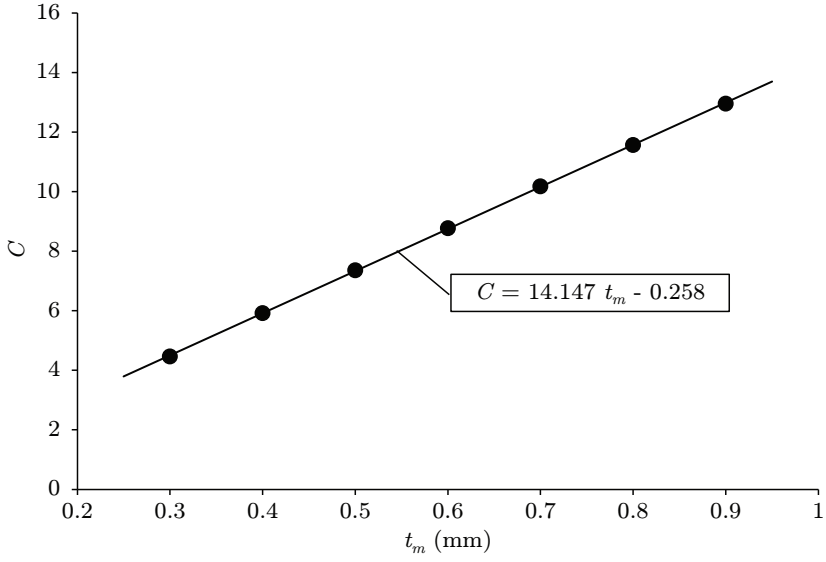


Figure 5.7: $C$-coefficient as function of $t_m$ fitted with a linear function.

For the optimisation procedure, the function coefficients for a crack initiation with stress concentration factor of $K_t = 3.0$, stress ratio $R = 0.05$ and prediction based on single S-N curve with $K_{t_{\text{S-N}}} = 2.0$ and $R_{\text{S-N}} = 0.0$ [4] for GLARE 2A, GLARE 4A and GLARE 4B and the *extended* design space of $n_m = 2 - 50$ layers and $t_m = 0.3 - 2.0$ mm are given in Table 5.3. In the optimisation procedure, the corresponding approximate functions are accessed when the lay-ups of the different grades are evaluated. The coefficients of GLARE 2A in Table 5.2 are slightly different than in Table 5.3, because of the increased design space. The approximate function is purely based on the trend between the prediction, increasing the design space makes sure that more points are fitted which in its turn makes the obtained relationship stronger.

| GLARE 2A | | GLARE 4A | | GLARE 4B | |
|---|---|---|---|---|---|
| $a_1$ | -0.141 | $a_1$ | 0.160 | $a_1$ | 0.144 |
| $a_2$ | 0.655 | $a_2$ | 0.672 | $a_2$ | -0.263 |
| $b_1$ | -1.761 | $b_1$ | -1.735 | $b_1$ | -2.155 |
| $b_2$ | -0.069 | $b_2$ | -0.156 | $b_2$ | -0.175 |
| $c_1$ | 13.868 | $c_1$ | 13.612 | $c_1$ | 15.48 |
| $c_2$ | 0.398 | $c_2$ | 0.649 | $c_2$ | 0.45 |

Table 5.3: FCI function coefficients with $K_t = 3.0$, $R = 0.05$ and prediction based on single S-N curve with $K_{t_{\text{S-N}}} = 2.0$ and $R_{\text{S-N}} = 0.0$ [4] for GLARE 2A, GLARE 4A and GLARE 4B and the extended design space of $n_m = 2 - 50$ and $t_m = 0.3 - 2.0$.

Due to the linear relationship of both the $n_m$ and $t_m$ parameters, it is expected that out-of-range lay-up prediction will result in a good accuracy, because the lay-ups are expected to follow the same linear trend. This statement is even strengthened when looking to the relation between the MVF and the FCI life. As long as, the laminates have the same grade and if the MVF matches, they will have the same cycles to initiation for the same applied stress. However, this is only assured for out-of-range lay-ups close the lay-up range of the approximate function. For other lay-ups the accuracy is not assured, because the fatigue behaviour of FML with high metal sheet thickness or high number of interfaces are not known or investigated.

### **5.2.2.** Verification

The approximate function is obtained for GLARE 2A, GLARE 4A and GLARE 4B and the function is verified with data points from the prediction method. There are three random verifications performed in which the laminate stress ($S_{\text{lam}}$), the metal layer thickness ($t_m$) or the number of metal layers ($n_m$) are varied for the different grades. The lines and their coefficients of determination ($R^2$) are given in Figs. 5.8, 5.9 and 5.10. In general, an accurate fit is obtained with a coefficient of determination between $R^2 \geq 0.804$ and $R^2 \leq 0.999$ for all grades.

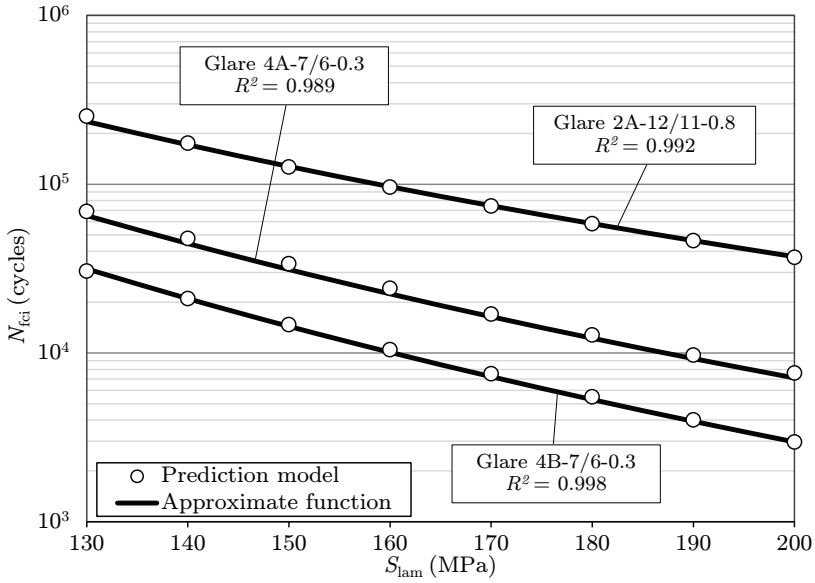


Figure 5.8: Verification of the approximate function of fatigue crack initiation with $K_t$ = 3.0, $R$ = 0.05, $K_{t_{\text{S-N}}}$ = 2.0 and $R_{\text{S-N}}$ for GLARE 2A-12/11-0.8, GLARE 4A-7/6-0.3 and GLARE 4B-7/6-0.3 for different $S_{\text{lam}}$.

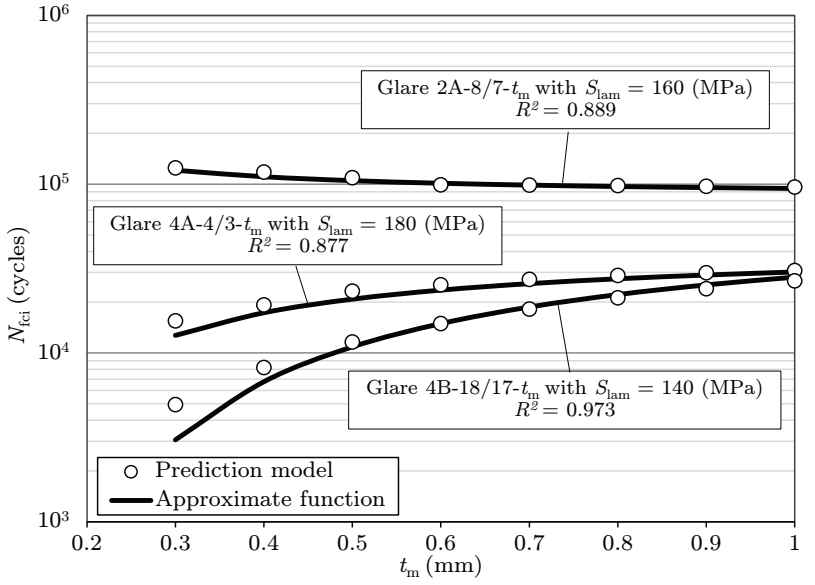


Figure 5.9: Verification of the approximate function of fatigue crack initiation with $K_t$ = 3.0, $R$ = 0.05, $K_{t_{\text{S-N}}}$ = 2.0 and $R_{\text{S-N}}$ for GLARE 2A-8/7-$t_m$ at 160 MPa, GLARE 4A-4/3-$t_m$ at 180 MPa and GLARE 4B-18/17-$t_m$ at 140 MPa for different $t_m$.

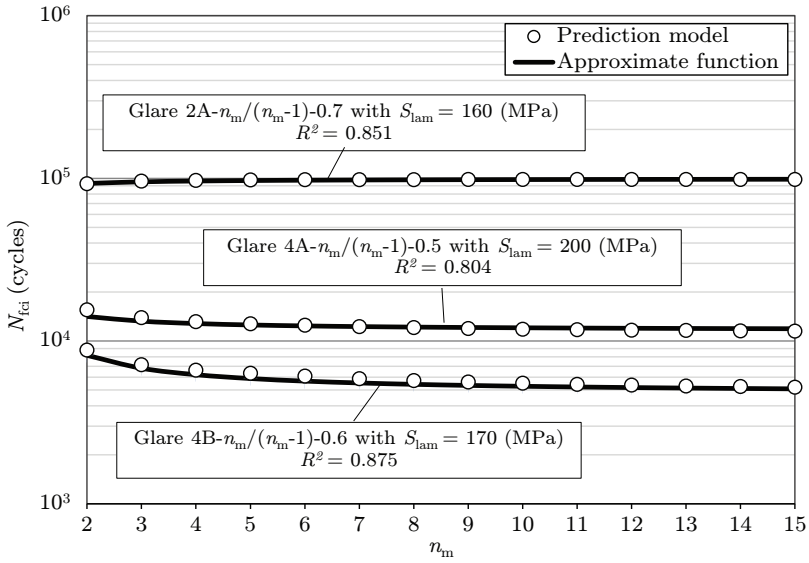


Figure 5.10: Verification of the approximate function of fatigue crack initiation with $K_t = 3.0$, $R = 0.05$, $K_{t_{S\text{-}N}} = 2.0$ and $R_{S\text{-}N}$ for GLARE 2A-$n_m/(n_m$-1)-0.7 at 160 MPa, GLARE 4A-$n_m/(n_m$-1)-0.5 at 200 MPa and GLARE 4B-$n_m/(n_m$-1)-0.6 at 170 MPa for different $n_m$.

## 5.3. Fatigue crack propagation

The design optimisation approach uses the FCP prediction model of Alderliesten, which is valid for symmetric lay-ups and longitudinal loads [5]. An approximation function is created for the FCP prediction by means of a regression analysis on a database that contains FCP data for different lay-up and applied stress combinations. The FCP data consist of the number of cycles ($N_{fcp}$) that takes to propagate the crack from the initial half crack length ($a_i$) to the critical half crack length ($a_c$). The initial half crack length is set as $a_i = 35$ mm and the critical half crack length as $a_c = 150$ mm in this particular situation and are kept constant next to the panel width ($W$), stress ratio ($R$) and other parameters related to the materials, such as the constituents properties which are given in Table 2.2. The Paris relation coefficients for crack growth and delamination are also given as input for the FCP prediction method. These coefficients are given Table 5.4 for GLARE.

To derive the approximate function, the GLARE 2A grade is again considered. The number of metal layers $n_m$ is varied between 2 and 10 layers and the thickness of the metal layers $t_m$ is varied between 0.3 and 0.7 mm. The applied laminate stress ($S_{lam}$) is also varied between 100 and 200 MPa. The constrained and the variable parameters are given in Table 5.5.

| Paris coefficients for GLARE | | |
|---|---|---|
| Crack growth Paris coefficient | $C_{cg}$ | $1.27 \cdot 10^{-11}$ |
| Crack growth Paris exponent | $n_{cg}$ | 2.94 |
| Delamination Paris coefficient | $C_d$ | 0.05 |
| Delamination Paris exponent | $n_d$ | 7.5 |

Table 5.4: Paris crack growth coefficients for GLARE [6] with $da/dN$ in mm/cycle and $K_{\text{eff}}$ in MPa$\sqrt{\text{mm}}$, and delamination coefficients for GLARE [7] with $db/dN$ in mm/cycle and $\sqrt{G_{\text{max}}} - \sqrt{G_{\text{min}}}$ in MPa·mm



| Constrained model variables | | |
|---|---|---|
| Half initial crack length (mm) | $a_i$ | 35 |
| Half critical crack length (mm) | $a_c$ | 150 |
| Stress ratio | $R$ | 0.05 |
| Width of specimen (mm) | $W$ | 600 |
| **Free variables** | | |
| Laminate stress (MPa) | $S_{\text{lam}}$ | $100 - 200$ [step: 10] |
| Thickness metal layer (mm) | $t_m$ | $0.3 - 0.7$ [step: 0.1] |
| Number metal layers | $n_m$ | $2 - 10$ [step: 1] |
| **Constrained lay-up variables** | | |
| Number fibre layers | $n_f$ | $n_m - 1$ |
| Thickness fibre ply (mm) | $t_{\text{ply}}$ | 0.133 |
| Grade | | $(0, 0)$ / GLARE 2A<br>$(0/90/0)$ / GLARE 4A<br>$(90/0/90)$ / GLARE 4B |

Table 5.5: Variables of the approximate function for fatigue crack propagation.

### **5.3.1.** Regression analysis

The approximate function is manually constructed by stepwise fitting a curve to the FCP data for a small range of lay-ups, in a similar analysis as was performed for FCI. The first step is creating a database of fatigue crack propagation life ($N_{\text{fcp}}$) by varying the applied laminate stress ($S_{\text{lam}}$) for different lay-ups. Fig. 5.11 is generated by plotting the $\log_{10}(N_{\text{fcp}})$ against $S_{\text{lam}}$ for variable $n_m$. The graph shows the cycles to propagation for GLARE 2A for an applied laminate stress between $S_{\text{lam}} = 100-200$ MPa, the number of metal layers is varied between $n_m = 2-10$ layers, and the thickness of metal layer is $t_m = 0.6$ mm. Similar graphs are also generated for other $t_m$ value.

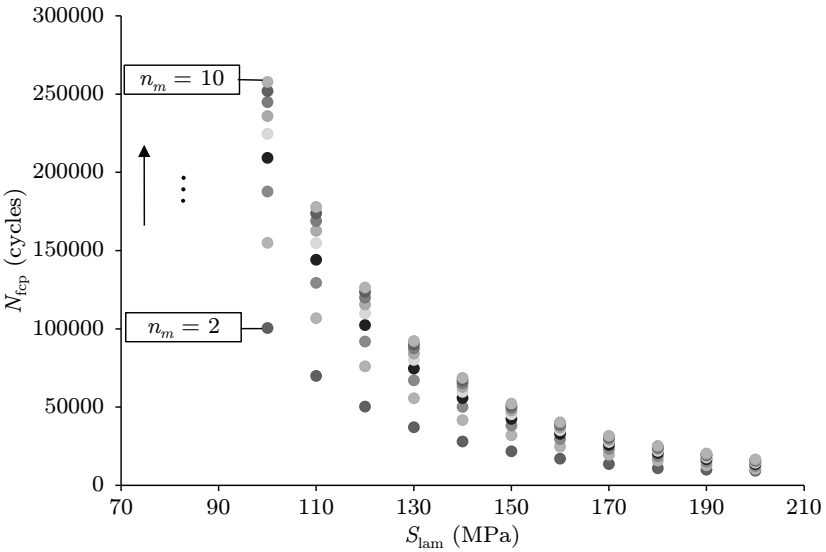


Figure 5.11: Data points of $N_{\text{fcp}}$ plotted versus $S_{\text{lam}}$ for different $n_m$ at $t_m = 0.6$ mm.

Next, the data points are structured to prepare for a good fit. As visible in Fig. 5.12, the $\log_{10}(N_{\text{fcp}})$ is multiplied by the corresponding $n_m$ to distantiate and align the curves with respect to each other. This is again done for the purpose of assuring a linear relationship between the coefficients of these curves. Furthermore, a natural logarithm of the $S_{\text{lam}}$ is taken, which makes these curves linear in log scale. The fit is described with the following equation:

$$n_m \cdot \log_{10} N_{\text{fcp}} = A_1 \cdot \ln(S_{\text{lam}}) + A_2 \tag{5.7}$$

The coefficient $A_1$ and $A_2$ of each curve is obtained for each $n_m$. This process is then repeated for all thicknesses in the range of $t_m = 0.3-0.7$ mm and the coefficients $A_1$ and $A_2$ are multiplied by the corresponding $t_m$, like the FCI analysis. This way the curves align with

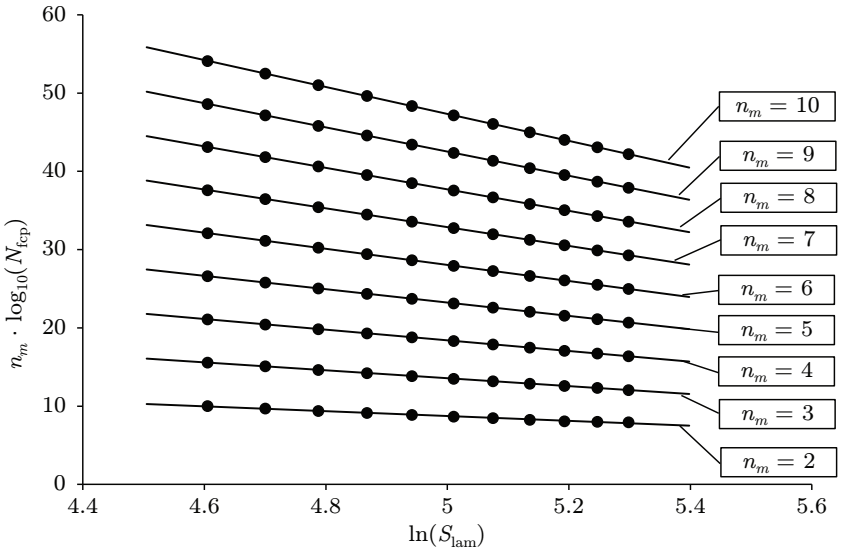


Figure 5.12: $n_m \cdot \log_{10}(N_{\text{fcp}})$ as function of $\ln(S_{\text{lam}})$ for different $n_m$ at $t_m = 0.6$ mm fitted with linear functions.

respect to each other and the coefficients will results in a linear relationship. These curves intersect at a point on the y-axis ($n_m = 0$), which is visible in Fig. 5.13 and 5.14, respectively for the two coefficients. The following equations are then used to describe these fits:

$$t_m \cdot A_1 = B \cdot n_m + a_1 \tag{5.8}$$

$$t_m \cdot A_2 = C \cdot n_m + a_2 \tag{5.9}$$

Looking at the graph of coefficient $A_1$ and $A_2$, only the slope $B$ and $C$ of the curves are changing depending on $t_m$. Therefore, the $a_1$ and $a_2$ coefficients are set to be constant as explained for the FCI case. The $B$ and $C$ coefficient are plotted against $t_m$ in Fig. 5.15 and 5.16.

As discussed before, the FCP model encounter a problem when a prediction is performed for laminates in combination of high thickness for the metal layers, low number of metal layers and high applied stress. The method is then unable to run, and gives no predictions in this specific situation. The relation between the coefficients and $t_m$ seems to be a linear fit according to Fig. 5.15 and 5.16. Increasing the thickness of the metal layer, neglecting the above described problem, and fitting the curves on the trend of the predictable results showed a stronger polynomial behaviour rather than a linear behaviour. For this reason, it is

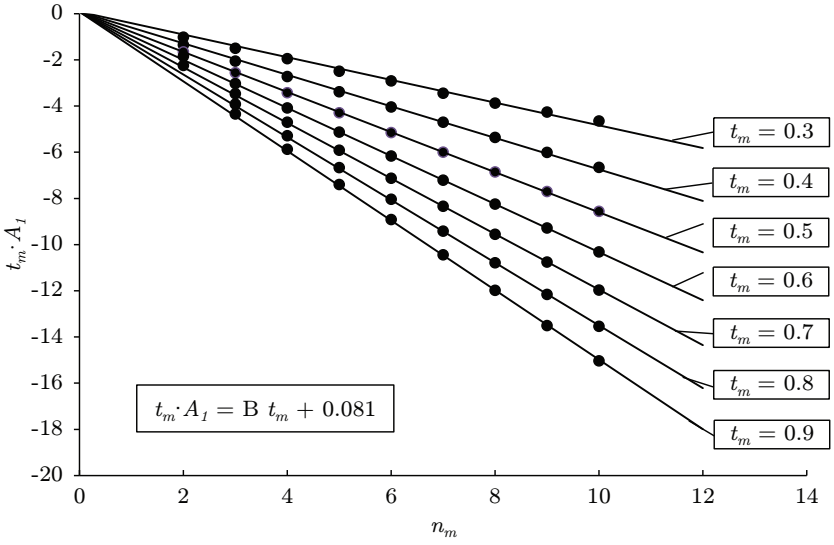


Figure 5.13: $A_1$-coefficient multiplied by the corresponding $t_m$ as function of $n_m$ for different $t_m$ fitted with linear functions with intersection at $(0, 0.026)$.

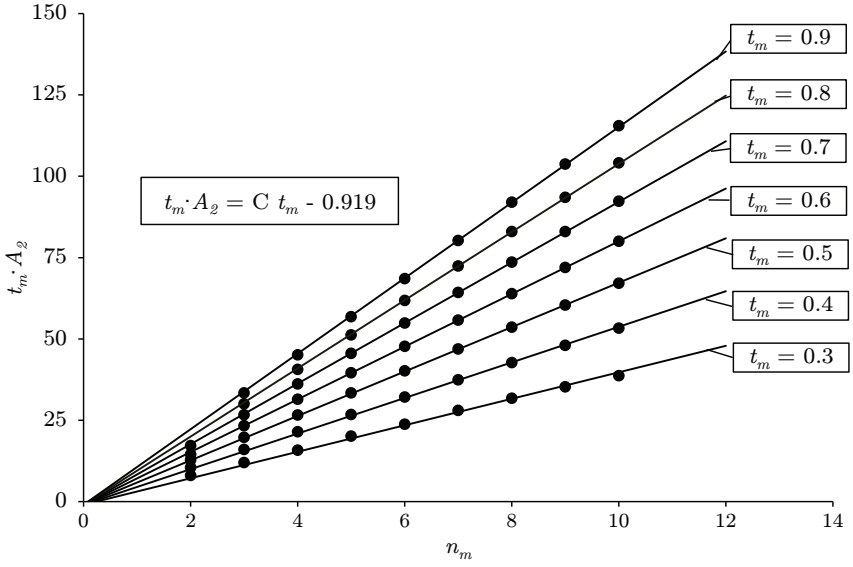


Figure 5.14: $A_2$-coefficient multiplied by the corresponding $t_m$ as function of $n_m$ for different $t_m$ fitted with linear functions with intersection at $(0, -0.578)$.

decided to approximate the coefficients with a second order polynomial function.

$$B = b_1 t_m^2 + b_2 t_m + b_3 \tag{5.10}$$

$$C = c_1 t_m^2 + c_2 t_m + c_3 \tag{5.11}$$

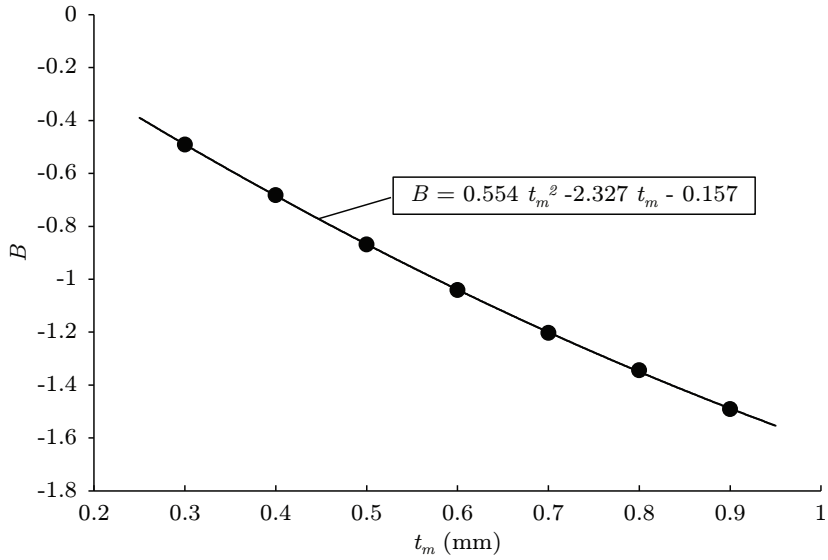


Figure 5.15: $B$-coefficient as function of $t_m$ fitted with a linear function.

Finally, the FCP approximate function is given by Eq. (5.12), which gives the fatigue life ($N_{\text{fcp}}$) as function of the laminate stress ($S_{\text{lam}}$), the number of metal layers ($n_m$) and the thickness ($t_m$) of metal layers.

$$\log_{10}(N_{\text{fcp}}) = \frac{1}{n_m} \cdot \left[ \left( \frac{n_m}{t_m} (b_1 t_m^2 + b_2 t_m + b_3) + a_1 \right) \ln(S_{\text{lam}}) + \left( \frac{n_m}{t_m} (c_1 t_m^2 + c_2 t_m + c_3) + a_2 \right) \right] \tag{5.12}$$

For the case presented in Figs. 5.11 to 5.16, the coefficients of the approximate functions are given in Table 5.6. The process is repeated for GLARE 2A, GLARE 4A and GLARE 4B, an extended design space of $n_m = 2-50$ layers and $t_m = 0.3-2.0$ mm, and an applied stress of $S_{\text{lam}} = 70-200$ MPa. The function coefficients for this design space with a crack propagation from half initial crack length of $a_i = 35$ mm until half critical crack length $a_c = 150$ mm are given in Table 5.7 per grade.

The approximate function is valid for $n_m \geq 2$. The relationship between $A_1 - A_2$ coefficients and $n_m$ is described by a linear curve and it is expected that lay-ups with higher $n_m$ will follow the same trend, but the accuracy of this extrapolation is not assured because again

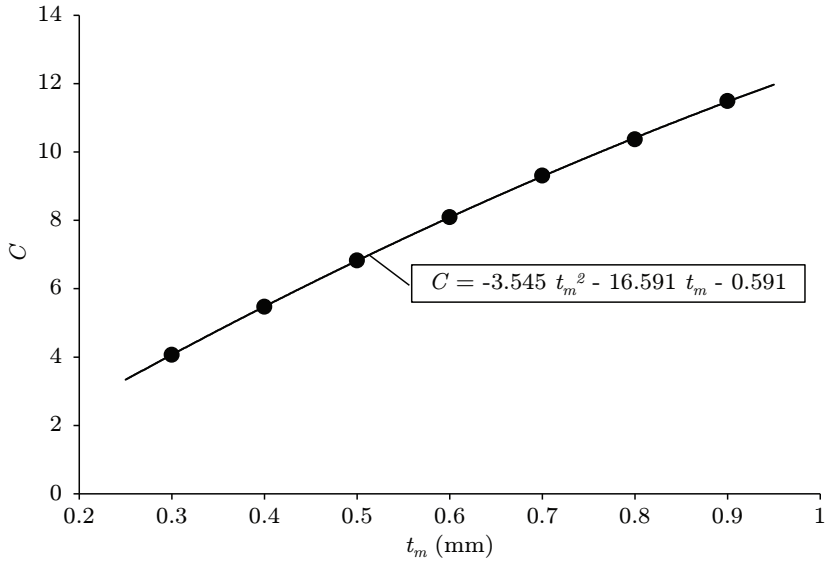


Figure 5.16: $C$-coefficient as function of $t_m$ fitted with a linear function.

| FCP function coefficients | | | | | |
|---|---|---|---|---|---|
| $a_1$ | 0.081 | $b_1$ | 0.554 | $c_1$ | −3.545 |
| $a_2$ | −0.919 | $b_2$ | −2.327 | $c_2$ | −16.591 |
| | | $b_3$ | −0.157 | $c_3$ | −0.591 |

Table 5.6: FCP function coefficients of GLARE 2A for the given case in Table 5.5 illustrated in Figs. 5.11 to 5.16.

the fatigue behaviour of these lay-ups are not investigated. Therefore, the function is limited valid for lay-ups with out-of-the-range layer numbers and the validity of the curve strongly depends on the validity of the prediction method as well.

The trend for thicker metal sheets is observed to be a second order polynomial. However, the cracking mechanism for thick sheet might work different and the material could behave different. The considered FCP method is not validated for these high sheet thicknesses, meaning that unreliable results are probably generated. Therefore, the trend for high metal layer thickness might be linear, but more research on thick FML solutions is required to prove this behaviour. In case of layer thickness, only values within the range should be considered, because the influence of $t_m$ cannot be predicted outside the range due to the non-linear effects, unless it is accounted for.

| GLARE 2A | | GLARE 4A | | GLARE 4B | |
|---|---|---|---|---|---|
| $a_1$ | $-0.136$ | $a_1$ | $-0.044$ | $a_1$ | $0.271$ |
| $a_2$ | $0.179$ | $a_2$ | $-0.211$ | $a_2$ | $-1.583$ |
| $b_1$ | $1.983$ | $b_1$ | $1.168$ | $b_1$ | $0.248$ |
| $b_2$ | $-4.592$ | $b_2$ | $-3.347$ | $b_2$ | $-1.848$ |
| $b_3$ | $1.001$ | $b_4$ | $0.544$ | $b_4$ | $-0.010$ |
| $c_1$ | $-10.682$ | $c_1$ | $-6.351$ | $c_1$ | $-1.432$ |
| $c_2$ | $28.115$ | $c_2$ | $21.473$ | $c_2$ | $13.391$ |
| $c_3$ | $-4.951$ | $c_3$ | $-2.603$ | $c_3$ | $0.168$ |

Table 5.7: FCP function coefficients from a half initial crack length of $a_i = 35$ mm until a half critical crack length $a_c = 150$ mm for GLARE 2A, GLARE 4A and GLARE 4B and the extended design space of $n_m = 2 - 50$ layers and $t_m = 0.3 - 2.0$ mm, and applied stress of $S_{\text{lam}} = 70 - 200$ MPa

### **5.3.2.** Verification



The approximate function is obtained for GLARE 2A, GLARE 4A and GLARE 4B and the function is verified with the prediction method. There are three random verifications performed in which the laminate stress ($S_{\text{lam}}$), the metal layer thickness ($t_m$) or the number of metal layers ($n_m$) are varied for the different grades. The lines and their coefficients of determination ($R^2$) are given in Figs. 5.17, 5.18 and 5.19. In general, an almost perfect fit is obtained with a coefficient of determination between $R^2 \geq 0.834$ and $R^2 \leq 1$ for all grades. The accuracy is very high in all cases and not related to the lay-up, but rather to the used function to fit the data. The lower accuracy of $R^2 = 0.834$ for GLARE 4B-$n_m$/($n_m$-1)-0.4 is due to the lower applied stress. At low stress, the fatigue life is very high and any small fluctuation on exponential scale influences the accuracy. The accuracy might change slightly if the validity range of the curve is changed, but in all cases the obtained accuracy is high enough to replace the prediction method.

### **5.3.3.** Influence on property

A good impression of the fatigue crack propagation behaviour of the laminates is given in Figs 5.17, 5.18 and 5.19 when the laminate stress ($S_{\text{lam}}$) or the lay-ups parameters ($n_m$ or $t_m$) are changed. In Fig. 5.17, it is visible that increasing $S_{\text{lam}}$ decreases the fatigue crack propagation life ($N_{\text{fcp}}$) of the laminates. In Fig. 5.18, it is observed that increasing $t_m$ decreases $N_{\text{fcp}}$. This is due to the metal volume fraction (MVF) increase and the simultaneous decrease of the fibre volume fraction (FVF) caused by the increasing $t_m$. The decrease of FVF means that there are less fibres for fibre bridging and thus more load has to be carried over the metal layers, which then causes the $N_{\text{fcp}}$ to decrease. In Fig. 5.19, the opposite behaviour is visible when the number of metal layers ($n_m$) are increased. The increase of

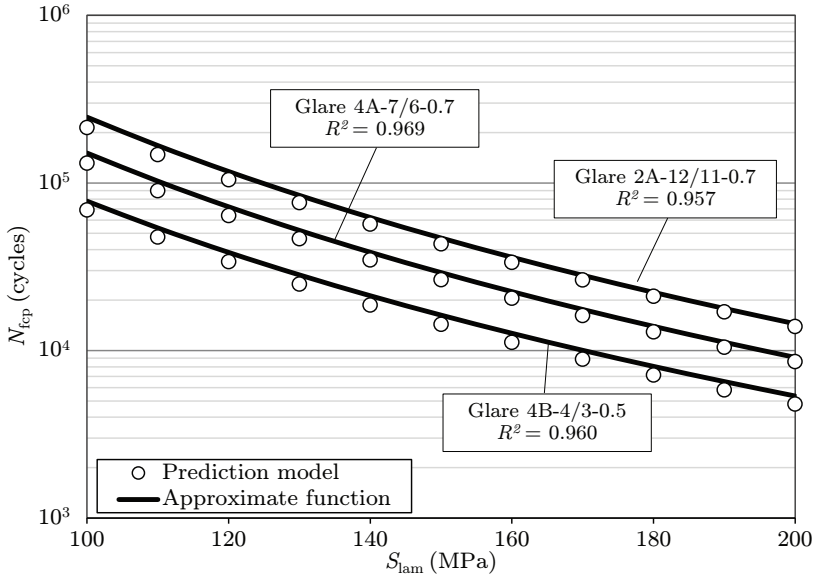


Figure 5.17: Verification of the approximate function of fatigue crack propagation from a crack length of $a_i$ = 35 mm until $a_c$ = 150 mm for GLARE 2A-12/11-0.7, GLARE 4A-7/6-0.7 and GLARE 4B-4/3-0.5 for different $S_{lam}$.

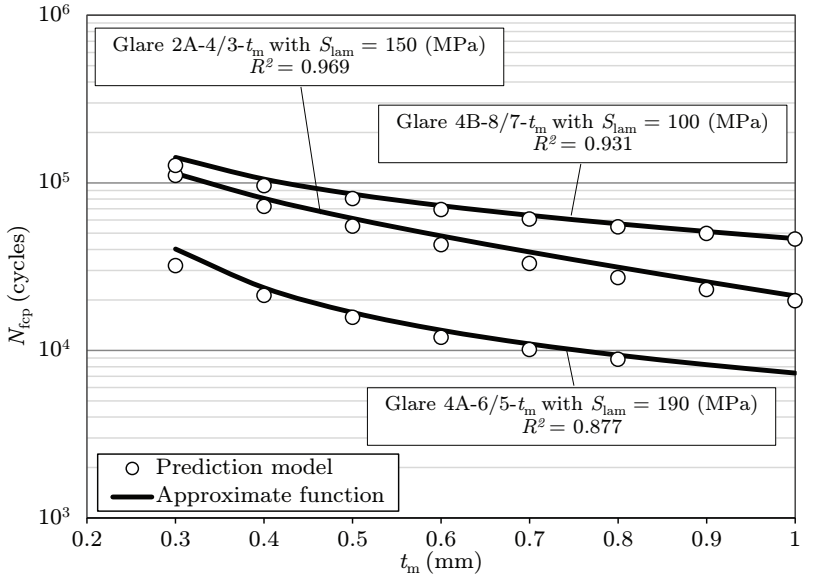


Figure 5.18: Verification of the approximate function of fatigue crack propagation from a crack length of $a_i$ = 35 mm until $a_c$ = 150 mm for GLARE 2A-4/3-$t_m$ at 150 MPa, GLARE 4A-6/5-$t_m$ at 190 MPa and GLARE 4B-8/7-$t_m$ at 100 MPa for different $t_m$.

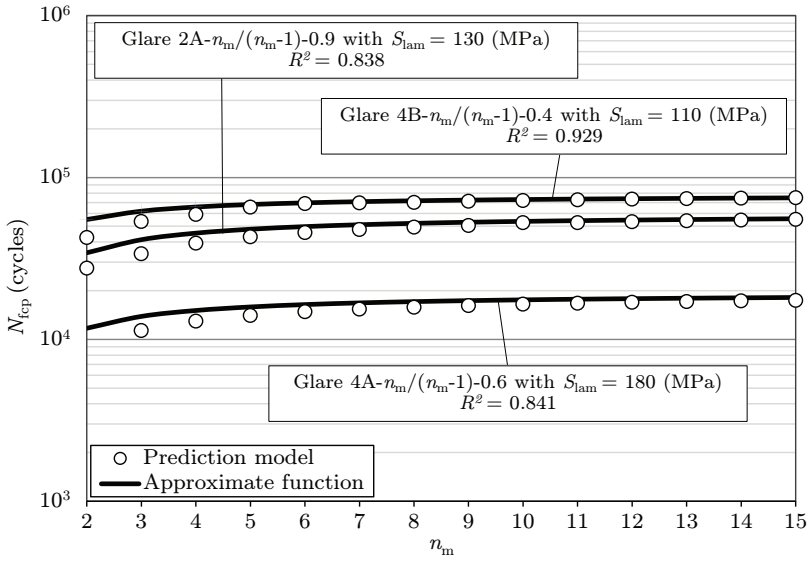


Figure 5.19: Verification of the approximate function of fatigue crack propagation from a crack length of $a_i$ = 35 mm until $a_c$ = 150 mm for GLARE 2A-$n_m/(n_m$-1)-0.9 at 130 MPa, GLARE 4A-$n_m/(n_m$-1)-0.6 at 180 MPa and GLARE 4B-$n_m/(n_m$-1)-0.4 at 110 MPa for different $n_m$.

$n_m$ automatically means the increase of the number of fibre layers ($n_f$) and a slight increase of FVF. Therefore, slightly more fibre bridging is observed and this improves the $N_{fcp}$.

## 5.4. Residual strength

A similar analysis was performed for the residual strength prediction model of Rodi [8]. The residual strength is defined as the load that a laminate can carry without failing in case of crack or damage. This value depends on the crack length and the lay-up. The model requires the crack dimensions and material properties as input. The lay-up parameters are the only variable in this analysis. The regression analysis is performed for the residual strength data generated from the parameters in Tables 2.2 and 5.8.

### 5.4.1. Regression analysis

First, the residual strength ($S_{rs}$) data is plotted against $t_m$ for each $n_m$ in Fig. 5.20. Visually in the graph, these data points overlap each other, making it difficult to observe a trend between the lay-up parameters and the residual strength. The dataset is further analysed and found that multiplying the $S_{rs}$ with $n_m$ results in a linear relationship between $n_m \cdot S_{rs}$ and the natural logarithm of the thickness ($\ln t_m$) as can be seen Fig. 5.21. The multiplication

| Constrained model variables | | |
|---|---|---|
| Half critical crack length (mm) | $a_c$ | 150 |
| Initial applied load (N) | $P$ | 10,000 |
| Fibre ultimate strain (%) | $\epsilon_{ult}$ | 0.45 |
| Width of specimen (mm) | $W$ | 600 |
| Length of specimen (mm) | $L$ | 600 |
| **Free variables** | | |
| Thickness metal layer (mm) | $t_m$ | 0.3 – 0.9 [step: 0.1 ] |
| Number metal layers | $n_m$ | 2 – 10 [step: 1] |
| **Constrained lay-up variables** | | |
| Number fibre layers | $n_f$ | $n_m - 1$ |
| Thickness fibre ply (mm) | $t_{\text{ply}}$ | 0.133 |
| Grade | | $(0,0)$ / GLARE 2A<br>$(0/90/0)$ / GLARE 4A<br>$(90/0/90)$ / GLARE 4B |

Table 5.8: Variables of the approximate function for residual strength.

assures that coefficients of this function form a linear relationship with $n_m$.

In a similar way as for the FCI and FCP analysis, the curves are fitted with the following function:

$$n_m \cdot S_{\text{rs}} = A \ln(t_m) + B \tag{5.13}$$

Plotting the coefficient against the corresponding $n_m$ gives the linear relationship as illustrated in Fig. 5.22 and 5.23, respectively for the $A$ and $B$ coefficients. These coefficients are consequently described with the following linear equations.

$$A = a_1 n_m + a_2 \tag{5.14}$$

$$B = b_1 n_m + b_2 \tag{5.15}$$

As a result, the equation is simplified to Eq. (5.16) that describes the residual strength $(S_{\text{rs}})$ as function of the number $(n_m)$ and thickness $(t_m)$ of metal layers.

$$S_{\text{rs}} = \frac{(a_1 n_m + a_2)\ln(t_m) + b_1 n_m + b_2}{n_m} \tag{5.16}$$

For the cases described in Figs. 5.20 to 5.23, the coefficients of the approximate functions are given in Table 5.9.

This approximation function for RS also describes the relationship per grade. The function coefficients for GLARE 2A, GLARE 4A and GLARE 4B with an extended design space of $n_m$ =

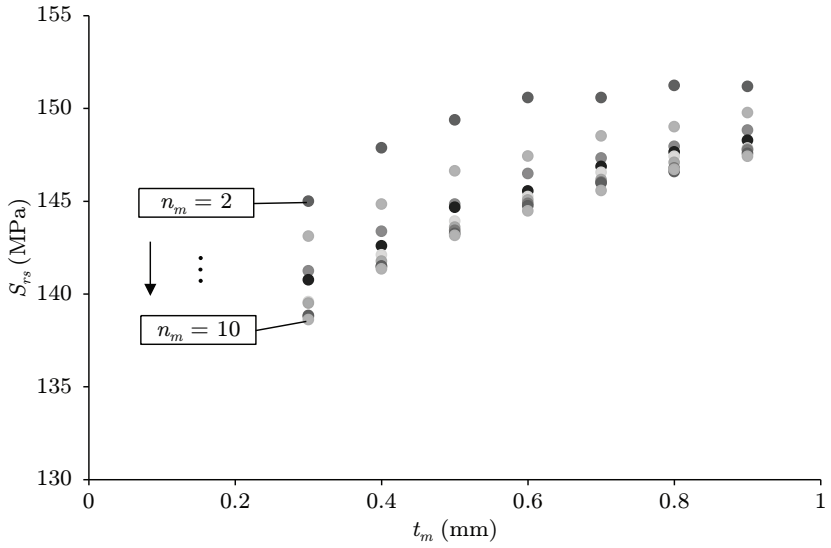


Figure 5.20: Data points of $S_{\text{rs}}$ plotted versus $t_m$ for different $n_m$.

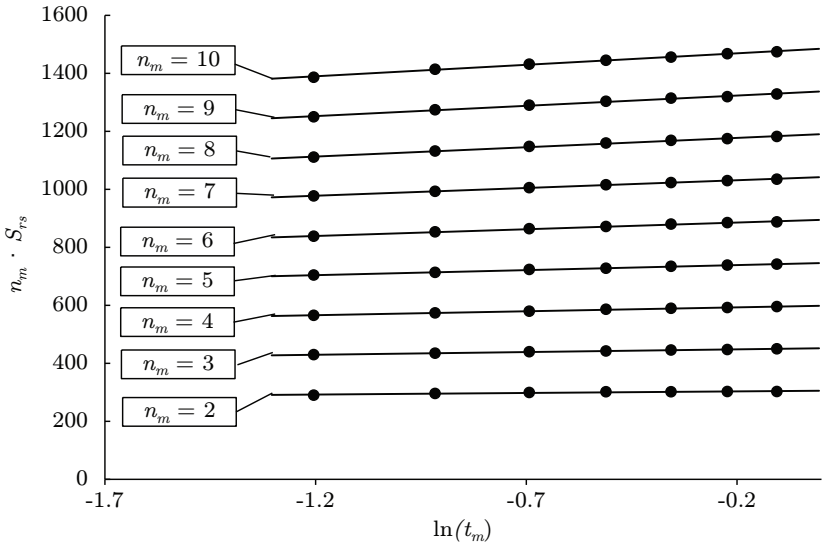


Figure 5.21: $n_m \cdot S_{\text{rs}}$ as function of $\ln(t_m)$ for different $n_m$ fitted with linear functions.

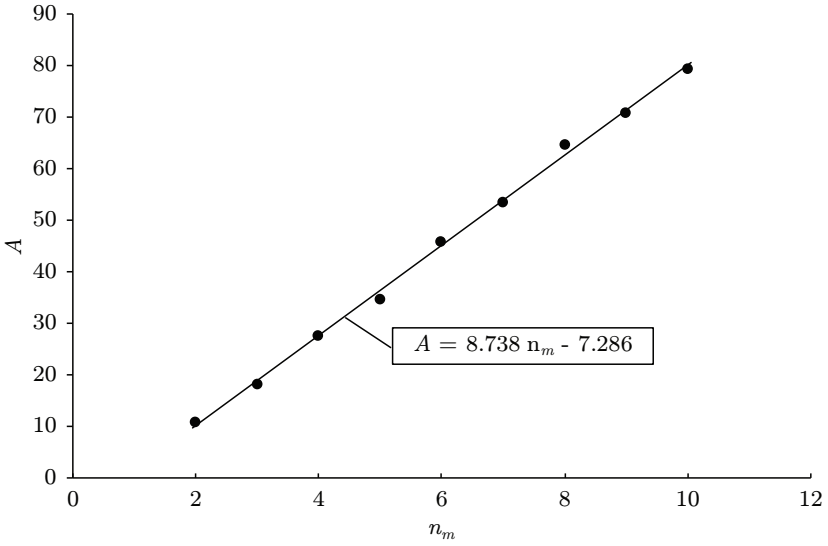


Figure 5.22: $A$-coefficient as function of $t_m$ fitted with a linear function.

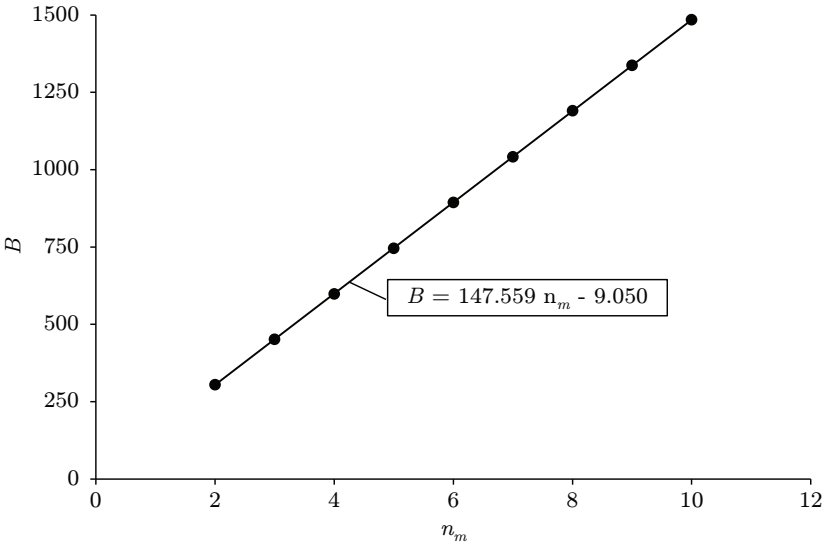


Figure 5.23: $B$-coefficient as function of $t_m$ fitted with a linear function.

| RS function coefficients | | | |
|---|---|---|---|
| $a_1$ | 8.738 | $b_1$ | 147.559 |
| $a_2$ | −7.286 | $b_2$ | 9.050 |

Table 5.9: RS function coefficients of GLARE 2A for the given case in Table 5.8 illustrated in Figs. 5.20 to 5.23.

| GLARE 2A | | GLARE 4A | | GLARE 4B | |
|---|---|---|---|---|---|
| $a_1$ | 7.104 | $a_1$ | 16.543 | $a_1$ | 24.822 |
| $a_2$ | −8.081 | $a_2$ | −10.611 | $a_2$ | −14.365 |
| $b_1$ | 146.512 | $b_1$ | 132.151 | $b_1$ | 120.596 |
| $b_2$ | 9.856 | $b_2$ | 19.578 | $b_2$ | 28.110 |

Table 5.10: RS function coefficients for a half initial crack length of $a_c = 150$ mm, GLARE 2A, GLARE 4A and GLARE 4B, and the extended space of $n_m = 2 - 50$ layers and $t_m = 0.3 - 2.0$ mm.



$2 - 50$ layers and $t_m = 0.3 - 2.0$ mm are given in Table 5.10. These coefficients will be used in the upcoming chapters for the optimisation cases.

The trend of a linear relationship is the same when the design range values of $n_m$ and $t_m$ are increased. This means a larger design space does not necessary change the obtained fit and an approximate function obtained by a smaller design space would still give accurate prediction for lay-ups that are out-of-range. This implies only for same grade lay-ups. But again, the extrapolation of the approximation function is not infinitely and at some points the failure mechanism of thick FML might work differently, meaning that either the approximate curve nor the prediction methods will give accurate results.

### **5.4.2.** Verification

The approximate function for residual strength is also verified with the prediction method obtained for GLARE 2A, GLARE 4A and GLARE 4B. There are two random verifications performed in which the metal layer thickness ($t_m$) or the number of metal layers ($n_m$) are varied for different grades. The lines and their coefficients of determination ($R^2$) are given in Figs. 5.24 and 5.25. In this case as well, a good fit is obtained with a coefficient of determination $0.832 \leq R^2 \leq 0.988$ for the residual strength function.

### **5.4.3.** Influence on property

In Fig. 5.24 and 5.25, a good impression is given on the residual strength behaviour if the lay-up parameters are changed. The opposite is observed for the residual strength behaviour

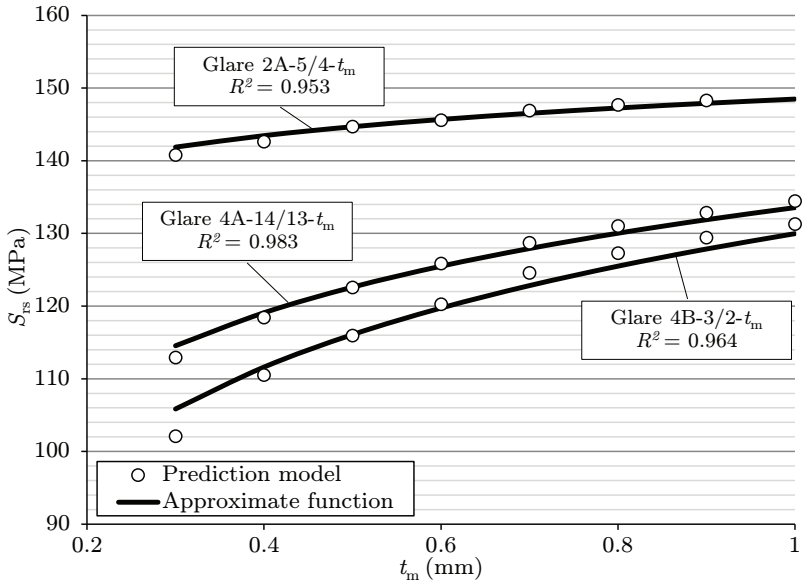


Figure 5.24: Verification of the approximate function of residual strength with an initial crack length of $a_c$ = 150 mm for GLARE 2A-5/4-$t_m$, GLARE 4A-14/13-$t_m$ and GLARE 4B-3/2-$t_m$ for different $t_m$.

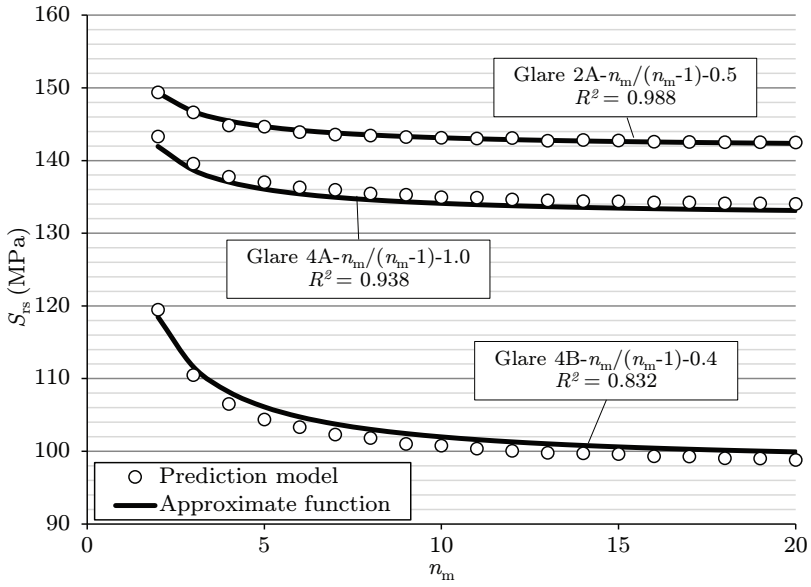


Figure 5.25: Verification of the approximate function of residual strength with an initial crack length of $a_c$ = 150 mm for GLARE 2A-$n_m/(n_m$-1)-0.5, GLARE 4A-$n_m/(n_m$-1)-1.0 and GLARE 4B-$n_m/(n_m$-1)-0.4 for different $n_m$.

compared to fatigue crack propagation, because a through-the-thickness crack scenario is assumed. In this crack scenario, it is assumed that the fibres directly fail along the crack without fibre bridging. Therefore, the metal layers are obliged to carry all the remaining loads of the structure, and therefore, it is thus beneficial to have less fibres and more metal in the laminate. Increasing $t_m$ (and thus MVF) increases the load carrying capabilities of the metal layers, which then improves the residual strength ($S_{\text{rs}}$) of the laminate, as can be seen in Fig. 5.24. Finally, in Fig. 5.25, it is visible that increasing $n_m$ (and thus FVF), decreases $S_{\text{rs}}$ for the same reason, but then the other way around.

## **5.5.** Conclusions

The approximate functions for the FCI, FCP and RS methods are obtained by means of regression analysis. The thickness and number of metal layers were used as input parameters for the lay-up. In case of FCI and FCP, the applied stress plays a role as design parameter, because it interacts with the running load and the laminate thickness. For this reason, the applied laminate stress is included in FCI and FCP approximate functions. The functions were defined per grade, because with the different fibre layer compositions no correlations was possible to link the different grades to each other. This way for each grade a separate function is obtained and in the optimisation routine to corresponding function is used to evaluate the lay-ups. Selecting a large lay-up range for the approximate function generally creates a better fit based on the trends, but for individual predictions more deviated predictions were obtained with sometimes less accurate predictions due to the influence of the logarithmic scale. In contrary, selecting a small lay-up range gives better predictions for the individual lay-ups. The functions replace the prediction methods with high $R^2$ and improved the computation time immensely, a comparison study is performed in Section 6.4. For the FCI prediction method, the approximate function does not have any significant time improvement. Therefore, it is advised to use the prediction method instead of the approximate function to assure high accuracy predictions.



## References

[1] I. Şen, R. Alderliesten, and R. Benedictus, *Approximate function for fatigue crack propagation in a design optimisation procedure for fibre metal laminates,* in *29th Congress of the International Council of the Aeronautical Sciences* (2014).

[2] H. Wu, L. Wu, W. Slagter, and J. Verolme, *Use of rule of mixtures and metal volume fraction for mechanical property predictions of fibre-reinforced aluminium laminates,* Journal of Material Science **29**, 4583 (1994).

[3] I. Şen, G. Delgrange, R. Alderliesten, and R. Benedictus, *Design optimization approach*

*for crack initiation in fml structures,* in *ICAF 2013 Symposium*, Vol. 2, edited by A. Brot (Paragon Israel - Dan Knassim Ltd., 2013).

[4] V. Hoang and L. Schwarmann, *Handbuch Struktur Berechnung (HSB), 63111-01 issue D: Zeitfestigkeit 3.1354 T3*, Tech. Rep. (1986).

[5] R. Alderliesten, *Analytical prediction model for fatigue crack propagation and delamination growth in glare,* International Journal of Fatigue **29**, 628 (2007).

[6] J. Homan, *Crack growth properties of thin aluminum sheets at various temperatures,* (2002), report B2V-02-39.

[7] R. Alderliesten, J. Schijve, and S. Zwaag, van der, *Application of the energy release rate approach for delamination growth in glare,* Engineering Fracture Mechanics **73**, 697 (2006).

[8] R. Rodi, *Residual strength in Fibre Metal Laminates*, Ph.D. thesis, Delft University of Technology, Delft (2012).

# 6

# Lay-up optimisation

*The procedure the design optimisation method was introduced in Chapter 4 and the approximations for the F&DT criteria were derived in Chapter 5. As a next step, the results and methodology of the (element) lay-up optimisation are presented and the important aspects influencing the design solutions are discussed in this chapter. First, by presenting a design case for the FCI criteria, the influence of the genetic algorithm settings are discussed. Next, the use of different S-N curves is explained with respect to the accuracy of the predictions and their influence on the design solutions. Additionally, a comparison is made between the approximate functions and the prediction methods for the FCP and RS criteria with respect to the prediction accuracy and the computation time. Finally, the influence of multi-criteria optimisation on the selection of design solutions is discussed for a given test case.*

## **6.1.** Introduction

The optimisation procedure consists of two types of optimisations: element and cross-section. In this chapter, the methodology of the element optimisation procedure is presented. The procedure is capable of finding a lowest weight solution which satisfies the F&DT requirement inside the defined design space. The design procedure is discussed with respect to accuracy, sensitivity and robustness of the model to ensure an appropriate design solution is obtained.

The result of being selected as an optimal design solution is effected by three conditions:

1. Being generated as a solution in the search procedure,

2. the predicted property of this solution,
3. and its satisfaction to the design requirement.

The first condition depends mainly on the settings used for GA. The influence of the settings will be discussed with respect to the FCI criteria in Section 6.2. The second condition relates to the output and accuracy of the prediction method and the fitness approximation used for the lay-up evaluation. Aspects concerning accuracy of S-N curves in the FCI method are discussed in Section 6.3 and the constraint approximations for FCP and RS methods are discussed in Section 6.4. The third condition is discussed by performing an analysis, where the influence of single and multi-criteria are shown on the design space in Section 6.5.

## **6.2.** Influence of GA settings

GA is a stochastic algorithm which means that it generates and uses random variables that result in coded strings representing FML lay-ups. The risk of this approach is that the *actual* optimal lay-up might not be found, simply because it is not generated and evaluated during the search procedure. The robustness of the search procedure depends on the setting of the GA function. These settings include parameters to control the genetic operators, like the probability to perform a crossover or mutation, the population size, the percentage of the generation that will migrate to the next generation, or the selection strategy. Incorrect selection of these parameters could lead to an incomplete exploration of the design space, and therefore, a different *optimal* solution will be obtained every time when the optimisation procedure is repeated. Tuning these settings will lead to a better design space exploration in which the best available solution is generated with high probability. This way the model will become more robust.



| | De Jong | Grefenstette 1 | Grefenstette 2 |
|---|---|---|---|
| Population size | 50 | 30 | 80 |
| Probability of crossover | 0.6 | 0.95 | 0.45 |
| Probability of mutation | 0.001 | 0.01 | 0.01 |
| Generation gap | 1 | 1 | 0.9 |
| Selection strategy | Elitist | Elitist | Non elitist |

Table 6.1: Settings for genetic algorithm: De Jong [1] and Grefenstette [2].

In the literature many settings are given that could be used for GA, e.g. settings proposed by De Jong [1], Grefenstette [2], and Eiben and Smit [3]. In order to show the impact of the GA settings on the output of the optimisation procedure, an analysis is performed for three settings to compare the performance and reliability. The three selected settings are listed in Table 6.1.

| Input | | Design range | Case 1 | Case 2 |
|---|---|---|---|---|
| $P$ (N/mm) | 1000 | Grade | GLARE 2A | GLARE 2A / 2B / 3 / 4A / 4B |
| $N_{\text{req}_{\text{fci}}}$ (cycles) | 20,000 | $n_m$ | $2-50$ | $2-50$ |
| $K_{t_{\text{S-N}}}$ | 2.7 | $t_m$ (mm) | $0.2-1.0$ | $0.2-1.0$ |
| $R$ | 0.05 | $t_{\text{ply}}$ (mm) | 0.133 | 0.133 |

Table 6.2: Design case to compare the influence of optimisation settings.

The optimal solution in all three design spaces is GLARE 2A-10/9-0.2. This solution is obtained by manually predicting the fatigue life for each solution and determining their corresponding weight. But this solution was not always found in the optimisation procedure. In fact, other optimal solutions were found when repeating the optimisation. In Fig. 6.1 and Fig. 6.2, the obtained solutions together with the number of appearances for Case 1 and 2 are given for the three settings of Table 6.1. The parameters for the design cases are given in Table 6.2. In Case 1 with a limited design space, the settings of De Jong and Grefenstette 2 gave in all situations the same optimal solution. Only Grefenstette 1 had a success rate of 83%. In Case 2, the setting given by De Jong had a success rate of 94% and the two settings of Grefenstette had a success rate of 51% and 100%, respectively. In these particular cases, Grefenstette 2 would assure that the best solution that exist in the two design spaces is always found.



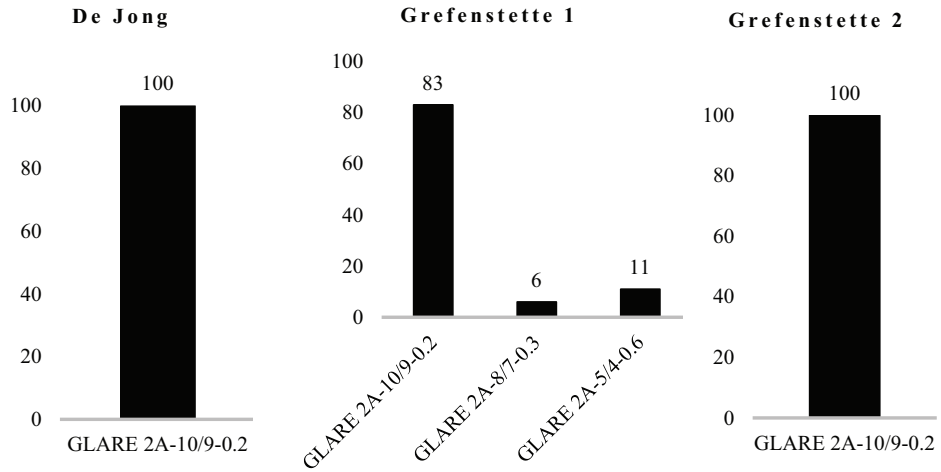


Figure 6.1: Optimal solutions for Case 1 based on 100 times repeating the search procedure.

The effectiveness of the settings are influenced by the complexity of the fitness function and by the size of the design population. If the fitness function or the design space is changed,

it is advised to repeat similar analysis for the settings to assure the settings will work in new situations. As it is clear from both test cases, when a small design space (Case 1) was selected, the optimal solution (GLARE 2A-10/9-0.2) was obtained more often with the three different settings.

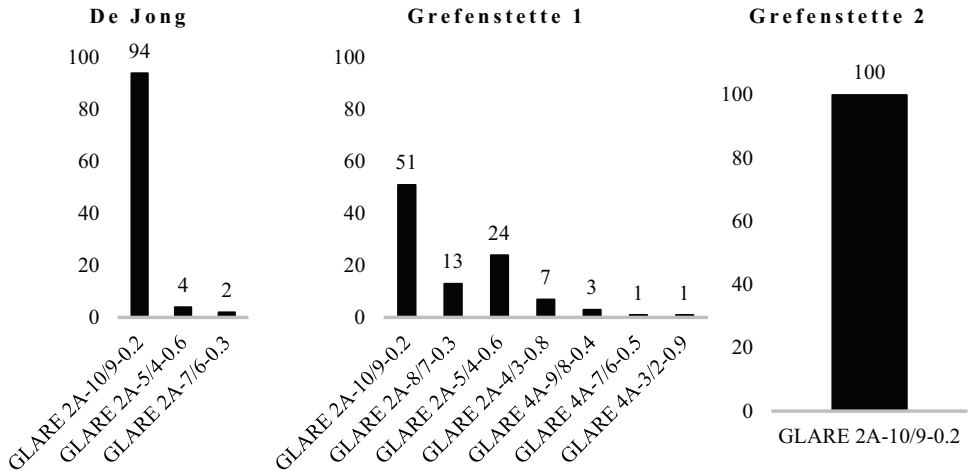


Figure 6.2: Optimal solutions for Case 2 based on 100 times repeating the search procedure.

Another criterion that depends on the GA settings is the performance related to the optimisation time. The average optimisation time for the two cases performed with the different settings is given in Table 6.3. The influence of the size of the design space is clearly visible; the optimisation for Case 2 takes a fraction more time with even 11 s difference in case of Grefenstette 2. The difference in optimisation time between the settings is caused by the selected population size. Grefenstette 1 responds the fastest, but in half of the cases the best solution was not given. Grefenstette 2 gave in all cases the best solution due to the high population size and probability of crossover, but on the other hand it was the slowest. The settings of De Jong had a good balance from both perspectives.

| | Time (s)[a] | | |
|---|---|---|---|
| | De Jong | Grefenstette 1 | Grefenstette 2 |
| Case 1 | 18 | 10 | 31 |
| Case 2 | 20 | 11 | 42 |

[a] The performance is depended on the computer. The values are here to compare the relative performance of each setting

Table 6.3: Average computation time of the settings.

In general, a larger design space would require a larger population size to create more variety.

This way the large domain is better explored with high probability of obtaining the global minimum instead of an local minimum. In contrary, a smaller population size responds faster and decreases the computation time. The same holds for crossover. Mutation is necessary to restore lost genes, but this should be kept low otherwise the GA procedure will perform a random search. Furthermore, it is desirable to use an elitist approach or a generation gap less than $100\%$. Then, it can be assured that the best solution is transferred to the next generation and is compared to its offspring. Otherwise, it will have the risk that the solution will be lost between the generations and it will not be present in the last generation.

The settings in the literature might not always give the best performance in different situations. Therefore, manual tuning of these settings is necessary to achieve the best performance and to assure the search procedure always results in the optimal design.

## **6.3.** Influence of FCI prediction methodology

The FCI methodology is used to evaluate the fatigue life of the generated lay-ups. The reliability of the prediction method is very important to make a correct judgement on the lay-ups. The accuracy of the prediction method determines whether the obtained optimal solution is actually the optimal solution. In case of crack initiation, the accuracy of the predicted fatigue life depends on the selected S-N data [4].



The S-N data is only valid for a laminate with the metal layer having the same stress concentration factor (SCF). In an ideal situation, a generated lay-up is compared to S-N data with same SCF. However, the available S-N data is limited and the same S-N curve should be used for lay-ups with different SCF values. Despite the corrections described in the guidelines [5] to estimate the fatigue life from S-N curves with different SCF values, the predicted fatigue life still differs depending on the S-N data used for predictions.

For example, a GLARE 4B-3/2-0.3 with a net section stress of $80$ MPa and a SCF of $K_{t_{\text{metal}}} = 2.7$ results in a fatigue life of $9739$ cycles when tested. However, for the same laminate a fatigue life of $8790$ cycles is predicted with $K_{t_{\text{S-N}}} = 2$ and $R_{\text{S-N}} = 0.0$, a life of $10,561$ cycles with $K_{t_{\text{S-N}}} = 2.5$ and $R_{\text{S-N}} = 0.0$ and of $11,699$ cycles for an interpolation between $K_{t_{\text{S-N}}} = 2.5$ & $3.6$ and $R_{\text{S-N}} = 0.0$. The predictions are fairly close to the test results, but this small difference in the prediction could make the difference of not being selected as an optimal solution, because the laminate for certain cases does not satisfy the required fatigue life.

In order to show the influence of the S-N data, two test cases are defined that are given in Table 6.4. For Case 3 only the number of metal layer is set as variable, while Case 4 has also the metal layer thickness as additional variable.

The obtained design solutions with its corresponding fitness value (equal to the weight in kg/m$^2$) are given in Table 6.5. Increasing the design space obviously introduces more near

| Input | | Design range | Case 3 | Case 4 |
|---|---|---|---|---|
| $P$ (N/mm) | $1000$ | Grade | GLARE 2A | GLARE 2A |
| $N_{\text{req}_{\text{fci}}}$ (cycles) | $20,000$ | $n_m$ | $2-20$ | $2-20$ |
| $K_{t_{\text{metal}}}$ | $2.7$ | $t_m$ (mm) | $0.5$ | $0.2-1.0$ |
| $R$ | $0.05$ | $t_{\text{ply}}$ (mm) | $0.133$ | $0.133$ |

Table 6.4: Design case to compare the influence of prediction method.

optimal solutions (difference between Case 3 & 4). In Case 3, for example looking at column 1, the two subsequent solutions have respectively a fitness value of $10.8$ and $12.7$. In between there are no solutions, because the laminate with an additional layer is the near optimal solution. For Case 4, it is clear that additional solutions are generated that have a lower fitness value than $12.7$, namely solutions with a fitness of $10.7$ and $11.7$.

It is also clear that the list of optimal and near optimal solutions changes depending on the S-N data used for the prediction. This difference is caused by the predicted fatigue life of each lay-up, see Table 6.6 for the detailed laminate prediction of the two solutions of Case 3 predicted with different S-N data. Furthermore, looking at the results of Case 4, it is clear that the algorithm aims to find the overall optimal solution. Due to this, not all near-optimal solutions are listed in the last generation. For example, GLARE 2A-11/10-0.2 in column 4 does not appear in column 1 or 3 despite the fact that it satisfies the fatigue criteria and has a lower weight than other given lay-ups. This makes it difficult to obtain the lightest near optimal solutions together with the optimal solution.



| | | 1 | 2 | 3 | 4 |
|---|---|---|---|---|---|
| | Rank | Single S-N<br>$K_{t_{\text{S-N}}} = 2.0$<br>$R_{\text{S-N}} = 0.25$ | Single S-N<br>$K_{t_{\text{S-N}}} = 2.5$<br>$R_{\text{S-N}} = 0.25$ | Closest S-N<br>(single)<br>$K_{t_{\text{S-N}}} = 2.0,\ 2.5,\ 3.6\ \&\ 5.2$<br>$R_{\text{S-N}} = 0.25$ | Closest S-N<br>(interpolation)<br>$K_{t_{\text{S-N}}} = 2.0,\ 2.5,\ 3.6\ \&\ 5.2$<br>$R_{\text{S-N}} = 0.25$ |
| Case 3 | 1 | GLARE 2A-6/5-0.5 = 10.8 | GLARE 2A-7/6-0.5 = 12.7 | GLARE 2A-6/5-0.5 = 10.8 | GLARE 2A-6/5-0.5 = 10.8 |
| | 2 | GLARE 2A-7/6-0.5 = 12.7 | GLARE 2A-8/7-0.5 = 14.6 | GLARE 2A-7/6-0.5 = 12.7 | GLARE 2A-7/6-0.5 = 12.7 |
| Case 4 | 1 | GLARE 2A-7/6-0.4 = 10.7 | GLARE 2A-6/5-0.6 = 12.5 | GLARE 2A-7/6-0.4 = 10.7 | GLARE 2A-7/6-0.4 = 10.7 |
| | 2 | GLARE 2A-6/5-0.5 = 10.8 | GLARE 2A-4/3-1.0 = 12.6 | GLARE 2A-9/8-0.3 = 11.4 | GLARE 2A-11/10-0.2 = 11.0 |
| | 3 | GLARE 2A-9/8-0.3 = 11.4 | GLARE 2A-7/6-0.5 = 12.7 | GLARE 2A-4/3-0.9 = 11.5 | GLARE 2A-4/3-0.9 = 11.5 |
| | 4 | GLARE 2A-4/3-0.9 = 11.5 | GLARE 2A-5/4-0.8 = 13.1 | GLARE 2A-4/3-1.0 = 12.6 | GLARE 2A-5/4-0.7 = 11.7 |
| | 5 | GLARE 2A-5/4-0.7 = 11.7 | GLARE 2A-6/5-0.7 = 14.1 | GLARE 2A-7/6-0.5 = 12.7 | GLARE 2A-8/7-0.4 = 12.3 |

Table 6.5: Design solutions obtained for Case 3 and 4 using different S-N data.

Hence, it is recommended to use multiple S-N curves for the optimisation procedure, where the closest S-N curve is selected for the fatigue life estimation per lay-up to ensure the best prediction. As discussed in Section C.3.3, fatigue life predictions by interpolating between two S-N curves have a smooth transition between different SCFs. In case of a prediction with one S-N curve, jumps in the predicted life can be expected when switching from one to another S-N curve if the closest S-N curve principle is used. Therefore, the interpolation

method with more than one S-N curves is preferred compared to the method using one S-N curve.

| Lay-up | $W$ (kg/m$^2$) | $K_{t_{\max}}$ | $S_a$ (MPa) | Single S-N $K_{t_{\text{S-N}}} = 2.0$ $R_{\text{S-N}} = 0.25$ | Single S-N $K_{t_{\text{S-N}}} = 2.5$ $R_{\text{S-N}} = 0.25$ | Closest S-N (single) $K_{t_{\text{S-N}}} = 2.0,\ 2.5,\ 3.6\ \&\ 5.2$ $R_{\text{S-N}} = 0.25$ | Closest S-N (interpolation) $K_{t_{\text{S-N}}} = 2.0,\ 2.5,\ 3.6\ \&\ 5.2$ $R_{\text{S-N}} = 0.25$ |
|---|---|---|---|---|---|---|---|
| GLARE 2A-6/5-0.5 | 10.8 | 2.09 | 109.7 | 27,147 | 13,818 | 27,147 | 27,732 |
| GLARE 2A-7/6-0.5 | 12.7 | 2.07 | 93.2 | 49,610 | 27,147 | 49,610 | 50,597 |

Table 6.6: Prediction results of the two main solutions of Case 3 in detail.

## 6.4. Influence of FCP and RS constraint approximation

The implementation of the approximate function is applied with the intention to improve the computation time. But, the functions do not perfectly replace the prediction methods, and therefore, the accuracy of the approximation might influence the obtained design solutions. This section aims to discuss this influence to assure the approximations would be able to replace the prediction methods in the optimisation procedure with giving solution based on inaccurate predictions. This influence is discussed for the FCP and RS criteria with the help of a case study, in which the applied load and in case of FCP, also the fatigue life requirement is varied. The FCI method is not discussed, because the constraint approximation of FCI does not significantly improve the computation time to justify the decrease in prediction accuracy.



### 6.4.1. Fatigue crack propagation

For the lay-up optimisation, the FCP criterion is evaluated with the approximate function presented in Section 5.3, with the coefficients listed in Table 5.7. The fatigue crack is assumed to propagate from $a_i = 35$ mm until $a_c = 150$ mm. The presented optimisation case includes three grades: GLARE 2A, GLARE 4A and GLARE 4B with $n_m$ varying between $2$ and $20$, and $t_m$ varied between $0.3$ and $1.0$ mm, are summarised in Table 6.7.

| Design range | Case 5 |
|---|---|
| Grade | GLARE 2A / GLARE 4A / GLARE 4B |
| $n_m$ | $2 - 20$ |
| $t_m$ (mm) | $0.3 - 1.0$ |
| $t_f$ (mm) | $0.133$ |

Table 6.7: Design case to asses the influence of constraint approximation

The results of the lay-up optimisation are given in Tables 6.8 and 6.9. In Table 6.8, the applied

load is varied and the fatigue life requirement is kept constant, and the design solution are then obtained for the different cases where the applied load is gradually increased. In Table 6.9, the fatigue life requirement is gradually increased, while the applied load is kept constant. Due to implementation issues of the FCP prediction method in the optimisation procedure as described in Section 5.1, it was not technically possible to perform this optimisation. In these cases, the obtained optimal solution of both optimisations were thus not compared, but the fatigue life of the optimal solution obtained by using the approximation was compared to the one from the prediction method. The error is between the two values is calculated with:

$$\text{Error} = (N_{\text{fcp}_{AF}} - N_{\text{fcp}_{PM}})/N_{\text{fcp}_{PM}} \tag{6.1}$$

Here, $N_{\text{fcp}_{AF}}$ refers to the fatigue life which is obtained with the case were the approximation is used as evaluation method and $N_{\text{fcp}_{AF}}$ refers the fatigue life which is obtained with the case were the prediction method is used as evaluation method. The solution is also checked, whether it would be included as design solutions in case the prediction method would have been used as evaluation method, by comparing the fatigue life of the laminate $(N_{\text{fcp}_{PM}})$ with the required fatigue life $(N_{\text{req}_{\text{fcp}}})$.



| 1 | 2 | 3 | 4 | 5 | 6 | 7 | 8 | 9 | 10 |
|---|---|---|---|---|---|---|---|---|---|
| $P$ (N/mm) | $N_{\text{req}_{\text{fcp}}}$ (cycles) | Lay-up | $t_{\text{lam}}$ (mm) | $W$ (kg/m$^2$) | $S_{\text{lam}}$ (MPa) | $N_{\text{fcp}_{AF}}{}^{a}$ (cycles) | $N_{\text{fcp}_{PM}}{}^{b}$ (cycles) | Solution$_{PM}{}^{c}$ | Error$^{d}$ |
| 250 | $1 \cdot 10^6$ | GLARE 2A-5/4-0.5 | 3.56 | 9.07 | 70.1 | $1.10 \cdot 10^6$ | $1.03 \cdot 10^6$ | yes | 6.8% |
| 500 | $1 \cdot 10^6$ | GLARE 2A-10/9-0.5 | 7.39 | 18.64 | 67.6 | $1.04 \cdot 10^6$ | $1.18 \cdot 10^6$ | yes | −11.9% |
| 750 | $1 \cdot 10^6$ | GLARE 2A-14/13-0.5 | 10.46 | 26.31 | 71.7 | $1.14 \cdot 10^6$ | $1.04 \cdot 10^6$ | yes | 14.0% |
| 1000 | $1 \cdot 10^6$ | GLARE 2A-18/17-0.5 | 13.52 | 33.97 | 74.0 | $1.03 \cdot 10^6$ | $0.97 \cdot 10^6$ | no | 6.2% |
| 1250 | $1 \cdot 10^6$ | GLARE 2A-20/19-0.6 | 17.05 | 43.37 | 73.3 | $1.06 \cdot 10^6$ | $0.92 \cdot 10^6$ | no | 15.2% |
| 1500 | $1 \cdot 10^6$ | GLARE 4A-20/19-1.0 | 27.58 | 70.61 | 54.4 | $0.92 \cdot 10^6$ | $1.05 \cdot 10^6$ | yes | −12.4% |

$^{a}$ AF: in case of approximation function as evaluation method.
$^{b}$ PM: in case of prediction method as evaluation method.
$^{c}$ Is the given design solution also an optimal solution in case of prediction method as evaluation method?
$^{d}$ Error = $(N_{\text{fcp}_{AF}} - N_{\text{fcp}_{PM}}/N_{\text{fcp}_{PM}})$

Table 6.8: Lay-up optimisation results for fatigue crack propagation from $a_i = 35$ mm until $a_c = 150$ mm for different applied loads.

Fatigue crack propagation depends on the laminate stress. Increasing the laminate stress decreases the fatigue life of a laminate. Thus for a certain applied load, the thickness and the laminate stress are balanced to find the matching fatigue life. The higher the load is, the thicker the laminate should be in general. The same is observed when the fatigue life requirement is increased. A high fatigue life is obtained at a lower laminate stress, and for this reason, the laminate thickness should be increased to lower the stress. When higher loads are applied the GLARE 2A laminates reach their limit in the design space. Therefore, the optimal solution switches to GLARE 4A that is thicker and can have a lower laminate stress so that the fatigue life criteria is met. Loads higher than $P = 1500$ N/mm do not result in any solution, because no lay-ups are found in the design range that satisfies the criteria. This is due to the fact that the design space is restricted to metal sheet thickness of

1.0 mm and 20 metal layers . Even the given solution at $P = 1500$ N/mm does not satisfy the optimisation criteria, but it was the closest solution to the requirement. This solution was given as output, with the notification that it did not satisfy the criteria. Checking the fatigue life of this solution with the prediction method showed that this solution would have satisfied the criteria if the prediction method was used as evaluation method.

| 1 | 2 | 3 | 4 | 5 | 6 | 7 | 8 | 9 | 10 |
|---|---|---|---|---|---|---|---|---|---|
| $P$ (N/mm) | $N_{\text{req}_{\text{fcp}}}$ (cycles) | Lay-up | $t_{\text{lam}}$ (mm) | $W$ (kg/m$^2$) | $S_{\text{lam}}$ (MPa) | $N_{\text{fcp}_{AF}}$ [a] (cycles) | $N_{\text{fcp}_{PM}}$ [b] (cycles) | Solution$_{PM}$ [c] | Error [d] |
| 1000 | $0.1 \cdot 10^6$ | GLARE 2A-11/10-0.3 | 5.96 | 14.44 | 167.8 | $0.12 \cdot 10^6$ | $0.10 \cdot 10^6$ | yes | 20.0% |
| 1000 | $0.3 \cdot 10^6$ | GLARE 2A-15/14-0.4 | 9.72 | 24.05 | 102.8 | $0.31 \cdot 10^6$ | $0.40 \cdot 10^6$ | yes | −22.5% |
| 1000 | $0.5 \cdot 10^6$ | GLARE 2A-15/14-0.5 | 11.22 | 28.22 | 89.1 | $0.52 \cdot 10^6$ | $0.55 \cdot 10^6$ | yes | −5.5% |
| 1000 | $0.7 \cdot 10^6$ | GLARE 2A-17/16-0.5 | 12.76 | 32.06 | 78.4 | $0.83 \cdot 10^6$ | $0.86 \cdot 10^6$ | yes | −3.5% |
| 1000 | $1.0 \cdot 10^6$ | GLARE 2A-18/17-0.5 | 13.52 | 33.97 | 74.0 | $1.03 \cdot 10^6$ | $0.97 \cdot 10^6$ | no | 6.2% |
| 1000 | $1.2 \cdot 10^6$ | GLARE 2A-19/18-0.5 | 14.29 | 35.89 | 67.0 | $1.27 \cdot 10^6$ | $1.02 \cdot 10^6$ | yes | 24.5% |
| 1000 | $1.5 \cdot 10^6$ | GLARE 2A-20/19-0.5 | 15.05 | 37.81 | 66.4 | $1.54 \cdot 10^6$ | $0.98 \cdot 10^6$ | no | 57.1% |
| 1000 | $2.0 \cdot 10^6$ | GLARE 2A-19/18-0.6 | 16.19 | 41.17 | 61.8 | $2.09 \cdot 10^6$ | $1.65 \cdot 10^6$ | no | 26.7% |
| 1000 | $2.5 \cdot 10^6$ | GLARE 2A-20/19-0.6 | 17.05 | 43.37 | 58.6 | $2.58 \cdot 10^6$ | $1.85 \cdot 10^6$ | no | 39.5% |
| 1000 | $3.0 \cdot 10^6$ | GLARE 2A-20/19-0.7 | 19.05 | 48.93 | 52.5 | $3.55 \cdot 10^6$ | $2.48 \cdot 10^6$ | no | 43.1% |
| 1000 | $4.0 \cdot 10^6$ | GLARE 2A-20/19-0.8 | 21.05 | 54.49 | 47.5 | $4.13 \cdot 10^6$ | $3.03 \cdot 10^6$ | no | 36.3% |

[a] AF: in case of approximation function as evaluation method.
[b] PM: in case of prediction method as evaluation method.
[c] Is the given design solution also an optimal solution in case of prediction method as evaluation method?
[d] Error = $(N_{fcp_{AF}} - N_{fcp_{PM}})/N_{fcp_{PM}}$

Table 6.9: Lay-up optimisation results for fatigue crack propagation from $a_i = 35$ mm until $a_c = 150$ mm for different life requirements.



Furthermore, a stress range of $S_{lam} = 70 - 200$ MPa is used to determine the coefficient of the FCP approximate function which are given in Table 5.7. The stress in the laminate of the design solutions should ideally be between this strange range. In column 6 of Table 6.8 and 6.9, it is visible that most of the laminate stresses are close to the lower stress boundary of 70 MPa. The cases in Table 6.9 with $N_{\text{req}_{\text{fcp}}} \geq 1.2 \cdot 10^6$ cycles are out-of-the-range, but still close to the lower limit of $S_{lam} = 70$ MPa. The predictions do not necessarily show a higher error compared to other cases.

The predictions with the approximate function and the prediction method are in general very close if the influence of the logarithmic scale is taken into consideration. However, the error starts to increase due to inaccurate predictions of the fatigue life. This has as result that some solutions are excluded. The main reason is that the approximate functions are created for stresses above 70 MPa, and for solutions close or above this stress result accurate predictions would be obtained. But for much lower stresses, the approximate function might follow a slightly different trend compared to prediction method. It is therefore advised to create an approximate function which includes to the full stress range as well as the lay-up range.

Despite the good fit of the approximate function, there were still mismatches in the predicted fatigue life between the prediction method and the approximate function. The average absolute error, for all cases listed in tables 6.8 and 6.9, is 21.6%. This introduces the risk that the optimisation procedure with the prediction method would exclude certain lay-ups

even if the error is very small, simply because the predicted value is just below the required fatigue life. As a result, not all design solutions obtained with the fitness approximation were listed as solution, if the prediction method would have been used as evaluation method. The problem is caused by the exponential behaviour of the fatigue life prediction, where small errors in logarithmic scale lead to a deviation up to $57.1\%$, in the particular case of $P = 1000$ N/mm and $N_{\text{req}_{\text{fcp}}} = 1.5 \cdot 10^6$ cycles. Nevertheless, $9$ of the $17$ optimisation cases would have been listed as a design solution.

The computation time is not listed for each specific case, but the average computation time decreased from $9500$ s to $8$ s. This means the constraint approximation helped to achieve the goal of improving the computation time. Furthermore, the procedural errors were eliminated for fatigue crack propagation.

### **6.4.2.** Residual strength

The design space for the RS design case is the same as for FCP and is given in Table 6.7. The approximate function derived in Section 5.4 with the coefficients from Table 5.10 are used as input. The optimisation procedure includes the same three grades as in the FCP analysis: GLARE 2A, GLARE 4A and GLARE 4B with $n_m$ varying between $2$ and $20$, and $t_m$ between $0.3$ and $1.0$ mm. The residual strength is predicted for a critical crack length of $a_c = 150$ mm. The optimisation results with additional information is given in Table 6.10. The applied load is stepwise varied from $500$ until $3500$ N/mm.

| 1 | 2 | 3 | 4 | 5 | 6 | 7 | 8 | 9 |
|---|---|---|---|---|---|---|---|---|
| $P$ (N/mm) | Lay-up | $t_{\text{lam}}$ (mm) | $W$ (kg/m$^2$) | $S_{\text{lam}}$ (MPa) | $S_{\text{rs}_{FA}}{}^b$ (MPa) | $S_{\text{rs}_{PM}}{}^c$ (MPa) | $\text{Time}_{FA}{}^b$ (s) | $\text{Time}_{PM}{}^c$ (s) |
| 500 | GLARE 2A-7/6-0.3 | 3.70 | 9.00 | 135.3 | 140.8 | 139.5 | 1 | 2482 |
| 1000 | GLARE 2A-14/13-0.3 | 7.66 | 18.52 | 130.6 | 139.4 | 138.4 | 1 | 3856 |
| 1500 | GLARE 2A-11/10-0.7 | 10.36 | 26.67 | 144.8 | 145.1 | 145.7 | 1 | 3940 |
| 2000 | GLARE 2A-12/11-0.9 | 13.73 | 35.82 | 145.7 | 146.7 | 147.2 | 1 | 4351 |
| 2500 | GLARE 2A-15/14-0.9 | 17.22 | 44.90 | 145.1 | 146.5 | 147.1 | 2 | 4843 |
| 3000 | GLARE 2A-18/17-0.9 | 20.72 | 53.99 | 144.8 | 146.4 | 146.9 | 2 | 4910 |
| 3500 | GLARE 2A-20/19-1.0 | 25.05 | 65.61 | 139.7 | 147.0 | 147.5 | 2 | 5347 |

Table 6.10: Lay-up optimisation results for RS with an initial crack length of $a_c = 150$ mm.

The optimisation for RS is also performed for two situations, namely the prediction method as evaluation method and the fitness approximation as evaluation method. This is done to verify that both procedures give the same lay-up as output. In this particular situation, all lay-ups listed in Table 6.10 are obtained with both procedures. This is obvious because the difference in the predicted residual strength values were almost identical in all cases, which thus resulted in the same design solutions.

Besides, the GLARE 2A laminate has the benefit over GLARE 4A and GLARE 4B laminates as design solution (same holds for fatigue crack propagation). This is due to the number of

fibre plies in GLARE 2A in which the two $0^\circ$-fibre plies contribute to fibre bridging, while in GLARE 4A, the additional $90^\circ$-fibre ply increases the laminate thickness without improving the residual strength property in longitudinal direction. In GLARE 4B, the single $0^\circ$-fibre layer worsens the residual strength behaviour, while the laminate thickness is equal to GLARE 4A, making it a non-attractive solution.

The computation time is monitored for all cases and in general, the higher the applied load the more computation time is required. The optimisation procedure starts at lay-up: $\begin{bmatrix}1 & 1 & 1\end{bmatrix}$. In general, when low load is applied, the design solution converges quickly, because the solution is at the begin of the design space (lower integer numbers in the vector means thin laminate solution). At high loads, the procedure has to explore more towards the end of the design space (higher integer numbers thus thick solutions), and therefore, the computation time is higher. Nevertheless, on average the computation time dropped from $4247$ s to less than $2$ s by using an approximation instead of the prediction method as evaluation method. It is shown that approximations improve the speed while keeping similar accuracy as the prediction method.

### **6.4.3.** General remarks



The presented criteria form the basis for F&DT design of FML. Applying a prediction method into an optimisation procedure is not efficient with respect to time. Therefore, the procedure is speed up with approximations, sometimes at the cost of accuracy. The obtained design solutions give an impression what type of lay-ups do fulfil the design requirements. The effectiveness of different grades can be compared, together with the influence of the layer number or thickness on the design criteria. In the presented optimisation cases, GLARE 4B never showed up due to its worse fatigue or residual strength performance, compared to GLARE 2A or GLARE 4A, caused by the $90^\circ$-fibre plies.

Furthermore, it was observed that the procedure rather prefers to increase the number of metal layers to achieve higher thickness instead of selecting a higher metal layer thickness. This is clearly visible in the results presented in Tables 6.8 and 6.9. Here, the layer number is increased and the thickness of metal layer is kept low to $0.3$-$0.5$ mm. Off course, with exception the case of high load together with high fatigue life requirement. In this case there was no other option other than increasing the layer thickness. The reason of preferring a high layer number instead of high layer thickness is that when the metal layer thickness is increased the MVF of the laminate increases while the number of interfaces stay the same. Consequently, this will decrease the stress in the fibre layers, which in his turn decreases the fibre bridging and thus worsens the fatigue or residual strength behaviour of the laminate. In conclusion, preferring more number of metal layers improves the fatigue and residual strength instead of increasing the metal layer thickness, because the increasing number of

metal layers decreases the MVF.

## 6.5. Influence of multi-constraint

Using single constraints, the influence of the prediction accuracy, of the GA settings, and of the approximate functions were discussed. However, combining different design constraints will result in different solutions that satisfy all applied criteria. In most cases one of the constraints appears critical. This means that selecting that single criterion or all criteria still result in that same lay-up solution of the critical constraint. However, there are cases where the optimal solution of each criteria is not overlapping with the design space of the other criteria. In those cases, the lightest solution that satisfies all criteria is selected to be optimal.

To discuss the influence of multi-constraint optimisation, a case study is performed, where the FCI, FCP and RS criteria are evaluated individually and combined to show the difference in the obtain solutions. For all three criteria the approximations are presented in Chapter 5 and used as evaluation criteria in the optimisation procedure. For FCI, FCP and RS, the coefficients in Table 5.3, 5.7 and 5.10 are respectively used in their corresponding approximate functions.



From the previous section, it is obvious that GLARE 2A is always the best performing lay-up, because for the fatigue life and residual strength calculation only load in longitudinal directions is considered. GLARE 2A is selected to illustrate the influence of the assessed design criteria. In Table 6.11, the design requirements and lay-up range are summarised. An optimisation is performed where the laminates should have a FCI life of at least $N_{\text{fci}} = 100,000$ cycles, a FCP life of at least $N_{\text{fci}} = 45,000$ cycles and the laminate stress should not exceed the residual strength ($S_{\text{lam}} \leq S_{\text{rs}}$). For each criteria separate and all criteria combined, the optimal lay-up is listed in Table 6.12.

| Input | | Design range | Case 6 |
|---|---|---|---|
| $P$ (N/mm) | $2000$ | Grade | GLARE 2A |
| $N_{\text{req}_{\text{fci}}}$ (cycles) | $1 \cdot 10^5$ | $t_m$ (mm) | $0.3 - 2.0$ |
| $N_{\text{req}_{\text{fcp}}}$ (cycles) | $0.45 \cdot 10^5$ | $n_m$ | $2 - 20$ |

Table 6.11: Design case for multiple constraint lay-up optimisation.

| Criteria | Lay-up | $t_{\text{lam}}$ (mm) | $W$ (kg/m$^2$) | $S_{\text{lam}}$ (MPa) | $N_{\text{fci}}$ (cycles) | $N_{\text{fcp}}$ (cycles) | $S_{\text{rs}}$ (MPA) |
|---|---|---|---|---|---|---|---|
| FCI | GLARE 2A-19/18-0.4 | 12.39 | 30.61 | 161.4 | $1.07 \cdot 10^5$ | $0.82 \cdot 10^5$ | 140.9 |
| FCP | GLARE 2A-12/11-0.3 | 6.53 | 15.8 | 306.4 | $0.06 \cdot 10^5$ | $0.47 \cdot 10^5$ | 139.6 |
| RS | GLARE 2A-12/11-0.9 | 13.73 | 35.82 | 145.7 | $1.42 \cdot 10^5$ | $0.35 \cdot 10^5$ | 145.7 |
| FCI + FCP + RS | GLARE 2A-19/18-0.5 | 14.29 | 35.89 | 140.0 | $1.89 \cdot 10^5$ | $0.99 \cdot 10^5$ | 142.4 |

Table 6.12: Results for of single and multiple criteria optimisation.

Meanwhile, the complete GLARE 2A design space is also manually evaluated per criteria to create an overview of all the lay-ups satisfying the criteria and to identify the position of the optimal solution obtained from the procedure. The optimal solution is expected to be on the boundary of the design space satisfying the criteria and in the direction of lay-ups with the lowest weight.

The design space evaluated for the FCI criteria is presented in Fig. 6.3. All the lay-ups satisfying solution are in the black area. The crossing of the vertical and horizontal grid lines represent the different design solutions. The aim of the optimisation is to choose the lightest solution, thus solutions with less $t_m$ or less $n_m$. Solutions with less $t_m$ and high $n_m$ are lighter than solutions with result in high $t_m$ and less $n_m$. In this case the optimal solution is GLARE 2A-19/18-0.4 as predicted by the algorithm, which is pointed out in Fig. 6.3 with a star. This solution confirms that GLARE 2A-19/18-0.4 is much lighter than for example GLARE 2A-6/5-2.0.

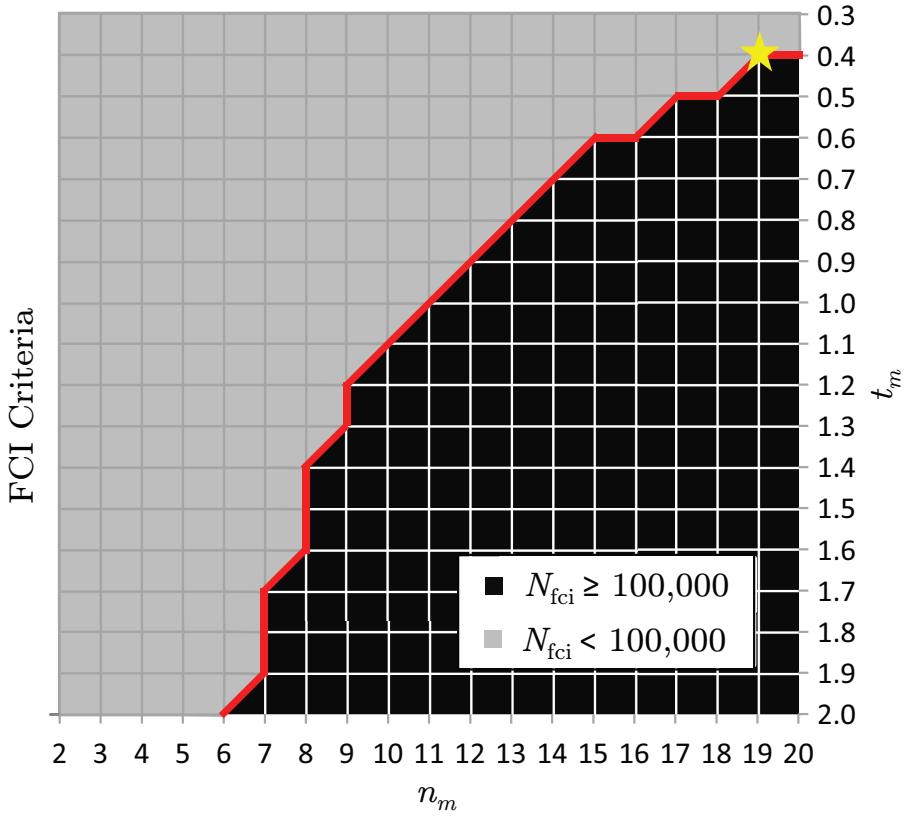


Figure 6.3: Lay-up options for GLARE 2A satisfying the FCI constraints at $P = 2000$ N/mm.

The same analysis is also performed for the FCP criteria and the design space satisfying the criteria becomes smaller compared to the FCI criteria as can be seen in Fig. 6.4. Looking to the design spaces in Figs. 6.3 and 6.4 reveals that there are overlapping solutions, meaning these lay-ups will satisfy both criteria in case the FCI and FCP criteria are evaluated together. In Fig. 6.4, the solution on the boundary line with $t_m = 0.3$ mm and $n_m \geq 12$ layers, thus GLARE 2A-12/11-0.3 is satisfying the FCP criteria, being the optimal solution. An interesting fact is that this lay-up has a very high laminate stress of $S_{lam} = 306.4$ MPa, so introducing additional criteria such as the residual strength will definitely eliminate this solution as it is clear from Fig. 6.5, where the RS criteria is evaluated.

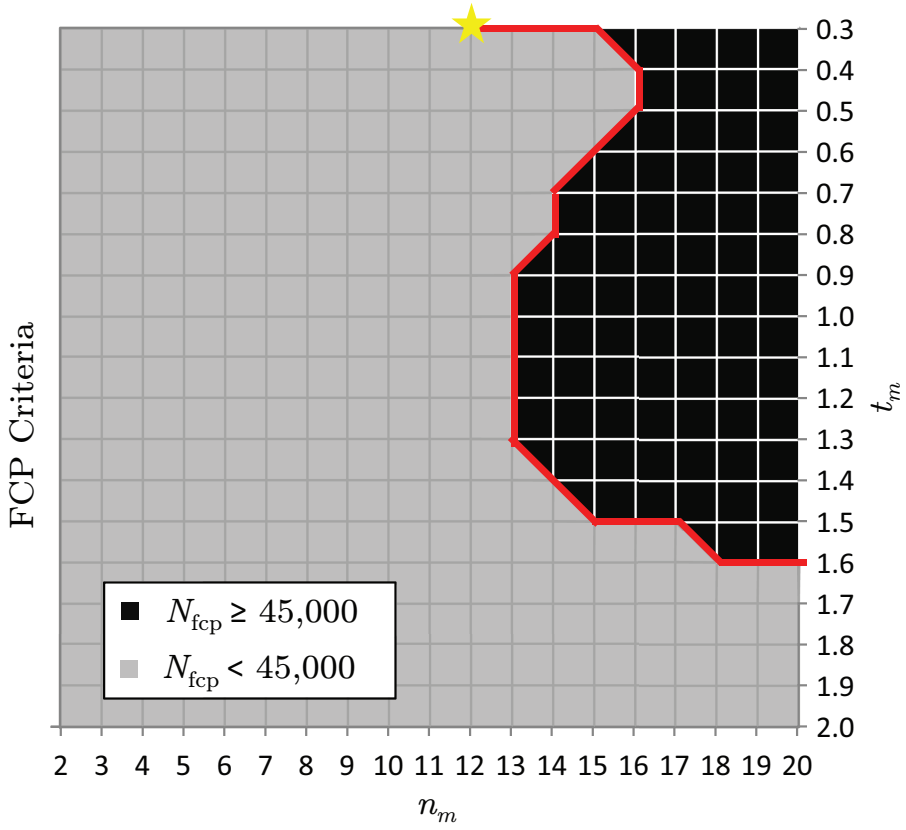


Figure 6.4: Lay-up options for GLARE 2A satisfying the FCP constraints at $P = 2000$ N/mm.

For the RS criteria, GLARE 2A-12/11-0.9 is the optimal solution within the design space given in Fig. 6.5. The residual strength of all GLARE 2A lay-ups are fairly close to each other. Therefore, the thickness of the lay-ups determines the laminate stress and thus the satisfaction to the RS criteria. Thin lay-ups have basically high laminates stresses and are

thus excluded for this case with a constant applied load of $P = 2000$ N/mm.

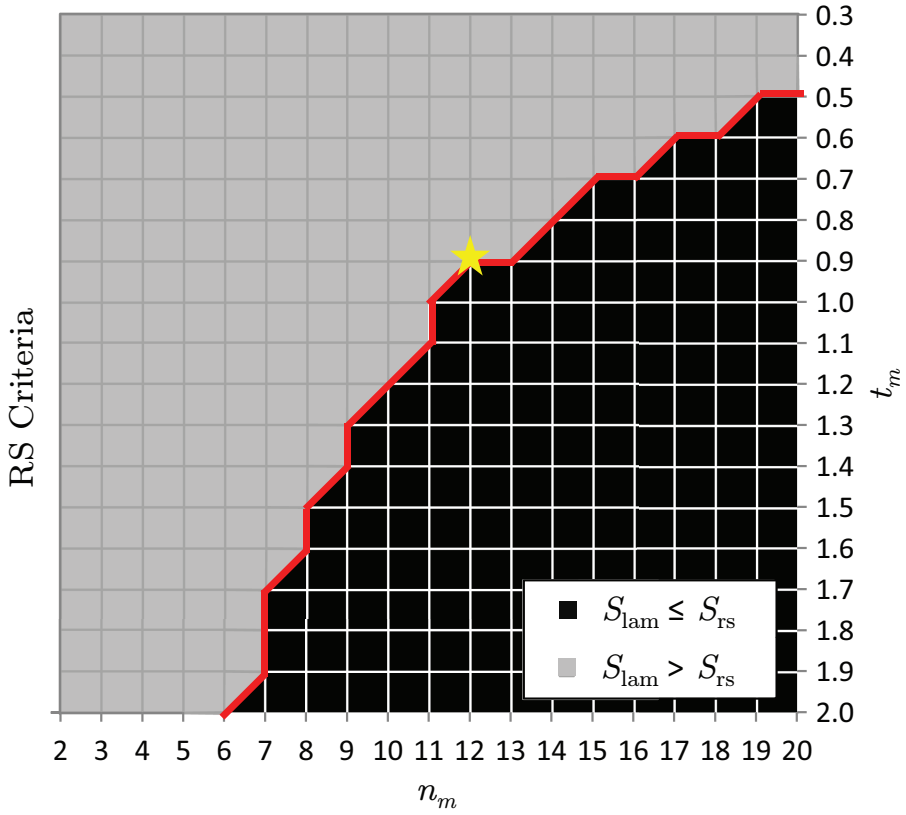


Figure 6.5: Lay-up options for GLARE 2A satisfying the RS constraints at $P = 2000$ N/mm.

Finally, the FCI, FCP and RS criteria are combined, a lay-up is obtained which satisfies all three criteria. In Fig. 6.6, the design space of the satisfying lay-ups are given. It is as expected the overlapping area of Figs. 6.3, 6.4 and 6.5. The optimal solution is GLARE 2A-19/18-0.5 as being the lightest solution in the design space. The optimal solution is not the optimal solution of the individual criteria, but it is the lightest solution that satisfies all the criteria.

Increasing the applied load, increases the laminate stress in all solutions. For example, at a load of $P = 3500$ N/mm, there are no solutions in the design space that satisfy all criteria, simply the FCP criteria is then not satisfied. Similarly, increasing the fatigue life requirement limits the design spaces. The only solution is to extend the design space or to consider different grades.

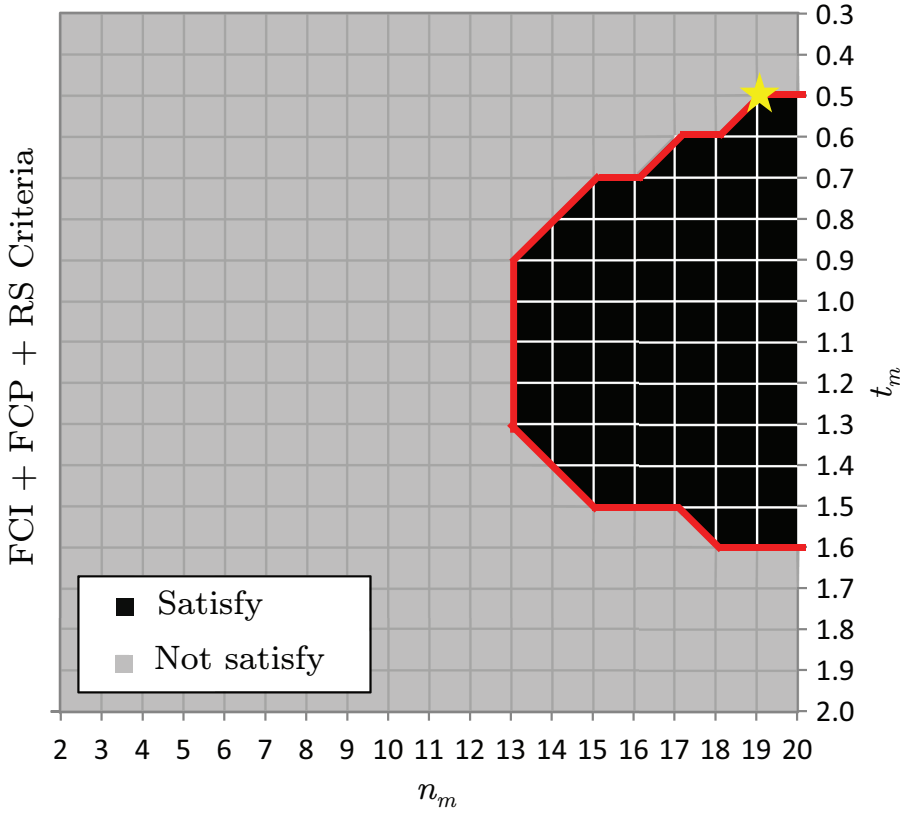


Figure 6.6: Lay-up options for GLARE 2A satisfying the FCI, FCP and RS constraints at $P = 2000$ N/mm.

## 6.6. Conclusions

In this chapter, the aspects influencing the evaluation of design solutions has been discussed from the perspective of GA settings, accuracy of the FCI prediction method, the application of the FCP and RS fitness approximation and the use of different design criteria.

The prediction accuracy for a lay-up directly influences the ranking in the GA procedure. The procedure does not compensate for any inaccuracy with respect to the prediction method itself. The influence of inaccuracy and sensitivity of predictions is still observed in the obtained results. Knowing the limitations of the prediction model beforehand makes it possible to take the influence of the accuracy into account when selecting the design solutions.

The effect of not obtaining the overall optimal solution could be eliminated by selecting different GA settings and repeating the analysis to assure the solution are converging. For this reason, it is necessary to tune the GA settings to assure that for selected prediction parameters and design space the best lay-up in the domain is obtained. Besides, receiving an appropriate design solution depends on the selected design space. A large domain could lead to immense amount of solutions, which is difficult to assess and to compare. It is advised to investigate and limit the design space beforehand.



Due to inefficiency with the application of prediction methods in the optimisation procedure, constraint approximations have been established, which prove to solve the inefficiency by replacing the prediction methods. The design solutions for both residual strength and fatigue crack propagation were presented. A comparison was made between the solutions of the prediction method and the approximation. For RS, in all situations the same design solutions were obtained, while the computation time was improved. For FCP, certain lay-ups were excluded due to differences in predicted fatigue life between the approximation function and the prediction method. The absolute average error was $21.6\%$, but considering the exponential behaviour of the fatigue life predictions, where small errors on logarithmic scale result in large fatigue life differences, this error is quite low. However, in return for the decreased accuracy, the application of constraint approximation improved the computation time significantly and solved the problems with respect to predicting the fatigue life for lay-ups under certain conditions.

The lay-up should satisfy multiple criteria and for this reason the satisfying design space is smaller compared to single criteria optimisation. A true benefit is that this way the best solution is obtained earlier. All in all, the design optimisation procedure for FML lay-ups is capable of finding the optimal solutions within the design space. The method showed its general applicability by discussing the implementation of three different design criteria into the GA environment. The method allows designers to explore a large design space and to limit their design choices towards an optimal solution.

# References

[1] K. D. Jong and W. Spears, *An analysis of the interacting roles of population size and crossover in genetic algorithms,* in *1st Workshop Parallel Problem Solving from Nature*, Vol. 496 (1991) pp. 38–47.

[2] J. Grefenstette, *Optimization of control parameters for genetic algorithms,* IEEE Transactions on Systems, Man and Cybernautics **16**, 122 (1986).

[3] A. Eiben and S. Smit, *Parameter tuning for configuring and analyzing evolutionary algorithms,* Swarm and Evolutionary Computation **1**, 19 (2011).

[4] S. Spronk, I. Şen, and R. Alderliesten, *Predicting fatigue crack initiation in fibre metal laminates based on metal fatigue test data,* International Journal of Fatigue **70**, 428 (2015).

[5] J. J. Homan, *Handbuch Struktur Berechnung (HSB), 62131-01 issue A: Guidelines for the prediction of the fatigue life for Kt values different to available databases*, Tech. Rep. (2009).

# 7

# Application to aircraft wings

*In the previous chapter, the optimisation procedure for FML lay-ups is presented and the element optimisation procedure is discussed with respect to the various influences on the design solutions. In this chapter, the step is set to wing optimisation by first discussing the single-sided wing box cross-section optimisation with loads as fixed input. Then, this optimisation is joined with the geometry- and load module so that the running loads for the wing cross-section are obtained based on defined load cases. The wing cross-section optimisation comprises both the upper and lower panels (double-sided), in which the upper panels are optimised for aluminium and the lower panels for FML. The developed method is tested with a design case where the weight of the wing cross-section solutions for different grades and metal sheet thicknesses are compared. Finally, the wing optimisation methodology is presented by obtaining an optimised wing solution satisfying the F&DT and compatibility criteria.*

## **7.1.** Introduction

In the literature, Cooper [1] created a design methodology for FML by incorporating ultimate strength and manufacturing constraints. The main difference with the work of Cooper is that the design method described here includes F&DT criteria to evaluate the lay-ups, which are the important ones for the development of FML. The implementation of this method also missed the link to the wing design environment by determining the running loads based on the wing geometry and flight loads.

For this reason, to support the design of wing structures, the design optimisation method is changed from element optimisation to cross-section optimisation. The wing running loads

are also linked to the cross-sectional segments to obtain the optimal solutions based on flight loads. The switch to cross-section optimisation is first tested by simply performing and multi-element optimisation or in other words a single-sided cross-section optimisation. Here after, as a final step in the design optimisation method, the FML optimisation routine is linked with the aluminium optimisation routine to finish the loop for the design of a wing by performing a double-sided cross-section optimisation. In Fig. 7.1, the difference between the single-sided and double-sided cross-section optimisation is illustrated. In which $x$ refers to the integers in the design vector given with Eq. (4.15).

First, in Section 7.2, a single-sided cross-section optimisation for the FML panel is performed for given loads. Hereafter, in Section 7.3, the cross-section optimisation is extended to a double-sided optimisation, where the upper and lower panels are optimised for different material solutions and design criteria, and the running loads for the evaluation are obtained from the geometry and load module, closing the wing design loop. In section 7.4, the cross-section optimisation is repeated along the wing length and a fully optimised wing is obtained.

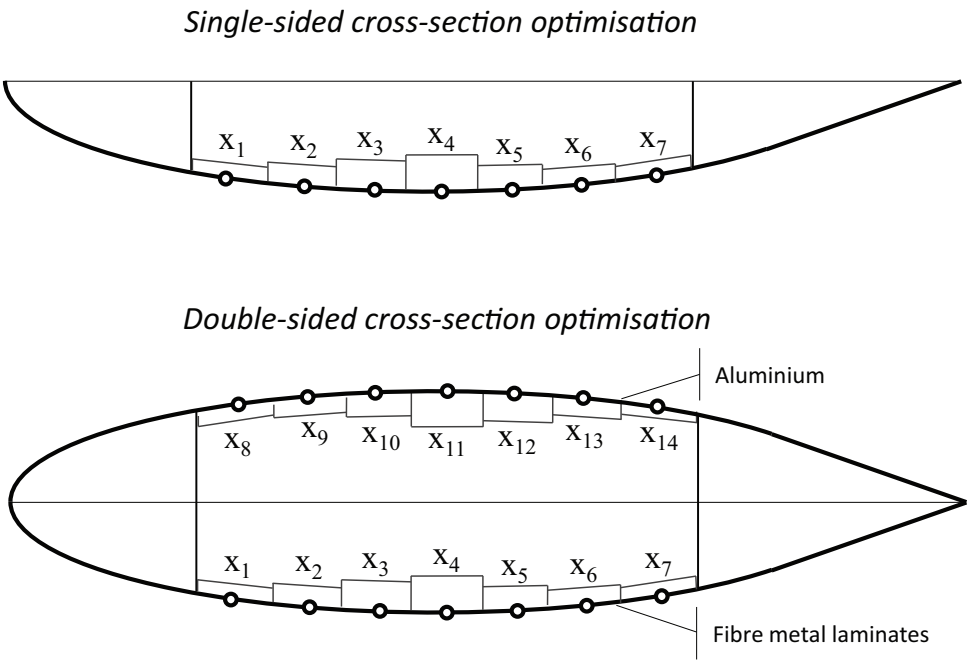


Figure 7.1: Illustration of single-sided and double-sided cross-section optimisation.

## **7.2.** Single-sided cross-section optimisation

The evaluation of a cross-section is mostly similar to the evaluation of an element. The difference relates to the definition of the design variables. For cross-section optimisation, the grade and thickness of the metal sheets $(t_m)$ are fixed, and the design vector represents the number of metal layers $(n_m)$ of each element. This means the vector length is increased from the initial three variables (grade, $n_m$ and $t_m$) to the number of elements in the cross-section, see Section 4.4.2. The challenge is to achieve convergence for the increased design vector due to the much larger design space and the fact that the same solution is simply not generated by the algorithm.

A convergence loop is implemented, where the GA procedure is repeated until the lightest solution of the optimisation is obtained. Hereby, the initial population of the algorithm is updated every time the optimisation is repeated during the convergence loop. The initial design vector is obtained after performing the optimisation for the first time and this vector is set as the initial population for the next optimisation. With this approach, it is assured that the previous optimal solution is again evaluated and the new optimal solution is indeed lighter than the previous one. This process is repeated till the solution converges and remains unchanged for a number of repetitions defined by the user. In Fig. 7.2, the convergence loop is illustrated with the exit value set to 5.

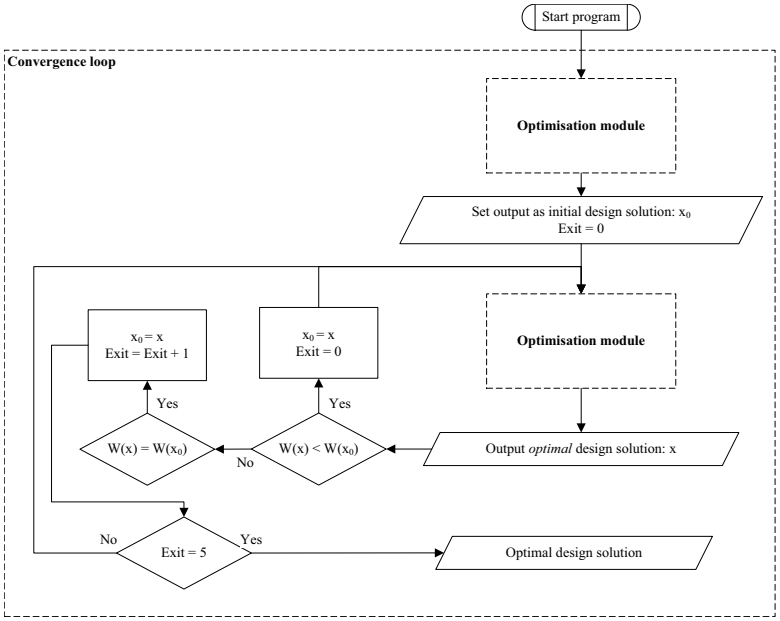


Figure 7.2: Convergence loop around the optimisation procedure.

From experience, this exit value of 5 would be enough to assure the lightest solution is obtained. Choosing a higher value does not necessary lead to a lighter solution. Because of the stochastic behaviour of GA, even with this convergence loop and tuned settings, it might be that the lightest solution is never generated. The initial solution also tends to force the algorithm to search in that direction, so the result of the first optimisation determines the direction in which part of the design space the algorithm should search for the lightest solution. Hence, the solution may converge to a different optimal solution, rather to the one which is really the lightest in the design space. Therefore, the algorithm tends to give multiple local optimum rather than a unique (theoretical) optimum. Sometimes, it happens that the algorithm does not find any design solution, because of the large design space. The issue is not that there are not satisfying solutions, but the solutions is not generated in this case. The initial solution could be set to the thickest laminate in the design solution (highest integer number in the design vector) to make sure a satisfying solution exist in the design space. So that the algorithm could proceed the operation of finding the optimal solution by using this solution as initial solution. If this thickest laminate is not satisfied then the design space is to small to have a valid solution, and increasing the upper boundary of the design space might be an option. Increasing the lower boundary would also benefit in this case, because the design space will become smaller and easier to explore.

### **7.2.1.** Design case



A design case is considered for single-sided cross-section optimisation of FML with the loads given as input. The design requirements and variables are given in table 7.1. In the optimisation, a maximum thickness step of $\Delta t_{\text{max}} = 3$ mm is considered for Eq. (4.5) to strict the thickness step between the elements. This value is purely selected to demonstrate the methodology. The thickness step is selected as criteria to assure that there are no additional stress concentrations between the segments. The thickness step is also necessary for the moment of inertia calculations that is consequently used for the running loads calculations as discussed in Appendix A. This calculation considers only the total area of the cross-section and ideally, it would put all the area in the centre of the cross-section. This will cause unrealistic cross-section designs with high thicknesses at the centre and very low thicknesses at the flanks. To avoid this problem, it is required to define a thickness step between the segments, so that the thicknesses are properly distributed on the cross-section.

An additional stacking layer for FML requires one metal sheet with $t_m = 0.5$ mm and two fibre plies with $t_{ply} = 0.133$ mm each, resulting in a total thickness step of $\Delta t_{\text{lam}} = 0.766$ mm. So by setting the criteria to $\Delta t_{\text{max}} = 3$ mm, the maximum thickness difference cannot be more than three additional metal layers for FML, thus $\Delta t_{\text{max}} = 2.30$ mm. This is simply checked by increasing the additional layers to four, then with $\Delta t = 3.1$ mm the thickness will exceed the maximum thickness step.

| Input | | Design range | Case 7 |
|---|---|---|---|
| $N_{\text{req}_{\text{fci}}}$ (cycles) | $100,000$ | Grade | GLARE 2A |
| $N_{\text{req}_{\text{fcp}}}$ (cycles) | $45,000$ | $t_m$ (mm) | $0.5$ |
| $\Delta t_{\text{max}}$ (mm) | $3$ | $n_m$ | $2-50$ |

Table 7.1: Design case for single-sided cross-section optimisation with fixed load condition.

The design solutions for the individual F&DT criteria and this criteria together including and excluding the thickness constraint are given in Table 7.2. The applied loads per element is given on top of the table. The integers indicate the number of metal layers per element for the given load. The weight is stated behind the solution, and an element width of $150$ mm is assumed to calculate the weight per unit span length. The weight of a cross-section per unit span length is calculated by summing up the element weight per unit multiplied with the element width ($w_e$). This weight is determined with Eq. (7.1), in which the second summation is to add the weight of the aluminium upper skin. This part will only be used for the double-sided cross-section optimisation that will be described in the next section.

$$W = \sum_{1}^{9} \rho_m n_m t_m w_e + \rho_f (n_m - 1) t_f w_e + \sum_{1}^{9} \rho_{al} t_{al} w_e \tag{7.1}$$

where, $\rho_m = 2820$ kg/m$^3$ is the density of metal layers in the FML skin, $\rho_f = 1980$ kg/m$^3$ is the density of fibre layers in the FML skin, and $\rho_{al} = 2820$ kg/m$^3$ is the density of the aluminium skin.



It is clearly visible that the RS criterion is the most critical one and the corresponding solution is also the lightest solution satisfying all the criteria. It is also clear that the number of layers are directly linked to the load, implying all the layers would have approximately similar layer stresses. This statement is confirmed when looking at Table 7.3, in which the design values for the FCI, FCP and RS criteria combined are given. Furthermore, the design values indicate that the FCI criteria ($N_{\text{fci}} \geq 100,000$ cycles), the FCP ($N_{\text{fcp}} \geq 45,000$ cycles) and RS ($S_{\text{lam}} \leq S_{\text{rs}}$) are met for each element. The thickness differences between elements are often high, because the maximum thickness step criteria is not used here.

The analysis is repeated with the thickness constraint limiting the thickness step between the elements. The influence of this criteria is visible in the design solutions. The number of layers are increased purely to meet the thickness step requirement and thus decreasing the stress in the corresponding element, which is clearly visible in Table 7.4. This way higher margins are obtained with respect to the stress and the F&DT requirements. Here again, all criteria are met including the thickness requirement. Due to this additional requirement the obtained solution became $32\%$ heavier ($32.5$ kg/m versus $24.6$ kg/m).

| Element number | 1 | 2 | 3 | 4 | 5 | 6 | 7 | 8 | 9 | |
|---|---|---|---|---|---|---|---|---|---|---|
| $P$ (N/mm) | 500 | 400 | 300 | 900 | 1700 | 1000 | 1500 | 1900 | 400 | |
| Criteria | Number of metal layers ($n_m$) | | | | | | | | | $W$ (kg/m) |
| FCI | 5 | 4 | 3 | 8 | 15 | 9 | 13 | 16 | 4 | 22.3 |
| FCP | 4 | 3 | 3 | 6 | 10 | 7 | 9 | 12 | 3 | 16.5 |
| RS | 5 | 4 | 4 | 9 | 16 | 10 | 15 | 18 | 4 | 24.6 |
| **FCI + FCP + RS** | 5 | 4 | 4 | 9 | 16 | 10 | 15 | 18 | 4 | **24.6** |
| FCI + $\Delta t$ | 5 | 6 | 9 | 12 | 15 | 12 | 13 | 16 | 13 | 29.3 |
| FCP + $\Delta t$ | 4 | 3 | 4 | 7 | 10 | 7 | 9 | 12 | 9 | 18.8 |
| RS + $\Delta t$ | 5 | 7 | 10 | 13 | 16 | 13 | 15 | 18 | 15 | 32.5 |
| **FCI + FCP + RS +** $\Delta t$ | 5 | 7 | 10 | 13 | 16 | 13 | 15 | 18 | 15 | **32.5** |

Table 7.2: Single-sided cross-section optimisation results for multiple criteria.

| Design values for FCI + FCP + RS | | | | | | | | | |
|---|---|---|---|---|---|---|---|---|---|
| Element number | 1 | 2 | 3 | 4 | 5 | 6 | 7 | 8 | 9 |
| $N_{\text{fci}}$ (cycles) | $1.85 \cdot 10^5$ | $1.69 \cdot 10^6$ | $6.09 \cdot 10^5$ | $2.15 \cdot 10^5$ | $1.79 \cdot 10^5$ | $2.19 \cdot 10^5$ | $2.32 \cdot 10^5$ | $1.86 \cdot 10^5$ | $1.69 \cdot 10^5$ |
| $N_{\text{fcp}}$ (cycles) | $8.34 \cdot 10^4$ | $7.34 \cdot 10^4$ | $2.215 \cdot 10^5$ | $1.05 \cdot 10^5$ | $9.38 \cdot 10^4$ | $1.07 \cdot 10^5$ | $1.16 \cdot 10^5$ | $9.77 \cdot 10^4$ | $7.34 \cdot 10^4$ |
| $S_{\text{rs}}$ (MPa) | 144.7 | 145.5 | 145.5 | 143.3 | 142.6 | 143.1 | 142.6 | 142.4 | 145.5 |
| $S_{\text{lam}}$ (MPa) | 140.3 | 143.0 | 107.2 | 135.8 | 141.8 | 135.2 | 133.6 | 140.5 | 143.0 |
| $t_{\text{lam}}$ (mm) | 3.56 | 2.80 | 2.80 | 6.63 | 11.99 | 7.39 | 11.22 | 13.52 | 2.80 |
| $\Delta t_{\text{lam}}$ (mm) | 0.76 | 0 | 3.83 | 5.36 | 4.60 | 3.83 | 2.3 | 10.72 | |

Table 7.3: Design values for multi-constraint optimisation without thickness constraint.

| Design values for FCI + FCP + RS + $\Delta t$ | | | | | | | | | |
|---|---|---|---|---|---|---|---|---|---|
| Element number | 1 | 2 | 3 | 4 | 5 | 6 | 7 | 8 | 9 |
| $N_{\text{fci}}$ (cycles) | $1.85 \cdot 10^5$ | $2.42 \cdot 10^6$ | $4.41 \cdot 10^7$ | $1.15 \cdot 10^6$ | $1.79 \cdot 10^5$ | $7.22 \cdot 10^5$ | $2.32 \cdot 10^5$ | $1.86 \cdot 10^5$ | $7.72 \cdot 10^7$ |
| $N_{\text{fcp}}$ (cycles) | $8.34 \cdot 10^4$ | $7.64 \cdot 10^5$ | $9.08 \cdot 10^6$ | $4.38 \cdot 10^5$ | $9.38 \cdot 10^4$ | $2.97 \cdot 10^5$ | $1.16 \cdot 10^5$ | $9.77 \cdot 10^4$ | $1.50 \cdot 10^7$ |
| $S_{\text{rs}}$ (MPa) | 144.7 | 143.8 | 143.1 | 142.8 | 142.6 | 142.8 | 142.6 | 142.5 | 142.6 |
| $S_{\text{lam}}$ (MPa) | 140.3 | 78.5 | 40.6 | 92.9 | 141.8 | 103.2 | 133.6 | 144.5 | 35.6 |
| $t_{\text{lam}}$ (mm) | 3.56 | 5.10 | 7.39 | 9.69 | 11.99 | 9.69 | 11.22 | 13.52 | 11.22 |
| $\Delta t_{\text{lam}}$ (mm) | 1.54 | 2.29 | 2.30 | 2.30 | 2.30 | 1.53 | 2.30 | 2.30 | |

Table 7.4: Design values for multi-constraint optimisation with thickness constraint.

## 7.3. Wing cross-section optimisation

The optimisation method is extended to perform a wing cross-section optimisation including both the optimisation of the upper and lower skin panels while using the wing running loads to evaluate the cross-section elements. The method optimises a complete cross-section at once finding the aluminium thickness for the upper panels and the number of metal layers for the FML solution. The wing running loads are determined using the geometry- and load module for each design solution generated by GA as described in Section 4.6. The shape of the cross-section is then incorporated, because the evaluated cross-sectional stresses depend on the moments of inertia and bending moment applied on this cross-section,

The aluminium upper panels are evaluated based on the Euler and local buckling criteria. The Euler buckling stress $(S_b)$ and critical local buckling stress $(S_{cr})$ are determined as described in Appendix B. The aluminium stresses $(S_{\text{al}})$ at each element should not exceed these buckling stresses:

$$S_{\text{al}} \leq S_b \tag{7.2}$$

$$S_{\text{al}} \leq S_{cr} \tag{7.3}$$

For the lower panels, the F&DT criteria given in Eqs. (4.2), (4.3) and (4.4) are used, while the thickness constraint in Eq. (4.6) or Eq. (4.6) is used for both panels. The upper aluminium skin is only optimised for buckling with the air load case of 2.5G (compression in upper panels). The same flight load case of 2.5G (tension in lower panels) is considered for the lower FML skin. The upper panel is selected to be aluminium 2024-T3 and the lower panel is considered to be GLARE 2A, GLARE 4A or GLARE 4B. Aluminium 2024-T3 is also considered for the stringers on both panels. The properties of this aluminium is given in Table 2.2. The stringer area is incorporated in the moment of inertia calculations and is fixed with respect to the skin thickness in terms of the stiffening ratio. The stiffening ratio for both the upper and lower wing is set to $\eta_{sf} = 0.33$ and the stringer spacing is $b_{str} = 150$ mm, more information about the definition of the skin stringer combination is given in Section A.4.1.

| Wing parameters | | |
|---|---|---|
| Bending moment on cross-section (N) | $M$ | $1.028 \cdot 10^6$ |
| Stringer spacing (mm) | $b_{str}$ | 150 |
| Stiffening ratio | $\mu$ | 0.33 |
| Rib spacing (mm) | $b_{rib}$ | 590 |

Table 7.5: Wing parameters at cross-section segment number 25.

The aircraft wing with a length of $L_{wing} = 15.1$ m as seen from the first rib till the wing tip is considered for the calculations. The wing is divided into 50 segments, resulting in a

segment length of $L_{seg} = 302$ mm. For the analysis, the segment $25$ is selected, which is half way the wing. At this location, the bending loads and the cross-sectional dimensions are obtained. The location and dimension of this cross-section segment is illustrated in Fig. 7.4. The bending moment of $M = 1.028 \cdot 10^6$ N is determined at segment $25$ by considering the load factor of $2.5$, in Fig. 7.3 the bending moments on the wing are given for the air load case of 2.5G.

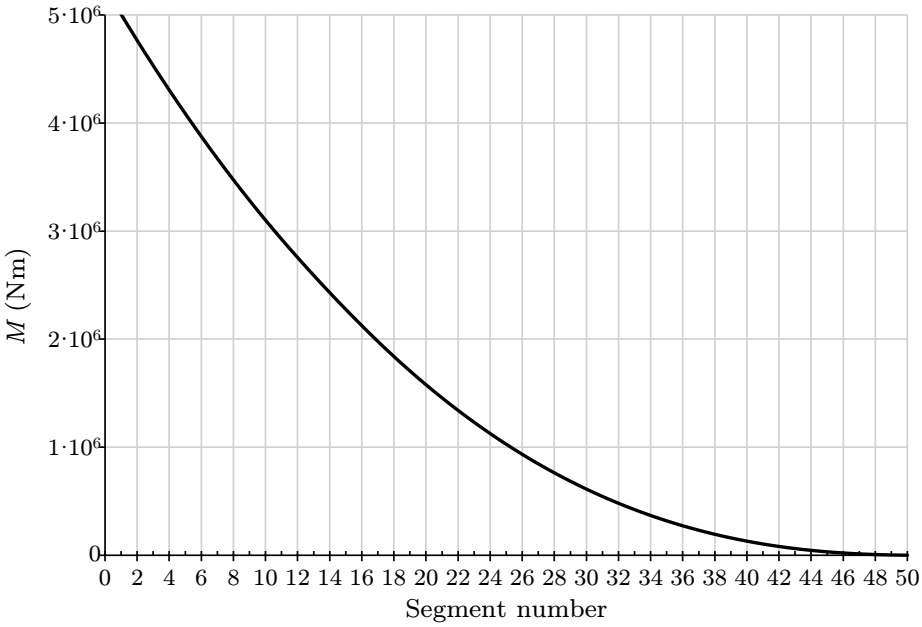


Figure 7.3: Bending moment on each segment at the flight load case of 2.5G.

The wing cross-section is considered the same along the length on a wing segment, and therefore, the obtained lay-up or skin thickness applies to one segment. The number of elements depends on the cross-section size, the selected stringer spacing and stiffening ratio, and is equal to $9$ for both the upper and lower panels at segment 25. The element width is set equal to the stringer spacing, and the critical crack length defined for the FCP and RS criteria to fulfil the two-bay-crack requirement is also set equal to the stringer spacing ($w_e = a_c = b_{str} = 150$ mm). Furthermore, a rib spacing of $b_{rib} = 590$ mm is assumed, this parameter is needed for the buckling calculations. These parameters are summarised in Table 7.5.

The optimisation routine is slightly changed with respect to the single-sided cross-section optimisation to cope with the optimisation of the full cross-section. The design vector is increased by additional integers that are representing the thickness of the upper panels.

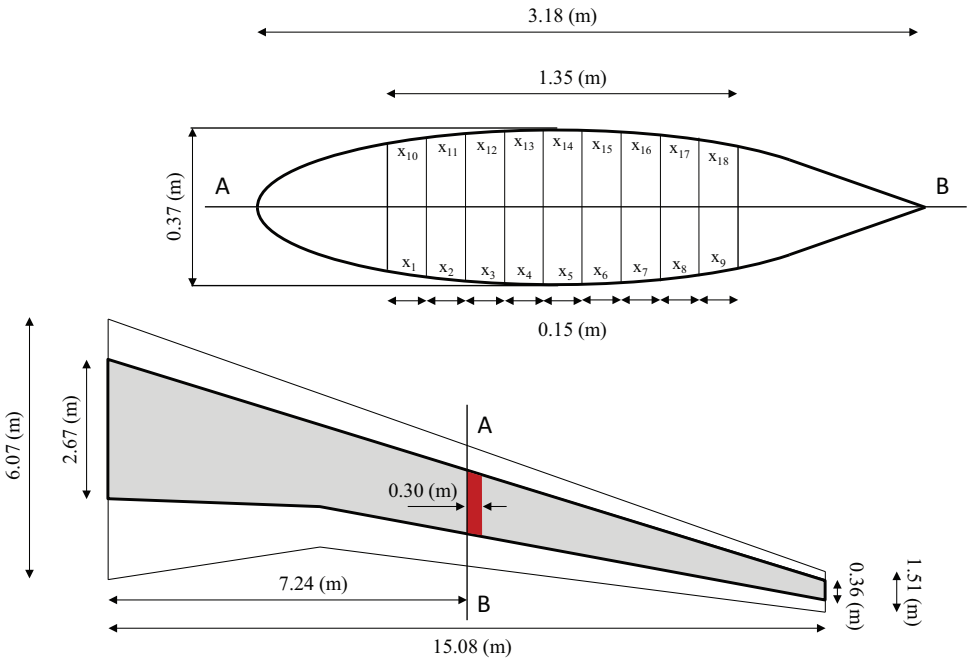


Figure 7.4: Cross-section location and dimensions of wing segment number 25.

An example of a design vector is given in Fig. 7.5. The optimisation procedure remained unchanged with the difference that the second part of the design vector is converted to the aluminium skin thickness which is used to calculate the laminate and buckling stresses for the evaluation of the upper skin.

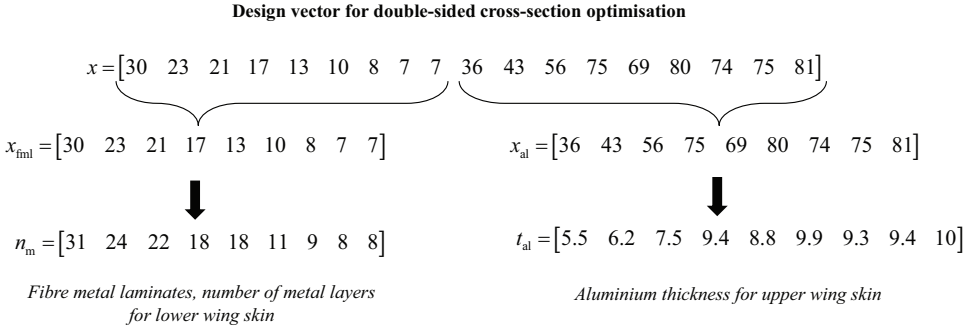


Figure 7.5: Example design vector for the double-sided cross-section optimisation.

The design requirements and the design variables for the upper and lower panels are given in Table 7.6. The optimisation is a joined optimisation in GA, where the thickness of aluminium $(t_{al})$ is selected to be a discrete value varied between 2 and 10 mm with steps of 0.1 mm.

The cases will use GLARE 2A, GLARE 4A or GLARE 4B with $t_m$ = 0.3, 0.4, 0.5, 0.6 or 0.7 mm in which $(n_m)$ is set as variable. This time for both skin panels to account for the thickness step, it is chosen to set a maximum percentage on the thickness step $(p_{\max})$ between the element, which is assumed to be 30%, thus a fraction of 0.3 in Eq. (4.6).

| Input | | Design range | Case 8 |
|---|---|---|---|
| $N_{\text{req}_{\text{fci}}}$ (cycles) | 100,000 | Grade | GLARE 2A, GLARE 4A or GLARE 4B |
| $N_{\text{req}_{\text{fcp}}}$ (cycles) | 45,000 | $t_m$ (mm) | 0.3, 0.4, 0.5, 0.6 or 0.7 |
| $p_{\max}$ | 0.3 | $n_m$ | 2 – 50 [step: 1] |
| | | $t_{al}$ (mm) | 2.0 – 10.0 [step: 0.1] |

Table 7.6: Design case for wing cross-section optimisation.

### 7.3.1. Optimisation results

The detailed optimisation results for the optimal cross-section consisting of GLARE 2A with $t_m$ = 0.5 mm is presented in Table 7.7. This lightest solution, that satisfies all the design criteria for the upper and lower panel, has a weight per unit span length of $W$ = 88.9 kg/m. The design values of the optimal cross-section were verified with the design requirements and it is concluded that all the requirements are met. For the upper panel, it is clearly visible that the obtained thickness meets the thickness constraint.



| Lower panel | | | | | | | | | |
|---|---|---|---|---|---|---|---|---|---|
| Element number | 1 | 2 | 3 | 4 | 5 | 6 | 7 | 8 | 9 |
| $n_m$ | 46 | 38 | 30 | 24 | 19 | 15 | 17 | 14 | 11 |
| $t_{\text{lam}}$ (mm) | 34.97 | 28.84 | 22.71 | 18.12 | 14.29 | 11.22 | 12.76 | 10.46 | 8.16 |
| $S_{\text{lam}}$ (MPa) | 131.1 | 124.5 | 116.2 | 104.1 | 89.7 | 73.5 | 55.5 | 36.1 | 15.5 |
| $N_{\text{fci}}$ (cycles) | $2.53 \cdot 10^5$ | $3.06 \cdot 10^5$ | $4.28 \cdot 10^5$ | $6.93 \cdot 10^5$ | $1.33 \cdot 10^6$ | $3.21 \cdot 10^6$ | $1.10 \cdot 10^7$ | $7.322 \cdot 10^7$ | $3.04 \cdot 10^9$ |
| $N_{\text{fcp}}$ (cycles) | $1.31 \cdot 10^5$ | $1.53 \cdot 10^5$ | $2.01 \cdot 10^5$ | $2.98 \cdot 10^5$ | $5.09 \cdot 10^5$ | $1.05 \cdot 10^6$ | $2.97 \cdot 10^6$ | $1.43 \cdot 10^7$ | $3.17 \cdot 10^8$ |
| $S_{\text{rs}}$ (MPa) | 141.9 | 142.0 | 142.1 | 142.2 | 142.4 | 142.6 | 142.5 | 142.7 | 143.0 |
| $\Delta t_{\text{lam}}$ (mm) | 6.13 | 6.13 | 4.59 | 3.83 | 3.07 | 1.54 | 2.30 | 2.30 | |
| $p_{\text{lam}}$ (%) | 21.3 | 27.0 | 25.3 | 26.8 | 27.3 | 13.7 | 22.0 | 28.2 | |

| Upper panel | | | | | | | | | |
|---|---|---|---|---|---|---|---|---|---|
| Element number | 10 | 11 | 12 | 13 | 14 | 15 | 16 | 17 | 18 |
| $t_{al}$ (mm) | 5.6 | 5.8 | 7.5 | 6.6 | 6.8 | 7.3 | 7.2 | 8.4 | 9.6 |
| $S_{al}$ (MPa) | 169.2 | 191.1 | 209.0 | 223.9 | 236.3 | 246.7 | 255.3 | 262.3 | 268.1 |
| $S_b$ (MPa) | 272.2 | 294.3 | 350.0 | 339.8 | 354.4 | 375.2 | 379.0 | 415.0 | 448.6 |
| $S_{cr}$ (MPa) | 372.5 | 399.6 | 668.2 | 517.5 | 549.3 | 633.1 | 615.8 | 838.2 | 1094.8 |
| $\Delta t_{\text{lam}}$ (mm) | 0.2 | 1.7 | 0.9 | 0.2 | 0.5 | 0.1 | 1.2 | 1.2 | |
| $p_{\text{lam}}$ (%) | 3.6 | 29.3 | 13.6 | 3.0 | 7.4 | 1.4 | 16.7 | 14.3 | |

Table 7.7: Detailed results of the cross-section optimisation for GLARE 2A with $t_m$ = 0.5 mm.

It is also clear that the selected stresses for the upper layer are not critical and are much lower than the buckling stresses. This is mainly related to the fact that the thickness of

the upper and lower panels influence the total running load and stress distribution on the cross-section. Thus, further decreasing the upper skin thickness will result in the increase of the stress in the lower panels, because the total area of the cross-section decreases. The optimum should find a balance between the aluminium skin thickness and the FML skin thickness. The lower panel is limited by the critical design requirement, thus any increase in the stress will make sure the fatigue life of the lower panel will exceed the requirement. The upper panel would thus require a larger margin to compensate for this effect. In this design case, the RS criteria seems to be the critical together with the thickness step criteria.

### **7.3.2.** Weight comparison

The analysis is repeated for other metal layer thicknesses and for GLARE 4A and GLARE 4B grades. The obtained solutions are the lightest solutions that satisfy all the criteria, but with consideration that it could be a local optimum. The weight of the optimal solutions are given in Table 7.8. The lightest solution is obtained with GLARE 2A and $t_m = 0.4$ mm with a weight per unit span length of $80.0$ kg/m.

| $t_m$ (mm) | $W$ (kg/m) | | |
|---|---|---|---|
| | GLARE 2A | GLARE 4A | GLARE 4B |
| 0.3 | 89.0 | 94.1 | – |
| 0.4 | 80.0 | 93.6 | 120.7 |
| 0.5 | 88.9 | 93.7 | 104.1 |
| 0.6 | 85.3 | 95.4 | 107.0 |
| 0.7 | 93.3 | 91.2 | 103.7 |

Table 7.8: Cross-sectional weight of optimal solution for GLARE 2A, GLARE 4A and GLARE 4B with different $t_m$.

In general, GLARE 4B performs the worst due to the two $90^\circ$-plies, because only longitudinal loads are considered in the optimisation process. The $90^\circ$-plies are only beneficial when lateral loads are applied. The same holds for GLARE 4A with one $90^\circ$-ply, making the structure slightly heavier compared to GLARE 2A, but performing better compared to GLARE 4B. For GLARE 4B with $t_m = 0.3$ mm, there was not an optimal solution in the design space, because the maximum laminate thickness that can be achieved with $50$ layers was not enough to bring the laminate stress down to reasonable levels to satisfy F&DT criteria.

## 7.4. Wing optimisation

The design case in Table 7.6 is this time used to perform a complete wing optimisation. The optimisation is repeated for each cross-section along the wing. This way a thickness distribution along the wing is obtained. The different cross-sections are optimised independently from each other, because there are no constraints linking the cross-sections to each other. The optimisation is performed for GLARE 2A with $t_m = 0.5$ mm and the results are presented here.

In Figs. 7.6 and 7.9 are respectively the FML skin thickness for lower panel and the aluminium skin thickness for the upper panel given. The corresponding $n_m$ for the FML thicknesses are given in Fig. 7.7. Furthermore, the corresponding skin stresses in the lower and upper panels are respectively given in Figs. 7.8 and 7.10. It is clear that the both thickness distributions are according to the defined step size. Due to use of a percentage instead of an absolute value, higher thicknesses are allowed to have a larger step size between the elements. Furthermore, the skin thicknesses for FML are quite high, especially at the wing root, caused by the high applied loads.

The prediction methods used for evaluation are only validated for low laminate thicknesses. The approximate functions replacing these prediction methods are used to extrapolate the predicted property to higher laminate thicknesses based on the trend. These extrapolation results are used for the evaluation, and therefore, the results obtained in procedure might be inaccurate. Nevertheless, this thesis describes the design optimisation methodology and the inaccuracy of the results is not caused by the methodology itself, but by the accuracy and validity of the prediction methods. The generic character of this design methodology allows the incorporation of other prediction methods that are validated for higher thickness in a later stage.

The most obvious on the results is that the lack of the thickness step criteria in lengthwise direction reflects on results. The algorithm generates independent solutions per cross-section. For some cross-sections the high thicknesses are more at the beginning of the cross-section, for example segment number 7 in Fig. 7.6. For other segments, the thickness is more centred or towards the end of the cross-section, for example segment number 6 in Fig. 7.6. This brings the issue that the thickness step in lengthwise direction might be higher than allowed, because it is not checked here. This effect of missing constraint is strongly observed between segments 29 and 30. This issue could be solved by switching from cross-section to a wing optimisation, where compatibility is checked with all neighbouring segments instead of the current two neighbouring elements.

Another issue visible in segments 14 to 29 is that the first elements becomes very thick taking most of the loads. This is why there should be a thickness step criteria limiting the step size between elements. In this case, the $30\%$ for thickness step difference is very loose, especially

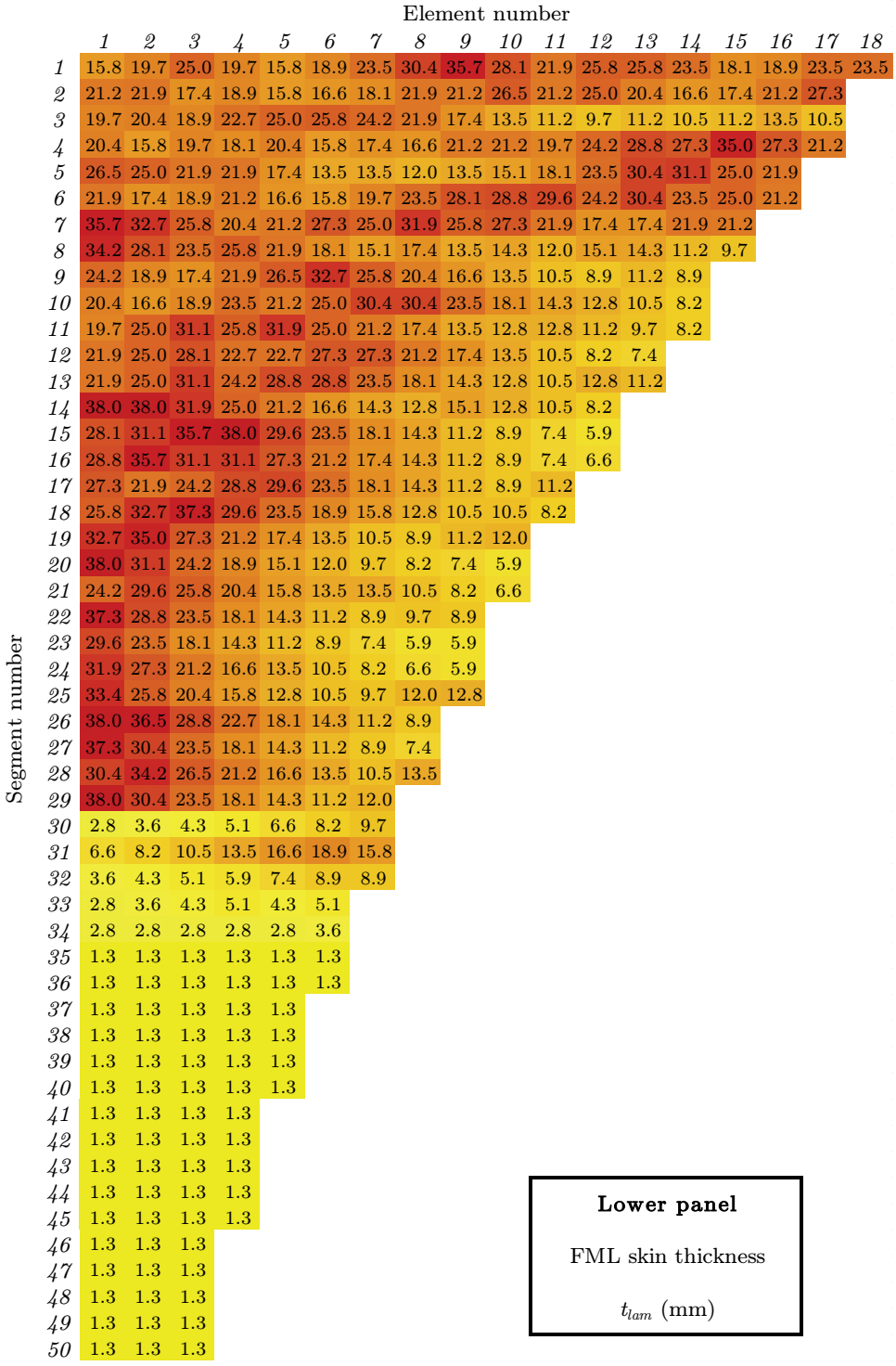




Figure 7.6: Lower skin thickness of the FML solution based on GLARE 2A with $t_m$ = 0.5 mm for wing optimisation.

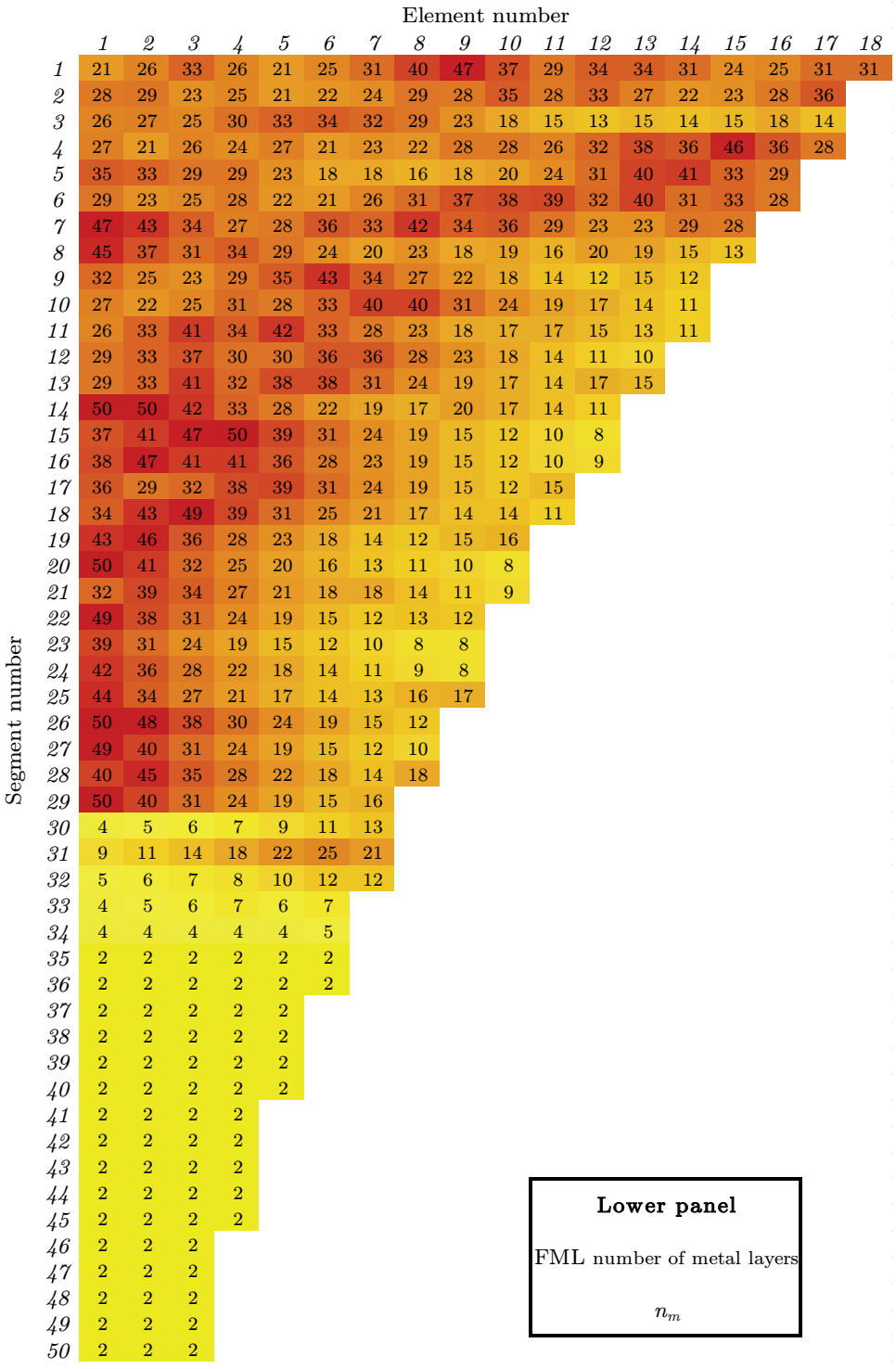


| Segment number | Element number 1 | 2 | 3 | 4 | 5 | 6 | 7 | 8 | 9 | 10 | 11 | 12 | 13 | 14 | 15 | 16 | 17 | 18 |
|---|---|---|---|---|---|---|---|---|---|---|---|---|---|---|---|---|---|---|
| 1 | 21 | 26 | 33 | 26 | 21 | 25 | 31 | 40 | 47 | 37 | 29 | 34 | 34 | 31 | 24 | 25 | 31 | 31 |
| 2 | 28 | 29 | 23 | 25 | 21 | 22 | 24 | 29 | 28 | 35 | 28 | 33 | 27 | 22 | 23 | 28 | 36 | |
| 3 | 26 | 27 | 25 | 30 | 33 | 34 | 32 | 29 | 23 | 18 | 15 | 13 | 15 | 14 | 15 | 18 | 14 | |
| 4 | 27 | 21 | 26 | 24 | 27 | 21 | 23 | 22 | 28 | 28 | 26 | 32 | 38 | 36 | 46 | 36 | 28 | |
| 5 | 35 | 33 | 29 | 29 | 23 | 18 | 18 | 16 | 18 | 20 | 24 | 31 | 40 | 41 | 33 | 29 | | |
| 6 | 29 | 23 | 25 | 28 | 22 | 21 | 26 | 31 | 37 | 38 | 39 | 32 | 40 | 31 | 33 | 28 | | |
| 7 | 47 | 43 | 34 | 27 | 28 | 36 | 33 | 42 | 34 | 36 | 29 | 23 | 23 | 29 | 28 | | | |
| 8 | 45 | 37 | 31 | 34 | 29 | 24 | 20 | 23 | 18 | 19 | 16 | 20 | 19 | 15 | 13 | | | |
| 9 | 32 | 25 | 23 | 29 | 35 | 43 | 34 | 27 | 22 | 18 | 14 | 12 | 15 | 12 | | | | |
| 10 | 27 | 22 | 25 | 31 | 28 | 33 | 40 | 40 | 31 | 24 | 19 | 17 | 14 | 11 | | | | |
| 11 | 26 | 33 | 41 | 34 | 42 | 33 | 28 | 23 | 18 | 17 | 17 | 15 | 13 | 11 | | | | |
| 12 | 29 | 33 | 37 | 30 | 30 | 36 | 36 | 28 | 23 | 18 | 14 | 11 | 10 | | | | | |
| 13 | 29 | 33 | 41 | 32 | 38 | 38 | 31 | 24 | 19 | 17 | 14 | 17 | 15 | | | | | |
| 14 | 50 | 50 | 42 | 33 | 28 | 22 | 19 | 17 | 20 | 17 | 14 | 11 | | | | | | |
| 15 | 37 | 41 | 47 | 50 | 39 | 31 | 24 | 19 | 15 | 12 | 10 | 8 | | | | | | |
| 16 | 38 | 47 | 41 | 41 | 36 | 28 | 23 | 19 | 15 | 12 | 10 | 9 | | | | | | |
| 17 | 36 | 29 | 32 | 38 | 39 | 31 | 24 | 19 | 15 | 12 | 15 | | | | | | | |
| 18 | 34 | 43 | 49 | 39 | 31 | 25 | 21 | 17 | 14 | 14 | 11 | | | | | | | |
| 19 | 43 | 46 | 36 | 28 | 23 | 18 | 14 | 12 | 15 | 16 | | | | | | | | |
| 20 | 50 | 41 | 32 | 25 | 20 | 16 | 13 | 11 | 10 | 8 | | | | | | | | |
| 21 | 32 | 39 | 34 | 27 | 21 | 18 | 18 | 14 | 11 | 9 | | | | | | | | |
| 22 | 49 | 38 | 31 | 24 | 19 | 15 | 12 | 13 | 12 | | | | | | | | | |
| 23 | 39 | 31 | 24 | 19 | 15 | 12 | 10 | 8 | 8 | | | | | | | | | |
| 24 | 42 | 36 | 28 | 22 | 18 | 14 | 11 | 9 | 8 | | | | | | | | | |
| 25 | 44 | 34 | 27 | 21 | 17 | 14 | 13 | 16 | 17 | | | | | | | | | |
| 26 | 50 | 48 | 38 | 30 | 24 | 19 | 15 | 12 | | | | | | | | | | |
| 27 | 49 | 40 | 31 | 24 | 19 | 15 | 12 | 10 | | | | | | | | | | |
| 28 | 40 | 45 | 35 | 28 | 22 | 18 | 14 | 18 | | | | | | | | | | |
| 29 | 50 | 40 | 31 | 24 | 19 | 15 | 16 | | | | | | | | | | | |
| 30 | 4 | 5 | 6 | 7 | 9 | 11 | 13 | | | | | | | | | | | |
| 31 | 9 | 11 | 14 | 18 | 22 | 25 | 21 | | | | | | | | | | | |
| 32 | 5 | 6 | 7 | 8 | 10 | 12 | 12 | | | | | | | | | | | |
| 33 | 4 | 5 | 6 | 7 | 6 | 7 | | | | | | | | | | | | |
| 34 | 4 | 4 | 4 | 4 | 4 | 5 | | | | | | | | | | | | |
| 35 | 2 | 2 | 2 | 2 | 2 | 2 | | | | | | | | | | | | |
| 36 | 2 | 2 | 2 | 2 | 2 | 2 | | | | | | | | | | | | |
| 37 | 2 | 2 | 2 | 2 | 2 | | | | | | | | | | | | | |
| 38 | 2 | 2 | 2 | 2 | 2 | | | | | | | | | | | | | |
| 39 | 2 | 2 | 2 | 2 | 2 | | | | | | | | | | | | | |
| 40 | 2 | 2 | 2 | 2 | 2 | | | | | | | | | | | | | |
| 41 | 2 | 2 | 2 | 2 | | | | | | | | | | | | | | |
| 42 | 2 | 2 | 2 | 2 | | | | | | | | | | | | | | |
| 43 | 2 | 2 | 2 | 2 | | | | | | | | | | | | | | |
| 44 | 2 | 2 | 2 | 2 | | | | | | | | | | | | | | |
| 45 | 2 | 2 | 2 | 2 | | | | | | | | | | | | | | |
| 46 | 2 | 2 | 2 | | | | | | | | | | | | | | | |
| 47 | 2 | 2 | 2 | | | | | | | | | | | | | | | |
| 48 | 2 | 2 | 2 | | | | | | | | | | | | | | | |
| 49 | 2 | 2 | 2 | | | | | | | | | | | | | | | |
| 50 | 2 | 2 | 2 | | | | | | | | | | | | | | | |





Figure 7.7: Number of metal layers of the FML solution based on GLARE 2A with $t_m$ = 0.5 mm.

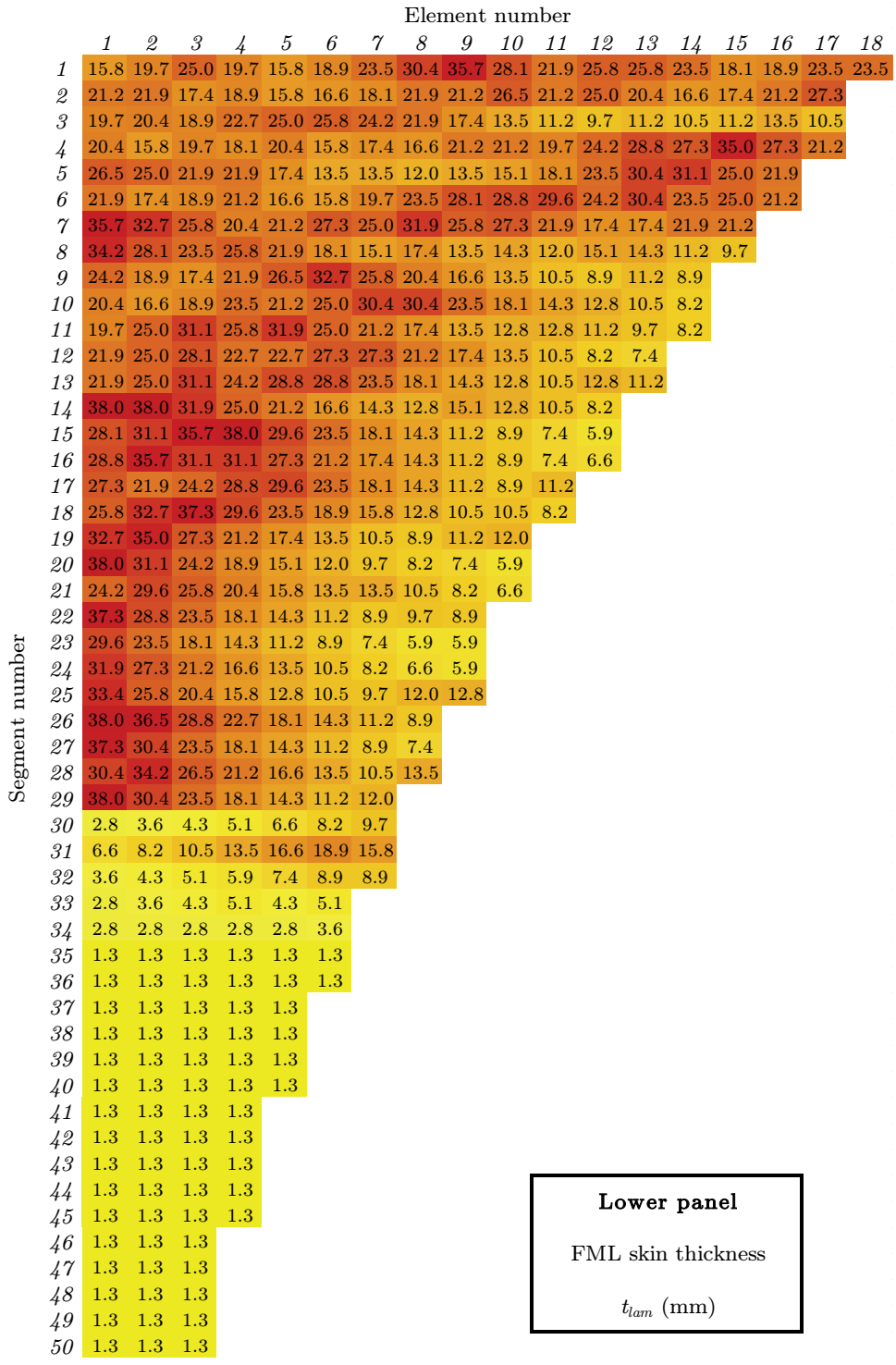






Figure 7.8: Skin stresses in the lower panel for GLARE 2A with $t_m$ = 0.5 mm.

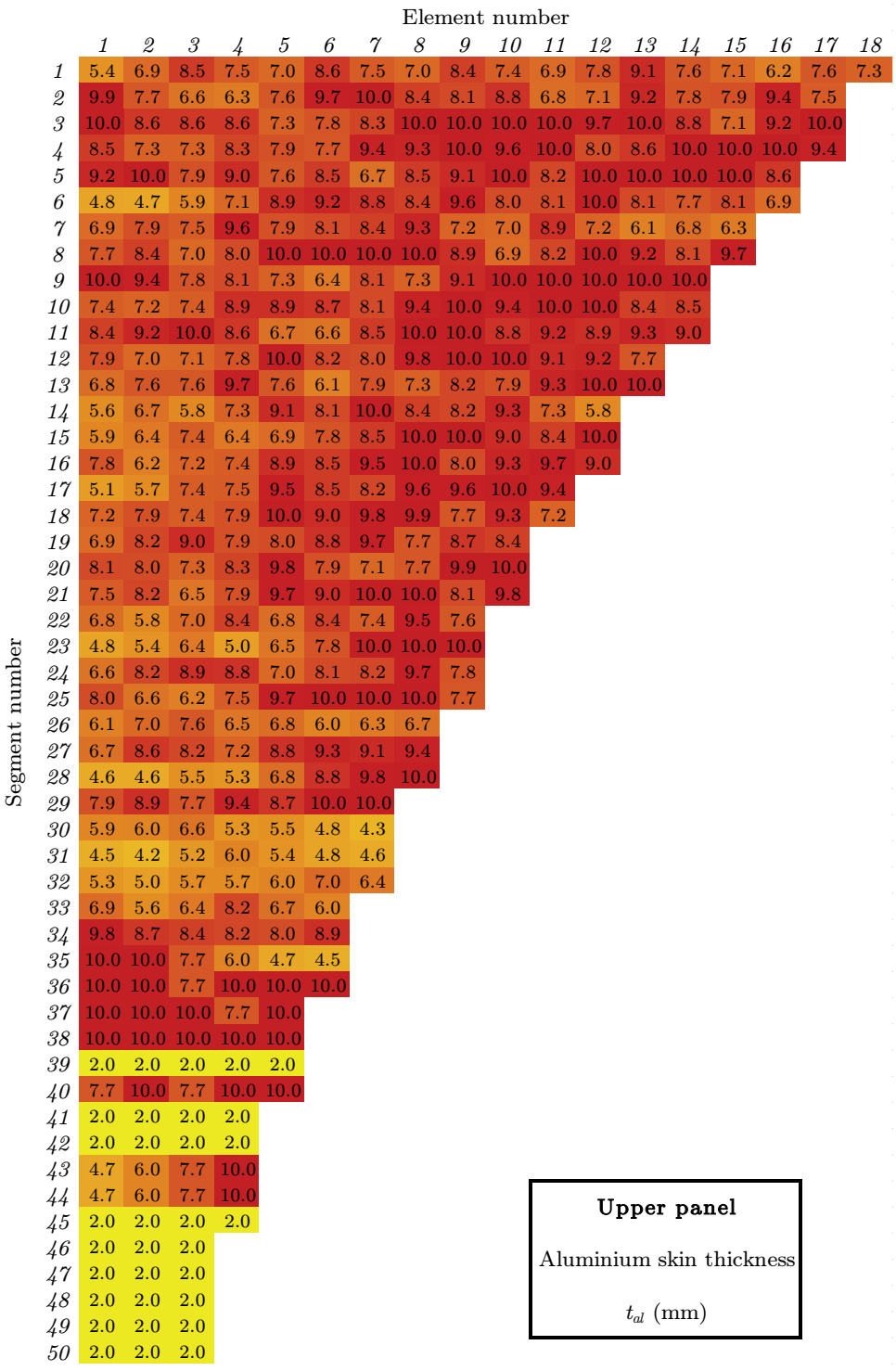


| Segment number | Element number 1 | 2 | 3 | 4 | 5 | 6 | 7 | 8 | 9 | 10 | 11 | 12 | 13 | 14 | 15 | 16 | 17 | 18 |
|---|---|---|---|---|---|---|---|---|---|---|---|---|---|---|---|---|---|---|
| 1 | 5.4 | 6.9 | 8.5 | 7.5 | 7.0 | 8.6 | 7.5 | 7.0 | 8.4 | 7.4 | 6.9 | 7.8 | 9.1 | 7.6 | 7.1 | 6.2 | 7.6 | 7.3 |
| 2 | 9.9 | 7.7 | 6.6 | 6.3 | 7.6 | 9.7 | 10.0 | 8.4 | 8.1 | 8.8 | 6.8 | 7.1 | 9.2 | 7.8 | 7.9 | 9.4 | 7.5 | |
| 3 | 10.0 | 8.6 | 8.6 | 8.6 | 7.3 | 7.8 | 8.3 | 10.0 | 10.0 | 10.0 | 10.0 | 9.7 | 10.0 | 8.8 | 7.1 | 9.2 | 10.0 | |
| 4 | 8.5 | 7.3 | 7.3 | 8.3 | 7.9 | 7.7 | 9.4 | 9.3 | 10.0 | 9.6 | 10.0 | 8.0 | 8.6 | 10.0 | 10.0 | 10.0 | 9.4 | |
| 5 | 9.2 | 10.0 | 7.9 | 9.0 | 7.6 | 8.5 | 6.7 | 8.5 | 9.1 | 10.0 | 8.2 | 10.0 | 10.0 | 10.0 | 10.0 | 8.6 | | |
| 6 | 4.8 | 4.7 | 5.9 | 7.1 | 8.9 | 9.2 | 8.8 | 8.4 | 9.6 | 8.0 | 8.1 | 10.0 | 8.1 | 7.7 | 8.1 | 6.9 | | |
| 7 | 6.9 | 7.9 | 7.5 | 9.6 | 7.9 | 8.1 | 8.4 | 9.3 | 7.2 | 7.0 | 8.9 | 7.2 | 6.1 | 6.8 | 6.3 | | | |
| 8 | 7.7 | 8.4 | 7.0 | 8.0 | 10.0 | 10.0 | 10.0 | 10.0 | 8.9 | 6.9 | 8.2 | 10.0 | 9.2 | 8.1 | 9.7 | | | |
| 9 | 10.0 | 9.4 | 7.8 | 8.1 | 7.3 | 6.4 | 8.1 | 7.3 | 9.1 | 10.0 | 10.0 | 10.0 | 10.0 | 10.0 | | | | |
| 10 | 7.4 | 7.2 | 7.4 | 8.9 | 8.9 | 8.7 | 8.1 | 9.4 | 10.0 | 9.4 | 10.0 | 10.0 | 8.4 | 8.5 | | | | |
| 11 | 8.4 | 9.2 | 10.0 | 8.6 | 6.7 | 6.6 | 8.5 | 10.0 | 10.0 | 8.8 | 9.2 | 8.9 | 9.3 | 9.0 | | | | |
| 12 | 7.9 | 7.0 | 7.1 | 7.8 | 10.0 | 8.2 | 8.0 | 9.8 | 10.0 | 10.0 | 9.1 | 9.2 | 7.7 | | | | | |
| 13 | 6.8 | 7.6 | 7.6 | 9.7 | 7.6 | 6.1 | 7.9 | 7.3 | 8.2 | 7.9 | 9.3 | 10.0 | 10.0 | | | | | |
| 14 | 5.6 | 6.7 | 5.8 | 7.3 | 9.1 | 8.1 | 10.0 | 8.4 | 8.2 | 9.3 | 7.3 | 5.8 | | | | | | |
| 15 | 5.9 | 6.4 | 7.4 | 6.4 | 6.9 | 7.8 | 8.5 | 10.0 | 10.0 | 9.0 | 8.4 | 10.0 | | | | | | |
| 16 | 7.8 | 6.2 | 7.2 | 7.4 | 8.9 | 8.5 | 9.5 | 10.0 | 8.0 | 9.3 | 9.7 | 9.0 | | | | | | |
| 17 | 5.1 | 5.7 | 7.4 | 7.5 | 9.5 | 8.5 | 8.2 | 9.6 | 9.6 | 10.0 | 9.4 | | | | | | | |
| 18 | 7.2 | 7.9 | 7.4 | 7.9 | 10.0 | 9.0 | 9.8 | 9.9 | 7.7 | 9.3 | 7.2 | | | | | | | |
| 19 | 6.9 | 8.2 | 9.0 | 7.9 | 8.0 | 8.8 | 9.7 | 7.7 | 8.7 | 8.4 | | | | | | | | |
| 20 | 8.1 | 8.0 | 7.3 | 8.3 | 9.8 | 7.9 | 7.1 | 7.7 | 9.9 | 10.0 | | | | | | | | |
| 21 | 7.5 | 8.2 | 6.5 | 7.9 | 9.7 | 9.0 | 10.0 | 10.0 | 8.1 | 9.8 | | | | | | | | |
| 22 | 6.8 | 5.8 | 7.0 | 8.4 | 6.8 | 8.4 | 7.4 | 9.5 | 7.6 | | | | | | | | | |
| 23 | 4.8 | 5.4 | 6.4 | 5.0 | 6.5 | 7.8 | 10.0 | 10.0 | 10.0 | | | | | | | | | |
| 24 | 6.6 | 8.2 | 8.9 | 8.8 | 7.0 | 8.1 | 8.2 | 9.7 | 7.8 | | | | | | | | | |
| 25 | 8.0 | 6.6 | 6.2 | 7.5 | 9.7 | 10.0 | 10.0 | 10.0 | 7.7 | | | | | | | | | |
| 26 | 6.1 | 7.0 | 7.6 | 6.5 | 6.8 | 6.0 | 6.3 | 6.7 | | | | | | | | | | |
| 27 | 6.7 | 8.6 | 8.2 | 7.2 | 8.8 | 9.3 | 9.1 | 9.4 | | | | | | | | | | |
| 28 | 4.6 | 4.6 | 5.5 | 5.3 | 6.8 | 8.8 | 9.8 | 10.0 | | | | | | | | | | |
| 29 | 7.9 | 8.9 | 7.7 | 9.4 | 8.7 | 10.0 | 10.0 | | | | | | | | | | | |
| 30 | 5.9 | 6.0 | 6.6 | 5.3 | 5.5 | 4.8 | 4.3 | | | | | | | | | | | |
| 31 | 4.5 | 4.2 | 5.2 | 6.0 | 5.4 | 4.8 | 4.6 | | | | | | | | | | | |
| 32 | 5.3 | 5.0 | 5.7 | 5.7 | 6.0 | 7.0 | 6.4 | | | | | | | | | | | |
| 33 | 6.9 | 5.6 | 6.4 | 8.2 | 6.7 | 6.0 | | | | | | | | | | | | |
| 34 | 9.8 | 8.7 | 8.4 | 8.2 | 8.0 | 8.9 | | | | | | | | | | | | |
| 35 | 10.0 | 10.0 | 7.7 | 6.0 | 4.7 | 4.5 | | | | | | | | | | | | |
| 36 | 10.0 | 10.0 | 7.7 | 10.0 | 10.0 | 10.0 | | | | | | | | | | | | |
| 37 | 10.0 | 10.0 | 10.0 | 7.7 | 10.0 | | | | | | | | | | | | | |
| 38 | 10.0 | 10.0 | 10.0 | 10.0 | 10.0 | | | | | | | | | | | | | |
| 39 | 2.0 | 2.0 | 2.0 | 2.0 | 2.0 | | | | | | | | | | | | | |
| 40 | 7.7 | 10.0 | 7.7 | 10.0 | 10.0 | | | | | | | | | | | | | |
| 41 | 2.0 | 2.0 | 2.0 | 2.0 | | | | | | | | | | | | | | |
| 42 | 2.0 | 2.0 | 2.0 | 2.0 | | | | | | | | | | | | | | |
| 43 | 4.7 | 6.0 | 7.7 | 10.0 | | | | | | | | | | | | | | |
| 44 | 4.7 | 6.0 | 7.7 | 10.0 | | | | | | | | | | | | | | |
| 45 | 2.0 | 2.0 | 2.0 | 2.0 | | | | | | | | | | | | | | |
| 46 | 2.0 | 2.0 | 2.0 | | | | | | | | | | | | | | | |
| 47 | 2.0 | 2.0 | 2.0 | | | | | | | | | | | | | | | |
| 48 | 2.0 | 2.0 | 2.0 | | | | | | | | | | | | | | | |
| 49 | 2.0 | 2.0 | 2.0 | | | | | | | | | | | | | | | |
| 50 | 2.0 | 2.0 | 2.0 | | | | | | | | | | | | | | | |





Figure 7.9: Upper skin thickness for the aluminium solution.

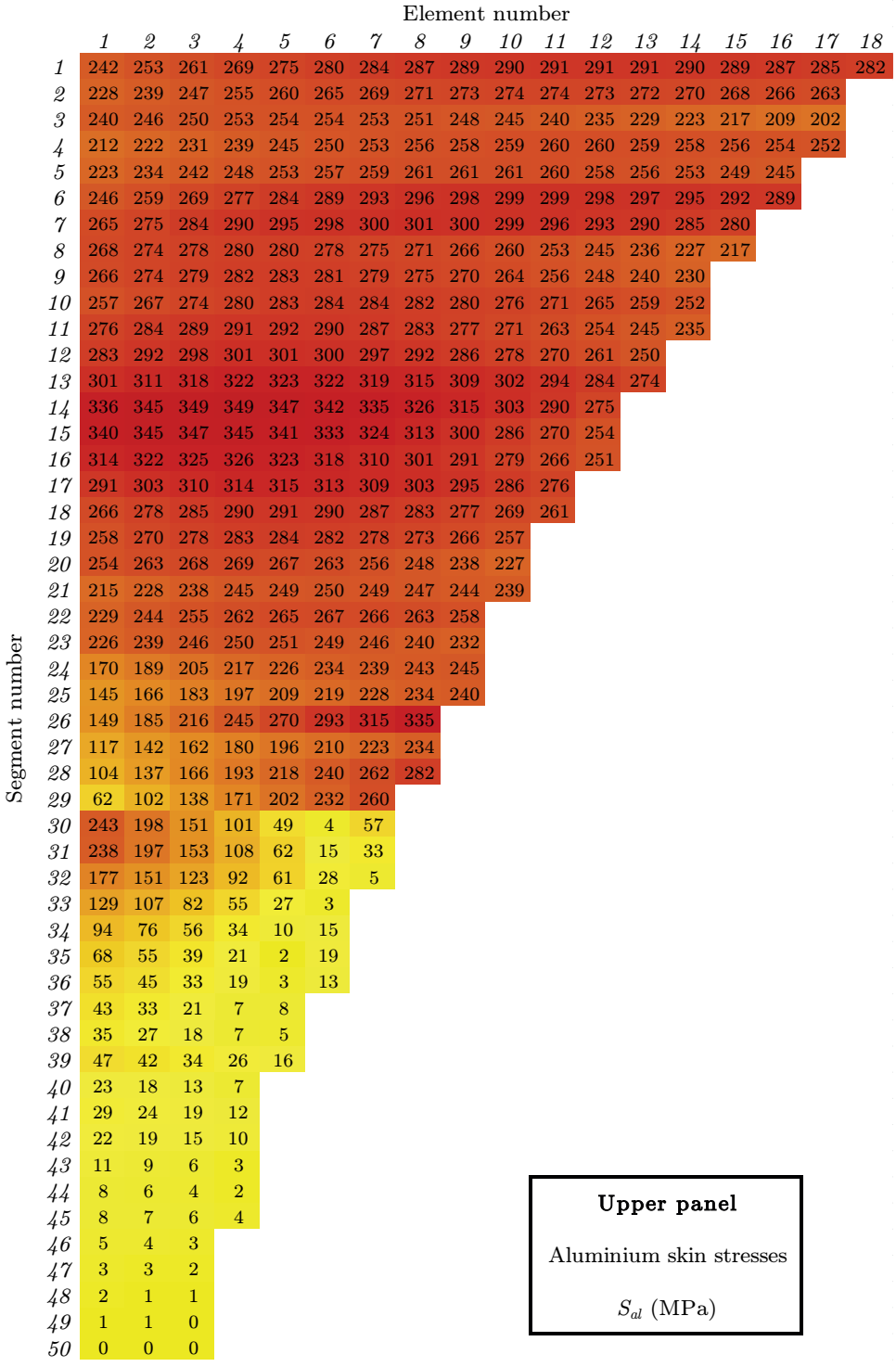


| Segment number | Element number 1 | 2 | 3 | 4 | 5 | 6 | 7 | 8 | 9 | 10 | 11 | 12 | 13 | 14 | 15 | 16 | 17 | 18 |
|---|---|---|---|---|---|---|---|---|---|---|---|---|---|---|---|---|---|---|
| 1 | 242 | 253 | 261 | 269 | 275 | 280 | 284 | 287 | 289 | 290 | 291 | 291 | 291 | 290 | 289 | 287 | 285 | 282 |
| 2 | 228 | 239 | 247 | 255 | 260 | 265 | 269 | 271 | 273 | 274 | 274 | 273 | 272 | 270 | 268 | 266 | 263 | |
| 3 | 240 | 246 | 250 | 253 | 254 | 254 | 253 | 251 | 248 | 245 | 240 | 235 | 229 | 223 | 217 | 209 | 202 | |
| 4 | 212 | 222 | 231 | 239 | 245 | 250 | 253 | 256 | 258 | 259 | 260 | 260 | 259 | 258 | 256 | 254 | 252 | |
| 5 | 223 | 234 | 242 | 248 | 253 | 257 | 259 | 261 | 261 | 261 | 260 | 258 | 256 | 253 | 249 | 245 | | |
| 6 | 246 | 259 | 269 | 277 | 284 | 289 | 293 | 296 | 298 | 299 | 299 | 298 | 297 | 295 | 292 | 289 | | |
| 7 | 265 | 275 | 284 | 290 | 295 | 298 | 300 | 301 | 300 | 299 | 296 | 293 | 290 | 285 | 280 | | | |
| 8 | 268 | 274 | 278 | 280 | 280 | 278 | 275 | 271 | 266 | 260 | 253 | 245 | 236 | 227 | 217 | | | |
| 9 | 266 | 274 | 279 | 282 | 283 | 281 | 279 | 275 | 270 | 264 | 256 | 248 | 240 | 230 | | | | |
| 10 | 257 | 267 | 274 | 280 | 283 | 284 | 284 | 282 | 280 | 276 | 271 | 265 | 259 | 252 | | | | |
| 11 | 276 | 284 | 289 | 291 | 292 | 290 | 287 | 283 | 277 | 271 | 263 | 254 | 245 | 235 | | | | |
| 12 | 283 | 292 | 298 | 301 | 301 | 300 | 297 | 292 | 286 | 278 | 270 | 261 | 250 | | | | | |
| 13 | 301 | 311 | 318 | 322 | 323 | 322 | 319 | 315 | 309 | 302 | 294 | 284 | 274 | | | | | |
| 14 | 336 | 345 | 349 | 349 | 347 | 342 | 335 | 326 | 315 | 303 | 290 | 275 | | | | | | |
| 15 | 340 | 345 | 347 | 345 | 341 | 333 | 324 | 313 | 300 | 286 | 270 | 254 | | | | | | |
| 16 | 314 | 322 | 325 | 326 | 323 | 318 | 310 | 301 | 291 | 279 | 266 | 251 | | | | | | |
| 17 | 291 | 303 | 310 | 314 | 315 | 313 | 309 | 303 | 295 | 286 | 276 | | | | | | | |
| 18 | 266 | 278 | 285 | 290 | 291 | 290 | 287 | 283 | 277 | 269 | 261 | | | | | | | |
| 19 | 258 | 270 | 278 | 283 | 284 | 282 | 278 | 273 | 266 | 257 | | | | | | | | |
| 20 | 254 | 263 | 268 | 269 | 267 | 263 | 256 | 248 | 238 | 227 | | | | | | | | |
| 21 | 215 | 228 | 238 | 245 | 249 | 250 | 249 | 247 | 244 | 239 | | | | | | | | |
| 22 | 229 | 244 | 255 | 262 | 265 | 267 | 266 | 263 | 258 | | | | | | | | | |
| 23 | 226 | 239 | 246 | 250 | 251 | 249 | 246 | 240 | 232 | | | | | | | | | |
| 24 | 170 | 189 | 205 | 217 | 226 | 234 | 239 | 243 | 245 | | | | | | | | | |
| 25 | 145 | 166 | 183 | 197 | 209 | 219 | 228 | 234 | 240 | | | | | | | | | |
| 26 | 149 | 185 | 216 | 245 | 270 | 293 | 315 | 335 | | | | | | | | | | |
| 27 | 117 | 142 | 162 | 180 | 196 | 210 | 223 | 234 | | | | | | | | | | |
| 28 | 104 | 137 | 166 | 193 | 218 | 240 | 262 | 282 | | | | | | | | | | |
| 29 | 62 | 102 | 138 | 171 | 202 | 232 | 260 | | | | | | | | | | | |
| 30 | 243 | 198 | 151 | 101 | 49 | 4 | 57 | | | | | | | | | | | |
| 31 | 238 | 197 | 153 | 108 | 62 | 15 | 33 | | | | | | | | | | | |
| 32 | 177 | 151 | 123 | 92 | 61 | 28 | 5 | | | | | | | | | | | |
| 33 | 129 | 107 | 82 | 55 | 27 | 3 | | | | | | | | | | | | |
| 34 | 94 | 76 | 56 | 34 | 10 | 15 | | | | | | | | | | | | |
| 35 | 68 | 55 | 39 | 21 | 2 | 19 | | | | | | | | | | | | |
| 36 | 55 | 45 | 33 | 19 | 3 | 13 | | | | | | | | | | | | |
| 37 | 43 | 33 | 21 | 7 | 8 | | | | | | | | | | | | | |
| 38 | 35 | 27 | 18 | 7 | 5 | | | | | | | | | | | | | |
| 39 | 47 | 42 | 34 | 26 | 16 | | | | | | | | | | | | | |
| 40 | 23 | 18 | 13 | 7 | | | | | | | | | | | | | | |
| 41 | 29 | 24 | 19 | 12 | | | | | | | | | | | | | | |
| 42 | 22 | 19 | 15 | 10 | | | | | | | | | | | | | | |
| 43 | 11 | 9 | 6 | 3 | | | | | | | | | | | | | | |
| 44 | 8 | 6 | 4 | 2 | | | | | | | | | | | | | | |
| 45 | 8 | 7 | 6 | 4 | | | | | | | | | | | | | | |
| 46 | 5 | 4 | 3 | | | | | | | | | | | | | | | |
| 47 | 3 | 3 | 2 | | | | | | | | | | | | | | | |
| 48 | 2 | 1 | 1 | | | | | | | | | | | | | | | |
| 49 | 1 | 1 | 0 | | | | | | | | | | | | | | | |
| 50 | 0 | 0 | 0 | | | | | | | | | | | | | | | |





Figure 7.10: Skin stresses in the upper panel for the aluminium solution.

at higher thicknesses. To solve this issue, the designer should choose a lower percentage or an absolute thickness step. This thickness concentration on one element could also be prevented by lowering the upper boundary limit, then the algorithm is forced to increase the thickness of other elements to get additional area to cope with the loads.

Besides, it should be stated that most aluminium elements have high skin stresses as visible in Fig. 7.10, because, the buckling criteria are far from critical. When additional constraints on the static strength would have been introduced, these stresses would have been much lower.

For the complete wing, the weight of the optimised aluminium and the FML cross-sections segments are obtained. In Fig. 7.3, it is visible that the bending moments are gradually decreasing towards the wing tip. For this reason, it is expected that the weight per segment will also reduce towards the wing tip. In Fig. 7.11, the weight of the optimised cross-section segments are given. Here, it is clearly seen that the weight is decreasing, but the curve is very bumpy. Solutions of segments with increasing numbers, which are expected to be lighter in weight, are sometimes higher than the preceding segment. This is caused by the algorithm that is unable to find the unique lighter solution and converges to a different solution that is best between the generated solutions rather than the best performing in the design space.

In this case, the segments 24 to 29 are heavier than the trend, so lighter design solutions are expected here when the optimisation is repeated on these segments. Unusual are also the aluminium thicknesses obtained for the segments 40, 43 and 44 (see Fig. 7.9). Looking at the neighbouring cross-sections, the design solutions for these segments are expected to be equal to the minimum solution in the design space as it is for the neighbouring segments.



Another issue is visible in Fig. 7.12, where the exit condition for each segment is given. A $1$ means the obtained solutions satisfies all design criteria and is the lightest solution between the generated design solutions. A value of $-2$ means that a satisfying solution is not found, but the given solution had the lowest penalty value and thus the best performing in the design space. For segments 30 and 31, a $-2$ was obtained, meaning these solutions do not satisfy the criteria. In case of segment 30, all the F&DT criteria were failed for the two last elements in the cross-section, and for segment 31, the stress in the last element exceeded the residual strength with only $0.1$ MPa. Satisfying solution were not generated within this optimisation, but when the analysis was repeated for these cross-sections, satisfying solutions were then obtained. This is another reason that could explain the bump between segments 29 and 30.

For segments 24 to 31, 40, 43 and 44, the analysis is repeated with the aim of finding a better solution that meets all criteria. Different to the normal procedure, some manual adaptations are made to the initial input to assure that a lighter satisfying solution is obtained. As proposed before, the thickest solution thus the design vector with the upper boundary of

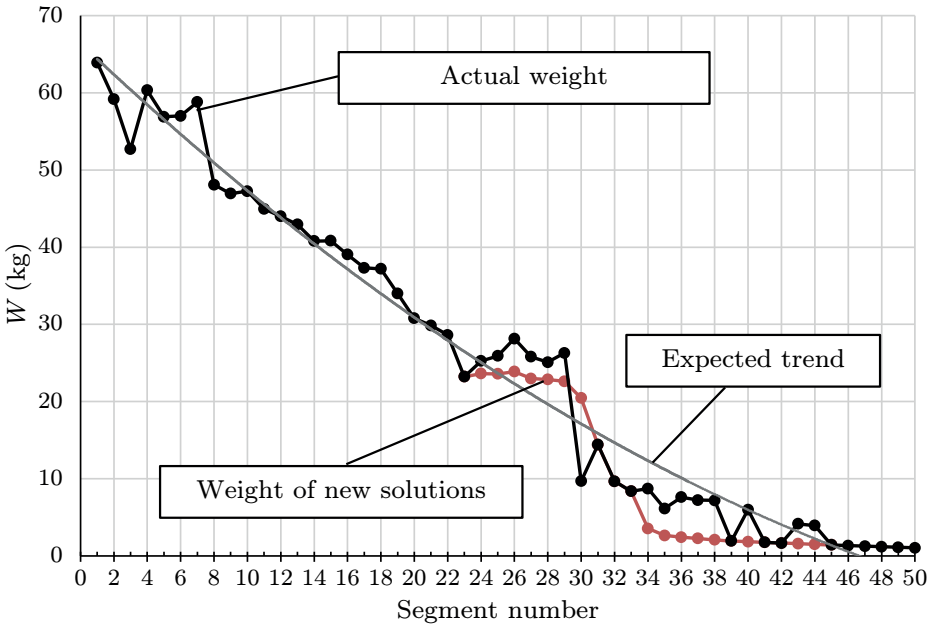


Figure 7.11: Weight of the optimal cross-section solution per segment.

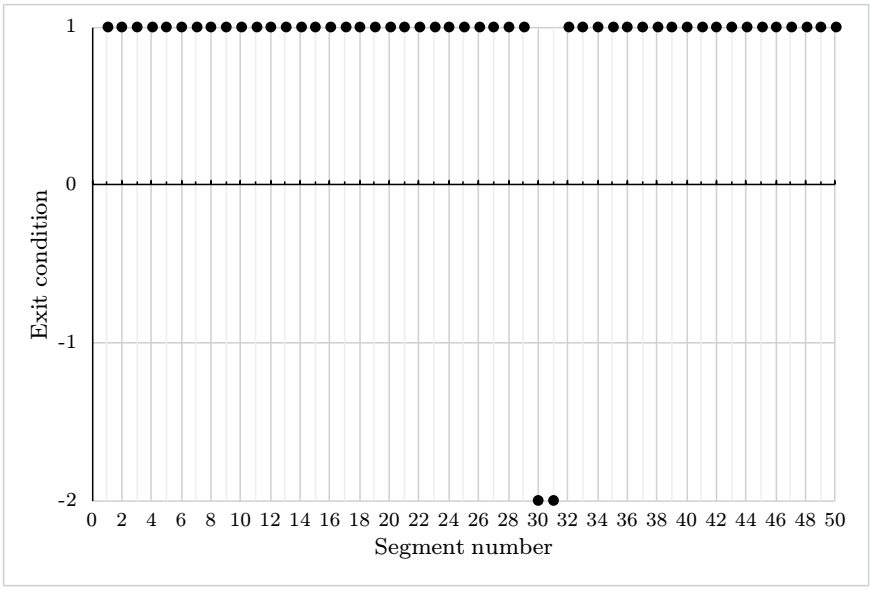


Figure 7.12: Exit condition of the optimisation procedure for each cross-section segment. Exit condition 1 means the solution satisfies all criteria, while −2 means the solution does not satisfy all solution, but has the lowest penalty value.

the design space is given as initial input for segments 30 and 31. This way it is checked whether there is a satisfying solution in the design space. In case of segments 30 and 31, satisfying solutions were obtained. Next step is to assure that the obtained solution is, to some extend, the lightest one. Therefore, the initial input is decreased to a solution with lower integer values. Then the optimisation procedure inclusive the convergence loop is repeated again, and the *optimal* solution is manually compared with the output of the previous optimisation. This process could be repeated for different input values more close to or at the lower boundary to somehow force the algorithm to search closer to the lower boundary. But this would sometimes result in no solution, in case the optimal solution is not close to the lower boundary. In general, selecting an initial input halfway the upper and lower boundary is useful to determine in which part of the design space the optimal solution is. Based on this information, the initial input could be selected, and the design space could be decreased to make the search more effective. This procedure which is used to obtain a better solutions is illustrated in Fig. 7.13.

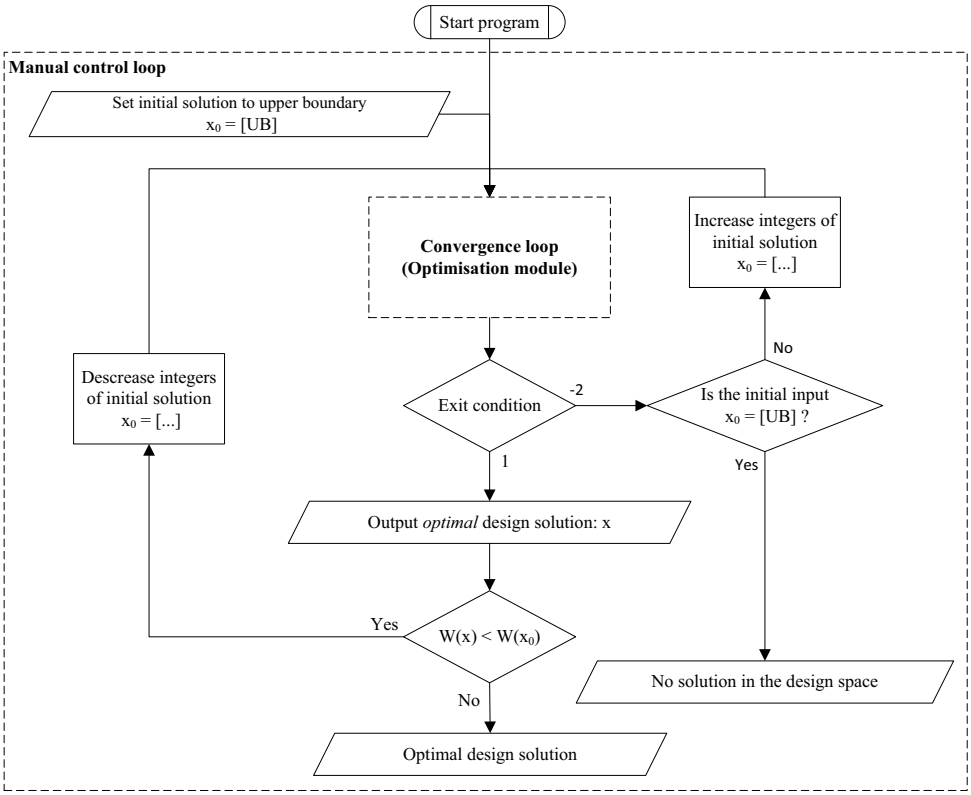


Figure 7.13: Manual control loop for the optimisation procedure.

The optimisation for these segments are repeated and the new solutions are updated in Fig.

7.14 and 7.15 for respectively the lower and upper skin. Segments 40, 43 and 44 have as expected a solution equal to the lower boundary of design space. For segments 30 and 31, a satisfying solution has been obtained while the weight of the solutions follow the trend of decreasing segment weight along the wing. The same is done for segments 24 to 29, for which lighter solutions are obtained by changing the initial design conditions. The weight reduction is clearly visible in Fig. 7.11, where also the weights of the new solutions are added.

In conclusion, an overall good performing design method is obtained for the wing structures. But manually eliminating the minor issues related to the algorithm and its limited capability of exploring large design spaces, is required to obtain proper solutions. Therefore, it is recommended for the designer to perform an additional check on the obtained solutions.

## 7.5. Limitations

As the design method is completely presented, the limitations are summarised below:

- The design solutions are dependent on the accuracy of the prediction methods.
- The approximate function should be created for different sets of model configurations.
- Approximate functions are only created per grade.
- The method currently extrapolated properties for thick lay-ups based on the trend.
- Prediction methods only consider longitudinal loads, so the design for lateral load is not possible at this stage.
- Lay-ups have only fibres with $0^\circ$ or $90^\circ$ orientation due to the limitations of the prediction methods.
- Settings of GA has to be optimised if the design space or requirements are changed.
- Only cross-sectional constraints are introduced, lengthwise constraints are not implemented.
- The design method is limited to three F&DT criteria and one thickness criteria.
- The FCI method is validated for GLARE and different type of FML solution, whereas the FCP and RS method are only validated for GLARE.

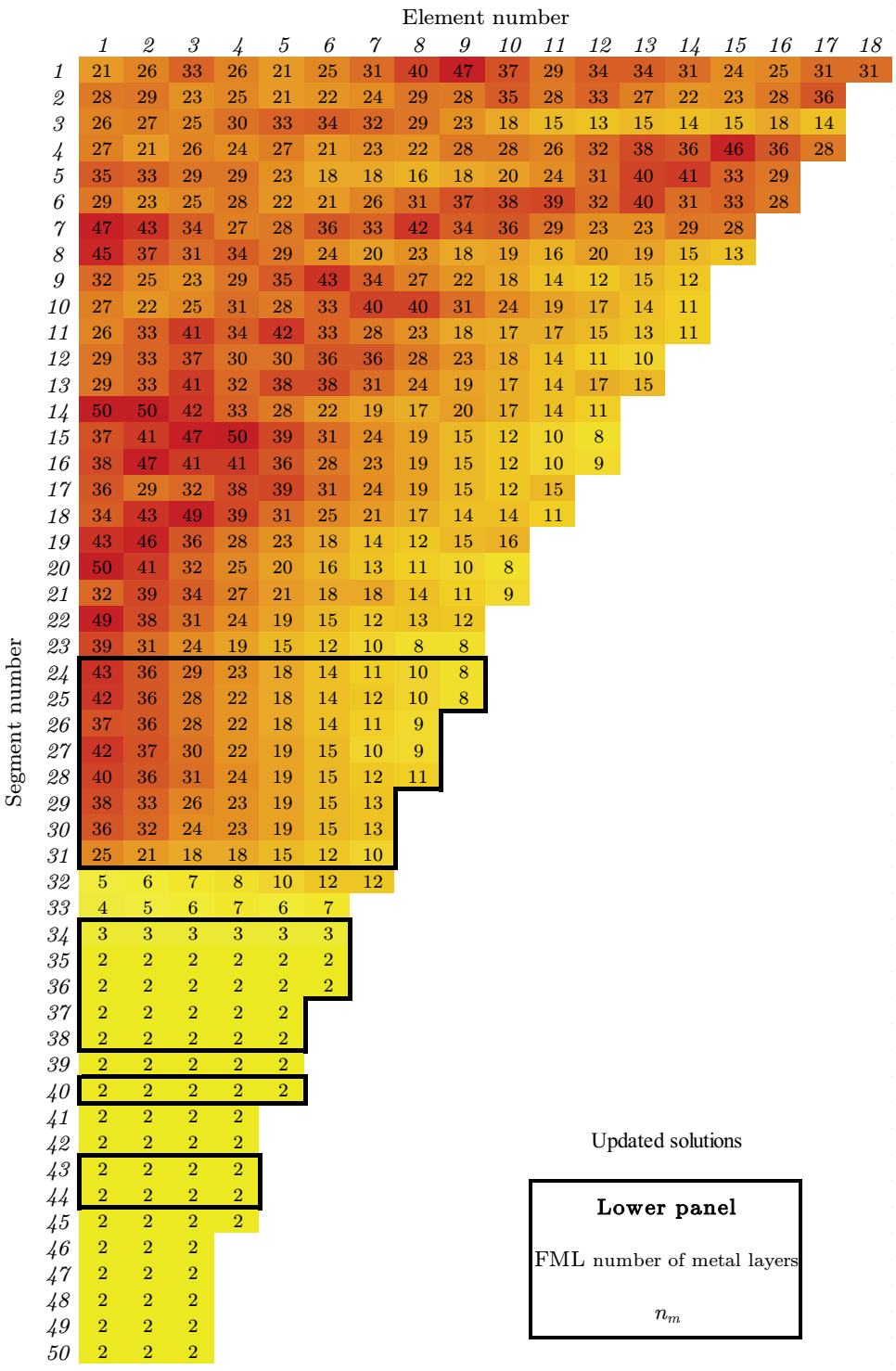


| Segment number | Element number 1 | 2 | 3 | 4 | 5 | 6 | 7 | 8 | 9 | 10 | 11 | 12 | 13 | 14 | 15 | 16 | 17 | 18 |
|---|---|---|---|---|---|---|---|---|---|---|---|---|---|---|---|---|---|---|
| 1 | 21 | 26 | 33 | 26 | 21 | 25 | 31 | 40 | 47 | 37 | 29 | 34 | 34 | 31 | 24 | 25 | 31 | 31 |
| 2 | 28 | 29 | 23 | 25 | 21 | 22 | 24 | 29 | 28 | 35 | 28 | 33 | 27 | 22 | 23 | 28 | 36 | |
| 3 | 26 | 27 | 25 | 30 | 33 | 34 | 32 | 29 | 23 | 18 | 15 | 13 | 15 | 14 | 15 | 18 | 14 | |
| 4 | 27 | 21 | 26 | 24 | 27 | 21 | 23 | 22 | 28 | 28 | 26 | 32 | 38 | 36 | 46 | 36 | 28 | |
| 5 | 35 | 33 | 29 | 29 | 23 | 18 | 18 | 16 | 18 | 20 | 24 | 31 | 40 | 41 | 33 | 29 | | |
| 6 | 29 | 23 | 25 | 28 | 22 | 21 | 26 | 31 | 37 | 38 | 39 | 32 | 40 | 31 | 33 | 28 | | |
| 7 | 47 | 43 | 34 | 27 | 28 | 36 | 33 | 42 | 34 | 36 | 29 | 23 | 23 | 29 | 28 | | | |
| 8 | 45 | 37 | 31 | 34 | 29 | 24 | 20 | 23 | 18 | 19 | 16 | 20 | 19 | 15 | 13 | | | |
| 9 | 32 | 25 | 23 | 29 | 35 | 43 | 34 | 27 | 22 | 18 | 14 | 12 | 15 | 12 | | | | |
| 10 | 27 | 22 | 25 | 31 | 28 | 33 | 40 | 40 | 31 | 24 | 19 | 17 | 14 | 11 | | | | |
| 11 | 26 | 33 | 41 | 34 | 42 | 33 | 28 | 23 | 18 | 17 | 17 | 15 | 13 | 11 | | | | |
| 12 | 29 | 33 | 37 | 30 | 30 | 36 | 36 | 28 | 23 | 18 | 14 | 11 | 10 | | | | | |
| 13 | 29 | 33 | 41 | 32 | 38 | 38 | 31 | 24 | 19 | 17 | 14 | 17 | 15 | | | | | |
| 14 | 50 | 50 | 42 | 33 | 28 | 22 | 19 | 17 | 20 | 17 | 14 | 11 | | | | | | |
| 15 | 37 | 41 | 47 | 50 | 39 | 31 | 24 | 19 | 15 | 12 | 10 | 8 | | | | | | |
| 16 | 38 | 47 | 41 | 41 | 36 | 28 | 23 | 19 | 15 | 12 | 10 | 9 | | | | | | |
| 17 | 36 | 29 | 32 | 38 | 39 | 31 | 24 | 19 | 15 | 12 | 15 | | | | | | | |
| 18 | 34 | 43 | 49 | 39 | 31 | 25 | 21 | 17 | 14 | 14 | 11 | | | | | | | |
| 19 | 43 | 46 | 36 | 28 | 23 | 18 | 14 | 12 | 15 | 16 | | | | | | | | |
| 20 | 50 | 41 | 32 | 25 | 20 | 16 | 13 | 11 | 10 | 8 | | | | | | | | |
| 21 | 32 | 39 | 34 | 27 | 21 | 18 | 18 | 14 | 11 | 9 | | | | | | | | |
| 22 | 49 | 38 | 31 | 24 | 19 | 15 | 12 | 13 | 12 | | | | | | | | | |
| 23 | 39 | 31 | 24 | 19 | 15 | 12 | 10 | 8 | 8 | | | | | | | | | |
| 24 | 43 | 36 | 29 | 23 | 18 | 14 | 11 | 10 | 8 | | | | | | | | | |
| 25 | 42 | 36 | 28 | 22 | 18 | 14 | 12 | 10 | 8 | | | | | | | | | |
| 26 | 37 | 36 | 28 | 22 | 18 | 14 | 11 | 9 | | | | | | | | | | |
| 27 | 42 | 37 | 30 | 22 | 19 | 15 | 10 | 9 | | | | | | | | | | |
| 28 | 40 | 36 | 31 | 24 | 19 | 15 | 12 | 11 | | | | | | | | | | |
| 29 | 38 | 33 | 26 | 23 | 19 | 15 | 13 | | | | | | | | | | | |
| 30 | 36 | 32 | 24 | 23 | 19 | 15 | 13 | | | | | | | | | | | |
| 31 | 25 | 21 | 18 | 18 | 15 | 12 | 10 | | | | | | | | | | | |
| 32 | 5 | 6 | 7 | 8 | 10 | 12 | 12 | | | | | | | | | | | |
| 33 | 4 | 5 | 6 | 7 | 6 | 7 | | | | | | | | | | | | |
| 34 | 3 | 3 | 3 | 3 | 3 | 3 | | | | | | | | | | | | |
| 35 | 2 | 2 | 2 | 2 | 2 | 2 | | | | | | | | | | | | |
| 36 | 2 | 2 | 2 | 2 | 2 | 2 | | | | | | | | | | | | |
| 37 | 2 | 2 | 2 | 2 | 2 | | | | | | | | | | | | | |
| 38 | 2 | 2 | 2 | 2 | 2 | | | | | | | | | | | | | |
| 39 | 2 | 2 | 2 | 2 | 2 | | | | | | | | | | | | | |
| 40 | 2 | 2 | 2 | 2 | 2 | | | | | | | | | | | | | |
| 41 | 2 | 2 | 2 | 2 | | | | | | | | | | | | | | |
| 42 | 2 | 2 | 2 | 2 | | | | | | | | | | | | | | |
| 43 | 2 | 2 | 2 | 2 | | | | | | | | | | | | | | |
| 44 | 2 | 2 | 2 | 2 | | | | | | | | | | | | | | |
| 45 | 2 | 2 | 2 | 2 | | | | | | | | | | | | | | |
| 46 | 2 | 2 | 2 | | | | | | | | | | | | | | | |
| 47 | 2 | 2 | 2 | | | | | | | | | | | | | | | |
| 48 | 2 | 2 | 2 | | | | | | | | | | | | | | | |
| 49 | 2 | 2 | 2 | | | | | | | | | | | | | | | |
| 50 | 2 | 2 | 2 | | | | | | | | | | | | | | | |



Figure 7.14: Number of metal layers in the FML lower skin based on GLARE 2A with $t_m$ = 0.5 mm with manually updated solutions.

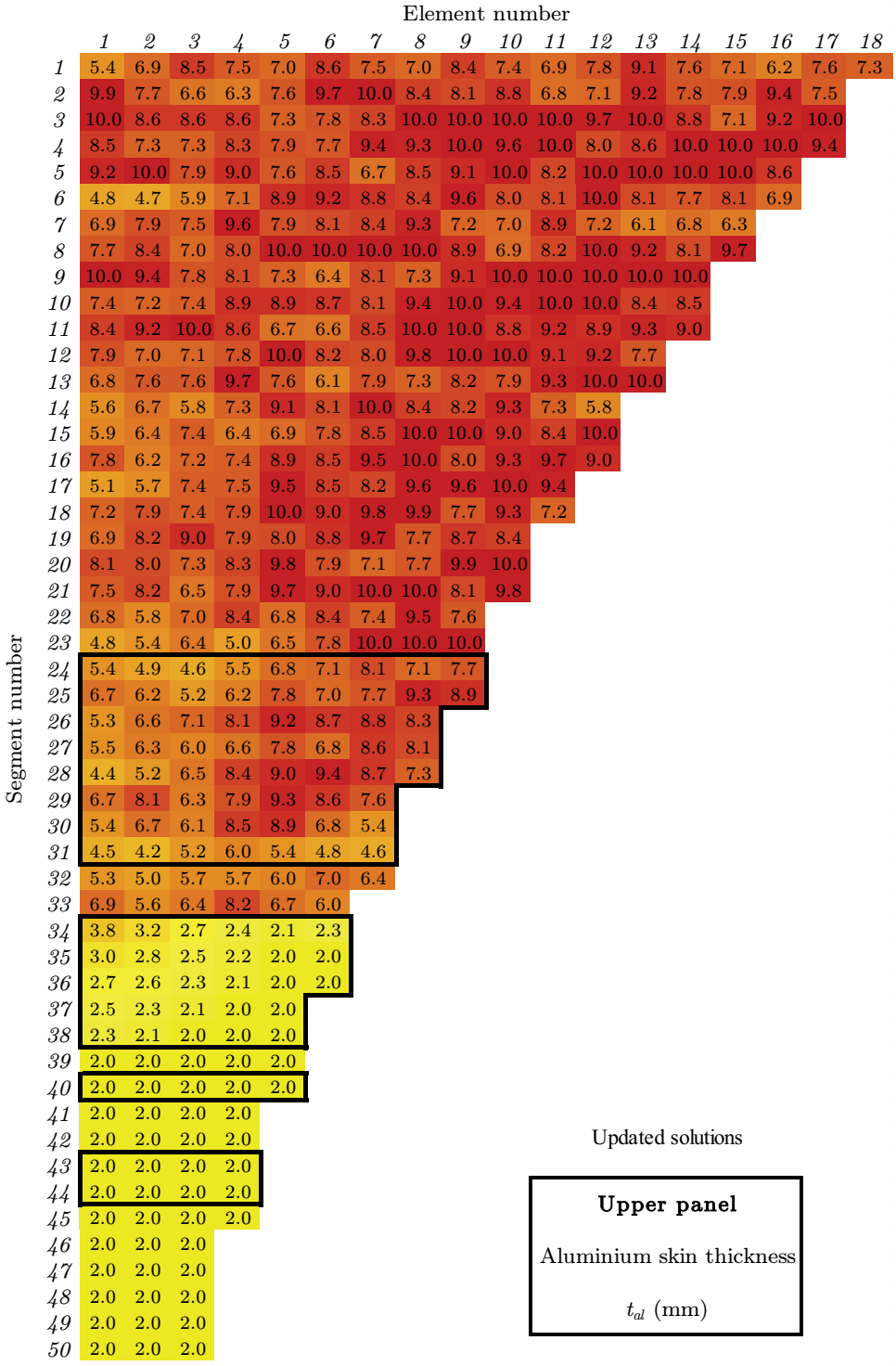


| Segment number \ Element number | 1 | 2 | 3 | 4 | 5 | 6 | 7 | 8 | 9 | 10 | 11 | 12 | 13 | 14 | 15 | 16 | 17 | 18 |
|---|---|---|---|---|---|---|---|---|---|---|---|---|---|---|---|---|---|---|
| 1 | 5.4 | 6.9 | 8.5 | 7.5 | 7.0 | 8.6 | 7.5 | 7.0 | 8.4 | 7.4 | 6.9 | 7.8 | 9.1 | 7.6 | 7.1 | 6.2 | 7.6 | 7.3 |
| 2 | 9.9 | 7.7 | 6.6 | 6.3 | 7.6 | 9.7 | 10.0 | 8.4 | 8.1 | 8.8 | 6.8 | 7.1 | 9.2 | 7.8 | 7.9 | 9.4 | 7.5 | |
| 3 | 10.0 | 8.6 | 8.6 | 8.6 | 7.3 | 7.8 | 8.3 | 10.0 | 10.0 | 10.0 | 10.0 | 9.7 | 10.0 | 8.8 | 7.1 | 9.2 | 10.0 | |
| 4 | 8.5 | 7.3 | 7.3 | 8.3 | 7.9 | 7.7 | 9.4 | 9.3 | 10.0 | 9.6 | 10.0 | 8.0 | 8.6 | 10.0 | 10.0 | 10.0 | 9.4 | |
| 5 | 9.2 | 10.0 | 7.9 | 9.0 | 7.6 | 8.5 | 6.7 | 8.5 | 9.1 | 10.0 | 8.2 | 10.0 | 10.0 | 10.0 | 10.0 | 8.6 | | |
| 6 | 4.8 | 4.7 | 5.9 | 7.1 | 8.9 | 9.2 | 8.8 | 8.4 | 9.6 | 8.0 | 8.1 | 10.0 | 8.1 | 7.7 | 8.1 | 6.9 | | |
| 7 | 6.9 | 7.9 | 7.5 | 9.6 | 7.9 | 8.1 | 8.4 | 9.3 | 7.2 | 7.0 | 8.9 | 7.2 | 6.1 | 6.8 | 6.3 | | | |
| 8 | 7.7 | 8.4 | 7.0 | 8.0 | 10.0 | 10.0 | 10.0 | 10.0 | 8.9 | 6.9 | 8.2 | 10.0 | 9.2 | 8.1 | 9.7 | | | |
| 9 | 10.0 | 9.4 | 7.8 | 8.1 | 7.3 | 6.4 | 8.1 | 7.3 | 9.1 | 10.0 | 10.0 | 10.0 | 10.0 | 10.0 | | | | |
| 10 | 7.4 | 7.2 | 7.4 | 8.9 | 8.9 | 8.7 | 8.1 | 9.4 | 10.0 | 9.4 | 10.0 | 10.0 | 8.4 | 8.5 | | | | |
| 11 | 8.4 | 9.2 | 10.0 | 8.6 | 6.7 | 6.6 | 8.5 | 10.0 | 10.0 | 8.8 | 9.2 | 8.9 | 9.3 | 9.0 | | | | |
| 12 | 7.9 | 7.0 | 7.1 | 7.8 | 10.0 | 8.2 | 8.0 | 9.8 | 10.0 | 10.0 | 9.1 | 9.2 | 7.7 | | | | | |
| 13 | 6.8 | 7.6 | 7.6 | 9.7 | 7.6 | 6.1 | 7.9 | 7.3 | 8.2 | 7.9 | 9.3 | 10.0 | 10.0 | | | | | |
| 14 | 5.6 | 6.7 | 5.8 | 7.3 | 9.1 | 8.1 | 10.0 | 8.4 | 8.2 | 9.3 | 7.3 | 5.8 | | | | | | |
| 15 | 5.9 | 6.4 | 7.4 | 6.4 | 6.9 | 7.8 | 8.5 | 10.0 | 10.0 | 9.0 | 8.4 | 10.0 | | | | | | |
| 16 | 7.8 | 6.2 | 7.2 | 7.4 | 8.9 | 8.5 | 9.5 | 10.0 | 8.0 | 9.3 | 9.7 | 9.0 | | | | | | |
| 17 | 5.1 | 5.7 | 7.4 | 7.5 | 9.5 | 8.5 | 8.2 | 9.6 | 9.6 | 10.0 | 9.4 | | | | | | | |
| 18 | 7.2 | 7.9 | 7.4 | 7.9 | 10.0 | 9.0 | 9.8 | 9.9 | 7.7 | 9.3 | 7.2 | | | | | | | |
| 19 | 6.9 | 8.2 | 9.0 | 7.9 | 8.0 | 8.8 | 9.7 | 7.7 | 8.7 | 8.4 | | | | | | | | |
| 20 | 8.1 | 8.0 | 7.3 | 8.3 | 9.8 | 7.9 | 7.1 | 7.7 | 9.9 | 10.0 | | | | | | | | |
| 21 | 7.5 | 8.2 | 6.5 | 7.9 | 9.7 | 9.0 | 10.0 | 10.0 | 8.1 | 9.8 | | | | | | | | |
| 22 | 6.8 | 5.8 | 7.0 | 8.4 | 6.8 | 8.4 | 7.4 | 9.5 | 7.6 | | | | | | | | | |
| 23 | 4.8 | 5.4 | 6.4 | 5.0 | 6.5 | 7.8 | 10.0 | 10.0 | 10.0 | | | | | | | | | |
| 24 | 5.4 | 4.9 | 4.6 | 5.5 | 6.8 | 7.1 | 8.1 | 7.1 | 7.7 | | | | | | | | | |
| 25 | 6.7 | 6.2 | 5.2 | 6.2 | 7.8 | 7.0 | 7.7 | 9.3 | 8.9 | | | | | | | | | |
| 26 | 5.3 | 6.6 | 7.1 | 8.1 | 9.2 | 8.7 | 8.8 | 8.3 | | | | | | | | | | |
| 27 | 5.5 | 6.3 | 6.0 | 6.6 | 7.8 | 6.8 | 8.6 | 8.1 | | | | | | | | | | |
| 28 | 4.4 | 5.2 | 6.5 | 8.4 | 9.0 | 9.4 | 8.7 | 7.3 | | | | | | | | | | |
| 29 | 6.7 | 8.1 | 6.3 | 7.9 | 9.3 | 8.6 | 7.6 | | | | | | | | | | | |
| 30 | 5.4 | 6.7 | 6.1 | 8.5 | 8.9 | 6.8 | 5.4 | | | | | | | | | | | |
| 31 | 4.5 | 4.2 | 5.2 | 6.0 | 5.4 | 4.8 | 4.6 | | | | | | | | | | | |
| 32 | 5.3 | 5.0 | 5.7 | 5.7 | 6.0 | 7.0 | 6.4 | | | | | | | | | | | |
| 33 | 6.9 | 5.6 | 6.4 | 8.2 | 6.7 | 6.0 | | | | | | | | | | | | |
| 34 | 3.8 | 3.2 | 2.7 | 2.4 | 2.1 | 2.3 | | | | | | | | | | | | |
| 35 | 3.0 | 2.8 | 2.5 | 2.2 | 2.0 | 2.0 | | | | | | | | | | | | |
| 36 | 2.7 | 2.6 | 2.3 | 2.1 | 2.0 | 2.0 | | | | | | | | | | | | |
| 37 | 2.5 | 2.3 | 2.1 | 2.0 | 2.0 | | | | | | | | | | | | | |
| 38 | 2.3 | 2.1 | 2.0 | 2.0 | 2.0 | | | | | | | | | | | | | |
| 39 | 2.0 | 2.0 | 2.0 | 2.0 | 2.0 | | | | | | | | | | | | | |
| 40 | 2.0 | 2.0 | 2.0 | 2.0 | 2.0 | | | | | | | | | | | | | |
| 41 | 2.0 | 2.0 | 2.0 | 2.0 | | | | | | | | | | | | | | |
| 42 | 2.0 | 2.0 | 2.0 | 2.0 | | | | | | | | | | | | | | |
| 43 | 2.0 | 2.0 | 2.0 | 2.0 | | | | | | | | | | | | | | |
| 44 | 2.0 | 2.0 | 2.0 | 2.0 | | | | | | | | | | | | | | |
| 45 | 2.0 | 2.0 | 2.0 | 2.0 | | | | | | | | | | | | | | |
| 46 | 2.0 | 2.0 | 2.0 | | | | | | | | | | | | | | | |
| 47 | 2.0 | 2.0 | 2.0 | | | | | | | | | | | | | | | |
| 48 | 2.0 | 2.0 | 2.0 | | | | | | | | | | | | | | | |
| 49 | 2.0 | 2.0 | 2.0 | | | | | | | | | | | | | | | |
| 50 | 2.0 | 2.0 | 2.0 | | | | | | | | | | | | | | | |



Figure 7.15: Upper skin thickness for the aluminium solution with manually updated solutions.

## 7.6. Conclusions

The methodology to obtain the results for the cross-section optimisation routine have been presented. The design method is capable of optimising a wing cross-section for upper panels consisting of aluminium and the lower panels consisting of FML. Hereby, the thickness of the upper panels are optimised, while for the lower FML panels, the number of metal sheet is selected as optimisation parameter. The thickness of the metal sheet and the grades is fixed during the optimisation. For various grades (GLARE 2A, GLARE 4A and GLARE 4B) and sheet thicknesses between $0.3$ and $0.7$ mm, the optimised lay-ups were obtained and the corresponding weight then compared. In this design case, GLARE 2A with $t_m = 0.4$ mm resulted in the lightest solution. Furthermore, the optimisation was repeated for all the cross-sections and a thickness and number of layer distribution for the full wing satisfying the F&DT and thickness step criteria were obtained. The important point that should be stated here is that the design methodology often finds local optima instead of the global optimum, simply because this global optimum is not generated in the large design space. The convergence loop partly assures that the design space is better explored. But the designer should be aware of this limitation caused by the large design space and the optimisation algorithm, and if necessary repeat the optimisation.

## References



[1] C. Cooper, *Development of a Methodology to Support Design of Complex Aircraft Wings*, Ph.D. thesis, Delft University of Technology, Delft (2011).

# 8

# Conclusions and recommendations

This chapter restates the aim and objectives of this research and summarises the conclusions that are gathered during the development of the design optimisation methodology for FML. Recommendations for further study are also discussed.

## **8.1.** Concluding remarks

The lower wing skin is one of the primary structures of an aircraft. To further improve the F&DT performance of the lower wing, FML are proposed as a new material solution. FML have a large design freedom and by varying the lay-up parameters, the laminate can be tailored for specific applications. Therefore, this study has been performed to explore the possibilities of FML and use it to design a wing structure.

The research aims *to develop a design optimisation methodology for FML that is used to design a wing skin where the F&DT criteria are met*. This aim has been successfully achieved with the stepwise development of the methodology as described in the previous chapters by fulfilling the engineering and scientific objectives.

**Engineering objective** — An analytical model is implemented in MATLAB that comprises all the functionality to design a wing skin consisting of FML lower panels and aluminium upper panels.

The model has a modular structure with the possibility to predict F&DT properties for given lay-ups, to create approximate functions for prediction models, to perform lay-up optimisation on element and cross-section level, to construct wing geometry and calculate running loads on predefined load cases, and finally, to perform a wing optimisation.

**Scientific objective** — A method has been successfully developed to reverse the prediction methods in order to find the lay-ups that satisfy the required property instead of determining the properties of a given lay-up.

Although mathematical reversion of the prediction methods was not possible due to the structure of the models. Approximate functions were created for these prediction methods by performing a regression analysis on the data of the prediction methods. The reversion of these functions was possible, and thus a reversed method could be developed. However, due to the multiple design variables for FML, an optimisation procedure was required to obtain the lay-ups. In this case, it was not necessary to mathematically reverse the prediction method, but with the implementation into this procedure a reversed method was obtained, in which lay-up for given properties are obtained. This procedure is improved by replacing the prediction methods by the earlier obtained approximate functions.

For these objectives, conclusions supported by this research are given below.

- Prediction methods are only predicting properties for given lay-ups. To obtain lay-ups for given properties requires the methodology to be reversed as stated by the scientific objective. An optimisation procedure was proposed to implement the prediction methods in this procedure. However, the procedure was not time efficient and procedural errors occurred for the FCP criteria, because the FCP method was unable to predict certain lay-ups due to its limitations. For this reason, an optimisation procedure with approximate function replacing the prediction methods was proposed now. The use of an approximation is with the cost of accuracy. But on the other side, the approximate function solved both issues by making the procedure efficient and giving the possibility to interpolate or extrapolate properties of solutions based on the trend of predictable lay-ups.
- Approximate functions were generated for the FCI, FCP and RS prediction methods. These function were only created for a single grade, because no correlation was found between the different grades. The thickness of the metal layers, the number of the metal layers and the laminate stress were selected as variables in the FCI and FCP functions, while the RS function had only the lay-up variables. The FCI method has a large dependency on S-N curves. Therefore, accurate prediction were sometimes difficult to assure due to the different S-N curves, each giving a different prediction for a solution. However, if the S-N curve was selected, the approximate function had a good agreement with the prediction data. The FCP approximate function had also in general a good fit. The exponential behaviour of fatigue life caused some deviations in the prediction results, but these were relatively small if the exponential behaviour is considered. For RS, a close to perfect fit was obtained.
- Inaccurate predictions influence the obtained optimal and near optimal design solutions. Due to this prediction, some solutions are ranked higher, while others are even unrighteously eliminated. The output of the optimal solution depends thus on the accuracy of the

prediction methods. Therefore, the designer should know the limitations of the prediction methods to assure that the obtained solutions are realistic ones.

- The method is implemented with GA, and it works fine when a single element is optimised. However, when switching to a cross-section optimisation, seldom it happened that satisfying solutions were not obtained. The size of a design space effects the output of the optimisation procedure. A larger design space is difficult to assess due to the immense amount of possible solutions. In this case, when there are no solutions obtained, this does not necessary mean that there are no satisfying solutions in the design space. The solutions were simply not generated due to the size of the design space or the selected settings for the algorithm. This problem could be solved by defining an initial input to the procedure, for example by giving the thickest laminate as input to check whether this laminate fulfils the criteria. If this solution does not satisfy either, then there are really no solutions available in the selected design space. Increasing the upper boundary of the design space would allow thicker laminates to be assessed. This way the laminate stresses will be lower, and the F&DT criteria will be met easier. An convergence loop has been implemented to solve this issue.
- GA also tends to give local minimum solutions affected by the initial solution instead of global minimum for large design spaces. This is because the design space is not thoroughly explored due to its size or again due to the defined settings. Making the design space smaller would help to obtain faster the global minimum. For example, for high applied loads the lower boundary of the design space could be increased as the thin solution might not satisfy anyway due to the high layer stresses. Another possibility is to adapt the GA setting, because then a better search performance might be obtained. Downside of the better search performance is that the computation time increases. Therefore, a balance has to be find between the different settings. Finding the best settings is a study on its own.
- With multi-criteria optimisation, each criteria has its own design space with solutions. Overlap between the design spaces is required to select the optimal solution satisfying all criteria. Sometimes it is required to increase the design space or the loosen one design criteria to have an optimal solution. So, the no solution situation is not always related to the algorithm.
- The developed design method has a generic character, and it considers both the design of aluminium and FML skin panel for a parametric wing geometry and various load cases. The cross-sections are obtained satisfying F&DT criteria and the thickness step criteria. The thickness step was introduced to prevent stress concentrations between the elements, but also to force a design with a distributed thickness. The method is able to design both panels while obtaining the thickness and number of metal layer distributions for the complete wing. The method determines the weight of each solutions and makes it possible to compare different solutions. The presented results were only to support and

demonstrate the methodology, as this study aims to develop the methodology to design a wing structure instead of the actual design.

With the two objectives met, it can now be stated that *a design optimisation methodology for FML that is used to design a wing skin where the F&DT criteria are met has been developed*. There is still a lot of work to be accomplished, but the initial method that designs a wing cross-section has been developed. With the use of this design method further research can be performed on the application of FML in aircraft structures.

## **8.2.** Future prospects

The following recommendations are suggested to improve and extent the design optimisation methodology:

- The prediction methods could be replaced by other methods with a more generic character to cover a larger design space. The prediction results for thick FML solutions should also be validated, because the wing requires higher skin thicknesses to bridge the higher loads.
- Verification and validation of the design results are required. In this thesis, the design methodology is proposed and developed, and the obtained results are just to demonstrate the methodology. As the prediction accuracy depends on the prediction methods and not on the design method, experimental testing or other verifications are required to check the design solutions.
- The current objective for the optimisation is defined as obtaining the minimum weight solution that satisfies F&DT criteria. Genetic algorithm supports the definition of multiple objectives, Therefore, additional objectives, such as the material and manufacturing cost could be introduced. This might be beneficial, for example, when different type of materials are assessed as FML constituents.
- The generic character of GA allows the definition of custom FML solution or additional variables, such as the material type. The method could be extended to design lay-up solutions that are different than the implemented GLARE ones.
- A sensitivity analysis is advised to identify the critical properties influencing the performance of a structure. This way the influence of the proposed improvements on the structure weight could be investigated. The developed design methodology is capable of being used for further studies on wing design and to create understanding on the influences of different properties on the design space.
- The wing cross-section optimisation does not have constraints between the different cross-section. The design method could be improved by introducing constraints between the cross-section. However, this requires the cross-section optimisation to be changed to a

wing optimisation, in which the compatibility is checked for four neighbouring segments instead of the current two.

- The thickness step constraint is the only manufacturing and compatibility criteria. Additional, criteria could be introduced to obtain a lightweight solution that is easier to manufacture. As initial step in the design, it is advised to start with a solution, where all cross-section elements have the same thickness. Depending on the results, the constraints on the thickness could be loosened to further decrease the cross-section weight.
- The method could be extended with detailed local optimisation to consider for local reinforcements, but more research is necessary on this topic.
- The computation time of optimisation procedure could be further improved by focussing on improvements related to the algorithm and its operators. Additionally, the improvement could also be achieved by simplifying the prediction methods by means of efficient programming, if approximate functions are not preferred to be used in the methodology.
- It is worth to perform a design study for aluminium versus FML to prove the efficiency of the FML concept in case of wing application.

# A

# Geometry and load calculations

*In this appendix, the geometry and load calculations are presented that are implemented in the design method. The shape and dimensions of the wing are defined by simplifying the wing geometry and making it parametric to support various wing types and sizes. The airfoil shape is variable and can be changed according to the need of the user. The wing is divided into lengthwise segments and the coordinates of each cross-section is determined in the global axis. Furthermore, the wing box dimensions are derived from the wing shape and the wing is cross-sectionally segmented by assuming a skin-stringer combination as a segment. For the load calculations, the weight and the elliptical lift distribution along the wing are estimated. The shear force and bending moment lines are determined and the running loads at the upper and lower skin segments are calculated based on these forces and moments. The running loads are used for further evaluation in the process of finding the minimum skin thickness in case of aluminium or the optimal lay-up in case of FML.*

## **A.1.** Introduction

The Airbus A320 transport aircraft is selected as reference aircraft and the geometry and load calculations are performed with the objective to perform material evaluation for the wing of this type of aircraft. In the geometry- and load module, the wing geometry is defined parametrically to support various wing types and the load cases are simplified. To facilitate these configurations, assumptions are made for the applied loads and the wing configuration. These assumptions are necessary to create an analytical model that is user friendly, easy to extend and accurate at the same time. The assumptions are states as followed:

A

- The method is designed for the wing of a commercial transport aircraft.
- The aircraft has one engine attached to the wing.
- The main landing gear is not attached to the wing.
- No cuts-outs are assumed in the wing (no inspection holes, etc.)
- The wing chord length en the wing thickness is linearly changing between the root, the kink and the tip section of the wing.
- The wing box width is a fixed percentage of the wing chord length.
- The wing is assumed to be clamped at root side.
- The lift distribution is assumed to be elliptical along the wing length.
- The wing weight is assumed to be a linear distribution along the wing length.
- When on the ground the lift forces are zero.
- When in the air the lift is equal to the aircraft weight.

## **A.2.** Geometry

### **A.2.1.** Shape and dimensions

The wing geometry is constructed based on the illustrations of the Airbus A320 transport aircraft, which are given in Fig. A.1. First, the wings do not have a straight taper, but a kink close to the engine attachment position on the wing. This kink is located at the discontinuity of the the wing taper, where a geometry transition occurs. Furthermore, the lower part of the wing has a parabolic shape starting from the root till approximately to the location of the kink, but for simplification reasons linear shapes are assumed for this section.

Using these simplifications, the wing shape as seen from the top is defined using the following parameters: the length of the wing $(l_w)$, the chord length at the root $(c_r)$, kink $\left(c_{k_1}\right)$ and tip $(c_t)$, and the sweep angle of the leading edge $(\Lambda)$. The wing shape as seen from the side is defined using the thickness at the root $(t_r)$, both kinks $\left(t_{k_1}, t_{k_2}\right)$ and tip $(t_t)$, and the dihedral $(\Gamma)$ of the wing. The schematic overview of the top view and side view are given in Fig. A.2 and A.3, respectively.

The wing chord is linearly changing along the wing between the input chord lengths and calculated by:

$$c = \begin{cases} c_r + \frac{c_{k_1} - c_r}{Y_{k_1}} Y & \text{for } 0 < Y \leq Y_{k_1} \\ c_{k_1} + \frac{c_t - c_{k_1}}{Y_t - Y_{k_1}} Y & \text{for } Y_{k_1} < Y \leq Y_t \end{cases} \tag{A.1}$$

where $c$ is the chord length at location $Y$, $c_r$ is the chord length at the root, $c_{k_1}$ is the chord length at the kink, $c_t$ is the chord length at the wing tip, $Y_{k_1}$ is the location of kink number

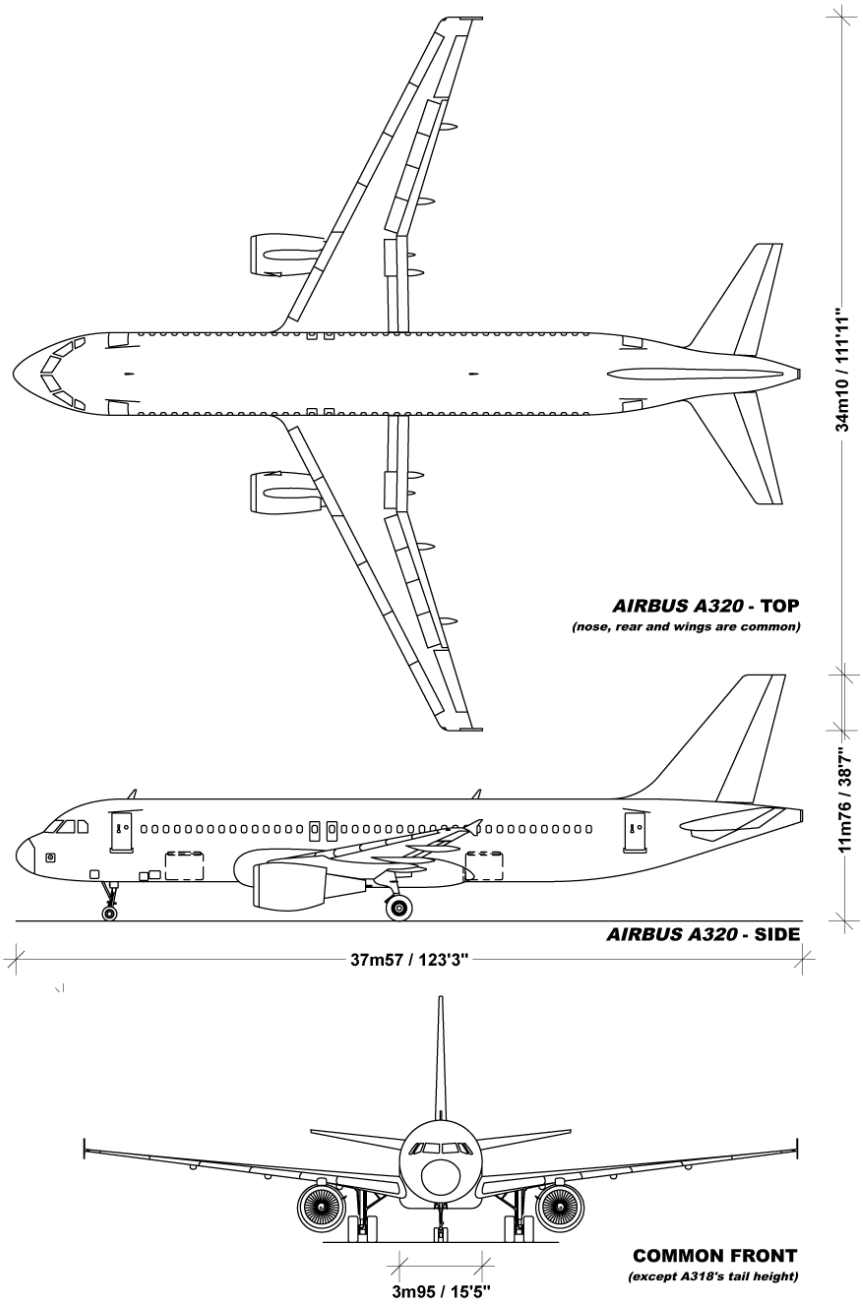


Figure A.1: Illustrations of an Airbus A320 transport aircraft [1].

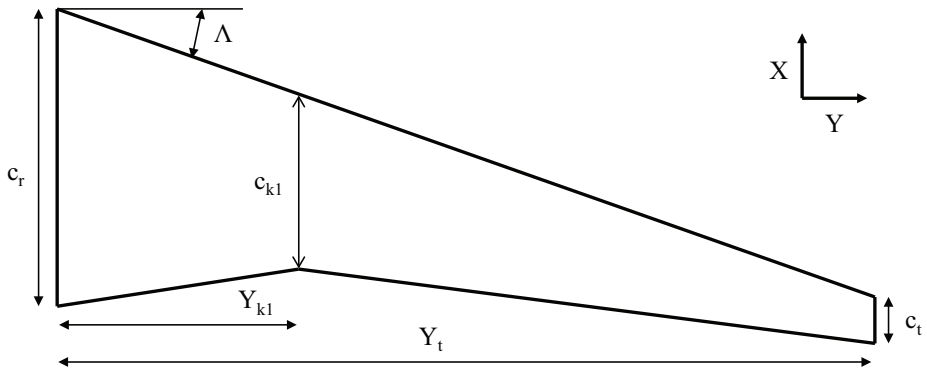


Figure A.2: Schematic top view of defined wing shape.

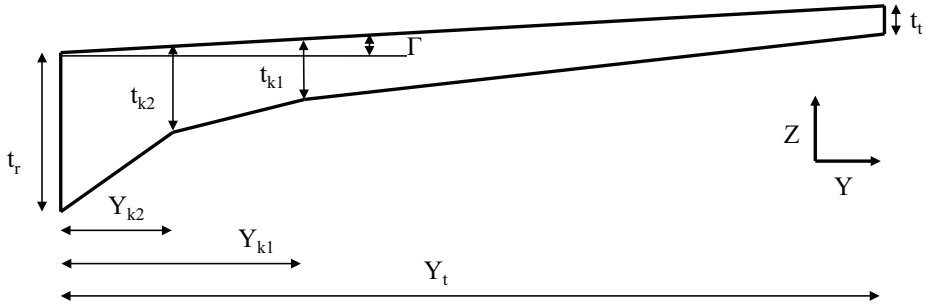


Figure A.3: Schematic side view of defined wing shape.

1 with respect to the root and $Y_t$ is the location of the wing tip, which is equal to the wing length $l_w$ and $Y$ is the location of the cross-section for which the chord length is determined along the wing length from 0 to $Y_t$. In Fig. A.4, the chord length along the wing is plotted for input data of the Airbus A320 aircraft. The parameter values to construct the wing are given in Table A.1.

| | | Root ($r$) | Kink 1 ($k_1$) | Kink 2[a] ($k_2$) | Tip ($t$) |
|---|---|---|---|---|---|
| Chord length (m) | $c$ | 6.075 | 3,757 | - | 1.496 |
| Thickness to chord ratio | $\frac{t}{c}$ | 0.1515 | 0.1175 | 0.1175 | 0.1084 |
| Location (m) | $Y$ | 0 | 4.46 | 4.46 | 15.085 |
| Front spar as fraction of chord | $\eta_p$ | 0.15 | 0.15 | 0.15 | 0.15 |
| Wing box width as fraction of chord | $\eta_b$ | 0.44 | 0.46 | 0.46 | 0.24 |
| Sweep angle (°) | $\Lambda$ | | 25 | | |
| Dihedral (°) | $\Gamma$ | | 5.11 | | |

[a] For the test case only one kink in the wing is assumed, kink 2 is at the same location as kink 1.

Table A.1: Wing parameters for the Airbus A320 aircraft.

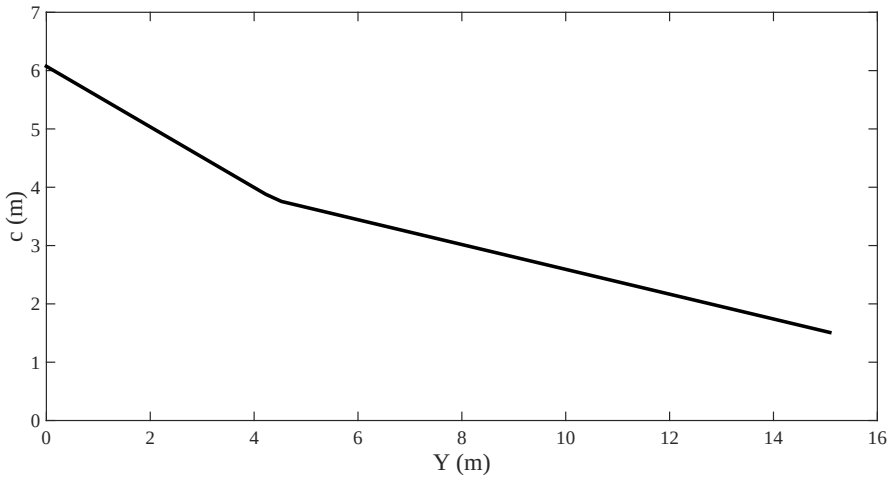


Figure A.4: Wing chord distribution along wing length for Airbus A320.

The wing thickness depends on the chord length. For this reason, the thickness to chord ratio of the wing $\left(\frac{t}{c}\right)$ is used to describe this dependency. On the lower section of the wing panel, there are two kinks assumed to replace the parabolic shape for simplification reasons

and $\frac{t}{c}$ at each location is assumed to be linearly changing and given by:

$$\frac{t}{c} = \begin{cases} \left(\frac{t}{c}\right)_r + \frac{\left(\frac{t}{c}\right)_{k_2} - \left(\frac{t}{c}\right)_r}{Y_{k_2}} Y & \text{for } 0 < Y \leq Y_{k_2} \\ \left(\frac{t}{c}\right)_{k_2} + \frac{\left(\frac{t}{c}\right)_{k_1} - \left(\frac{t}{c}\right)_{k_2}}{Y_{k_1} - Y_{k_2}} Y & \text{for } Y_{k_2} < Y \leq Y_{k_1} \quad \text{Note: } Y_{k_2} \leq Y_{k_1} \\ \left(\frac{t}{c}\right)_{k_1} + \frac{\left(\frac{t}{c}\right)_t - \left(\frac{t}{c}\right)_{k_1}}{Y_t - Y_{k_1}} Y & \text{for } Y_{k_1} < Y \leq Y_t \end{cases} \tag{A.2}$$

where $\left(\frac{t}{c}\right)_r$ is thickness to chord ratio at the root, $\left(\frac{t}{c}\right)_{k_1}$ is the thickness to chord ratio at kink number 1, $\left(\frac{t}{c}\right)_{k_2}$ is the thickness to chord ratio at kink number 2 which is between the root and kink number 1, $\left(\frac{t}{c}\right)_t$ is the thickness to chord ratio at the wing tip, $\Gamma$ is the dihedral of the wing, $Y_{k_1}$ is the location of kink number 1 with respect to the root, $Y_{k_2}$ is the location of kink number 2 with respect to the root, $Y_t$ is the location of the wing tip and $Y$ is the location of the cross-section for which the thickness to chord ratio is determined along the wing length from $0$ to $Y_t$. In Fig. A.5, the wing thickness along the wing is plotted for input data of the Airbus A320 aircraft.

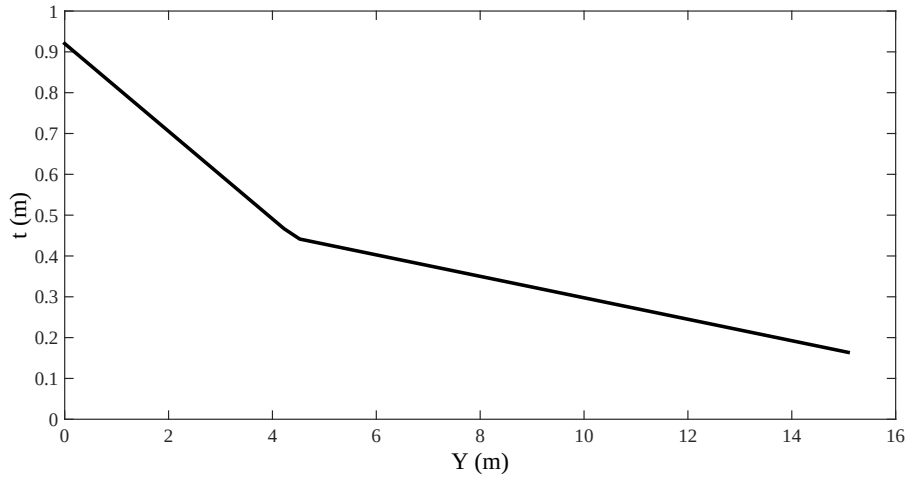


Figure A.5: Wing thickness distribution along wing length for Airbus A320.

The global coordinate system is defined with the axis origin at the front-upper section of the wing root. Using the sweep angle $(\Lambda)$ the position and X-coordinates of the front spars $(X_{\text{front}})$ are calculated. The position of rear spar $(X_{\text{rear}})$ is then found by subtracting the chord length $(c)$ at location $Y$.

$$X_{\text{front}} = -Y \tan(\Lambda) \tag{A.3}$$

$$X_{\text{rear}} = X_{\text{front}} - c \tag{A.4}$$

The X-coordinates of the front and rear spars of the reference aircraft is plotted in Fig. A.6.

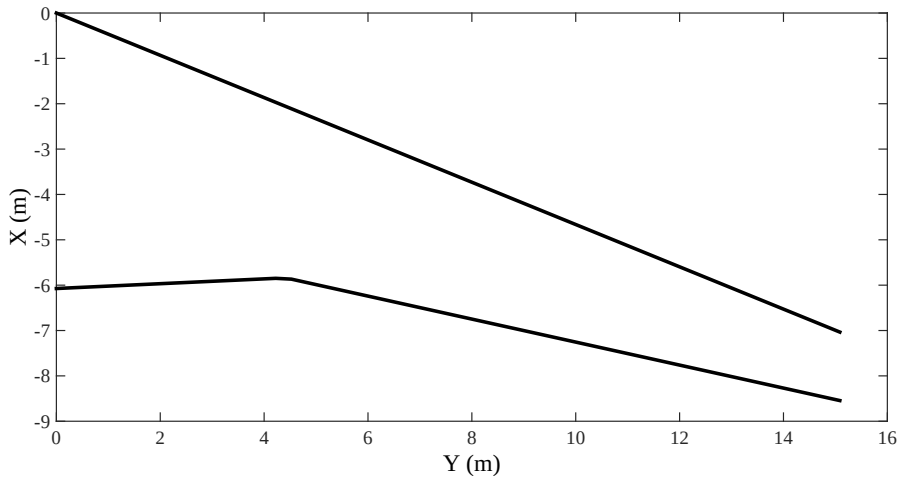


Figure A.6: Front and rear spars coordinates for Airbus A320.

Using the dihedral ($\Gamma$), the Z-coordinates ($Z_{\text{top}}$) of the top cover is calculated, while the Z-coordinates of the bottom cover ($Z_{\text{bottom}}$) is found by subtracting the wing thickness from $Z_{\text{top}}$ at each $Y$ location.

$$Z_{\text{top}} = Y \tan(\Gamma) \tag{A.5}$$

$$Z_{\text{bottom}} = Z_{\text{top}} - \left(\frac{t}{c}\right) c \tag{A.6}$$

These Z-coordinates represent the maximum distance between the upper and lower cover and at these points the airfoil shape will be the thickest. The airfoil has a closing shape and it will be defined from the midpoint between the top and bottom panel. Therefore, the calculation of the midpoint coordinate ($Z_{\text{mid}}$) is necessary.

$$Z_{\text{mid}} = \frac{Z_{\text{top}} + Z_{\text{bottom}}}{2} \tag{A.7}$$

The Z-coordinates of the top and bottom cover of the reference aircraft is given in Fig. A.7.

### **A.2.2.** Airfoil

The symmetric 4-digit NACA airfoil is considered [2] as the shape for the wing cross-section. The shape of the airfoil is described by the following formula:

$$\begin{aligned} y = \frac{t}{0.2} c \Bigg[ & 0.2969 \sqrt{\frac{x}{c}} - 0.1260 \left(\frac{x}{c}\right) \\ & -0.3516 \left(\frac{x}{c}\right)^2 + 0.2843 \left(\frac{x}{c}\right)^3 - 0.1015 \left(\frac{x}{c}\right)^4 \Bigg] \end{aligned} \tag{A.8}$$

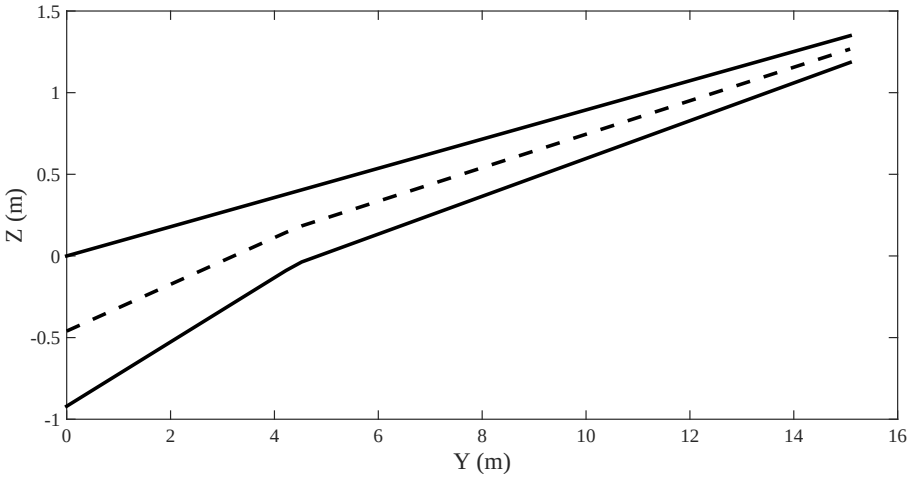


Figure A.7: Top and bottom cover coordinates for Airbus A320.

where $c$ is the chord length, $x$ is the position along the chord from 0 to $c$, $y$ is the half thickness at a given value of $x$ (centreline to surface) and $t$ is the maximum thickness as a fraction of the chord. $x$ en $y$ are defined as the local axis with the nose of the airfoil as the origin of the axis. The schematic view of the airfoil described by Eq. (A.8) is given in Fig. A.8.

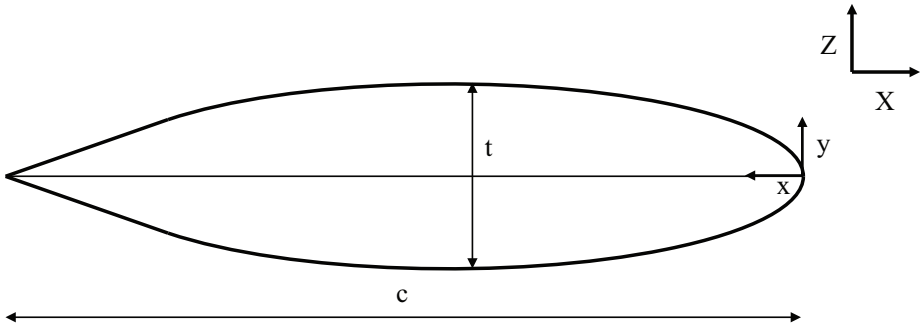


Figure A.8: Schematic cross-sectional view of the wing.

The global coordinates of the cross-section is found by adding or subtracting the local coordinates from the global ones. The coordinates of the upper section is calculated as:

$$Z_{\text{upper}} = Z_{\text{mid}} + y \tag{A.9}$$

$$X_{\text{upper}} = X_{\text{front}} - x \tag{A.10}$$

The coordinates of the lower section is calculated as:

$$Z_{\text{lower}} = Z_{\text{mid}} - y \tag{A.11}$$

$$X_{\text{lower}} = X_{\text{mid}} - x \tag{A.12}$$

The cross-sectional view of the wing is given in Fig. A.9.

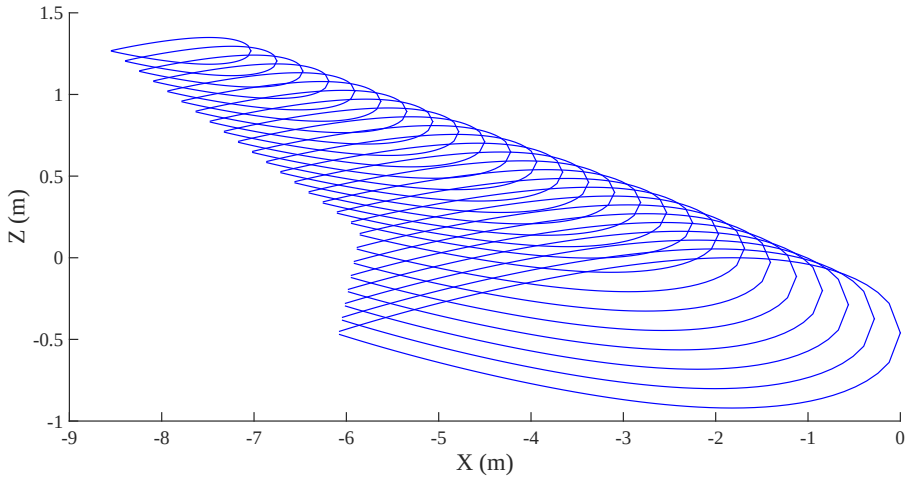


Figure A.9: Cross-sectional view of the defined wing shape.

### **A.2.3.** Segmentation

The wing is lengthwise divided into segments with a length of $dY$. Each segment has its own cross-sectional shape and size depending on the airfoil and the position on the wing. The chord length $(c)$ and the thickness to chord ratio $\left(\frac{t}{c}\right)$ is calculated for each segment and then the exact dimensions of the cross-section is found using the airfoil formula given by Eq. A.8. This cross-section is then assumed for the segment length $dY$. The position of the fuel tank and the engine is linked to the closest segments and these segments are assumed to be the actual position of the fuel tank and the engine. The number of segments is changeable depending on the required accuracy. An illustration of the segmented wing is given in Fig. A.10.

Each cross-section is divided into two parts: the upper and lower panel. The upper and lower panels are segmented and the coordinates of each segments is determined in to the global axis. The width of each segment is set as $dc$ and assumed to be straight lines for simplification reasons, which is illustrated in Fig. A.11.

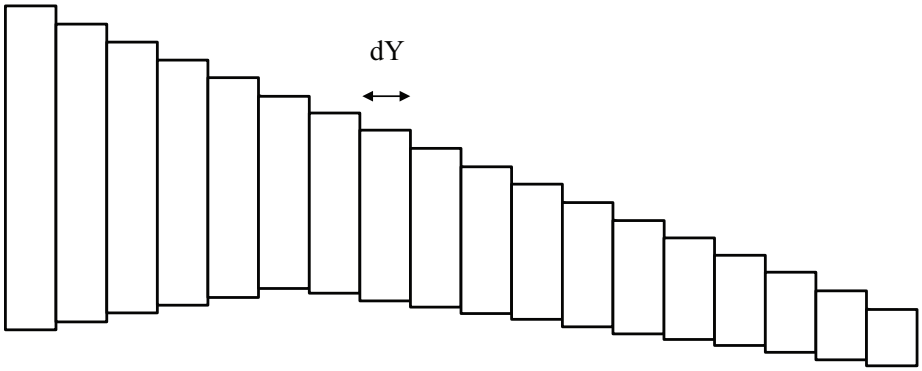


Figure A.10: Segmentation of the wing in lengthwise direction.

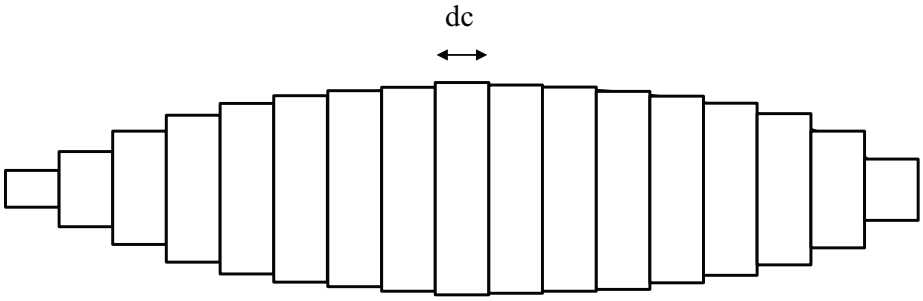


Figure A.11: Segmentation of the wing in cross-sectional direction.

### **A.2.4.** Wing box

The wing box width ($b_w$) is assumed to be a fixed percentage of the chord length ($b_w = \eta_b c$). This value is given as input for the root, kink and tip section. Hereafter, the wing box width is linearly interpolated for each segment. The start position of the wing box ($p_w$) is given as a percentage of the chord length with respect to the front spar ($p_w = \eta_p c$). )The illustration of the wing box cross-section and the shape along the wing length are illustrated in Fig. A.12 and A.13, respectively. These values are given in Table A.1.

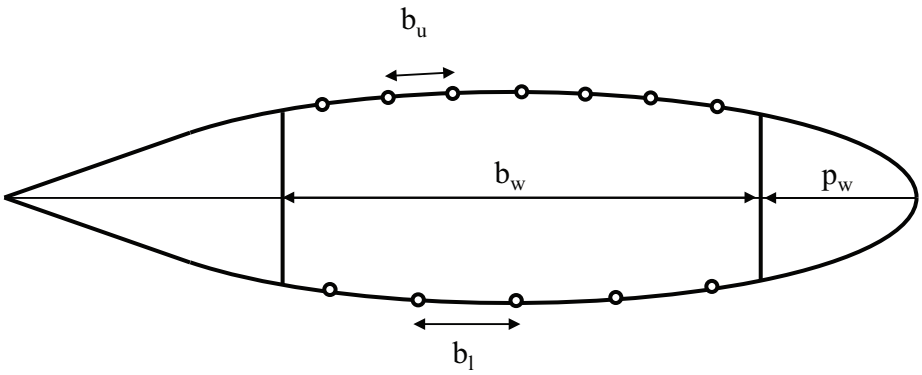


Figure A.12: Schematic view of the wing box cross-section.

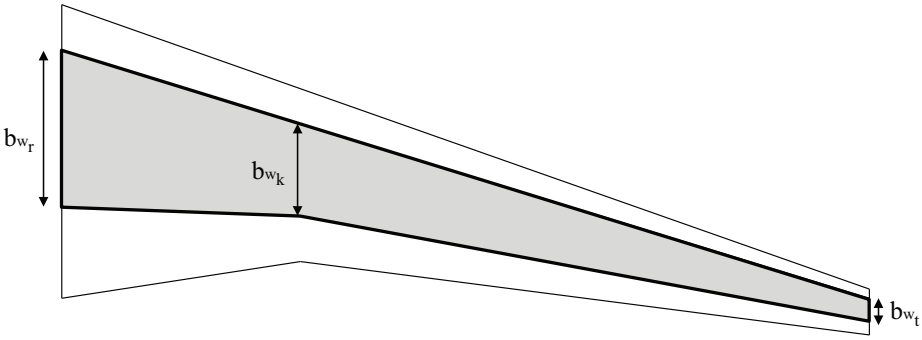


Figure A.13: Schematic view of the wing box as seen from the top.

## **A.3.** Loads

Once the geometry is modelled, the load calculations are performed by determining the forces and the moments on the wing and deriving the running loads on the skin panels. There are two general load cases defined [3, 4]:

1. Air
2. Ground (no lift)

The load calculations are simplified and only two aspects contribute to the running loads, namely the weight and lift distribution along the wing. These distributions are obtained by means of estimations described by Torenbeek [5] and are used to derive the force and moment lines along the wing length.

### **A.3.1.** Weight

The total wing weight is assumed to be $9\%$ of the aircraft weight $(W)$ based on weight estimations of aircraft with similar size discussed in [5]. The aircraft weight is set equal to the Maximum Take-off Weight (MTOW) of $66,000$ (kg). The weight of one wing $(W_w)$ is then assumed to be the half of this percentage, $W_w = 0.045W$. The weight at the tip $(W_{w_t})$ is assumed to be $5\%$ of the wing weight, $W_{w_t} = 0.05W_w$ [5]. The weight at the root $(W_{w_r})$ is obtained with $W_{w_r} = \frac{W_w}{l_w} - W_{w_t}$, and then the weight distribution $\frac{dW_w}{dY}$ is assumed to be linearly decreasing along the wing from the root till the tip ($Y = 0$ to $Y = Y_t$) [5].

$$\frac{dW_w}{dY} = W_{w_r} - \frac{W_{w_r} - W_{w_t}}{l_w} Y \tag{A.13}$$

The weight of the fuel stored in the wing contributes to the wing weight, and therefore taken considered for the weight calculations. The fuel weight $(W_f)$ is assumed to be distributed evenly along the fuel tank. Therefore, the fuel distribution $(\frac{dW_f}{dY})$ is described by:

$$\frac{dW_f}{dY} = \frac{W_f}{l_{tk}} \tag{A.14}$$

where $l_{tk}$ is the length of the fuel tank and calculated with:

$$l_{tk} = Y_{tk_e} - Y_{tk_b} \tag{A.15}$$

where $Y_{tk_b} = 0$ m and $Y_{tk_e} = 11.368$ m are respectively the begin and end location of the fuel tank.

Likewise, the weight of the engine is considered for the weight calculations. The total engine weight $(W_e)$ is obtained by considering a correction factor $(a_e) = 1.5$ over the engine weight $(W_{eng}) = 1980$ kg to include the additional weight for the nacelle and engine mounting .

$$W_e = a_e W_{eng} \tag{A.16}$$

The engine weight is considered as a concentrated force at location $Y = Y_e$, in case the width of the engine is smaller than the width of the wing segment $(w_e < dY)$. However, if

the engine width is larger then the segment width $(w_e > dY)$, then the weight of engines will be spread out to several segments. In this case, the weight distribution of the engine for $Y_{e_b} = Y_e - l_e$ to $Y_{e_e} = Y_e + l_e$ is described by:

$$\frac{dW_e}{dY} = \frac{W_e}{2l_e} \tag{A.17}$$

where $l_e = 0.75$ m is the length of the area where the engine spreads. The weight distribution is plotted in Fig. A.14, where the contribution of the engine weight and fuel weight is clearly visible.

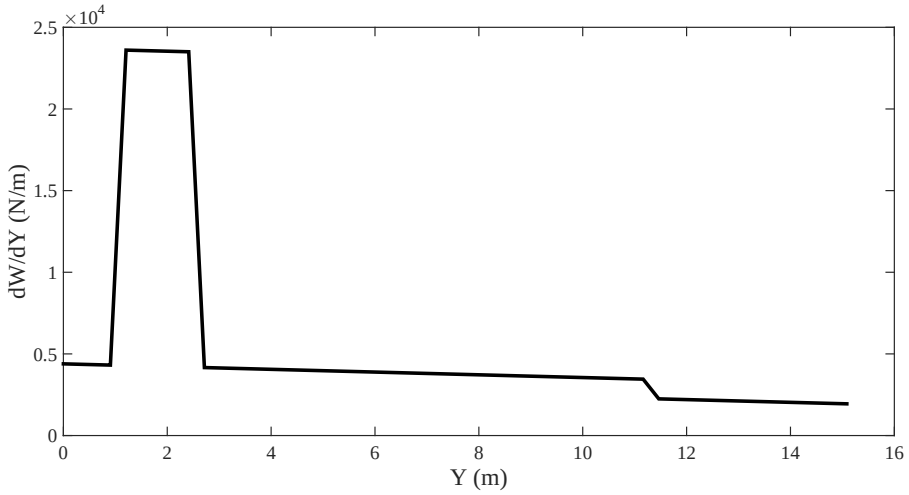


Figure A.14: Weight distribution along wing length for Airbus A320

### A.3.2. Lift

The other important force acting on the wing is the lift. The total lift is assumed to be equal to the weight of the aircraft $(L = W)$. The lift generated by both wings is assumed to be $90\%$ of the total lift, the remaining $10\%$ is accounted for the fuselage and other sections [5]. The lift per wing is thus assumed to be $45\%$ of the total lift, $(L_w = 0.45L)$. Furthermore, the lift distribution is assumed to be elliptical with $1\%$ of the lift at the tip $(L_t = 0.01L_w)$. The lift at the root $(L_r)$ is then determined by:

$$L_r = \frac{L_w}{l_w} - L_t \tag{A.18}$$

Hereafter, the elliptical lift distribution is described by:

$$\frac{dL}{dY} = L_r \sqrt{1 - \left( \frac{Y}{l_w \sqrt{1 - \left(\frac{L_t}{L_r}\right)^2}} \right)} \tag{A.19}$$

The lift distribution is valid along the wing length from $Y = 0$ to $Y = Y_t$ and is given in Fig. A.15.

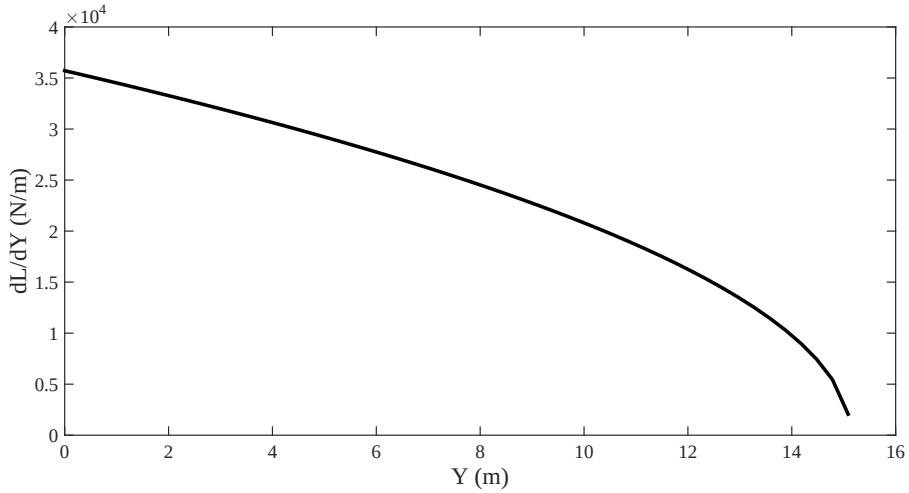


Figure A.15: Lift distribution along the wing length for Airbus A320.

### A.3.3. Force and moment

Once the acting forces on the wing are known the net force is calculated. The variables are considered as a vector in which each position refers to the corresponding force in the segment. This means that the vector for engine weight and fuel weight are zero outside their application region.

$$\frac{dV}{dY} = \frac{dL}{dY} - \left( \frac{dW_w}{dY} + \frac{dW_e}{dY} + \frac{dW_f}{dY} \right) \tag{A.20}$$

Summing up $\frac{dV}{dY}$ along the wing length and multiplying it with the segment length of $dY$ gives the force line $(V)$ along the wing. Furthermore, the summation of $V$ multiplied by the corresponding segment location $Y$ gives the moment line $(M)$ along the wing.

$$V = \sum \frac{dV}{dY} dY \tag{A.21}$$

$$M = \sum VY \tag{A.22}$$

The moment line along the wing length for the reference aircraft is given in Fig. A.16.

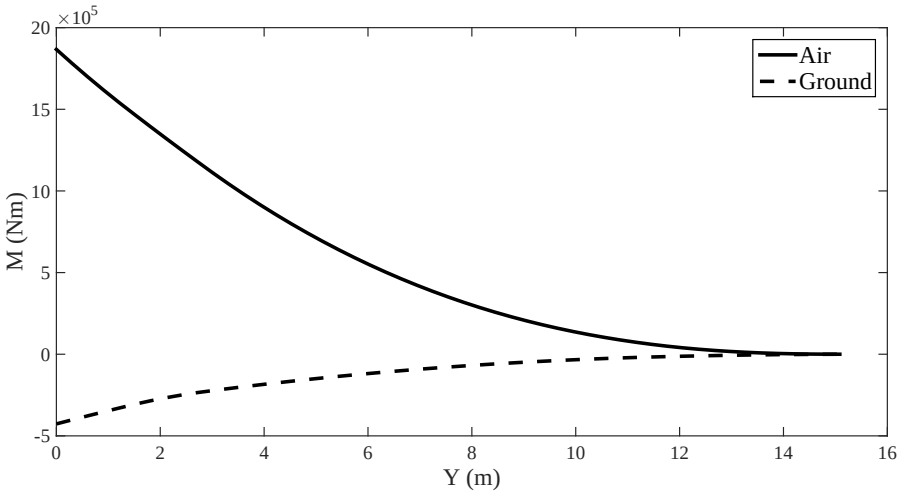


Figure A.16: Moment line along the wing length for Airbus A320.

## A.4. Running loads

The running loads on the skin panels are used for the wing analysis and these are determined using the applied shear and bending forces on the cross-section. The stresses resulting from the torsion moment and normal force are not considered. For further analysis, the wing box is considered together with the skin panels, stringers, spars and caps, and all other parts are neglected for the moment of inertia calculations.

### A.4.1. Skin and stringer

The wing cross-section is split into bays and stringers, where the stringer pitch ($b_{str}$) is assumed to be equal to the width of a skin bay ($b_{sk}$). The number of stringers ($N_{str}$) is determined by dividing the wing box width ($b_w$) by the stringer pitch and rounding off the value to the nearest integer. The stringers are distributed on the skin panel while there are no stringers considered at the corners. The distance to the corner from the closest stringer is half the stringer pitch. The coordinates of each stringer is found, which is then used for the calculation of the stresses at specific locations. The skin and stringer are simplified to a skin-stringer combination with a stringer placed in the centre of a skin bay and assumed to be a smeared thickness in the moment of inertia calculations. An illustration of these

parameters is given in Fig. A.17.

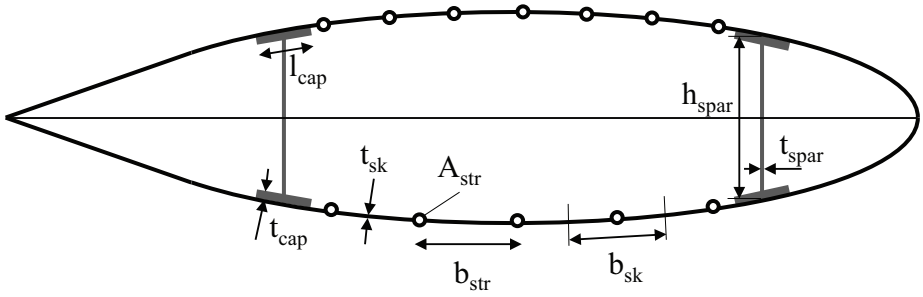


Figure A.17: Illustration of the wing cross-section with the stringers, spars and caps.

An estimate is made for the initial thickness of the skin panels to perform the load calculations. The stringer area is linked to the skin thickness by the stiffening factor $(\eta_{sf})$ [6]. This means there is a fixed ratio between the stringer and skin area, namely:

$$\eta_{sf} = \frac{E_{str}A_{str}}{E_{str}A_{str} + E_{sk}A_{sk}} \tag{A.23}$$

where $A_{sk}$ is the area of the skin, $A_{str}$ is the area of the stringer, $E_{sk}$ is the E-modulus of the skin and $E_{str}$ is the E-modulus of the stringer. The skin area $(A_{sk})$ is found by multiplying the skin thickness $(t_{sk})$ by stringer pitch $(b_{sk})$ and the stringer area $(A_{str})$ is found by using the stiffening factor $(\eta_{sf})$.

$$A_{sk} = t_{sk}b_{sk} \tag{A.24}$$

$$A_{str} = \frac{\eta_{sf}E_{sk}A_{sk}}{(1-\eta_{sf})E_{str}} \tag{A.25}$$

For further calculation, an equivalent thickness is used to represent the skin-stringer combination. The upper and lower panel are separately configured by defining a different stringer pitch, materials and stiffening factor.

### **A.4.2.** Spars and caps

The wing spar thickness $(t_{\text{spar}})$ and the wing cap thickness $(t_{\text{cap}})$ are given as input for the root and tip. In between, the thickness is interpolated based on the location on the wing. The spar height $h_{\text{spar}}$ is determined by taken the difference of the Z-coordinates of the begin of the wing box for the front spar and the end of the wing box for the rear spar. The wing cap length $(l_{\text{cap}})$ is given as input and the positions of the caps are respectively the four corners of the wing box, see Fig. A.17. The area of the spar $A_{\text{spar}}$ and the cap $A_{\text{cap}}$ are needed for

the moment of inertia calculations and are calculated as:

$$A_{\text{spar}} = t_{\text{spar}} h_{\text{spar}} \tag{A.26}$$

$$A_{\text{cap}} = t_{\text{cap}} l_{\text{cap}} \tag{A.27}$$

### **A.4.3.** Weighted area

The possibility of considering different material for the stringer and skin are implemented in the design tool. For this reason, the weighted area of the skin-stringer combination is calculated by normalizing the E-modulus of the materials [4]. The mean E-modulus $(E_{\text{mean}})$ is given:

$$E_{\text{mean}} = \frac{E_{sk} A_{sk} + E_{str} A_{str}}{A_{sk} + A_{str}} \tag{A.28}$$

where $E_{sk}$ is the E-modulus of the skin, $E_{str}$ is the E-modulus of the stringer, $A_{sk}$ is the area of the skin and $A_{str}$ is the area of the stringer.

Consequently, the equivalent area $(A_e)$ and the equivalent thickness $(t_e)$ is found [4].

$$A_e = \frac{E_{sk}}{E_{\text{mean}}} A_{sk} + \frac{E_{str}}{E_{\text{mean}}} A_{str} \tag{A.29}$$

$$t_e = \frac{A_e}{b_{sk}} \tag{A.30}$$

### **A.4.4.** Neutral line

Once the area and the coordinates of each skin-stringer combination is known, the neutral line of the wing box cross-section is obtained. The neutral line is a straight line and goes through the centre of gravity of the cross-section. It is calculated by summing up the equivalent area and multiplying it by the location coordinates and dividing it by the total area of the skin-stringers [7]. The neutral line on both axis is defined as:

$$X_{nl} = \frac{\sum A_e X + \sum A_{\text{spar}} X_{\text{spar}} + \sum A_{\text{cap}} X_{\text{cap}}}{\sum A_e + \sum A_{\text{spar}} + \sum A_{\text{cap}}} \tag{A.31}$$

$$Z_{nl} = \frac{\sum A_e Z + \sum A_{\text{spar}} Z_{\text{spar}} + \sum A_{\text{cap}} Z_{\text{cap}}}{\sum A_e + \sum A_{\text{spar}} + \sum A_{\text{cap}}} \tag{A.32}$$

where $X_{nl}$ is the $X$-coordinate of the neutral line in the global axis, $X$ is the corresponding $X$-coordinate of the skin-stringer combination, $X_{\text{spar}}$ is the $X$-coordinate of the spars, $X_{\text{cap}}$ is the $X$-coordinate of the caps, $Z_{nl}$ is the $Z$-coordinate of the neutral line in the global axis, $Z$ is the corresponding $Z$-coordinate of the skin-stringer combination, $Z_{\text{spar}}$ is the $Z$-coordinate of the spars and $Z_{\text{cap}}$ is the $Z$-coordinate of the caps.

### **A.4.5.** Moment of inertia

The moment of inertia $(I_{xx}, I_{zz}, I_{xz})$ of the wing box cross-section on both the $X$ and $Z$ axis are defined by [7]:

$$I_{xx} = \sum A_e(Z - Z_{nl})^2 + \sum A_{\text{spar}}(Z_{\text{spar}} - Z_{nl})^2 + \sum A_{\text{cap}}(Z_{\text{cap}} - Z_{nl})^2 \tag{A.33}$$

$$I_{zz} = \sum A_e(X - X_{nl})^2 + \sum A_{\text{spar}}(X_{\text{spar}} - X_{nl})^2 + \sum A_{\text{cap}}(X_{\text{cap}} - X_{nl})^2 \tag{A.34}$$

$$I_{xz} = \sum A_e(X - X_{nl})(Z - Z_{nl}) + \sum A_{\text{spar}}(X_{\text{spar}} - X_{nl})(Z_{\text{spar}} - Z_{nl}) + \sum A_{\text{cap}}(X_{\text{cap}} - X_{nl})(Z_{\text{cap}} - Z_{nl}) \tag{A.35}$$

### **A.4.6.** Bending stresses

The bending moment $M_x$ causes the wing to bend. The upper part of the wing is subjected to compression, while the lower part is in tension during flight. The line separating these regions is called the neutral line. The bending stress $(\sigma_y)$ applied on the wing at each location is calculated [7].

$$\sigma_y = -\frac{M_x(I_{zz}(Z - Z_{nl}) - I_{xz}(X - X_{nl}))}{I_{xx}I_{zz} - I_{xz}^2} \tag{A.36}$$

This equation only includes the bending moment around the X-axis. The contribution of the bending moment around the Z-axis $M_z$ is neglected, and therefore, assumed to be zero.

For design purposes, the running load $(P)$ is used rather then the bending stress, since the running load does not include the skin thickness, which makes it easier to define the thickness as a design parameter. For the running load calculation, it is assumed that skin-stringer combination has a smeared thickness, which is the equivalent thickness $(t_e)$.

$$P = \sigma_y t_e \tag{A.37}$$

Next, the separate stress in the skin and the stringer is obtained and the actual force $(F)$ is determined on the same location, since the applied force on skin and stringer are equal.

$$F = \frac{\sigma_y}{A_e} \tag{A.38}$$

The strain $(\epsilon)$ of the skin and stringer is equal, because the skin-stringer are attached to each other. The elastic deformation is determined with the mean E-modulus $(E_{mean})$ and the equivalent area $(A_e)$ of the skin and stringer [4].

$$\epsilon = \frac{F}{E_{mean}A_e} \tag{A.39}$$

Using the strain of the skin and stringer, the actual stress on the skin and stringer is determined:

$$\sigma_{sk} = \epsilon E_{sk} \tag{A.40}$$

$$\sigma_{str} = \epsilon E_{str} \tag{A.41}$$

The running load for the skin panel is finally found, which is used for further evaluation.

$$P_{sk} = \sigma_{sk} t_{sk} \tag{A.42}$$

## References


[1] *Airbus A320 - Airplane Characteristics For Airport Planning AC*, Airbus S.A.S. (1995).

[2] E. Jacobs, K. Ward, and R. Pinkerton, *The Characteristics of 78 related Airfoil Sections from Tests in the Variable-Density Wind Tunnel*, Report No. 460 (National Advisory Committee for Aeronautics, 1935).

[3] P. Astori, J. Hupperets, and M. Tooren, van, *Loads Development for Two Aircraft Fuselages using FAR criteria and parametrised FE-models*, CR#2003#01 (Delft University of Technology, 2003).

[4] I. Şen, *Aircraft Fuselage Design Study*, Master's thesis, Delft University of Technology, Delft (2010), available via `http://repository.tudelft.nl/`.

[5] E. Torenbeek, *Synthesis of Subsonic Airplane Design* (Kluwer Academic Publishers Group, Delft, 1982).

[6] C. Poe, Jr., *Fatigue crack propagation in stiffened panels,* American Society for Testing and Materials **Damage Tolerance in Aircraft Structures**, 79 (1971).

[7] T. Megson, *Aircraft Structures for Engineering Students*, 4th ed. (Butterworth-Heinemann, 2007).

# B

# Design criteria for aluminium

*In this appendix, the design criteria for the assessment of aluminium as skin material are presented. The criteria includes static, fatigue and damage tolerance criteria, such as yield and ultimate strength, buckling, fatigue crack initiation, fatigue crack propagation and fracture toughness.*

## **B.1.** Introduction

The design methodology considers both the design of the upper and lower wing panels. The upper wing skin remains aluminium, while the lower wing skin is optimised for FML. To make sure the lower wing skin optimisation is performed with the correct running loads, both skin panels are needed to be optimised together. This is because the moment of inertia calculations of the wing cross-section depend on the skin thicknesses of both panels. For this purpose, aluminium design methods are needed to optimise the upper wing skin for aluminium. The important design methods for aluminium are summarised in this appendix. With these methods, the minimum skin thickness and the design allowables for aluminium are determined. The upper panels are mainly loaded in compression and are checked for static strength and buckling. Additionally, F&DT criteria for the tensile loaded lower wing are also presented, for in case, the lower wing will be optimised for aluminium. The latter is possible due to the generic nature of the presented design methodology in this thesis.

## **B.2.** Static strength

The static strength evaluation includes assessment of tension and compression loads for the yield and ultimate strength criteria. Furthermore, buckling criteria are used to assess the skin panels for compression loads.



### **B.2.1.** Yield and ultimate strength

The actual stress on the wing panels are compared to the yield strength $(S_{yld})$ of the material and the actual stresses times $1.5$ is compared to the ultimate strength $(S_{ult})$ of the material [1]. The required skin thickness based on the yield and ultimate is determined with following equations:

$$t_{yld} = \frac{P}{S_{yld}} \tag{B.1}$$

$$t_{ult} = 1.5\frac{P}{S_{ult}} \tag{B.2}$$

where $P$ is the running load on the panel segment, $t_{yld}$ is required thickness to satisfy the yield strength and $t_{ult}$ is required thickness to satisfy the ultimate strength criteria.

### **B.2.2.** Buckling

The buckling criteria are considered for the upper panel in case of compression loads. The criteria is evaluated based on Euler buckling and local buckling.

#### Euler buckling

The allowable buckling stress $(\sigma_b)$ is obtained by Euler buckling formula [2].

$$\sigma_b = \eta\sqrt{\frac{PE}{b_{rib}}} \tag{B.3}$$

where $P$ is the running load on the panel, $E$ the elastic modulus of the material and $b_{rib}$ is the rib spacing.

Hence, the minimum required thickness for buckling $(t_b)$ is then calculated.

$$t_b = \frac{P}{\sigma_b} \tag{B.4}$$

#### Local buckling

The critical stress for local buckling $(\sigma_{cr})$ criteria is described by [2]:

$$\sigma_{cr} = \frac{\pi^2 k_c E}{12(1-\nu^2)}\left(\frac{t}{b_{str}}\right)^2 \tag{B.5}$$

where $\sigma_{cr}$ is the critical buckling stress, $b_{str}$ is the stringer pitch, $\nu$ is the Poisson's ratio of the material and $k_c$ is the buckling coefficient which depends on edge boundary conditions and sheet aspect ratio $\frac{a}{b}$. In generally, the $k_c$ is equal to 4 for simply supported panels.

The required thickness for local buckling $(t_{lc})$ is found by solving the following equation:

$$t_{lc} = \sqrt[3]{\frac{12(1-\nu^2)P}{\pi^2 k_c E b_{str}}} \tag{B.6}$$

where the minimum thickness is again the real and absolute solution of this equation.

## **B.3.** Fatigue and damage tolerance

The fatigue life under cyclic loading consists of two phases, the crack initiation life followed by a crack growth period and finally the last stage of final failure. This is represented in a block diagram, see Fig. B.1. Each phase is evaluated separately with corresponding design methods.

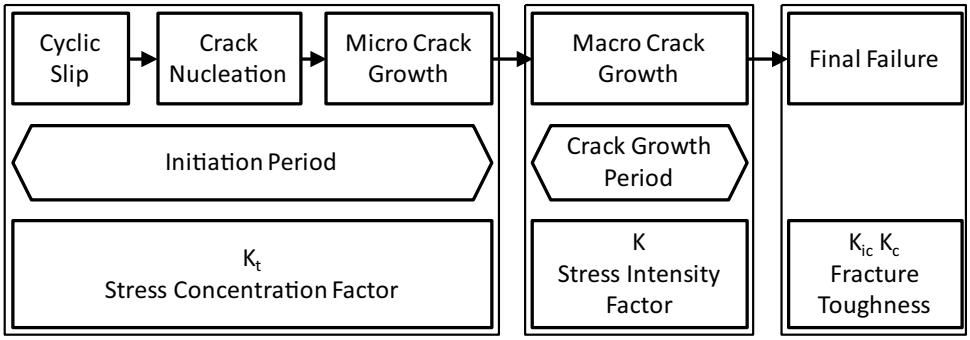


Figure B.1: Different phases of the fatigue life in metals together with relevant factors [3].

### **B.3.1.** Fatigue crack initiation

The fatigue crack initiation is a criteria that is used to set the inspection threshold for the aircraft. The inspection threshold is the is the number of flight cycles when the aircraft should be inspected for the first time for cracks. The evaluation of this design criteria is performed using S-N curves of the material, which is dependent on the stress concentration factor $(K_t)$ of the notch and stress ratio $(R)$. The allowable fatigue stress of the material is determined using the available S-N curves. The HSB database [4] is used as reference S-N data for

aluminium 2024-T3. The S-N curves are described by the following equation:

$$S_a = C_1 + \frac{C_2 - C_1}{\exp\left(\frac{\log N}{C_3}\right)^{C_4}} \tag{B.7}$$

where $S_a$ is the stress amplitude, $N$ is the number of cycles and $C_{1,2,3,4}$ are constants of the S-N curves depending on the material type, stress ratio $R$ and stress concentration factor $K_t$.

The maximum fatigue stress $(S_{\text{fci}})$ that is allowed to have at least the defined number of cycles is determined with [5]:

$$S_{\text{fci}} = \frac{2S_a}{(1-R)} \tag{B.8}$$

The minimal required thickness for fatigue crack initiation $(t_{\text{fci}})$ is calculated with:

$$t_{\text{fci}} = \frac{P}{S_{\text{fci}}} \tag{B.9}$$

where $P$ is the running load on the wing skin.

### **B.3.2.** Fatigue crack propagation

The stress intensity factor gives the correlation between the crack growth rate $\left(\frac{da}{dN}\right)$ and the stress intensity factor range $(\Delta K)$. The stress intensity factor $(K)$ is given as function of the crack length $(a)$.

$$\Delta K = \beta \Delta S \sqrt{\pi a} \tag{B.10}$$

where $\beta$ is the geometry constant and is considered to be $1$, in case of a wing skin without stiffening.

The Forman relationship describes the fatigue crack propagation in metals and is given with [5]:

$$\frac{da}{dN} = \frac{C_F \Delta K^m}{(1-R)K_F - \Delta K} \tag{B.11}$$

Rewriting and integration of this function gives the number of cycles $(N)$ as function of the crack length $(a)$.

$$N = \int_{a_i}^{a_c} \frac{(1-R)K_F - \Delta K}{C_F \Delta K^m} da \tag{B.12}$$

For the design, the number of cycles for crack propagation is derived from the inspection period. For a required number of cycles $(N)$, initial crack length $(a_i)$ and critical crack length $(a_c)$, the $\Delta S$ is obtained by means of solving Eq. (B.12).

The allowable fatigue stress for crack growth $(S_{\text{fcp}})$ is then obtained by:

$$S_{\text{fcp}} = \frac{\Delta S}{(1-R)} \tag{B.13}$$

The minimal required thickness for fatigue crack growth ($t_{\text{fcp}}$) is calculated with:

$$t_{\text{fcp}} = \frac{P}{S_{\text{fcp}}} \tag{B.14}$$



If the contribution of the stringers is considered, a new value for geometry constant ($\beta$) should be calculated that matches the change in geometry due to the stringers. The geometry constant is determined for the actual stiffening ratio and stringer pitch using the method described by Rans et al. [6]. This method considers bonded stiffeners and assumes that there is a crack in the skin with a broken central stringer. In this case, the allowable stress for fatigue crack growth is lower, because the skin should compensate for the loads of the broken stringer. This case is selected as a critical condition.

### **B.3.3.** Fracture Toughness

Fracture toughness is the property which describes the ability of a material containing a crack to resist fracture, and is an important property of a material for design. It is denoted as $K_{ic}$ and the crack length ($a_c$) depends on fracture toughness [5, 7].

$$K_{ic} = \beta S_c \sqrt{\pi a_c} \tag{B.15}$$

where $S_c$ is the critical stress and $\beta$ is the geometry constant. The fracture toughness property ($K_{ic}$) depends on the material of the skin. Furthermore, the critical crack length ($a_c$) is set equal to the length of stringer pitch.

Hence, the critical stress ($S_c$) is calculated by:

$$S_c = \frac{K_{ic}}{\sqrt{\pi a_c}} \tag{B.16}$$

Finally, the minimum thickness ($t_{ft}$) at each location is found for the fracture toughness criteria.

$$t_{ft} = \frac{P}{S_c} \tag{B.17}$$

Additionally, the critical stress could be divided by a safety factor of 1.15 to meet the two-bay-crack criteria [8]. The two-bay-crack criterion states that a crack through a frame (and thus crack in two bays) should not result in catastrophic failure. This criteria is also applicable to a stringer on a skin.

## **B.4.** Reserve factor

A reserve factor ($RF$) is introduced to identify the critical design criteria and the margin between these criteria. This reserve factor defines the potential for improvement of a single

allowable until the minimum thickness is limited by the next critical criteria.

$$RF = \frac{t_1}{t_2} \tag{B.18}$$



where $t_1$ is the current limiting thickness and $t_2$ is the next limiting thickness.

Besides, the margin of safety $(MS)$ is used to determine the space for improvement.

$$MS = RF - 1 \tag{B.19}$$

If the reserve factor is close to $1$ or the safety margin close to $0$, then the thickness of the next criteria is very close to the current limiting thickness. This means the improvement of the current criteria will not directly result in a structural weight improvement, because the other criteria will be the limiting one.

## References


[1] I. Şen, *Aircraft Fuselage Design Study*, Master's thesis, Delft University of Technology, Delft (2010), available via `http://repository.tudelft.nl/`.

[2] E. Bruhn, *Analysis and Design of Flight Vehicle Structures* (Tr-State Offset Company, 1973).

[3] S. Beden, S. Abdullah, and A. Ariffin, *Review of fatigue crack propagation models for metallic components,* European Journal of Scientific Research **28**, 364 (2009).

[4] V. Hoang and L. Schwarmann, *Handbuch Struktur Berechnung (HSB), 63111-01 issue D: Zeitfestigkeit 3.1354 T3*, Tech. Rep. (1986).

[5] J. Schijve, G. Campoli, and A. Monaco, *Fatigue of structures and secondary bending in structural elements,* International Journal of Fatigue **31**, 1111 (2009).

[6] C. Rans, R. Rodi, and R. Alderliesten, *Analytical prediction of mode i stress intensity factors for cracked panels containing bonded stiffeners,* Engineering Fracture Mechanics **97**, 12 (2013).

[7] S. Suresh, *Fatigue of Materials* (Cambridge University Press, 1998).

[8] A. Rothwell, *Structural design and optimisation, Part II* (Delft University of Technology, 2001).

# C

# Accuracy of FCI predictions

*In this appendix, the adaptations to the FCI prediction method are explained to assure an accurate fatigue life prediction for FML using S-N data of aluminium. Two adaptations are applied: first, the load cycle is matched to the mean stress of the S-N curve, and second, the load cycle is matched to the stress concentration factor of the S-N curve by using a load factor or a interpolation between two or three S-N curves. The difference between the two stress concentration factor adaptations are discussed with respect to accuracy, and finally, the FCI method is validated using test data.*

## C.1. Introduction

The accuracy of the FCI prediction method implemented in the optimisation routine shows a strict dependency on S-N data. This method described by Spronk et al. [1] is an extended version of the method described by Homan [2]. Homan's paper stops at the calculation of the stress cycle at the notch and leaves the implementation of predicting the fatigue life to the designer. The extension that will be discussed in this appendix describes how to predict the actual fatigue life of FML by comparing the stresses in the metal layers with S-N data of the monolithic aluminium. Each S-N curve represents a stress concentration factor and a stress ratio depending on the test set-up and specimen shape, and in most of the cases, these two values do not match with the values determined for the FML load cycle. Therefore, the method considers two adaptations to ensure that an accurate prediction of the fatigue life is obtained by means of S-N data:

1. Adapting the load cycle to match the mean stress of the S-N curve.
2. Adapting the load cycle to match the stress concentration factor of the S-N curve.

In this section, both adaptations for predicting the fatigue life are discussed, and hereafter, the results of the fatigue life prediction are compared with experimental data of GLARE by using different S-N data from the literature. Finally,the accuracy of the predictions are evaluated and the sensitivity of the estimated fatigue life is discussed.

## **C.2.** Predicting the cycles to crack initiation



Once the occurring stress cycle has been determined, the fatigue initiation life can be estimated by looking up a calculated stress amplitude in S-N data available in the literature. The calculation of the stress cycle is described in detail in [1]. The combination of nominal stress amplitude, ($S_{a,\ nom}$) and peak stress ratio ($R_{\text{peak}}$) are used as the reference stress cycle. This allows for a comparison on the basis of nominal stress, while using the correct stress ratio occurring at the point of interest.

It has been found that the cycles to failure of notched monolithic aluminium specimens is close to the cycles to a crack length of 1 mm in the aluminium layers of FML with the same shape [3, 4]. Crack initiation, therefore, is assumed to have taken place at this crack length, and S-N data for monolithic aluminium will be treated as S-$N_i$ data for the metal layers in FML, and no factor is used to account for a possible discrepancy between the two.

The question remains which stress to compare to the S-N curve? The stress ratio for this stress and the SCF in the analysed case should be equal to the stress ratio and SCF of the S-N data for a correct estimation. In case they are not, correction formulae need to be applied to correct for the difference.

### **C.2.1.** Adapting the load cycle to match the mean stress

The reference stress cycle has to be converted towards the mean stress level that was used to produce the S-N data with which the amplitude of this stress cycle is to be compared.

The mean value and the amplitude of the reference stress occurring in a layer can be calculated using:

$$S_{m,\,\text{nom}} = \left(\frac{1 + R_{\text{nom}}}{2}\right) S^{\max}_{k,\,\text{nom}} \tag{C.1}$$

$$S_{a,\,\text{nom}} = \left(\frac{1 - R_{\text{nom}}}{2}\right) S^{\max}_{k,\,\text{nom}} \tag{C.2}$$

The amplitude for zero mean reference stress is calculated using the Goodman relation instead of alternative relations, because it is generally a conservative approximation [5]:

$$S_{a,\,\text{nom}}\big|_{S_m=0} = \frac{S_{a,\,\text{nom}}}{1 + \frac{S_{m,\,\text{nom}}}{S_u}} \tag{C.3}$$

To find the amplitude of the stress cycle in the S-N curve ($S_{a,\,\text{S-N}}$) that is equivalent to the stress cycle of the test case, the Goodman relation is used once again, this time with the stress ratio of the S-N curve ($R_{\text{S-N}}$):

$$S_{a,\,\text{S-N}} = S_{a,\,\text{nom}}\big|_{S_m=0}\left(1 - \frac{S_{m,\,\text{S-N}}}{S_u}\right) \tag{C.4}$$

where the same amplitude for zero mean stress as in Eq. (C.3) is used, because it characterises the stress cycle of the analysed case.



The mean value of the equivalent stress cycle in the S-N data ($S_{m,\,\text{S-N}}$) is still an unknown. The mean value of any constant-amplitude load cycle can be written as a function of the corresponding amplitude with use of the stress ratio:

$$S_{\text{max}} = \left(\frac{2}{1-R}\right)S_a \tag{C.5}$$

in which the denominator will never be zero because $R = 1$ would mean there is no load variation. Hence, for the mean value of the peak stress of a load cycle described by the S-N curve, it follows that:

$$\begin{aligned} S_{m,\,\text{S-N}} &= S_{\text{max,\,S-N}} - S_{a,\,\text{S-N}} \\ &= \left(\frac{2}{1-R_{\text{S-N}}} - 1\right)S_{a,\,\text{S-N}} \end{aligned} \tag{C.6}$$

Eq. (C.4) can be rewritten using Eq. (C.6) to obtain a relation for $S_{a,\,\text{S-N}}$ that is solely dependent on terms that are known. This results in Eq. (C.7) which gives the peak stress amplitude in the S-N data that is equivalent to the reference stress amplitude $S_{a,\,\text{nom}}$ occurring in a metal layer of the laminate:

$$\begin{aligned} S_{a,\,\text{S-N}} &= S_{a,\,\text{nom}}\big|_{S_m=0}\left(1 - \frac{\left(\frac{2}{1-R_{\text{S-N}}} - 1\right)S_{a,\,\text{S-N}}}{S_u}\right) \\ &= \frac{S_{a,\,\text{nom}}\big|_{S_m=0}}{1 + S_{a,\,\text{nom}}\big|_{S_m=0}\left(\frac{\frac{2}{1-R_{\text{S-N}}}-1}{S_u}\right)} \end{aligned} \tag{C.7}$$

### **C.2.2.** Adapting the load cycle to match the SCF

A different stress distribution in a plate loaded by a repetitive load leads to a different fatigue life, even if the peak stress remains the same [5]. The shape of the stress distribution is determined by, among others, the SCF. Thus, using S-N data with a different SCF value than the case at hand may lead to a wrong life estimation. The reference stress amplitude, therefore, needs another translation to be suitable for comparison to the S-N data used. In

HSB 62131-01 [6], a method for the prediction of the fatigue life for cases with SCF values different to available S-N data is described. The method makes a distinction between two translation methods which are termed 'method 1,' and 'method 2' for the remainder of this appendix.

If one S-N curve is used, SCF translation method 1 is applied, which entails multiplying the stress amplitude with a load factor $f$ to account for different SCF values of the S-N curve. In general, the closer the SCF values, the more accurate the obtained prediction will be. The load factors are calculated using:



$$f = \begin{cases} K_t & K_{t,\,\text{S-N}} = 1,\ K_t \geq 1 \\ \frac{K_t}{K_{t,\,\text{S-N}}} & K_{t,\,\text{S-N}} > 1,\ K_t > K_{t,\,\text{S-N}} \\ 1 & K_{t,\,\text{S-N}} > 1,\ K_t \leq K_{t,\,\text{S-N}} \end{cases} \tag{C.8}$$

and thus the corrected stress amplitude is determined with:

$$S_{a,\,\text{corrected}} = f \cdot S_{a,\,\text{S-N}} \tag{C.9}$$

which is used to predict the cycles to crack initiation from the corresponding S-N curve.

If more than one S-N curve is available, SCF correction method 2 can be used, where two S-N curves with the same stress ratio are selected to perform an interpolation or extrapolation, depending on the choice of curves, to predict the cycles to crack initiation. A prediction for the cycles to crack initiation is made using each chosen S-N curve, making use of the stress amplitude $S_{a,\,\text{S-N}}$ from Section C.2.1, after which the final result is obtained with:

$$\begin{aligned} \log(N) = \log(N_2) + \\ (\log(N_2) - \log(N_1))\,\frac{\log(K_t) - \log(K_{t,\,\text{S-N2}})}{\log(K_{t,\,\text{S-N2}}) - \log(K_{t,\,\text{S-N1}})} \end{aligned} \tag{C.10}$$

where $N$ is the resulting amount of cycles to initiation, $N_1$ and $N_2$ are the cycles to initiation using the individual S-N curves, and $K_{t,\,\text{S-N1}}$ and $K_{t,\,\text{S-N2}}$ the SCF values of the corresponding S-N curves used. The index 1 always points to the S-N curve with the lower SCF value of the two.

The applicability of both the SCF correction methods mentioned above is limited to high cycle fatigue ($N > 5 \cdot 10^3$ cycles) [6].

## C.3. Evaluation of predictions

Homan and Schra [3] have tested the cycles to crack initiation on GLARE 4B laminates. The results of one test series on GLARE 4B-3/2-0.3 is given in Table C.1. This material has a stiffness of 48.7 GPa and a nominal tensile yield and ultimate strength of respectively 251

MPa and 572 MPa in longitudinal direction [7]. The constituent mechanical properties are given in Table 2.2. More information about (this type of) Glare is given in Section 2.1.1. The cycles to initiation were obtained as a function of net section stress amplitude ($S_{a,\,\text{net}}$). The prediction methodology for cycles to crack initiation, described in Section C.2, Section 2.4.2 and in more detail in [1], is used in this section to predict the cycles to initiation in the same situations. The material properties that were used in the simulation for the Glare constituents were those given by Homan [2] which are given in Table 2.2.



| $S_{a,\,\text{net}}$ (MPa) | $N_i$ (cycles) | $S_{a,\,\text{nom}}$ (MPa) | $R_{\text{peak}}$ (-) | $K_{t,\,\text{max}}$ (-) |
|---|---|---|---|---|
| 110 | 2599 | 160.4 | 0.073 | 2.879 |
| 100 | 3993 | 145.8 | 0.075 | 2.866 |
| 90 | 6118 | 131.2 | 0.078 | 2.850 |
| 80 | 9739 | 116.6 | 0.082 | 2.831 |
| 70 | 18427 | 102.1 | 0.086 | 2.807 |
| 60 | 34706 | 87.5 | 0.092 | 2.775 |
| 50 | 68583 | 72.9 | 0.099 | 2.733 |

Table C.1: Crack initiation life test data and corresponding calculated nominal stress amplitude in the metal layers, peak stress ratio and maximum SCF for GLARE 4B-3/2-0.3 with $K_{t,\,\text{iso}} = 2.7$, $R = 0.05$ [3]

The predicted cycles to initiation using S-N curves of monolithic notched metal plates are compared to S-$N_i$-test results of notched FML plates in this section. The accuracy of the predictions is evaluated using the absolute value of the ratio of the predicted cycles to crack initiation with the expected value, i.e. the test result, as a measure of relative error:

$$\eta = \left| \frac{N_{\text{predicted}}}{N_{\text{expected}}} - 1 \right| \tag{C.11}$$

Table C.2 contains the average error of the prediction of multiple data points for the FCI in notched GLARE 4B-3/2-0.3 using various S-N curves for notched aluminium. A value in the table belongs to predictions that are made using the S-N curve(s) of the $R$- and $K_t$-values indicated. These values show the average error to predict the cycles to initiation for each data point in Table C.1, which is determined using Eq. (C.11) for each data point and taking the average value of the set of results.

S-N curves with $K_t = 1$ give only run-outs for the tested laminate and are thus excluded from the comparison in Table C.2. The various load levels that were also excluded from a large part of the table entries are a result of the method failing to produce an answer when the stress amplitude lies above the highest value of the S-N curve.

The data in Table C.2 shows that the accuracy of the prediction methodology is strongly influenced by the choice of S-N data that is to serve as the base of the predictions. It is important to realise that a bad agreement of a prediction with test results, therefore, does

not necessarily disprove the validity of the method. It can simply mean that the S-N data does not represent the metal layers in the FML. The opposite is also true: a good agreement between predictions and test result does not validate the method, but could be a lucky choice of S-N data.

| | | $R_{\text{S-N}}$ | | | |
|---|---|---|---|---|---|
| | $K_{t,\text{ S-N}}$ | 0.25 | 0.0 | −0.5 | −1.0 |
| Method 1 | 2.0 | $0.27^{2}$ | $0.19^{2}$ | $0.29^{2}$ | $0.64^{2}$ |
| | 2.5 | 0.45 | 0.33 | $0.49^{1}$ | $0.88^{2}$ |
| | 3.6 | $0.51^{1}$ | $0.51^{1}$ | $0.41^{2}$ | $0.46^{2}$ |
| | 5.2 | $0.67^{1}$ | $0.72^{2}$ | $0.71^{3}$ | $0.71^{3}$ |
| Method 2 | 2.0 & 2.5 | 0.76 | 0.38 | $0.54^{1}$ | $0.76^{1}$ |
| | 2.0 & 3.6 | $0.30^{1}$ | $0.31^{1}$ | $0.57^{2}$ | $1.60^{2}$ |
| | 2.0 & 5.2 | $0.95^{1}$ | $0.66^{2}$ | $1.10^{3}$ | $2.87^{3}$ |
| | 2.5 & 3.6 | $0.53^{1}$ | $0.34^{1}$ | $0.57^{2}$ | $1.07^{2}$ |
| | 2.5 & 5.2 | $0.90^{1}$ | $0.52^{2}$ | $0.71^{3}$ | $1.34^{3}$ |
| | 3.6 & 5.2 | $0.36^{1}$ | $0.30^{2}$ | $0.38^{3}$ | $0.69^{3}$ |

Excluding [1] 110, [2] 100 and 110, and [3] 90, 100, and 110 MPa

Table C.2: Average error $\eta$, see Eq. (C.11), of fatigue crack initiation life predictions for GLARE 4B-3/2-0.3 with $K_{t,\text{ iso}} = 2.7$, $R = 0.05$ [3] to replicate the test results of Table C.1.

### C.3.1. Accuracy of the predictions

The average error over all rows equals 0.57, 0.43, 0.58, and 1.10 for S-N data with $R =$ 0.25, 0.0, −0.5, and −1.0, respectively. The applied load cycle has $R = 0.05$, leading to $0.073 \leq R_{\text{peak}} \leq 0.099$. The S-N curves with the closest value for the load ratio have $R = 0.0$, and the average error of the column with this value for $R$ is also the lowest of the four. This leads to the conclusion that indeed the best predictions are obtained when the load ratio of the S-N data equals the case analysed.

The case analysed has $K_{t,\text{ max}} = 2.807$, so in this case the S-N curve with $K_{t,\text{ S-N}} = 2.5$ lies closest to this value. It can be seen in Table C.2 that the error using a single S-N curve with this value of $K_t$ is not the smallest in comparison to using other curves to predict crack initiation. This is probably a result of scatter of the test data that is used to evaluate the accuracy, and could be solved using a larger dataset.

Based on the trends in the average error values using method 1, it seems that it is beneficial to use S-N data that has a lower $K_t$ value than the case for which a prediction is made, rather than a higher one. This is probably a result of Eq. (C.8), which only corrects the prediction in case the SCF of the S-N curve falls below the case analysed.

### **C.3.2.** Method 1 versus method 2

It was mentioned earlier that the column with the most accurate results is $R = 0.0$. The average error of the predictions in this column using method 1 equals $0.44$. The average error is $0.42$ when method 2 is applied. It thus appears that both methods produce predictions that seem equally accurate on average and no decision can be made on whether one method is significantly better than the other. A slight preference of method 1 over method 2 could be based on the high errors seen using the latter method when the $R$ value is far off from the case analysed, while method 1 remains relatively accurate.



The result of the two prediction methods is plotted with the test results for a variety of stress amplitudes in Fig. C.1. The error, as defined by Eq. (C.11), is plotted per stress level in Fig. C.2. For each data point, the S-N curves were used that had the smallest difference in $K_t$ and $R$ values with the case analysed: $K_{t,\text{ S-N}} = 2.5$ for method 1, and $K_{t,\text{ S-N}} = 2.5$ and $3.6$ for method 2, and $R = 0$ for all S-N data used.

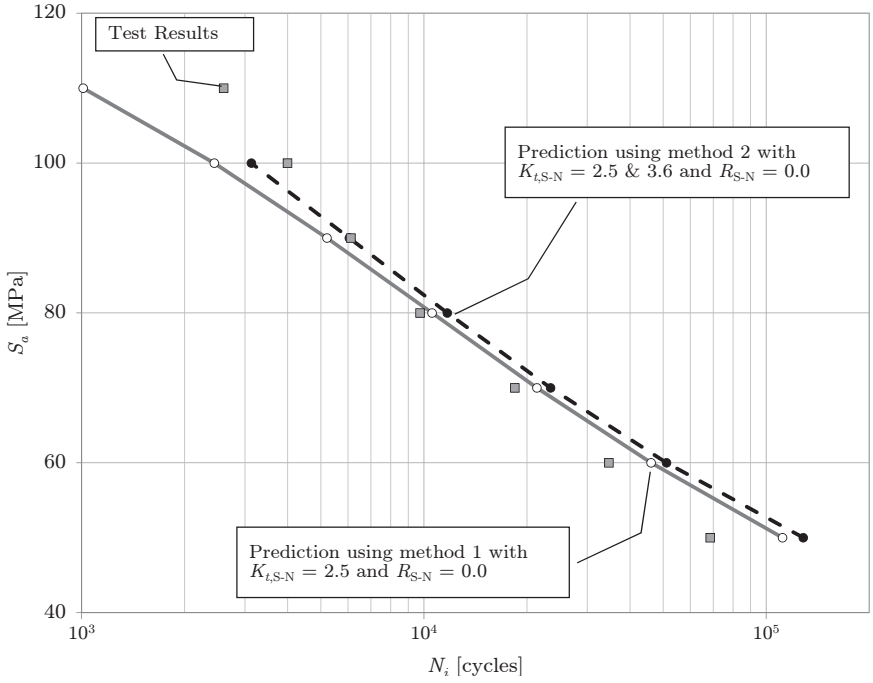


Figure C.1: Fatigue crack initiation life predictions for GLARE 4B-3/2-0.3 at several stress amplitudes using both methods mentioned in Section C.2.2 compared to test results from Table C.1.

It can be seen in the figures that both prediction methods approach the test results quite well. The error is low at stress amplitudes in the middle of the range tested, and increases when the applied stress amplitude either decreases or increases. The high error towards

a higher applied load is a result of the fact that the S-N data used is not valid below $10^4$ cycles [8], but it is still used to make a prediction. The error towards a lower applied load is a result of the decreasing slope of the S-N curves towards the fatigue limit. This causes a larger variation in cycles to initiation as compared to a higher load, for the same variation in stress amplitude.

There is no data point for method 2 at $S_a$ = 110 MPa, because the method predicts failure below a single cycle as a result of trying to find a value above the upper stress limit of the curve that constitutes the S-N data [8]. It is decided not to include any result outside the limits of the curve, which lie at $10^0$ and $10^7$ cycles.

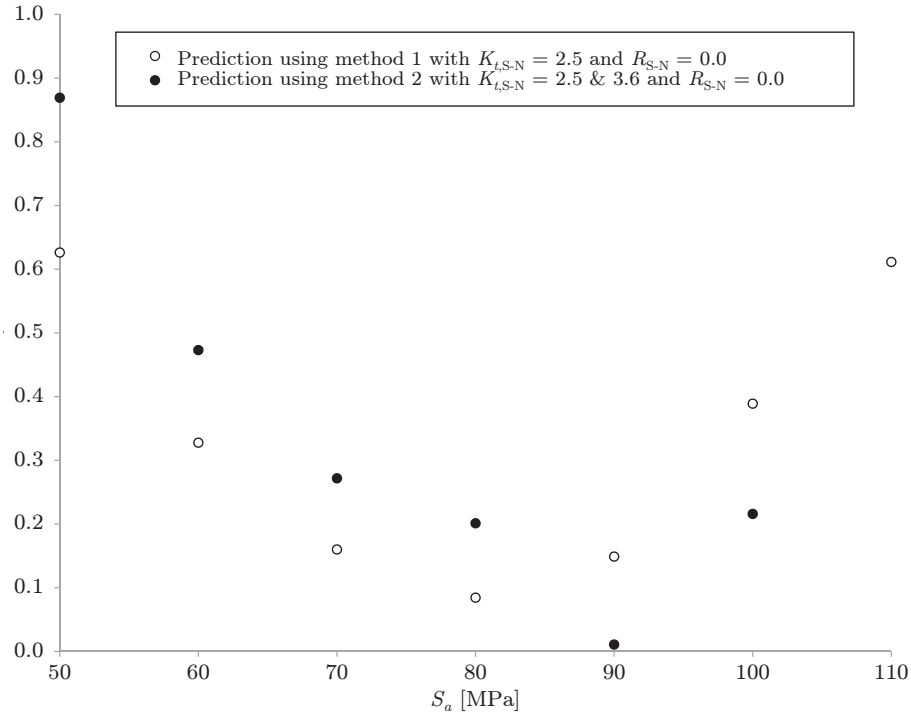


Figure C.2: Error $\eta$ of the crack initiation predictions for GLARE 4B-3/2-0.3 in Fig. C.1 compared to test results in Table C.1, calculated using Eq. (C.11).

### **C.3.3.** Sensitivity of estimated fatigue life

Two methods were explained above to correct the SCF for the estimation of the cycles to initiation. In Fig. C.3, the results of both estimation methods are compared for a large range of $K_t$ values.

The sudden steps or slope changes in the results clearly show the switch from using one

(set of) S-N curve(s) to another. Method 1, moreover, keeps giving the same life estimation if the $K_t$ value of the closest S-N curve is higher than the occurring $K_t$ value, as can be seen by the horizontal portion of the solid grey line in the figure.

Method 2 shows a smoother transition from interpolating using one set of curves to another. This behaviour is preferred especially in case of automated optimisation of FML layups for crack initiation, because it means the optimiser will see a gradient in the results which it can use to find an optimum. No horizontal sections can be seen in the dashed line, indicating that the estimation below the lowest S-N curve is probably more accurate using interpolation. This was already concluded from the lower observed error in Section C.3.1.



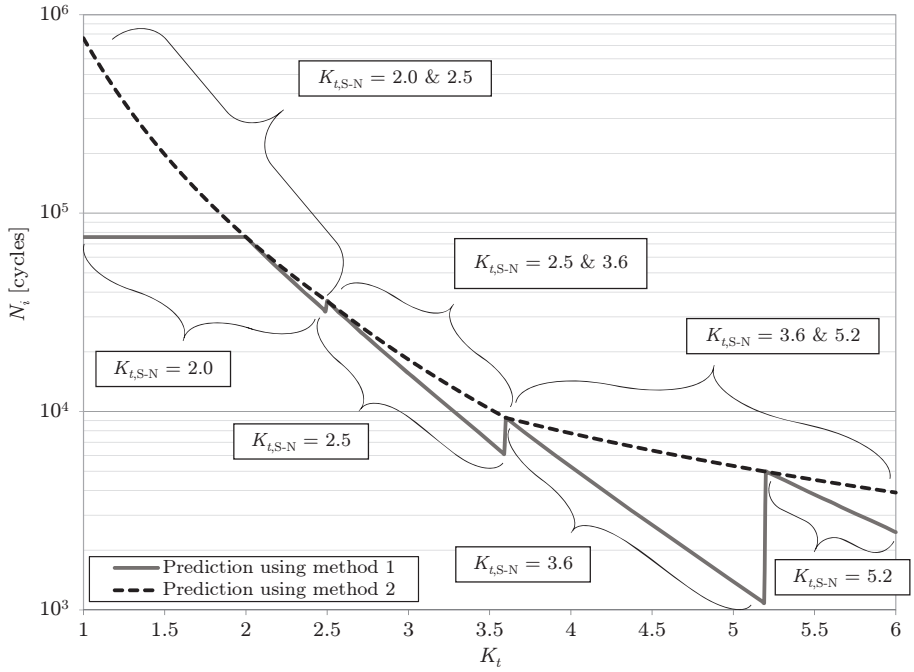


Figure C.3: Prediction based on $S_{a,\,\text{nom}} = 102.1$ MPa, $R_{\text{peak}} = 0.859$ varied between $K_t = 1.0$ and $K_t = 6.0$ using the closest available S-N data with $R_{\text{S-N}} = 0$.

## C.4. Conclusions

Two methods were described to use S-N data with a different $K_t$ value than the case analysed to predict the cycles to crack initiation: a correction and an interpolation method. Both methods showed a comparable accuracy in predicting the test results that were used to validate the complete methodology. In a optimisation environment, though, the interpolation method has preference over the correction method, because it shows a smoother dependence on

the SCF as compared to the correction method.

It was shown that the number of cycles to crack initiation of several types of FML can be predicted accurately using the presented methodology. The obtained accuracy depends on the S-N data that is used to make the predictions with. It was shown for GLARE 4B-3/2-0.3 that the closer the value of $R$ of the S-N data approaches the value of the case analysed, the higher the accuracy obtained. Such a trend was not observed for the $K_t$ value, although a choice for S-N data with a different $K_t$ can cause a significant change in precision.



## References


[1] S. Spronk, I. Şen, and R. Alderliesten, *Predicting fatigue crack initiation in fibre metal laminates based on metal fatigue test data,* International Journal of Fatigue **70**, 428 (2015).

[2] J. Homan, *Fatigue initiation in fibre metal laminates,* International Journal of Fatigue **28**, 366 (2006).

[3] J. J. Homan and L. Schra, *Application of aluminium alloy 2024-T3 fatigue life data to Glare laminates, GTP methods projects 2.4.3.2-B, 2.4.3.3-B and 2.3.3.4-B*, NLR Report NLR-CR-2002-185 (National Aerospace Laboratory of the Netherlands, 2002).

[4] R. Alderliesten, *Fatigue & damage tolerance of hybrid materials & structures - some myths, facts & fairytales,* in *ICAF 2009, Bridging the Gap between Theory and Operational Practice*, edited by M. Bos (Springer Netherlands, 2009) pp. 1245–1260.

[5] J. Schijve, *Fatigue of Structures and Materials* (Springer, 2009) iSBN-13: 978-1-4020-6807-2.

[6] J. J. Homan, *Handbuch Struktur Berechnung (HSB), 62131-01 issue A: Guidelines for the prediction of the fatigue life for Kt values different to available databases*, Tech. Rep. (2009).

[7] A. Vlot and J. W. Gunnink, *Fibre Metal Laminates, an introduction* (Kluwer Academic Publishers, Dordrecht, The Netherlands, 2001).

[8] V. Hoang and L. Schwarmann, *Handbuch Struktur Berechnung (HSB), 63111-01 issue D: Zeitfestigkeit 3.1354 T3*, Tech. Rep. (1986).

# Summary

The lower wing skin is one of the primary structures of an aircraft. To further improve the fatigue and damage tolerance (F&DT) performance of the lower wing, fibre metal laminates (FML) are proposed as a new material solution. FML consist of thin metal layers bonded with layers of fibre composites. This concept has potentially a large design freedom and its lay-ups could be tailored for specific applications by varying the number, thickness, orientation, and material type of the metal and fibre constituents. This study has been performed to explore the possibilities of lay-up optimisation for FML and to apply the concept of FML to a wing structure.

This research aimed to develop a design optimisation methodology for FML that satisfies F&DT criteria. The optimisation methodology should reveal the contribution of individual criteria to the obtained solutions. Furthermore, the method will be used to design a lower wing skin consisting of FML where F&DT and additional compatibility criteria are met. As a result, an analytical model is developed that comprises all the functionality to design a wing structure consisting of FML lower panels and aluminium upper panels. The lay-up solutions are obtained by evaluating the laminates for fatigue crack initiation (FCI), fatigue crack propagation (FCP) and residual strength (RS). These properties are obtained by means of prediction methods, which are implemented into a genetic algorithm optimisation environment. The scientific contribution is delivered by developing a method to reverse the prediction methods to find the lay-ups that satisfy the required property instead of determining the properties of a given lay-up.

The lay-up solutions are defined by three parameters: thickness of metal layers, number of metal layers and the grade of a laminate. The amount and orientation of the fibre plies are defined in this grade. With the optimisation method, the lowest weight solution in the design space is determined by generating solutions based on crossover and mutation operators and ranking the satisfying solutions based on their weight. The method considers the optimisation of flat-plates and wing cross-sections. For cross-section optimisation, only the numbers of metal layers along the cross-section are optimised to comply with manufacturing constraints. Additionally, a thickness step constraint is introduced to prevent stress concentrations between elements and to force a distributed thickness along the cross-section.

As a final step, the cross-section optimisation is linked to a wing design module that is now capable of dimensioning an aircraft wing structure with the lower panel consisting of FML and the upper panel of aluminium. The thickness of the aluminium skin is defined as variable

for the upper skin and evaluated using buckling criteria. As output, a complete optimized cross-section is obtained. To further improve the computation time and to simply the optimisation routine, a regression analysis is performed on the prediction methods for FCI, FCP and RS to obtain approximations for these methods. These approximate functions replace the prediction methods with high correlation and with assurance that the same solutions are obtained as output. The functions are replaceable with other functions representing different criteria to have a generic design method.

The influence of optimisation settings, approximations and different design criteria are extensively investigated. The output of the design method depends on the accuracy of the prediction methods and the accuracy of the performed regression, because a small difference in prediction influences the obtained optimal and near optimal design solutions. Further, genetic algorithm proved to be a robust method when optimising single elements or flat-plates when the settings are well-defined. In case of cross-section optimisation, due to the increasing size of the design space the method proved to be inefficient sometimes with the case that once in a while satisfying solutions were not obtained or were stuck at local minima. This problem is solved by defining an initial input to the procedure and increasing or decreasing the upper and lower boundary of the design space. A convergence loop for genetic algorithm is implemented to automate this process in this design method.

In conclusion, the method has the ability to compare and evaluate material configurations, to investigate the influence of various design criteria on the lay-up solutions and to optimise the wing material for minimised weight for different sets of load cases and wing geometries.

# Samenvatting

De huid van de ondervleugel is één van de primaire constructies van een vliegtuig. Vezelmetaallaminaten (VML) zijn geïntroduceerd als nieuwe materiaaloplossing om de vermoeiing en schadetolerantie (V&ST) prestaties van de ondervleugel te verbeteren. VML bestaan uit dunne metaallagen gelijmd met vezelcomposietlagen. Dit concept heeft een potentiële grote ontwerpvrijheid en de lay-ups kunnen voor specifieke toepassingen op maat gemaakt worden door het aantal, de dikte, de oriëntatie en het materiaaltype van de metaal- en vezelbestanddelen te variëren. Deze studie is uitgevoerd om de mogelijkheden van lay-upoptimalisatie te ontdekken en het VML-concept op een vleugelconstructie toe te passen.

Dit onderzoek heeft daarom als doel een ontwerp- en optimalisatiemethode voor VML te ontwikkelen waarbij aan V&ST-criteria wordt voldaan. De optimalisatiemethode moet de bijdrage van de individuele criteria aan de verkregen oplossingen onthullen. Bovendien zal deze methode gebruikt worden om een onderste vleugelhuid te ontwerpen dat voldoet aan de V&ST en aanvullende compatibiliteitscriteria. Als resultaat is er een analytisch model ontwikkeld die alle functionaliteit bevat om een vleugelconstructie bestaande uit VML onderpanelen en aluminium bovenpanelen te ontwerpen. De lay-upoplossingen zijn verkregen door de laminaten te evalueren voor vermoeiingsscheurinitiatie (VSI), vermoeiingsscheurgroei (VSG) en reststerkte (RS). Deze eigenschappen zijn verkregen met behulp van voorspellingsmethodes die in een genetische algoritme optimalisatieomgeving zijn geïmplementeerd. De wetenschappelijke bijdrage wordt geleverd door het ontwikkelen van een methode om de voorspellingsmethoden te omkeren zodat lay-ups die voldoen aan de geëiste eigenschappen worden gevonden in plaats van de eigenschappen van een gegeven lay-up te bepalen.

De lay-upoplossingen zijn gedefinieerd aan de hand van drie parameters: de dikte van de metaallagen, het aantal van de metaallagen en de gradatie van het laminaat. Het aantal en de oriëntatie van de vezellagen zijn gedefinieerd in deze gradatie. Met deze optimalisatiemethode worden de oplossingen met het laagste gewicht in de ontwerpruimte bepaald door verschillende oplossingen met behulp van cross-over- en mutatieoperatoren te genereren en de oplossingen die voldoen te rangschikken op hun gewicht. De methode werkt zowel voor de optimalisatie van vlakke platen als mede voor vleugeldwarsdoorsneden. In het geval van vleugeldwarsdoorsneden zijn alleen het aantal metaallagen langs de dwarsdoorsnede geoptimaliseerd om aan de productiebeperkingen te voldoen. Tevens is er een diktestapbeperking geïntroduceerd om spanningsconcentraties tussen de elementen te voorkomen en een dikteverdeling langs de dwarsdoorsnede te forceren.

Als laatste stap is de dwarsdoorsnedeoptimalisatie gekoppeld aan een vleugel ontwerpmodule dat nu instaat is om een vleugelconstructie te dimensioneren met het onderpaneel bestaande uit VML en het bovenpaneel bestaande uit aluminium. De dikte van de aluminiumhuid is gedefinieerd als variabele voor de bovenhuid en wordt geëvalueerd aan de hand van knik criteria. Als output wordt dan een volledig geoptimaliseerde dwarsdoorsnede verkregen. Om de rekentijd te verbeteren en de optimalisatieroutine te vereenvoudigen, is er een regressieanalyse uitgevoerd op de voorspellingsmodellen voor VSI, VSG en RS, zodat er een benadering voor deze methodes wordt verkregen. Hierbij worden de voorspellingsmethodes met goede correlatie en zekerheid dat dezelfde oplossingen als output worden verkregen, vervangen door benaderingsfuncties. Deze functies zijn vervangbaar door andere functies die andere design criteria voorstellen, zodat er een generiek ontwerpmethode verkregen wordt.

De output van de ontwerpmethode hangt af van de nauwkeurigheid van de voorspellingsmethode en de nauwkeurigheid van de uitgevoerde regressie, immers een kleine afwijking in de voorspelling beïnvloedt de verkregen optimale en bijna-optimale oplossingen. Bovendien heeft genetisch algoritme bewezen dat het een robuuste methode is in geval van een enkel element- of vlakke plaatoptimalisatie indien de optimalisatie instellingen goed gedefinieerd zijn. In geval van dwarsdoorsnedeoptimalisatie bleek de methode inefficiënt te zijn vanwege de toenemende grootte van de ontwerpruimte waarbij af en toe voldane oplossingen niet verkregen werden of vastzaten bij lokale minima. Deze probleem is verholpen door een initiële input te definiëren en door de boven- en ondergrens van de ontwerpruimte te verhogen of te verlagen. Om dit proces te automatiseren is er een convergentielus voor genetisch algoritme geïmplementeerd in deze ontwerpmethode.

Concluderend, de methode is instaat om materiaalconfiguraties te vergelijken en te evalueren, de invloed van verschillende ontwerpcriteria op de lay-upoplossingen te onderzoeken en het vleugelmateriaal voor verschillende belastinggevallen en vleugelgeometrieën te optimaliseren aan de hand van de minimale gewichtsdoelstelling.

# About the author

## Ilhan Şen

Ilhan Şen was born in 1986 in The Hague, The Netherlands. He started in 2005 with his BSc Aerospace Engineering at the Delft University of Technology, which he finished with distinction in 2008. Consequently, he commenced with his MSc Aerospace Engineering, where he mainly focused on the design of aircraft. At his internship at KVE Composites, he got familiar with the concept of composites and during his graduation project in corporation with Tata Steel, he got the affinity for developing design methods for aircraft structures. With his master thesis *Aircraft Fuselage Design Study* as output for the graduation period, he focused on the design and optimisation of aluminium for fuselage using buckling and fatigue and damage tolerance criteria. After finishing his MSc study in 2010, he stayed in Delft to perform his PhD. In 2011, he started the project in corporation with Constellium for which this thesis is the output. During this period, he experienced the concept of Fibre Metal Laminates and followed his work of method development for design optimisation of structures. Here, he specialised in the field of fatigue and damage tolerance of structures, which he now decided to pursue as a future career.

# Propositions

accompanying the dissertation

## Lay-up Optimisation of Fibre Metal Laminates

Development of a Design Methodology for Wing Structures

by

**Ilhan Şen**

1. The design methodology presented in this thesis cannot be used for designing a wing.
2. The local optima generated with genetic algorithms in this design method are as good as the global optimum.
3. Despite the potentially large design freedom of fibre metal laminates, the design choices are limited to a handful solutions.
4. Fibre metal laminates are a business opportunity for aluminium suppliers instead of danger to their business case.
5. The combination of Italian flavours with Japanese simplicity provides the basis for undiscovered dishes.
6. Social media give people the impression of being social, but in fact people become asocial.
7. The cold war between the West and East never ended, it was just frozen.
8. Feeling non-Dutch in the Dutch society is typically Dutch.
9. Despite all the knowledge and experience reported in the literature, the wheel will be reinvented again. And again.
10. Science is served by describing what a model cannot do instead of what it can do.
11. Universities pay with subscriptions for knowledge they share for free.

These propositions are regarded as opposable and defendable, and have been approved as such by the supervisor prof. dr. ir. R. Benedictus.

# Stellingen

behorende bij het proefschrift

## Lay-up Optimisation of Fibre Metal Laminates

Development of a Design Methodology for Wing Structures

door

**Ilhan Şen**

1. De ontwerpmethode gepresenteerd in dit proefschrift kan niet gebruikt worden om een vleugel te ontwerpen.
2. De lokale optima gegenereerd met genetisch algoritme in deze ontwerpmethode zijn even goed als het globale optimum.
3. Ondanks de potentiële grote ontwerpvrijheid van vezelmetaallaminaten zijn de ontwerpkeuzes beperkt tot een handvol oplossingen.
4. Voor aluminiumleveranciers zijn vezelmetaallaminaten een ondernemingskans in plaats van gevaar voor hun bedrijfsvoering.
5. De combinatie van Italiaanse smaken met Japanse eenvoud vormt de basis voor onontdekte gerechten.
6. Sociale media geeft mensen de impressie dat zij sociaal zijn, maar in feite worden mensen asociaal.
7. De koude oorlog tussen het Westen en Oosten is nooit beëindigd, het was alleen bevroren.
8. Het niet-Nederlands voelen in de Nederlandse samenleving is typisch Nederlands.
9. Ondanks dat alle kennis en ervaring geraporteerd wordt in de literatuur zal de wiel toch opnieuw uitgevonden worden. En weer opnieuw.
10. Wetenschap wordt gediend bij het beschrijven van wat een model niet kan in plaats van het beschrijven wat een model wel kan.
11. Universiteiten betalen in de vorm van abonnementen voor kennis die zij gratis delen.

Deze stellingen worden opponeerbaar en verdedigbaar geacht en zijn als zodanig goedgekeurd door de promotor prof. dr. ir. R. Benedictus.